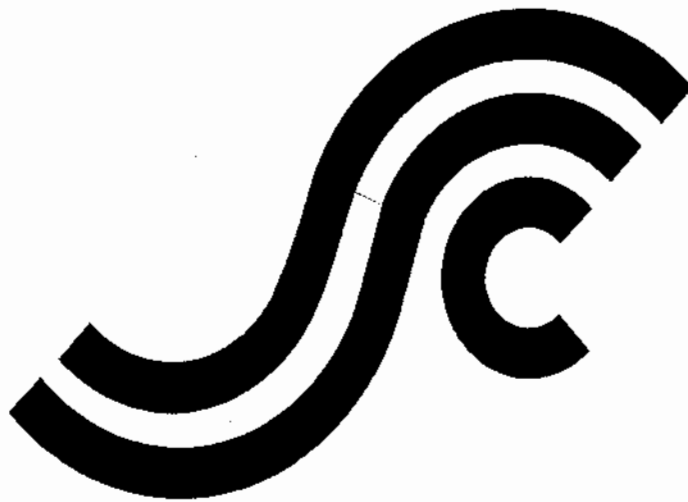


SSC-430

**FRACTURE TOUGHNESS OF A SHIP
STRUCTURE**



This document has been approved
For public release and sale; its
Distribution is unlimited

**SHIP STRUCTURE COMMITTEE
2003**

SHIP STRUCTURE COMMITTEE

RADM Thomas H. Gilmour
U. S. Coast Guard Assistant Commandant,
Marine Safety and Environmental Protection
Chairman, Ship Structure Committee

Mr. W. Thomas Packard
Director,
Survivability and Structural Integrity Group
Naval Sea Systems Command

Dr. Donald Liu
Senior Vice President
American Bureau of Shipping

Mr. Joseph Byrne
Director, Office of Ship Construction
Maritime Administration

Mr. Gerard A. McDonald
Director General, Marine Safety,
Safety & Security
Transport Canada

Mr. Thomas Connors
Director of Engineering
Military Sealift Command

Dr. Neil Pegg
Group Leader - Structural Mechanics
Defence Research & Development Canada - Atlantic

CONTRACTING OFFICER TECHNICAL REP.
Chao Lin / MARAD
Natale Nappi / NAVSEA
Robert Sedat / USCG

EXECUTIVE DIRECTOR
Lieutenant Eric M. Cooper
U. S. Coast Guard

SHIP STRUCTURE SUB-COMMITTEE

AMERICAN BUREAU OF SHIPPING

Mr. Glenn Ashe
Mr. Yung Shin
Mr. Phil Rynn
Mr. William Hanzalek

DEFENCE RESEARCH & DEVELOPMENT ATLANTIC

Dr David Stredulinsky
Mr. John Porter

MARITIME ADMINISTRATION

Mr. Chao Lin
Mr. Carlos Setterstrom
Mr. Richard Sonnenschein

MILITARY SEALIFT COMMAND

Mr. Joseph Bohr
Mr. Rick A. Anderson
Mr. Michael W. Touma

NAVAL SEA SYSTEMS COMMAND

Mr. Jeffery E. Beach
Mr. Edward E. Kadala
Mr. Allen H. Engle
Mr. Charles L. Null

TRANSPORT CANADA

Mr. Jacek Dubiel

UNITED STATES COAST GUARD

Mr. Rubin Sheinberg
Mr. Robert Sedat
Commander Ray Petow

CANADIAN COAST GUARD

Mr. Daniel Gauvin

Member Agencies:

*American Bureau of Shipping
Defence Research Establishment Atlantic
Maritime Administration
Military Sealift Command
Naval Sea Systems Command
Society of Naval Architects & Marine Engineers
Transport Canada
United States Coast Guard*



**Ship
Structure
Committee**

Address Correspondence to:

Executive Director
Ship Structure Committee
U.S. Coast Guard (G-MSE/SSC)
2100 Second Street, SW
Washington, D.C. 20593-0001
Ph: (202) 267-0003
Email: ecooper@comdt.uscg.mil

**SSC – 430
SR – 1429**

November 2003

FRACTURE TOUGHNESS OF A SHIP STRUCTURE

This project demonstrated the fracture susceptibility of a ship structure. It further illustrated the application of failure assessment techniques to aid ship owners and operators in evaluating the susceptibility of their vessels and thus support maintenance activities.

The results of this project include a description of the analysis approach and provide background on key elements of the supporting data and analysis techniques. The demonstration considered various fracture toughness levels, residual stress levels, and locations within the vessel on failure probabilities.

The sample application considered a bulk carrier as a platform for the demonstration of the concepts involved in this project. The failure assessment process was applied to this vessel to demonstrate the implementation of numerical and analytical modeling techniques by considering the six-step process outlined in the introductory sections of the report. These steps include vessel particular identification, structural section and component definition, load assessment, definition of local detail characteristics, failure assessment, and application of the results. Results of the failure assessment are presented for the bulk carrier and are discussed to illustrate trends and how they may be applied in practice. Potential applications could be extended to the improvement of vessel design and maintenance practice including inspection focusing, repair prioritization, identification of critical details, and gauging the significance of each structural member. The report reviews the strengths and weaknesses of the analysis techniques and recommends further research areas to improve the viability of the techniques demonstrated in this report.


T. H. GILMOUR

Rear Admiral, U.S. Coast Guard
Chairman, Ship Structure Committee

1. Report No. SSC-430	2. Government Accession No. PB2004-101321	3. Recipient's Catalog No. SR-1429	
4. Title and Subtitle FRACTURE TOUGHNESS OF A SHIP STRUCTURE		5. Report Date December 2003	
		6. Performing Organization Code	
7. Author(s) A.S. Dinovitzer, N. Pussegoda		8. Performing Organization Report No. 5383C.DFR	
9. Performing Organization Name and Address BMT Fleet Technology Ltd. 311 Legget Drive Kanata, Ontario Canada K2K 1Z8		10. Work Unit No. (TRAIS)	
		11. Contract or Grant No.	
12. Sponsoring Agency Name and Address Ship Structure Committee C/O Commandant (G-MSE/SSC) United States Coast Guard 2100 Second Street, SW Washington, DC 20593-0001		13. Type of Report Final Report	
		14. Sponsoring Agency Code G-M	
15. Supplementary Notes Sponsored by the Ship Structure Committee and its member agencies			
<p>16. Abstract</p> <p>The report presenting the results of this project includes a description of the analysis approach and provides background on key elements of the supporting data and analysis techniques. Based upon this review, this demonstration project assembled sample material data, vessel loading, a failure criterion, and developed flaw location and size scenarios. The demonstration considered various fracture toughness levels, residual stress levels, and locations within the vessel on failure probabilities.</p> <p>The sample application considered a bulk carrier as a platform for the demonstration of the concepts involved in this project. The failure assessment process was applied to this vessel to demonstrate the implementation of numerical and analytic modeling techniques by considering the six-step process outlined in the introductory sections of the report. These steps include vessel particular identification, structural section and component definition, load assessment, definition of local detail characteristics, failure assessment, and application of the results. Results of the failure assessment are presented for the bulk carrier and are discussed to illustrate trends in the results and how they may be applied in practice.</p> <p>It is proposed that the potential applications could, in the future, be extended to the improvement of vessel design and maintenance practice. Some applications could include inspection focusing, repair prioritization, identification of critical details, and gauging the significance of each structural member.</p>			
17. Key Words		18. Distribution Available From: National Technical Information Service U.S. Department of Commerce Springfield, VA 22151 Ph. (703) 605-6000	
19. Security Classif. (of this report) Unclassified	20. Security Classif. (of this page) Unclassified	21. No. of Pages 160	22. Price PC - \$48 (A09) ED - \$29(A00)

CONVERSION FACTORS
(Approximate conversions to metric measures)

To convert from	to	Function	Value
LENGTH			
inches	meters	divide	39.3701
inches	millimeters	multiply by	25.4000
feet	meters	divide by	3.2808
VOLUME			
cubic feet	cubic meters	divide by	35.3149
cubic inches	cubic meters	divide by	61,024
SECTION MODULUS			
inches ² feet ²	centimeters ² meters ²	multiply by	1.9665
inches ² feet ²	centimeters ³	multiply by	196.6448
inches ⁴	centimeters ³	multiply by	16.3871
MOMENT OF INERTIA			
inches ² feet ²	centimeters ² meters	divide by	1.6684
inches ² feet ²	centimeters ⁴	multiply by	5993.73
inches ⁴	centimeters ⁴	multiply by	41.623
FORCE OR MASS			
long tons	tonne	multiply by	1.0160
long tons	kilograms	multiply by	1016.047
pounds	tonnes	divide by	2204.62
pounds	kilograms	divide by	2.2046
pounds	Newtons	multiply by	4.4482
PRESSURE OR STRESS			
pounds/inch ²	Newtons/meter ² (Pascals)	multiply by	6894.757
kilo pounds/inch ²	mega Newtons/meter ² (mega Pascals)	multiply by	6.8947
BENDING OR TORQUE			
foot tons	meter tons	divide by	3.2291
foot pounds	kilogram meters	divide by	7.23285
foot pounds	Newton meters	multiply by	1.35582
ENERGY			
foot pounds	Joules	multiply by	1.355826
STRESS INTENSITY			
kilo pound/inch ² inch ^{1/2} (ksi√in)	mega Newton MNm ^{3/2}	multiply by	1.0998
J-INTEGRAL			
kilo pound/inch	Joules/mm ²	multiply by	0.1753
kilo pound/inch	kilo Joules/m ²	multiply by	175.3

ABSTRACT

This Ship Structure Committee project was developed to demonstrate the fracture susceptibility of a ship structure. This demonstration was intended to illustrate the application of failure assessment technique and how these analysis techniques could be used to aid ship owners and operators in evaluating the susceptibility of their vessels and thus support maintenance activities. It is proposed that the potential applications could, in the future, be extended to the improvement of vessel design and maintenance practice. Some applications could include inspection focusing, repair prioritization, identification of critical details, and gauging the significance of each structural member.

The report presenting the results of this project includes a description of the analysis approach and provides background on key elements of the supporting data and analysis techniques. Based upon this review, this demonstration project assembled sample material data, vessel loading, a failure criterion, and developed flaw location and size scenarios. The demonstration considered various fracture toughness levels, residual stress levels, and locations within the vessel on failure probabilities.

The sample application considered a bulk carrier as a platform for the demonstration of the concepts involved in this project. The failure assessment process was applied to this vessel to demonstrate the implementation of numerical and analytic modeling techniques by considering the six-step process outlined in the introductory sections of the report. These steps include vessel particular identification, structural section and component definition, load assessment, definition of local detail characteristics, failure assessment, and application of the results. Results of the failure assessment are presented for the bulk carrier and are discussed to illustrate trends in the results and how they may be applied in practice.

It is noted that the load analysis in the sample applications and theory described in this report consider only the vessel's linear response to wave induced bending. Practical design or analysis of ship structures for fracture resistance may require the consideration of effects not described in this report such as slamming, shock or impact, thermal effects, non-linear extreme sea response, hydro-elasticity and/or ice interaction loads.

The report concludes with a review of the strengths and weaknesses of the analysis techniques and recommends further research areas to improve the viability of the techniques demonstrated in this report. In general, it is concluded that the techniques presented in this project can be applied, however, they require automation of the analysis process and the support of material (fracture toughness) data.

TABLE OF CONTENTS

	<u>Page</u>
1. INTRODUCTION.....	1
1.1 Report Layout	1
2. PROJECT OBJECTIVE.....	3
2.1 Project Overview and Scope of Work	3
3. VESSEL FRACTURE ASSESSMENT TECHNIQUE	5
3.1 Vessel Particular Identification.....	5
3.1.1 Structural Analysis Techniques.....	6
3.1.2 Material Property (Fracture Toughness) Data.....	6
3.1.3 Correlation Initiation Fracture Toughness with Other Fracture Toughness Parameters.....	9
3.1.4 Tensile Properties.....	10
3.1.5 Future Development.....	13
3.2 Structural Section and Component Definition.....	14
3.2.1 Future Development.....	16
3.3 Load Estimation.....	16
3.3.1 Load Analysis Data Requirements.....	17
3.3.2 Load Analysis Process.....	18
3.3.3 Vertical and Horizontal Moment Interaction.....	20
3.3.4 Future Development.....	21
3.4 Definition of Local Detail Characteristics.....	22
3.4.1 Nominal Stress Transfer Function.....	23
3.4.2 Component Cross-Section Geometry.....	23
3.4.3 Stress Concentration Effects.....	24
3.4.4 Stress Intensity Factor Solution.....	24
3.4.5 Residual Stress.....	26
3.4.6 Finite Element Modeling.....	28
3.4.7 Future Development.....	35
3.5 Failure Assessment.....	36
3.5.1 Construction of Failure Assessment Curves.....	37
3.5.2 Detail: Example of an Assessment of the State of the Cracked Detail.....	42
3.5.3 Detail: Determine the Safety Margin of the Cracked Detail.....	43
3.6 Application of the Results.....	46
3.7 References.....	47
4. DEMONSTRATION OF THE FAILURE ASSESSMENT TECHNIQUE.....	49
4.1 Centre Cracked Stiffened Panel.....	49
4.1.1 Introduction.....	49
4.1.2 Stress Intensity Factor and Reference Stress Formulations.....	49
4.1.3 Computational Method.....	52
4.1.5 Results of Analyses.....	56
4.1.6 Discussion.....	60
4.2 Cracked Deck Longitudinal.....	60
4.2.1 Introduction.....	60

4.2.2	Model Geometry.....	61
4.2.3	Shear lag in Deck Plate	62
4.2.4	Stress Intensity Factor and Reference Stress Formulations	62
4.2.5	Failure Assessment of the Composite Section	66
4.2.6	Effect of Load Shedding.....	68
4.2.7	Discussion	70
4.3	References.....	70
5.	DEMONSTRATION OF THE VESSEL FAILURE ASSESSMENT TECHNIQUE	71
5.1	Vessel Particular Identification.....	71
5.2	Structural Segment and Component Definition.....	72
5.3	Load Assessment	75
5.3.1	Vertical Bending Moment.....	77
5.3.2	Bi-Axial Bending	79
5.4	Definition of Local Detail Characteristics.....	82
5.4.1	Material Properties	83
5.4.2	Stress and Stress Intensity Transfer Function Development.....	84
5.4.3	Component Cross-Section Geometry.....	96
5.4.4	Residual Stress	97
5.5	Failure Assessment	100
5.5.1	General Approach.....	100
5.5.2	Derivation of Detail Stress Exceedence Probabilities.....	100
5.5.3	Definition of Crack Critical Stress Levels	102
5.5.4	Definition of Crack Failure Probabilities	106
5.6	Application of the Results.....	107
6.	CRITICAL REVIEW OF THE ANALYSIS APPROACH LIMITATIONS.....	112
6.1	Vessel Particular Identification.....	112
6.2	Structural Section and Component Definition.....	113
6.3	Load Assessment	113
6.4	Definition of Local Detail Characteristics.....	114
6.5	Failure Assessment	114
6.6	Application of the Results.....	115
7.	CONCLUSIONS AND RECOMMENDATIONS.....	116
7.1	Conclusions.....	116
7.2	Recommendations.....	116

APPENDICES

APPENDIX A1: BS 7910 ELABORATION

APPENDIX A2: SAMPLE FAILURE ASSESSMENT DIAGRAMS FOR VARIOUS SHIP
STEELS

APPENDIX B: MATERIAL FRACTURE TOUGHNESS

APPENDIX C: STRESS INTENSITY FACTOR SOLUTION DERIVATIONS

LIST OF FIGURES

Figure 2.1: Proposed Project Overview	4
Figure 3.1: Samples of Structural Models Available at BMT FTL	7
Figure 3.2: ABS Grade B Plate (T-L orientation)-Intermediate and QS Rate Transition Curves..	8
Figure 3.3: ABS Grade EH 36 Plate (T-L orientation)-Intermediate and QS Rate Transition Curves.....	9
Figure 3.4: Relation Between NDT and 0.2 mm CTOD Transition Temperature Covering the Ship Plate Grades Tested [Pussegoda et al 1996]	10
Figure 3.5: True Stress vs. True Strain Curves of the Low-C Bainite/Ferrite Steel Tested at Different Temperatures and a Strain Rate of 0.00075 s^{-1}	11
Figure 3.6: Comparison of Predicted Stress-Strain Curves	11
Figure 3.7: Characterization of the Yield Strength and Tensile Strength Using the Rate Dependent Parameter R.....	12
Figure 3.8: Vessel Longitudinal Segment Definition	14
Figure 3.9: Definition of Typical Frames for a Given Ship Segment.....	15
Figure 3.10: Definition of Typical Structural Details.....	15
Figure 3.11: Example Load Spectrum	20
Figure 3.12: Typical Vessel Load Interaction Plot.....	22
Figure 3.13: Component Geometric Definition	23
Figure 3.14: Sample Ship Structure SCF Formulations	25
Figure 3.15: Three Modes of Cracking.....	26
Figure 3.16: Typical Distributions of Residual Stresses at Welds	28
Figure 3.17: Global Finite Element Model of Bulk Carrier (ABS 1994).....	30
Figure 3.18: Local Finite Element Model of Ship Detail	31
Figure 3.19: Recommended Element Sizes for Local Detail FEA	32
Figure 3.20: Collapsed Node Isoparametric Crack Tip Element.....	33
Figure 3.21: Example of 2-D Crack Model of an Edge Cracked Plate	34
Figure 3.22: Example of 3-D Crack Mesh for Semi-Elliptical Surface Crack	34
Figure 3.23: A Schematic of the Generic FAC, the FAP and Safety Margin.....	36
Figure 3.24: Lüders Plateau ϵ_L , Measured Values and Estimation Equation of BS 7910:1999 with Amendment 1	39
Figure 3.25: Strain Hardening Exponents for Steel Plate, Sheet, and Bar	39
Figure 3.26: BS 7910:1999 Level 2 FAC's – ABS EH 36 Steel.....	40
Figure 3.27: Comparison of BS 7910:1999 Level 2 FAC's with the simplified Level 2B Curve – ABS EH 36 Steel.....	41
Figure 3.28(a): BS 7910:1999 Simplified Level 2B FAC – ABS A, B, D, E Steels – $\sigma_{res} = 0$...45	
Figure 3.28(b): BS 7910:1999 Simplified Level 2B FAC – ABS A, B, D, E Steels – $\sigma_{res} = \sigma_y$...45	
Figure 4.1: Central, Through-Thickness, Cracked Panel with Stiffened Edges.....	50
Figure 4.2: Stiffened Edge SIF Correction Factors	51
Figure 4.3: Screen Capture - $\beta = 0$, $\sigma_y = 50 \text{ ksi}$, $\sigma_{res} = 0$, $\delta_c = 0.004 \text{ in}$, $2a_i = 0.1 \text{ in}$	52
Figure 4.4: Screen Capture - $\beta = 0$, $\sigma_y = 50 \text{ ksi}$, $\sigma_{res} = 25 \text{ ksi}$, $\delta_c = 0.004 \text{ in}$, $2a_i = 0.1 \text{ in}$	53
Figure 4.5: Screen Capture - $\beta = 0$, $\sigma_y = 50 \text{ ksi}$, $\sigma_{res} = 0$, $\delta_c = 0.080 \text{ in}$, $2a_i = 1.0 \text{ in}$	53
Figure 4.6: Screen Capture - $\beta = 0$, $\sigma_y = 50 \text{ ksi}$, $\sigma_{res} = 25 \text{ ksi}$, $\delta_c = 0.080 \text{ in}$, $2a_i = 1.0 \text{ in}$	54
Figure 4.7: Screen Capture - $\beta \rightarrow \infty$, $\sigma_y = 50 \text{ ksi}$, $\sigma_{res} = 0$, $\delta_c = 0.004$, $2a_i = 1.0 \text{ in}$	54

Figure 4.8: Screen Capture - $\beta \rightarrow \infty$, $\sigma_y = 50$ ksi, $\sigma_{res} = 25$ ksi, $\delta_c = 0.004$, $2a_i = 0.1$ in.	55
Figure 4.9: Screen Capture - $\beta \rightarrow \infty$, $\sigma_y = 50$ ksi, $\sigma_{res} = 0$, $\delta_c = 0.080$, $2a_i = 1.0$ in.	55
Figure 4.10: Screen Capture - $\beta \rightarrow \infty$, $\sigma_y = 50$ ksi, $\sigma_{res} = 25$ ksi, $\delta_c = 0.080$, $2a_i = 1.0$ in.	56
Figure 4.11: Critical Crack Length $2a_f$ vs. Membrane Stress, σ_m , $2b = 1024$ in (26 m), $\beta = 0$	59
Figure 4.12: Critical Crack Length $2a_f$ vs. Membrane Stress, σ_m , $2b = 1024$ in (26 m), $\beta \rightarrow \infty$.	59
Figure 4.13: Composite Section – Deck Plate and Bulb Flat Longitudinals	61
Figure 4.14: Equivalent Flat Plate Longitudinal for Fracture Mechanics Analysis	63
Figure 4.15: Failure Assessment Diagram for Composite Section.....	66
Figure 4.16: Critical Stress vs. Crack Length for Composite Section.....	67
Figure 4.17: Load Shedding in Composite Section	69
Figure 5.1: Bulk Carrier Particulars.....	71
Figure 5.2: General Arrangement of Segments and Frames in the Bulk Carrier.....	73
Figure 5.3: Section View of the Bulk Carrier Describing Component Location	74
Figure 5.4: Loaded Condition Vertical Bending Moment Exceedence Probability	78
Figure 5.5: Ballast Condition Vertical Bending Moment Exceedence Probability	79
Figure 5.6: Segment 1 Bending Moment Interaction Load Cycle Probability Envelopes	80
Figure 5.7: Segment 2 Bending Moment Interaction Load Cycle Probability Envelopes	80
Figure 5.8: Segment 3 Bending Moment Interaction Load Cycle Probability Envelopes	81
Figure 5.9: Segment 4 Bending Moment Interaction Load Cycle Probability Envelopes	81
Figure 5.10: Segment 5 Bending Moment Interaction Load Cycle Probability Envelopes	82
Figure 5.11: Sample Application Cracking Locations of Interest and Crack Types	83
Figure 5.12: Estimated AH36 Fracture Toughness Transition Curve	83
Figure 5.13: Sample Ship Structure SCF Formulations	86
Figure 5.14: Three Modes of Cracking.....	87
Figure 5.15: ALGOR Shell Finite Element Model.....	88
Figure 5.16: Basic ANSYS Primary Shell Solid Model Geometry.....	88
Figure 5.17: Through Crack Shell Finite Element Model	90
Figure 5.18: Edge Crack Shell Finite Element Model.....	90
Figure 5.19: Through-Crack Brick Finite Element Model	91
Figure 5.20: Edge Crack Brick Finite Element Model	91
Figure 5.21: View of Solid Model along Z-Axis (All Dimensions in mm).....	92
Figure 5.22: View of Solid Model along X-Axis (All Dimensions in mm)	93
Figure 5.23: Component Geometric Definition.....	97
Figure 5.24: Typical Distributions of Residual Stresses at Welds	99
Figure 5.25: Sample Numeric Vertical Bending Moment Local Stress Exceedence Probabilities.....	101
Figure 5.26: Sample Analytic Vertical Bending Moment Local Stress Exceedence Probabilities.....	101
Figure 5.27: Sample Numeric Combined Vertical and Horizontal Bending Moment Local Stress Exceedence Probabilities.....	102

LIST OF TABLES

Table 3.1. Steel Grades with Stress-Strain Curves	42
Table 3.2. Values of X and E	43
Table 3.3: Safety Margins — Failure Assessment Using the Simplified Level 2B FAC.....	44
Table 4.1: Results, $\beta = 0$, $\sigma_y = 50$ ksi, $2b = 1024$ in.	57
Table 4.2: Results, $\beta \rightarrow \infty$, $\sigma_y = 50$ ksi, $2b = 1024$ in.....	58
Table 4.3: Properties of Deck Longitudinal.....	61
Table 4.4: Plasticity Correction Factors.	65
Table 4.5: Failure Assessment Results	67
Table 4.6: Increase in Critical Stress due to Load Shedding.....	69
Table 5.1: Vessel Segment and Frame Type Distribution.....	72
Table 5.2: Vessel Component Characteristics for Frame Types 1 and 2**	76
Table 5.3: Bulk Carrier Joint Probability of Speed and Sea State.....	76
Table 5.4: Bulk Carrier Joint Probability of Relative Heading and Sea State.....	77
Table 5.5: Bulk Carrier Vertical Bending Moment Exceedence Probabilities.....	78
Table 5.6: Vessel Analytic Stress Transfer Functions (Section Properties).....	84
Table 5.7: Crack Model Description.....	92
Table 5.8: Global FE Model Load Case Summary.....	93
Table 5.9: Analytic and Numeric Edge Crack SIF and Stress Summary	94
Table 5.10: Analytic and Numeric Through Crack SIF and Stress Summary.....	95
Table 5.11: Edge Crack Transfer Functions	96
Table 5.12: Through Crack Transfer Functions.....	96
Table 5.13: Edge Crack Critical Stresses.....	104
Table 5.14: Through Crack Critical Stresses	105
Table 5.15: Edge Crack Critical Crack Lengths; 0% Yield Residual Stress	108
Table 5.16: Edge Crack Critical Crack Lengths; 100% Yield Residual Stress	109
Table 5.17: Through Crack Critical Crack Lengths; 0% Yield Residual Stress	110
Table 5.18: Through Crack Critical Crack Lengths; 100% Yield Residual Stress	111

1. INTRODUCTION

The mandate of the Ship Structure Committee is to promote research and disseminate its results to the marine community in an effort to improve the quality of ship design, construction, maintenance and life cycle management.

This project was developed to support the investigation and demonstration of the feasibility of techniques to aid ship owners and operators to better understand the significance of crack-like flaws to the integrity of their vessel. This integrity assessment involves the consideration of the potential for fracture or plastic collapse as described in a variety of defect assessment standards and the SSC developed Guide to Damage Tolerance (SSC-409). In more detail, the assessment considers both the crack driving force and resistance to crack extension which are influenced by the following factors:

Crack Driving Force

- flaw size and orientation
- flaw location within the structure
- local and global structural geometry
- magnitude and direction of structural loads and residual stresses

Resistance to Crack Extension

- material chemistry, thickness and manufacturing process
- in-service deformation history
- in-service temperature
- applied loading strain rate

Successful completion of this project will permit the owner or operator of a vessel to easily identify the areas in the ship most likely to give rise to crack defects, and to focus on quality during construction and subsequent maintenance and repair on these areas. The project will provide guidance on the most suitable, cost effective and practical approach to fracture probability assessment for ship structures. In a sense, this project may be seen as the logical extension of the SSC Guide to Damage Tolerance of Ship Structures in that it seeks to develop and demonstrate the techniques outlined therein.

1.1 Report Layout

The following report presents the results of a research project aimed at demonstrating vessel fracture assessment techniques. This report is presented as a demonstration of the concepts involved and as a first step towards the final development of these techniques. The report is presented in seven sections as follows:

- Section 1 - Introduction

Introduces the justification for the project and describes the layout of the report.

- Section 2 - Project Objective

Defines the project objectives and scope of the investigation.

- Section 3 - Vessel Fracture Assessment Techniques

Presents the vessel fracture assessment techniques along with its process, analytic approaches and defines the assessment data requirements.

- Section 4 - Demonstration of the Fracture Assessment Techniques

Presents two worked examples to demonstrate the analysis process and results.

- Section 5 - Demonstration of Vessel Fracture Assessment Techniques

Presents worked examples to demonstrate the analysis data, process and results when the proposed analysis techniques are applied to a ship structure.

- Section 6 - A Critical Review of the Analysis Approach Limitations

Discusses the benefits of the analysis techniques along with those areas in need of further development.

- Section 7 - Conclusions and Recommendations

Presents conclusions outlining what has been learned in this project and recommends areas for further development.

2. PROJECT OBJECTIVE

The primary objective of this project is:

to demonstrate the feasibility of modeling the fracture toughness of a ship structure as an entity.

The ability to evaluate a vessel's fracture toughness or resistance to unstable crack extension, allows the project's second objective to be achieved:

to allow vessel owners or operators to understand the risk of fracture throughout their vessel and thus focus inspection, maintenance or design efforts to reduce this risk.

2.1 Project Overview and Scope of Work

The project was divided into two phases including: (1) technology and data review; and (2) development and demonstration of the fracture assessment methodology. These two phases included several tasks to achieve the project objectives. It was proposed that a project break or decision point be considered after the completion of the first phase. If the technology and data review demonstrated significant gaps in the current state of practice or knowledge, the project team would have recommended that the project not proceed further. The final decision was made by the project technical committee with the support of the project team's interim report, describing the findings of Phase 1, that sufficient information existed to proceed with Phase 2.

It was suggested in this proposal to include three approaches to fracture assessment in the development and demonstration phase of the project. The three approaches are used to demonstrate and compare the advantages and disadvantages of: (1) analytic, (2) hybrid numerical and analytic, and (3) numeric techniques that may be used to complete the desired fracture assessment. The advantage of this approach is that it will demonstrate the three techniques to individually assess their practicability and compare their effectiveness. The overall project approach is outlined in Figure 2.1. In order to perform the work required for completion of this project, the scope of work was divided into tasks as listed in Figure 2.1.

During the execution of the project, the project team and technical committee decided that the project scope should be changed to focus on a single vessel in the sample applications, rather than considering two vessels. This project scope modification was made to permit the development of analysis results with greater detail and a broader investigation of the applied loading

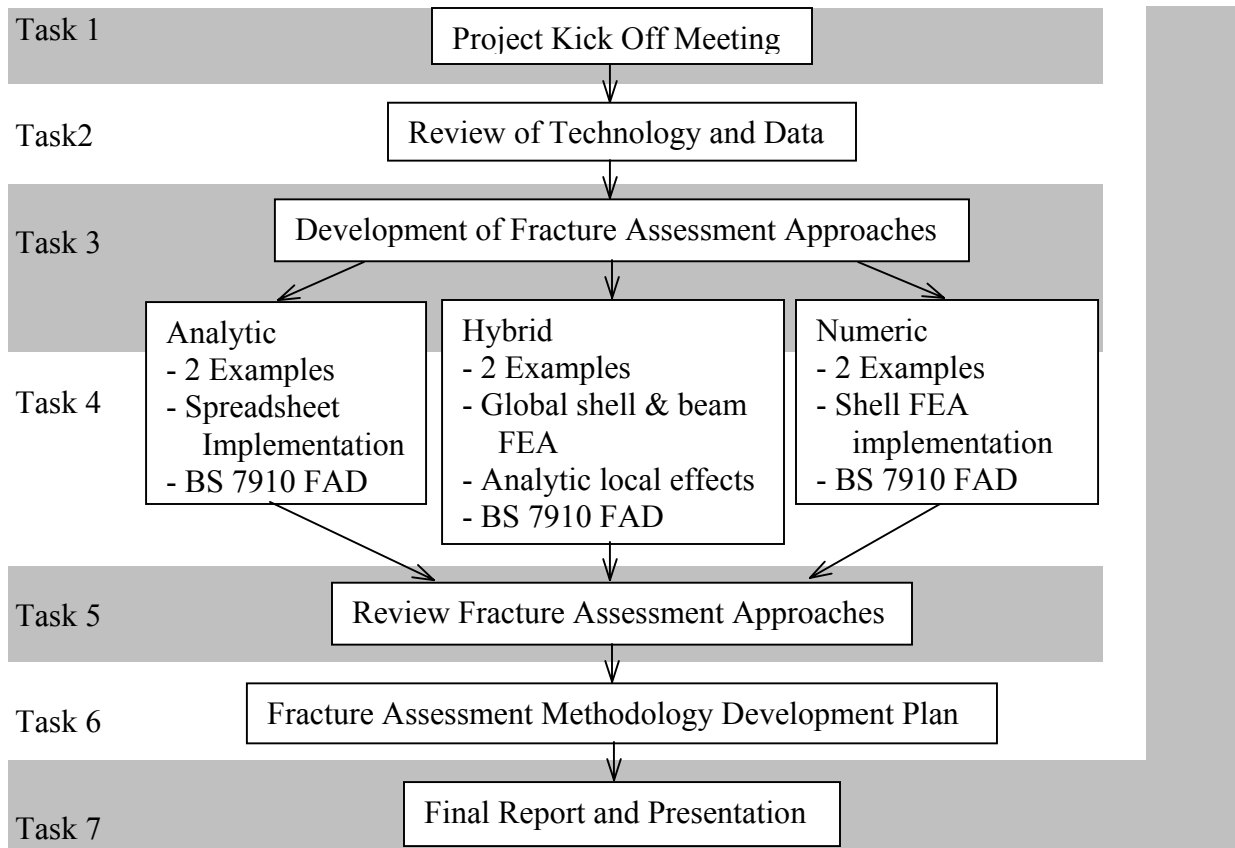


Figure 2.1: Proposed Project Overview

3. VESSEL FRACTURE ASSESSMENT TECHNIQUE

The vessel fracture assessment approach developed in this project involves a six step process including:

- Vessel Particular Identification,
- Structural Section and Component Definition,
- Load Assessment,
- Definition of Local Detail Characteristics,
- Failure Assessment
 - Fracture and/or plastic collapse
- Application of the Results
 - Critical flaw size definition for design load scenarios
 - Critical load level for specified flaw size
 - Critical component definition
 - Identification of damage tolerance assessment on design

The sections that follow describe these steps and discuss their application, providing some additional information on their limitations and inherent assumptions. In addition, alternative approaches to those proposed for the case study examples are described.

It should be noted that the approach has been assembled with an alternate failure assessment approach that is described in Appendix A. This alternate approach is used to reduce the level of conservatism inherent in the analysis and to simplify the assessment and thus facilitate the demonstration of vessel fracture assessment.

The approach presented in this report was developed after the completion of a literature review to identify the state of practice. An overview of the results of the literature review is provided in this section.

3.1 Vessel Particular Identification

In this step, the subject vessel is described in terms of its:

- Structural configuration and scantlings
- Materials, and
- Hull form and weight distribution

The structural configuration information, which may be described by general arrangement drawings, is used to subdivide the ship structure into discrete compartments with different environments (e.g., ballast tanks, work and cargo spaces). The scantlings will be used to define the structural components used in the fracture assessment calculations along with the material property information. The scantling and section information will also be used to describe typical hull girder sections used to calculate section moduli and/or develop finite element models to support the assessment.

3.1.1 Structural Analysis Techniques

The structural analysis proposed for this project was to be completed along three avenues with differing levels of numerical complexity. These techniques include analytic, hybrid numeric and analytic as well as fully numeric. Samples of these levels of analysis are shown in Figure 3.1 that illustrate geometric forms and levels of detail they provide. It is noted that that the deflections and Von Mises stresses presented in these figures are not used in fracture assessment.

The "Analytic" approach employs spreadsheets to calculate vessel section properties and local nominal stresses. These stresses are modified by global structural stress concentration factors to incorporate the effects of openings or other changes in structural members. As needed, local stress concentration effects are considered. These stresses are used along with analytic stress intensity factor solutions to estimate the crack driving force.

The "hybrid" approach employs a global finite element model to resolve local member stresses including global stress concentration effects. These stresses, magnified by local stress concentration factors, are used along with analytic stress intensity factor solutions to estimate the crack driving force.

The "numeric" approach to demonstrating the fracture toughness of a ship structure demonstrates a fully numeric approach to the problem in which sub-structured finite element models are used to consider numerically derived stress intensity factors from finite element models explicitly including crack tip elements.

3.1.2 Material Property (Fracture Toughness) Data

The proposed sample vessel fracture assessment is presented based upon simple hull girder analytic calculations as well as using sub-structured linear elastic finite element modeling. In both cases, the material property data requirements are modest. For the current example, the material property data requirements include:

Analytic Analysis

- Steel yield and ultimate tensile strengths
- Modulus of elasticity, and
- Steel and/or weld metal fracture toughness transition curve

Numerical (FE) Analysis

- Steel yield and ultimate tensile strengths
- Modulus of elasticity
- Poisson's ratio (0.3), and
- Steel and/or weld metal fracture toughness transition curve

The critical assessment of the ship structure details has been evaluated on damage tolerance methodology for some preliminary cases. The sensitivity study has shown that a fracture critical situation arises only for long cracks at the low-end bound of the CTOD toughness (0.25 mm). In these situations, we would usually be assessing fatigue cracks at the toe of a fillet weld. These long cracks reside mostly in the base metal and therefore the focus was on the availability of base material fracture toughness data.

The paragraphs that follow provide some insight into the effect of loading rate and temperature on fracture toughness. While the effect of temperature is commonly considered in material characterization, the effect of loading rate is not as commonly considered and thus there is much less data available describing this effect. Ideally in the future, material properties generated for dynamic loading rates would be considered in design, however, the state of practice does not currently support the consideration of dynamic loading rate material characterization.

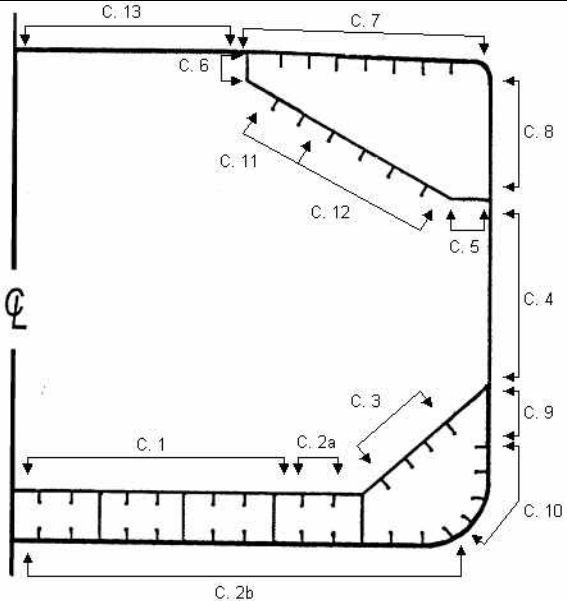
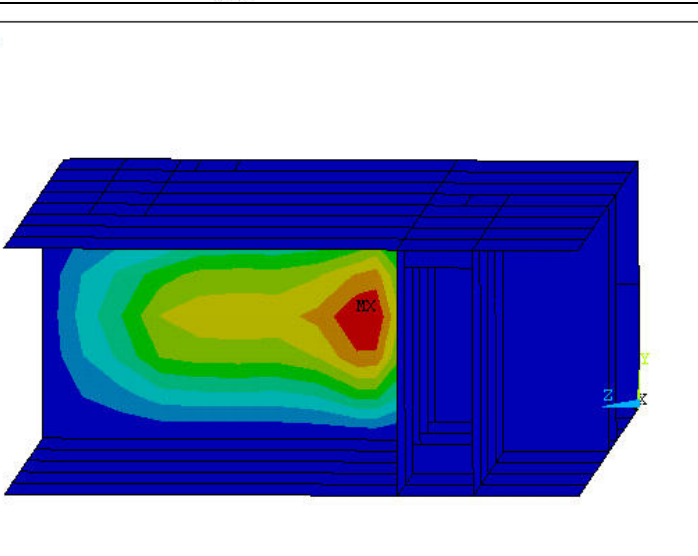
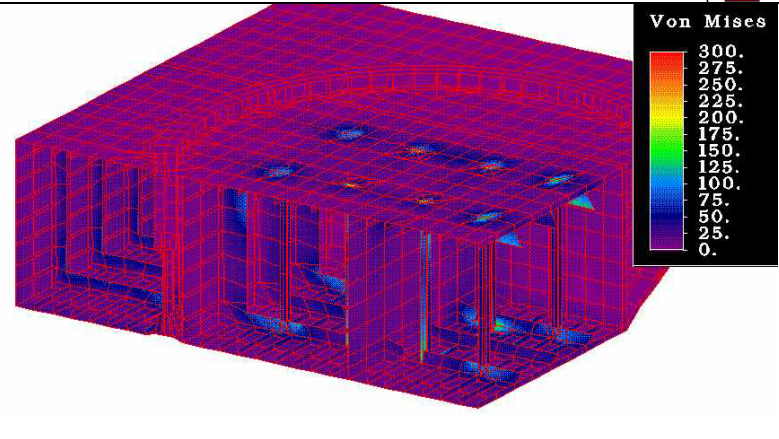
<p>Analytic</p> <ul style="list-style-type: none"> - Tanker - Bulk Carrier - Warship <p>Spreadsheets outlining properties of stiffened plate structural components and calculating section properties</p>	
<p>Hybrid</p> <ul style="list-style-type: none"> - Tank Barge - Power Barge <p>Full ship FE models developed using shell elements for the hull and bulkheads and beam elements for longitudinal and transverse stiffening</p>	 <pre> ANSYS 5.6.1 MAR 5 2001 11:51:59 NODAL SOLUTION STEP=3 SUB =1 TIME=3 USUM TOP RSYS=0 DMX =31.307 SEPC=73.58 SMX =31.307 0 3.479 6.957 10.436 13.914 17.393 20.871 24.35 27.828 31.307 </pre>
<p>Numeric</p> <ul style="list-style-type: none"> - Oil Tanker - Bulk Carrier - Work Barge - Asphalt Tanker - Semi Submersible <p>Full ship and three hold FE models using shell elements for all hull, bulkhead, frames and longitudinals</p>	 <pre> Von Mises 300. 275. 250. 225. 200. 175. 150. 125. 100. 75. 50. 25. 0. </pre>

Figure 3.1: Samples of Structural Models Available at BMT FTL

The initiation fracture toughness of steel plate data that is needed is in the form of crack tip opening displacement (CTOD). Standard methods for performing these tests are specified in both British Standards and ASTM standards. These standards are applicable at the quasi-static loading rate, whereas in a ship structure, the load is dynamic. Fracture toughness data at dynamic loading rates are less readily available. In applying the CTOD toughness in Engineering Critical Assessment (ECA) for the case of ship structural details, it is important to consider the loading rate effect as well as the effect of temperature on toughness. In ferritic steels (ship plate belongs to this type), we also have the generic fracture transition behavior, i.e., the ductile to brittle, as the temperature drops below the transition. These effects have been described in the literature by Barsom and Rolfe.[1999] Figures 3.2 and 3.3 show the effect of strain (loading) rate and temperature on the transition behavior of ship plate. In summary, the findings show the following:

- The CTOD-temperature transition curves for the intermediate rate loading, 6.5×10^3 MPa $\sqrt{\text{m/s}}$ representing slamming, were shifted to the right of the Quasi Static (QS) rate transition curves.
- At 0.25 mm CTOD lower bound, a design temperature of 0°C is safe for QS loading rate. At the intermediate loading rate the DH and B grade give CTOD values lower than 0.25 mm.
- Work done later at “impact” rate loading using cross head rates approaching 4 ms^{-1} , showed that the transition curves shifted further to the right, while the degree of the shift was less than the shift from QS to intermediate loading rate [Pussegoda et al 1996].

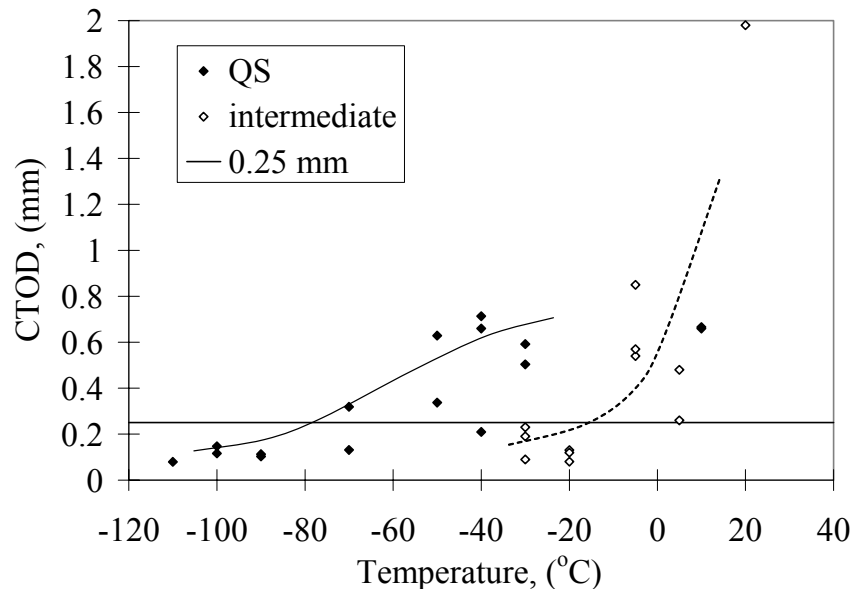


Figure 3.2: ABS Grade B Plate (T-L orientation)-Intermediate and QS Rate Transition Curves

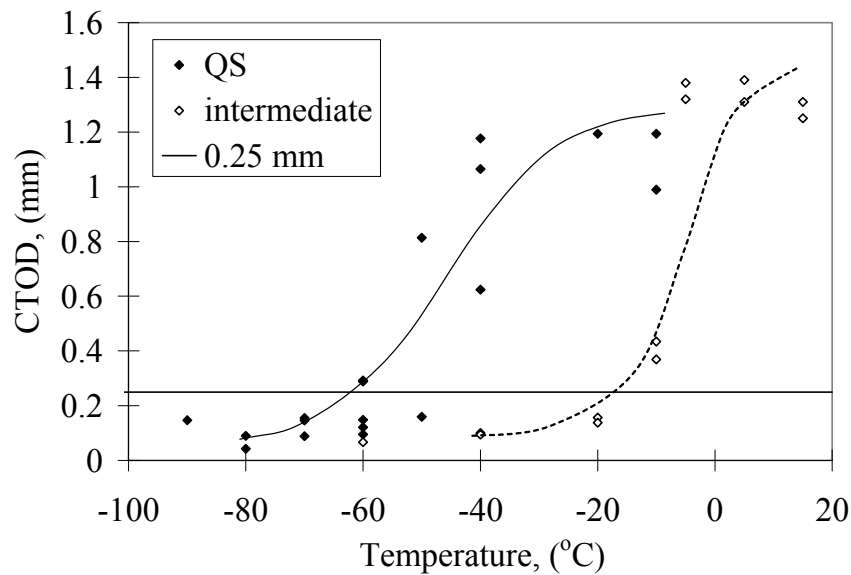


Figure 3.3: ABS Grade EH 36 Plate (T-L orientation)-Intermediate and QS Rate Transition Curves

Figure 3.3 shows the generic transition curve shape, i.e., the lower shelf (brittle fracture), brittle-to-ductile transition and the upper shelf ductile fracture, and this figure clearly shows that at the higher strain rate, the transition curve is shifted to the right and is typical of other published literature on fracture toughness transition. The CTOD values are also identified with the type of failure, for example, δ_m category is crack growth from the fatigue crack tip by ductile tearing (upper shelf in the transition curve), δ_u is brittle extension after minor ductile growth (transition region), δ_c is brittle extension from the facture crack tip after crack blunting (lower shelf).

CTOD toughness of ship and offshore grades from Japanese publications are available. Among these, one publication had relevant information on fracture transition behaviour and the strain rate effect for CTOD toughness of 490 MPa tensile strength (TS) class steels [F. Minami et al. 1998]. The summary findings are below:

The yield strength (YS) of the steels is about 350 MPa with yield to tensile strength ratio (Y/T) of about 0.7. The steel composition indicates 0.15 C/1.3 Mn steel with some Ti addition in one. The carbon equivalent (CE) is about 0.4 (CSA W59 expression).

CTOD transition data are available for these two grades at QS (cross-head rate 0.1 mm/s) and intermediate rate (10 mm/s). The CTOD values at 0°C is about 1 mm (δ_m) at QS loading (strain rate) and at intermediate rate falls in the range of 0.2 (δ_c) to 1.2 mm (δ_m)

3.1.3 Correlation Initiation Fracture Toughness with Other Fracture Toughness Parameters

In the past, correlations have been presented between nil-ductility transition (NDT) temperature (ASTM E208) and dynamic fracture toughness transition temperature. Early work has been presented to show that the termination of the lower shelf K base toughness at about 10^3 s^{-1} strain rate is close to the NDT temperature [Barsom and Rolfe, 1999]. This relation is shown for A36, ABS - C and ASTM A572 grades. Such relations have been validated for more recent ABS grades as well.

Figure 3.4 shows this relationship in terms of CTOD transition temperature and NDT temperature for ABS and DNV grades. The difference from the K based data is that the NDT temperature is slightly below the 0.2 mm intermediate loading rate CTOD transition temperature and 20°C below the 0.2 mm impact (dynamic) loading rate CTOD transition temperature. As the K values at 0.2 mm CTOD are higher than 30 MPa√m used in the K based relation, the results in Figure 3.4 and those in reference [Barsom and Rolfe, 1999] are consistent.

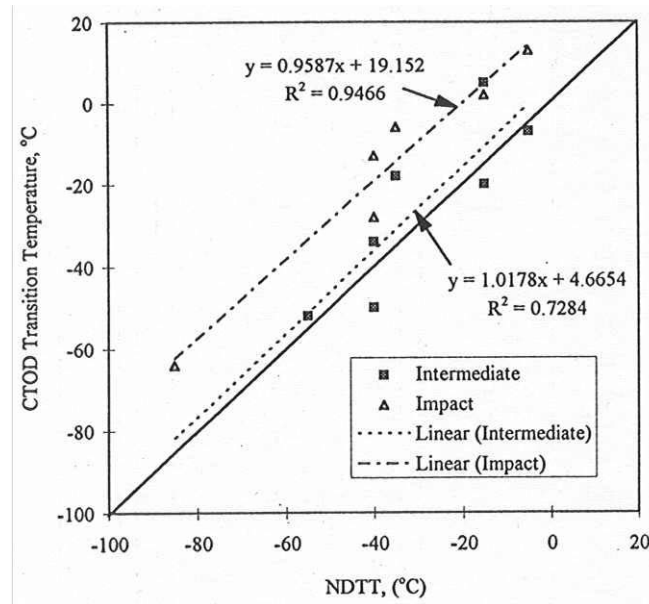


Figure 3.4: Relation Between NDT and 0.2 mm CTOD Transition Temperature Covering the Ship Plate Grades Tested [Pussegoda et al 1996]

In summary, the above relationships and the generic shape of the transition curve can be reliably used to estimate dynamic and intermediate loading rate CTOD values in the transition temperature range from NDT temperature for these types of steels. A lesser accurate estimation of the 0.2 mm CTOD transition temperature and CTOD values in the transition temperature range at QS rate can be estimated from this methodology.

3.1.4 Tensile Properties

Room temperature tensile properties of structural steels at QS loading rate are not scarce in the literature, the more difficult properties to obtain in the literature in perspective of this program is at lower temperature and at higher strain rate. Figure 3.5 and 3.6 are presented to demonstrate in a generic way the effect of temperature and strain rate on flow properties of steel [S. Xu et al. 2001]. The curves in Figure 3.5 are presented in ascending temperature order for the indicated temperatures.

A number of expressions in the literature are available to account for the temperature and strain rate effects on yield strength of steels. In the case of Figure 3.6, the temperature and strain rate dependent term is:

$$\sigma^* = \left[27.86 - 0.00393 T \ln \left(\frac{10^8}{\dot{\epsilon}} \right) \right]^2 \quad (3.1)$$

where, σ^* is the strain rate and temperature dependant yield stress, T is the temperature in $^{\circ}\text{K}$ that effects the stress strain behaviour.

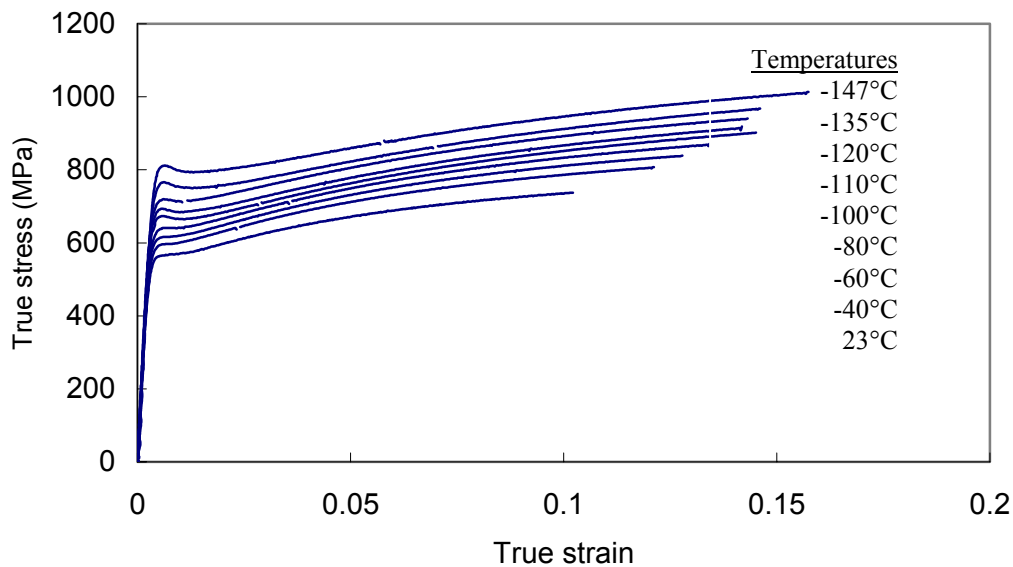


Figure 3.5: True Stress vs. True Strain Curves of the Low-C Bainite/Ferrite Steel Tested at Different Temperatures and a Strain Rate of 0.00075 s^{-1}

In Figure 3.6, the curves from the top to the bottom correspond to test temperatures from low to high as indicated in the legend.

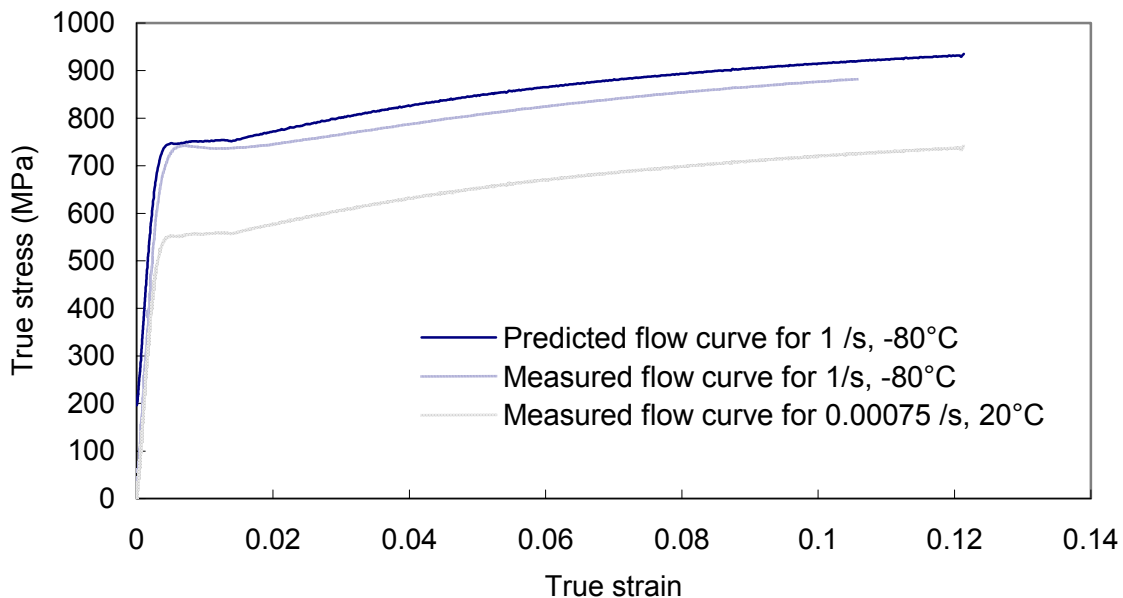


Figure 3.6: Comparison of Predicted Stress-Strain Curves

(adding the thermal component of stress to the athermal stress-strain curve, i.e., at room temperature and static loading rate) with an experimental stress-strain curve of the low-C bainite/ferrite steel at 1 s^{-1} and at -80°C).

For an intermediate rate of loading (strain rate of 0.05 s^{-1}), representing slamming, the yield strength of steels were fitted to a rate dependent expression:

$$\sigma_y = \left[A - B T \ln \left(\frac{10^8}{\dot{\epsilon}} \right) \right]^2 \quad (3.2)$$

where A and B are constants determined by curve fitting for each steel grade.

Similar forms of relationships have been developed by others to fit experimentally observed temperature dependence on yield strength and flow strength. Figure 3.7 shows such an example from literature. The rate parameter expression in this case is:

$$R = \left[T \ln \left(\frac{A}{\dot{\epsilon}} \right) \right] \quad (3.3)$$

where A and R are constants as defined in Figure 3.7 [F.M. Bennett and G.M. Sinclair (1965) and M. Tada (1995)].

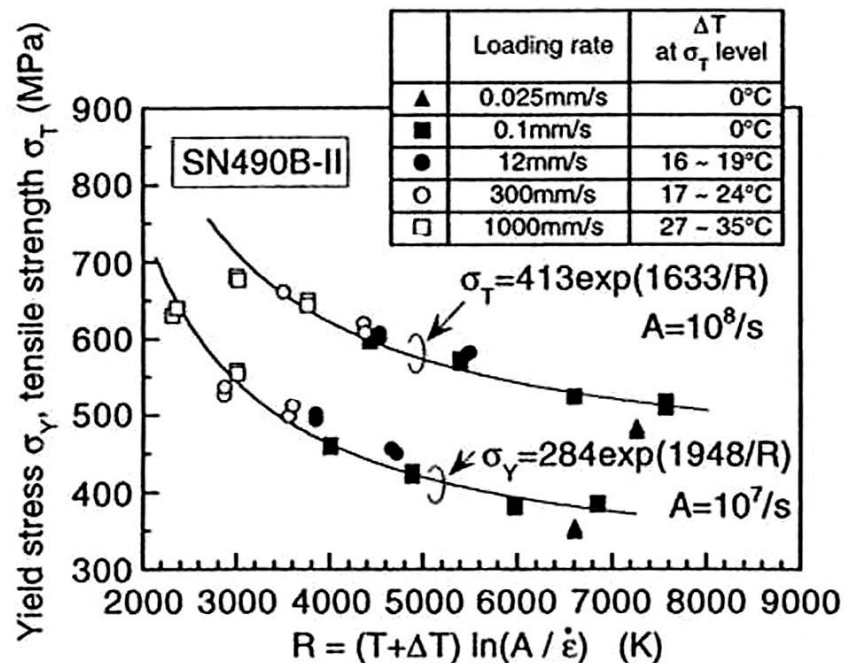


Figure 3.7: Characterization of the Yield Strength and Tensile Strength Using the Rate Dependent Parameter R

In summary, data in the form of complete stress-strain curves is limited. However, standard behaviour of Marine and Offshore grades can be categorized in a generic way into two types:

- A flow curve that has discontinuous yield (displaying the Luder's plateau) with strain hardening. The higher strength steels usually have lower strain hardening.
- A flow curve that has continuous yielding behaviour.

It is possible that if the yield strength and tensile strength and elongation is available, a generic curve fit could be employed to assess the collapse portion of the failure assessment curve (FAC). For this, an estimate of the uniform elongation is required. More complete definitions and description of the failure assessment diagram is provided in later sections of this report and in Appendix A.

The low temperature and higher strain effects increase the yield strength and the flow curve and this could affect the failure assessment point (FAP) by reducing the load ratio (L_r) due to the yield strength value that is in the denominator for the expression of L_r . This could make the FAP more fracture sensitive. Here an assumption is that the strain rate does not significantly affect the applied stress.

3.1.5 Future Development

It is expected that in software developed specifically for ship structure fracture assessment, much of the required material property or performance information would be stored in a database. The description of the vessel particulars would be defined using a Graphical User Interface (GUI). The contents of the database would be made available to the user through a GUI allowing selections to be made from lists or pull-down menus.

While some material property data to support the analyses of interest are available, it is suggested that a concerted effort to collect a marine structural material property database to support fracture assessment or damage tolerance analysis would be in order. The collection effort or testing program should consider both strain rate effect and temperature on fracture properties.

3.2 Structural Section and Component Definition

The objective of this step in the assessment process is to subdivide the ship structure into a more manageable number of representative sections and components. The subdivision process is essential for the analytic approach but may not be required for the numerical analysis approach depending on the size of the global finite element model and the level of sophistication of the applied load analysis.

Vessel subdivision is accomplished by first dividing the structure into N longitudinal segments as shown in Figure 3.8. The division of the ship into segments should be performed such that the segments are small enough to be considered to have uniform applied loads and be subjected to common environmental effects (i.e., temperature). Ship segment ends should ideally start and stop at the forward and aft ends of compartments and or convenient mid-frame locations.

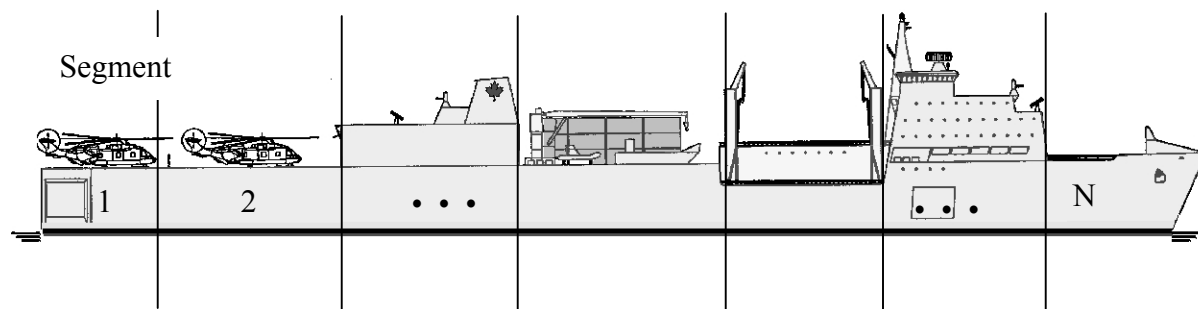


Figure 3.8: Vessel Longitudinal Segment Definition

The second step in the vessel subdivision process for an analytic assessment is to define one or more typical frame structures within each segment. This step would involve the definition of M typical frame sections similar to that shown in Figure 3.9. If the same number of frames is defined in each segment, then $M \times N$ frames have been defined in total. At this time, the number of frames that is characterized by a given frame is also recorded.

The third and final step in the subdivision process involves the identification of typical structural details. By grouping, structural details which:

- are structurally similar,
- are fabricated with the same materials,
- are subjected to similar loads, and
- operate under the same environmental conditions.

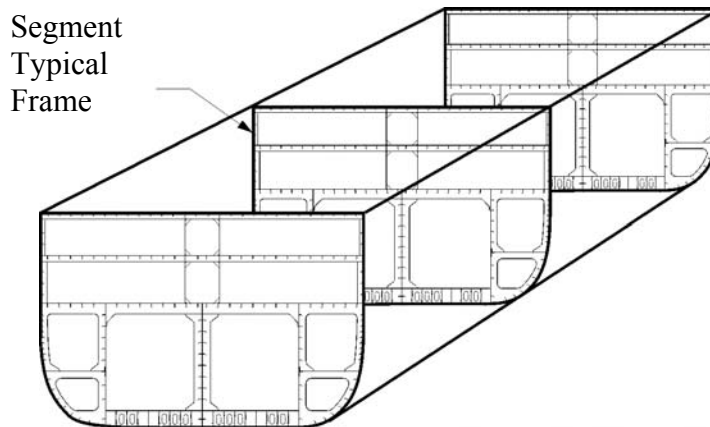


Figure 3.9: Definition of Typical Frames for a Given Ship Segment

This final subdivision step for an analytic formulation of the problem is accomplished as shown in Figure 3.10, in which the main deck longitudinal/frame intersections are grouped. In this structural detail grouping process J typical structural detail types are defined. The number of repetitions of each structural detail in each group needs to be reported.

Based on this definition scheme, any structural detail characteristic could be related to its segment, frame and component based on a three dimensional subscript system (e.g., $Area_{m,n,j}$). In addition, the level of discretization detail would be determined by the user, and thus would be appropriate to their needs.

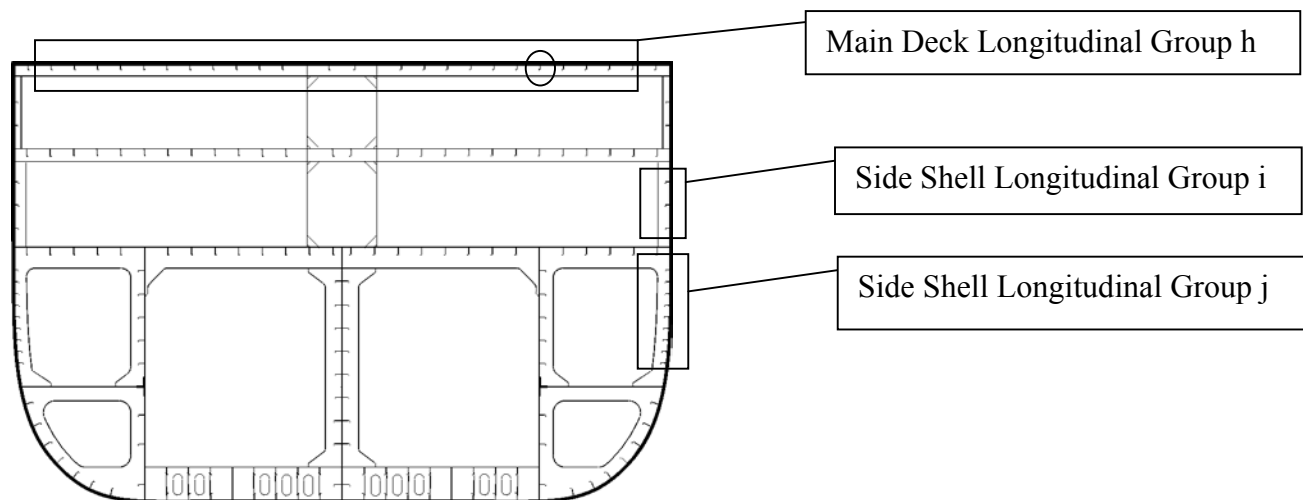


Figure 3.10: Definition of Typical Structural Details

3.2.1 Future Development

This structural segment, frame and component definition could be completed in a database environment in which a pictorial representation of the longitudinal structure is presented. The user could specify the number of frames in the hull, the frame spacing, location of the segment boundaries and typical frames. The number of typical frame groups and proportion of the segment's frames represented by each typical frame could be defined. Finally, the user could group and define typical structural details for each frame by picking from a pictorial listing of structural details.

Based on the approach outlined for structural discretization, it is possible to include any appropriate level of detail. For instance every frame and structural component may be described or a more approximate approach which takes advantage of the ability to group like components and frames, assuming that their performance will be similar, can be applied.

3.3 Load Estimation

The objective of this step in the assessment process is to define the loads applied to the vessel. This is accomplished through a statistical analysis of the loads generated based on a defined operational profile to estimate extreme load distributions for the failure (fracture) assessment calculations. These wave-induced loads are added to the still water load distribution in the fracture assessment.

The still water load distribution may be estimated based on the hull geometry and weight distribution data. While the analysis completed in this project did not consider the uncertainty in still water bending moment, this source of uncertainty for a given vessel longitudinal position may be considered by characterizing the still water moment with a normal distribution. It has been suggested [Ayyub & Assakkaf 2000] that the ratio of the mean to nominal still water moments are 0.4 to 0.6 for commercial vessels and 0.7 for warships. The variability in terms of the coefficient of variation was estimated as 0.3 to 0.9 for commercial vessels and 0.15 for warships.

An operational profile may be defined simply by stating a general area of operation (e.g., North Atlantic) and an endurance or service speed. At the other extreme, a full operational profile for a specific loading condition or a mission may state how much time the vessel will spend in various areas of the world, and at what times in the year, as well as the distribution of its speed and headings. This data can be then combined with a statistical representation of the wave climate in the areas of operation to provide a complete picture of the vessel's "sea operational profile". The net result is a matrix expressing the probability of occurrence of a given wave height, period and ship speed condition. This wave encounter data statistical analysis computation may be completed using software such as LOS³A, for example.

The next step in the load analysis process is to evaluate vessel response to wave encounters (load cycle amplitude) and thus develop a load level exceedence probability for the operational profile. The net result of this portion of the analysis process is to develop a load spectrum specific to the vessel operational profile. If more than one operational profile is defined for a vessel, the procedure is repeated and an *overall* load spectrum is obtained as a weighted sum of the individual operational profiles based on the proportions of time spent in each operational profile.

In the sample applications, two sets of applied load spectra will be developed. The first characterization of the load will consider only the vessel vertical bending moment statistical distribution along the length of the vessel, whereas, the second load characterization will consider the interaction of vertical and horizontal bending along the length of the vessel.

It is noted that the load analysis in the sample applications and theory described in the sections that follow consider only the vessel's linear response to wave induced bending. Practical design or analysis of ship structures for fracture resistance may require the consideration of effects not described in this report such as slamming, shock or impact, thermal effects, non-linear extreme sea response, hydro-elasticity and/or ice interaction loads.

3.3.1 Load Analysis Data Requirements

Two “sets” of data are required for long-term load calculations including the vessel operational profile and reference loads for all operational conditions. The operational profile information required includes:

- The projected route of the vessel described in terms of areas of operation and the percent time spent in these areas;
- Vessel loading conditions or mission and relative time spent in each mode; (loading conditions are appropriate for commercial vessels, while the mission may be more appropriate for military or patrol vessels);
- Vessel average speed ranges and relative amount of time spent at each speed in a particular sea state or wave height. In statistical terms this refers to joint probability distribution (or conditional probability distribution) of speed and sea state (wave height);
- Joint probability distribution (or conditional probability) of relative heading and sea state (wave height); and
- Statistical representation of the wave climate for each area of operation.

The ship loads information includes load Response Amplitude Operators (RAO's) and corresponding load zero crossing periods in irregular seaways for all relevant combinations of ship speed, relative heading and sea state. Load RAO values refer to a particular (predetermined) load location (e.g., midships) and for a specific loading mode (e.g., vertical bending moment).

In order to make the calculations feasible, each of the parameters in the operational profile is discretized in some manner. For example, the route can be divided into Marsden Zones (or zones of latitude and longitude transited by the vessel) and the time spent in these zones. Loading can be treated in terms of standard conditions. Relative heading can be simplified into head, bow beam, quartering and following seas; and speed can be treated as sets of speed ranges.

When a new design will follow the same operational profile as an existing ship, the existing ship's operation may be studied and characterised from operational logs. For new designs, operational profiles can be generated from the operator's plans. The level of discretization of operational profile and/or environmental data should correspond to the certainty in the operational profile information.

The process of developing a detailed operational profile requires the development of input joint probability or conditional probability diagrams, including ship speed versus sea state (or wave height), and relative heading versus sea state (or wave height). These are obtained either from historical data or perhaps from operating directions for the vessel.

Vessel response RAO values are usually obtained utilising state of the art load calculating software. Two types of sea load calculating programs have been successfully used in this project. One is the linear strip theory program ShipmoPC, Version 3.0, and the other is PRECAL, a frequency domain panel code for load calculations, however, many seakeeping codes could be used.

3.3.2 Load Analysis Process

Exceedence probabilities for load cycle may be calculated using the procedure given in [FTL 1998]. The sea loads applied on vessels can be predicted numerically for each combination of ship speed (V), heading (β), significant wave height (H), and peak wave period (T). For vessels operating on random seaways, the sea load probability computations depend on the joint probabilities of operational profiles, $p(V, \beta, H, T)$.

On the other hand, the assumptions of linearity and narrow bandedness permit load amplitude in a random seaway to be modeled using a Rayleigh distribution as follows:

$$f_{X_{cycle}}(X_{cycle}) = \frac{X_{cycle}}{\sigma^2} e^{-\frac{X_{cycle}^2}{2\sigma^2}} \quad (3.4)$$

The probability for load amplitude $X > X_{cycle}$ will be

$$q(X > X_{cycle}) = e^{-\frac{X_{cycle}^2}{2\sigma^2}} \quad (3.5)$$

Therefore, the exceedence probability for load cycle amplitude X_{cycle} in a random seaway can be expressed as:

$$\begin{aligned} Q_{X_{cycle}}(X_{cycle}) &= \iiint\limits_{V \beta H T} p(V, \beta, H, T) \frac{f_Z}{\bar{f}_Z} e^{-\frac{X_{cycle}^2}{2\sigma^2}} dV d\beta dH dT \\ &\cong \sum_{i=1}^{N_V} \sum_{j=1}^{N_\beta} \sum_{k=1}^{N_H} \sum_{l=1}^{N_T} p(V_i, \beta_j, H_k, T_l) \frac{f_{Zijkl}}{\bar{f}_Z} \exp\left(-\frac{1}{2} \cdot \left(\frac{X_{cycle}(V_i, \beta_j, H_k, T_l)}{\sigma(V_i, \beta_j, H_k, T_l)}\right)^2\right) \end{aligned} \quad (3.6)$$

where, X_{cycle} is the load amplitude; σ is the RMS load in a seaway; f_Z is the zero crossing frequency in a seaway; \bar{f}_Z is the average zero-crossing loading frequency for all the operational conditions given by

$$\bar{f}_Z = \sum_{i=1}^{N_V} \sum_{j=1}^{N_\beta} \sum_{k=1}^{N_H} \sum_{l=1}^{N_T} p(V_i, \beta_j, H_k, T_l) f_{Zijkl} \quad (3.7)$$

Equation (3.6) is used to determine extreme load amplitude level under given design load probability. In addition, a table of load amplitude and the associated exceedence probability, as well as the number of cycles a vessel may experience during a specific duration, can be compiled based on equation (3.6), which can be utilized for fatigue analysis.

It should be noted that equation (3.6), the probability of load amplitude exceedence, may be applied for each individual load mode, such as vertical bending moment, horizontal bending moment, torsion, vertical shear force and/or horizontal shear force, because the load amplitude for each load mode follows Rayleigh distribution based on the assumption of linearity and narrow bandedness.

Thus, a target load amplitude, either V_{BM}^* for vertical bending moment or H_{BM}^* for horizontal bending moment can be determined by equation (3.6) at given design probability levels on a route.

The three major assumptions inherent in this approach include:

- stationarity of wave conditions, i.e., wave parameters given by significant wave height and zero crossing period are assumed fixed for a certain period of time (usually two to three hours),
- wave loading process is narrow banded. This permits load amplitude in a random seaway to be modelled using a Rayleigh distribution,
- when an operational profile is developed in the absence of historical data, speed, sea state (wave height) and relative heading are assumed to be independent quantities. This may not always be the case, as in severe sea states, the practice is to reduce speed and to orient the ship in preferred directions. From the fatigue point of view, the bulk of damage arises from the exposure to moderate conditions. Because the amount of time spent in these severe sea states is not as significant as that spent in more moderate conditions, the assumption of independence is reasonable.

The cumulative probability distribution of lifetime loading is calculated from the knowledge of number of cycles in the ship life N_{cycle} as:

$$F_{X_{life}}(X_{life}) = [F_{X_{cycle}}(X_{cycle})]^{N_{cycles}} \quad (3.8)$$

The calculated lifetime load spectrum can be presented in either tabular or graphical form. Also, as previously mentioned, calculations can be done for individual load amplitudes or for load amplitude ranges. For example, Figure 3.11 shows in graphical form load exceedence probabilities based on individual load cycle amplitudes.

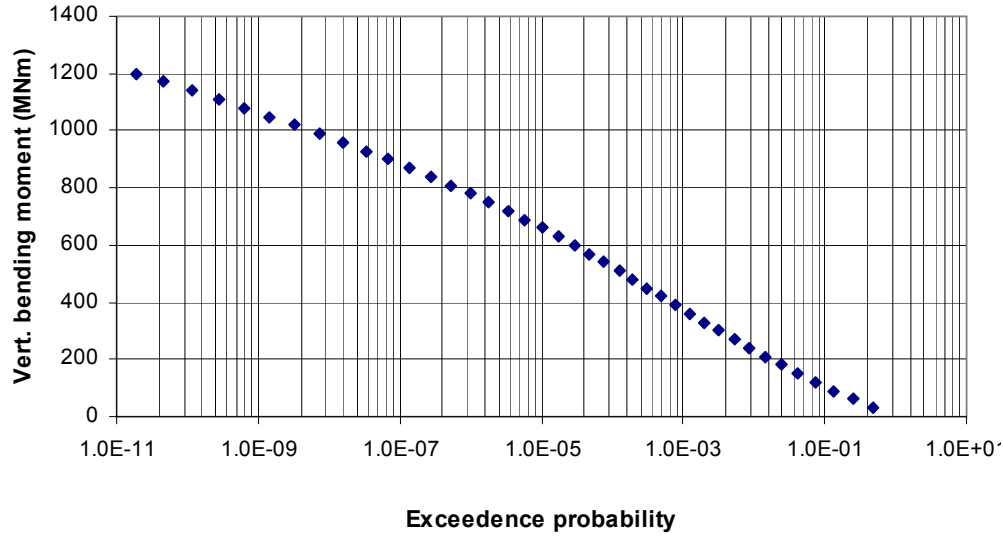


Figure 3.11: Example Load Spectrum

This type of data presentation is well suited if short-term analysis is sought, i.e., finding an individual load cycle corresponding to a certain probability of exceedence in the ship lifetime.

3.3.3 Vertical and Horizontal Moment Interaction

In practice, some or all the loading components are applied to vessels at the same time for a given seaway/operational condition. For example, both vertical and horizontal bending moments are exerted on a vessel in quartering seas. A load envelope for combined vertical and horizontal bending moments can then be defined as follows.

Let the $(H_{BM}^*, 0)$ and $(0, V_{BM}^*)$ be the two intercept points on the load envelope curve.

Additional points on the load envelope curve may be located by finding a set of magnitudes of horizontal bending moments satisfying the design probability, under specified load magnitudes of vertical bending moments that are between 0 and V_{BM}^* . Alternatively, points on the curve can also be located by finding a set of magnitudes of vertical bending moments satisfying the design probability, under specified load magnitudes of horizontal bending moments that are between 0 and H_{BM}^* . Nevertheless, the two approaches should yield the same load envelope curve.

In the development of the load envelope curve, we denote V_{BM} and H_{BM} to be the vertical bending amplitude and horizontal bending amplitude, respectively. Similar to above procedure, we have the exceedence probability of horizontal bending amplitude under the condition of vertical bending amplitude level exceeding specific level on a route as follows:

$$Q_{H_{BM}}(H_{BM} | V_{BM} \geq \alpha V_{BM}^*) = \int \int \int \int [p(V, \beta, H, T) p(V_{BM} \geq \alpha V_{BM}^*)] \frac{f_Z}{f_Z} e^{-\frac{H_{BM}^2}{2\sigma_h^2}} dV d\beta dH dT \quad (3.9a)$$

$$0 \leq \alpha \leq 1$$

Similarly,

$$Q_{V_{BM}}(V_{BM} | H_{BM} \geq \alpha H_{BM}^*) = \int \int \int \int [p(V, \beta, H, T) p(H_{BM} \geq \alpha H_{BM}^*)] \frac{f_Z}{f_Z} e^{-\frac{V_{BM}^2}{2\sigma_V^2}} dV d\beta dH dT \quad (3.9b)$$

$$0 \leq \alpha \leq 1$$

Equations (3.6) and (3.9) are employed to determine wave-induced load amplitude level at the desired design probability level. Figure 3.12 shows an example of load amplitude envelope at the midship section of a warship on a winter North Atlantic transit route. The load interaction curve should be expected to be symmetric about the vertical axis and thus only half of the plot is given. This interaction curve, Figure 3.12, is developed for the extreme load anticipated in a vessel transit and thus has a probability of exceedence of $1/N_{\text{transit}}$, where N_{transit} is the expected number of wave encounters for the transit.

This approach to the development of a load envelope includes several assumptions including:

Load event probabilities may be expressed in terms of event frequencies (probabilities) without a time base since they were developed from a frequency domain. A time base for probabilities can be fitted by considering the average wave period or design life of the vessel.

The approach conservatively assumes that the peaks of the two load components being considered occur at the same time. This is generally not true and could be modified by considering the phase angles of each of the load components.

The RAO data used to estimate the load magnitudes are appropriate for ultimate strength analysis. This assumption will need to be addressed in the future through the application of a non-linear hydrodynamics code in the future.

3.3.4 Future Development

The definition of operational profiles and, in general, the load calculations may be completed using the LOS³A software in which a map based system is used to define the operational profile. RAO's can be generated using Shipmo⁷ for the vessel sections and operating conditions of interest.

By assembling the software in a modular fashion, any RAO generating software may be used with the LOS³A software to estimate the applied load spectrum.

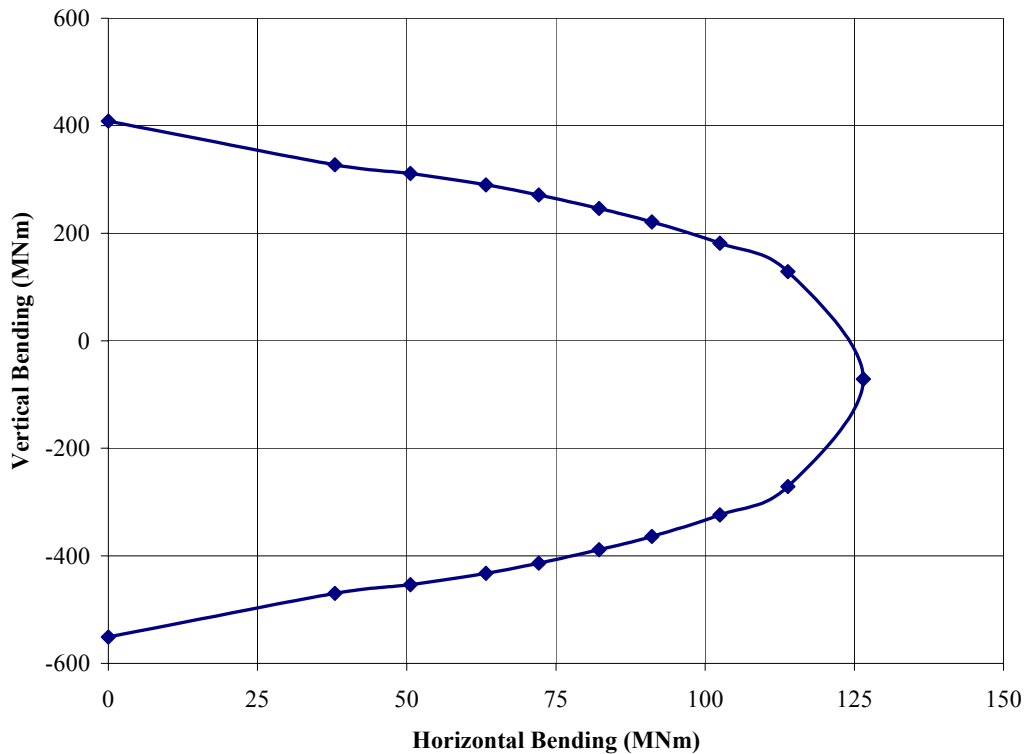


Figure 3.12: Typical Vessel Load Interaction Plot

3.4 Definition of Local Detail Characteristics

In this stage of the problem solution process, the characteristics of the previously defined structural details (see Section 3.2) are assigned. The characteristics of interest to this investigation include:

- nominal stress transfer functions,
- detail scantling or geometry,
- stress concentration effects,
- stress intensity factor solutions for cracked structural components, and
- residual stress levels.

In general, the bulk of the information defined at this stage of the solution process is related to the analytic or hybrid analysis approach. The numerical (FE) approach will explicitly identify, stress concentrations, stress intensity factors for given flaw sizes and all of the required stress transfer functions. In the case of the numerical modeling approach, the global and detail finite element model would be assembled in this step.

3.4.1 Nominal Stress Transfer Function

The nominal stress transfer coefficient is used to identify the local nominal stress applied to each component. In the approach which will be implemented, the nominal stress transfer coefficient is the vertical distance of component m,n,j from the vessel keel ($Y_{m,n,j}$). This information will be used to estimate the location of the section neutral axis ($Y_{cg_{m,n}}$) and the moment of inertia ($I_{m,n}$). The difference between the neutral axis height from the keel and the component distance from the keel will be used to estimate the component nominal stress ($\sigma_{m,n,j}$) considering the section moment $M_{m,n}$ as follows:

$$\sigma_{m,n} = M_{m,n} \frac{(Y_{cg_{m,n}} - Y_{m,n,j})}{I_{m,n}}$$

The section moment of inertia and neutral axis location need to be calculated for each axis of bending (horizontal and vertical moment).

3.4.2 Component Cross-Section Geometry

Section properties ($Y_{cg_{m,n}}$ and $I_{m,n}$) will be estimated based on the geometry of the structural components. Local component geometries will be defined in terms of the as-built area of plating and stiffeners as shown below.

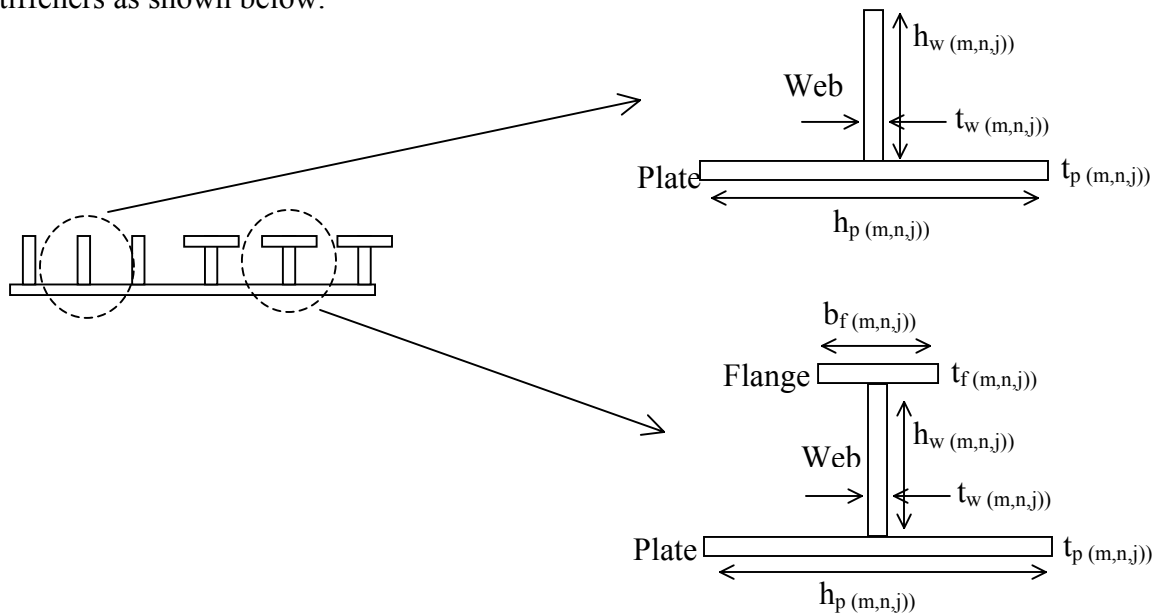


Figure 3.13: Component Geometric Definition

Depending on the location of cracks (e.g., plating vs. stiffening element) of interest, the basic structural component geometry is defined in terms of the component stiffener and plate thickness and lengths as defined above. In assigning these section properties, effective thicknesses will have to be assigned for stiffeners with flanges to ensure that the stiffener area is preserved. In calculating section moments of inertia, the contribution of the component moment of inertia about its own axis will be neglected. The centroid of the component area will be defined by the keel offset ($Y_{m,n,j}$) defined previously for nominal stress calculation.

3.4.3 Stress Concentration Effects

Local (peak) stresses considering the geometry of the connection detail may be estimated based on parametric approximations of stress concentration factors for ship details, when these are available. Stress concentration factors (SCF) for a range typical of ship structure details are given by [Stambaugh et al (1994), ABS (1992), Cramer et al (1995), and Yoneya et al (1992)] for example. Stress concentration factors for typical ship structural details (K_g) and for misalignment effects (K_{te} , $K_{t\alpha}$) are presented in Appendix B of the Fatigue Design Guide [Glen 1999].

The analyst must exercise extreme care when applying stress concentration factors from different sources to ensure that the correct nominal stress definition is used. For example, in some cases the nominal stress is defined at the intersection point of a connection, in other cases the global nominal stress may be defined at the weld toe or some distance from the weld toe.

Furthermore, the analyst should be aware that sometimes the published stress concentration factor solutions are designed to calculate the "hot spot" stress or the "notch" stress as opposed to the local nominal stress. The analyst should make certain which form of peak stress will result from the application of the SCF.

Local stress concentration effects will be considered using handbook definitions of local stress concentration effects for ship structural details. Figure 3.14 is a sample of the analytic ship structure detail stress concentration factors (SCF) that could be used in a non-numeric analysis. More of these local and global SCF formulations are listed in the SSC Fatigue Design Guide Appendix C. Stress concentration effects are considered explicitly when a numerical (FEA) approach to the problem is considered.

3.4.4 Stress Intensity Factor Solution

A key requirement of local damage tolerance assessment for fatigue and fracture is the ability to evaluate stress intensity factors (SIF) for ship structural details containing cracks. The rigorous derivation of the SIF can be found in most advanced texts on fracture mechanics and so only a brief overview will be presented here. A crack represents a very sharp notch (i.e., notch radius $\rightarrow 0$) and in an ideal elastic body the stresses approach infinity at the crack tip. By studying the conditions near the tip of a crack in an elastic body, it can be shown that the stress and displacement fields can be expressed in terms of three elastic SIF's corresponding to the three modes of fracture (Figure 3.15, [Almer-Naess 1985]): K_I for Mode I (Opening Mode), K_{II} for Mode II (Sliding Mode), and K_{III} for Mode III (Tearing Mode). Any crack problem can be considered to be a combination of these three basic modes of fracture.

However, since there is always a tendency for a brittle fracture to propagate in the direction that minimizes the shear loading (i.e., perpendicular to the maximum principal stress), the first mode is generally regarded as the most important and in this application only the mode I fracture is considered.

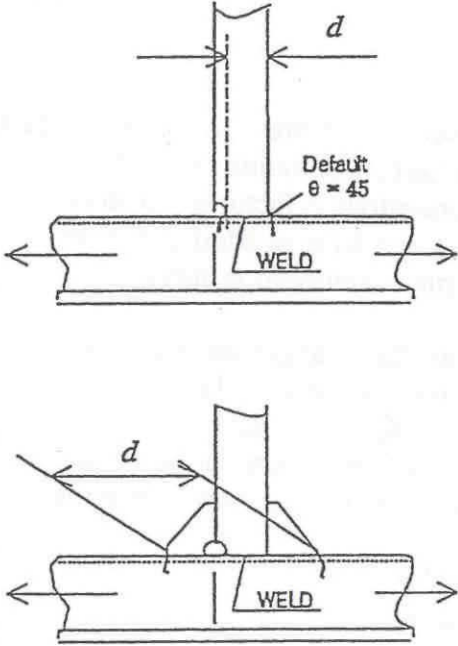
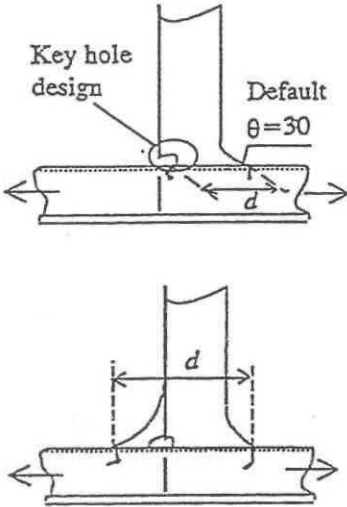
Geometry	K-factor								
<p>B.2.a</p> 	<p>For supporting members welded to stiffener flange:</p> <table border="0"> <tr> <td>$K_g \cdot K_w = 1.8$</td> <td>$d \leq 50$</td> </tr> <tr> <td>$K_g \cdot K_w = 1.9$</td> <td>$50 < d \leq 100$</td> </tr> <tr> <td>$K_g \cdot K_w = 2.0$</td> <td>$100 < d \leq 150$</td> </tr> <tr> <td>$K_g \cdot K_w = 2.2$</td> <td>$d > 150$</td> </tr> </table> <p>For supporting members welded to stiffener web by overlap with weld throat thickness as given in $\beta.5a$ (Table $\beta.5$), the above factors are to be multiplied by a factor 1.15</p> <p>Note: The weld connection area between supporting members and stiffener flange must fulfil the requirements in Rules.</p>	$K_g \cdot K_w = 1.8$	$d \leq 50$	$K_g \cdot K_w = 1.9$	$50 < d \leq 100$	$K_g \cdot K_w = 2.0$	$100 < d \leq 150$	$K_g \cdot K_w = 2.2$	$d > 150$
$K_g \cdot K_w = 1.8$	$d \leq 50$								
$K_g \cdot K_w = 1.9$	$50 < d \leq 100$								
$K_g \cdot K_w = 2.0$	$100 < d \leq 150$								
$K_g \cdot K_w = 2.2$	$d > 150$								
<p>B.2.b</p> 	<table border="0"> <tr> <td>$K_g \cdot K_w = 1.6$</td> <td>$d \leq 50$</td> </tr> <tr> <td>$K_g \cdot K_w = 1.7$</td> <td>$50 < d \leq 100$</td> </tr> <tr> <td>$K_g \cdot K_w = 1.8$</td> <td>$100 < d \leq 150$</td> </tr> <tr> <td>$K_g \cdot K_w = 2.0$</td> <td>$d > 150$</td> </tr> </table> <p>For supporting member welded to stiffener, flange only. It is assumed that the weld is kept clear of flange edge.</p> <p>Note: The weld connection area between supporting members and stiffener flange must fulfil the requirements in Rules.</p>	$K_g \cdot K_w = 1.6$	$d \leq 50$	$K_g \cdot K_w = 1.7$	$50 < d \leq 100$	$K_g \cdot K_w = 1.8$	$100 < d \leq 150$	$K_g \cdot K_w = 2.0$	$d > 150$
$K_g \cdot K_w = 1.6$	$d \leq 50$								
$K_g \cdot K_w = 1.7$	$50 < d \leq 100$								
$K_g \cdot K_w = 1.8$	$100 < d \leq 150$								
$K_g \cdot K_w = 2.0$	$d > 150$								

Figure 3.14: Sample Ship Structure SCF Formulations

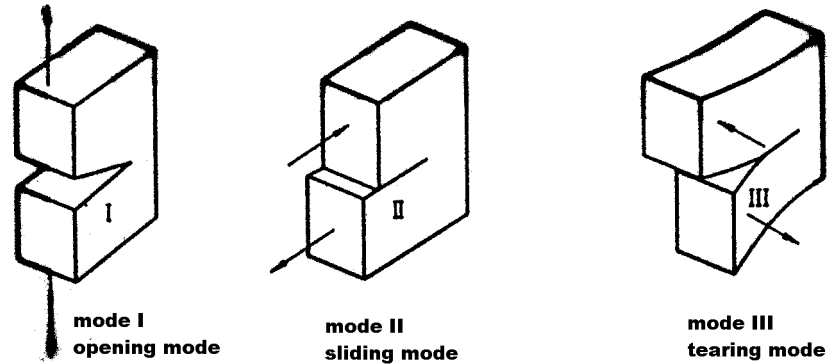


Figure 3.15: Three Modes of Cracking

Various techniques are available to calculate stress intensity factors. When time and resources do not permit the direct (FE based) calculation of K_I , estimates can be obtained using handbook solutions for simplified geometries and loadings that most closely resemble the actual conditions at the crack location. Stress intensity factor solutions are commonly presented in the following form:

$$K_I = \sigma \cdot Y \cdot \sqrt{(\pi a)} \quad (3.10)$$

where:

- σ = a reference local nominal or "field" stress at the crack location
- Y = stress intensity factor correction
- a = crack size parameter

The stress intensity magnification factor, Y , is a function of crack geometry, structural geometry and mode of loading. The reference nominal stress at the crack location is determined from a local stress analysis of the uncracked body. For residual strength assessments, the reference nominal stress corresponds to the stresses under the extreme load condition (including residual stresses).

The membrane and bending components of stress usually require separate correction functions and thus the stress intensity factor solution is somewhat more complex than that outlined above.

3.4.5 Residual Stress

Residual stresses caused by welding and fabrication are self-equilibrating stresses necessary to satisfy compatibility in the structure. These stresses in themselves do not contribute to plastic collapse since they arise from strain/displacement limited phenomena, and therefore do not influence the abscissa in the Failure Assessment Diagram (FAD) (S_r or L_r) (see Section 3.5). However, residual stresses do add to the crack driving force and therefore have to be included in the calculation of K_{app} for residual strength assessments.

Ideally, one would establish the residual stress magnitude based on actual measurements and resolve them into their membrane and bending components (i.e., σ_{rm} and σ_{rb}). However that is impractical and, therefore, conservative estimates of residual stresses based on findings in the technical literature and on the location of the flaw (weld zone or base metal) and orientation with respect to the weld, are incorporated in the analysis.

The following guidelines can be used to estimate the magnitude of residual stresses to be incorporated into the residual strength assessment. As before, the approach depends on the level of detail of the fracture assessment being performed. For the assessment being performed:

- If the actual distribution of residual stresses is known, then these can be incorporated by linearizing the distribution such that the assumed residual stresses are greater than the actual (measured) stresses over the flaw depth. The linearized residual stress distribution can then be separated into its membrane and bending components.
- A reasonable estimate of residual stresses can be based on some typical residual stress distributions given in (BS7910) for butt, fillet and pipe welds (see Figure 3.16). Parametric equations have been developed corresponding to these distributions and their use can reduce the conservatism in the assumption of "yield strength residual stresses in as-welded joints". Still, the use of these parametric equations pre-supposes some knowledge of the weld joint restraint during fabrication.
- The most conservative approach remains the assumption of uniform, yield strength level, residual stresses.

If the reference (net section) stress is deemed high enough to cause plasticity at the crack tips, a certain amount of residual stress relief occurs and the residual stress can be appropriately reduced to the minimum of:

- a) σ_y
- b) σ_r based on approximate distributions
- c) $(1.4 - \sigma_n / \sigma_f) \sigma_y$ for Level 2 FAD with S_r abscissa
- d) $(1.4 - \sigma_n / 1.2\sigma_y) \sigma_y$ for Level 2 FAD's with L_r abscissa

The evaluation of reference stress, σ_n , the stress in the presence of the flaw, is presented in Section 3.5. Clearly, the reference stress must be of the order of 50% of the yield strength in order to get any residual stress relief due to plasticity.

When the flaw tips are in the base metal and away from the weld (2 to 3 plate thicknesses), then the weld residual stresses are negligible. However, there are some longer range assembly and construction stresses that still may be present. These may be relieved to some extent with service (shake down effect) or as the crack grows. However, this effect is difficult to predict and therefore, as a conservative measure, longer range residual stresses equal to 20% of the yield strength are recommended to be included in a fracture analysis.

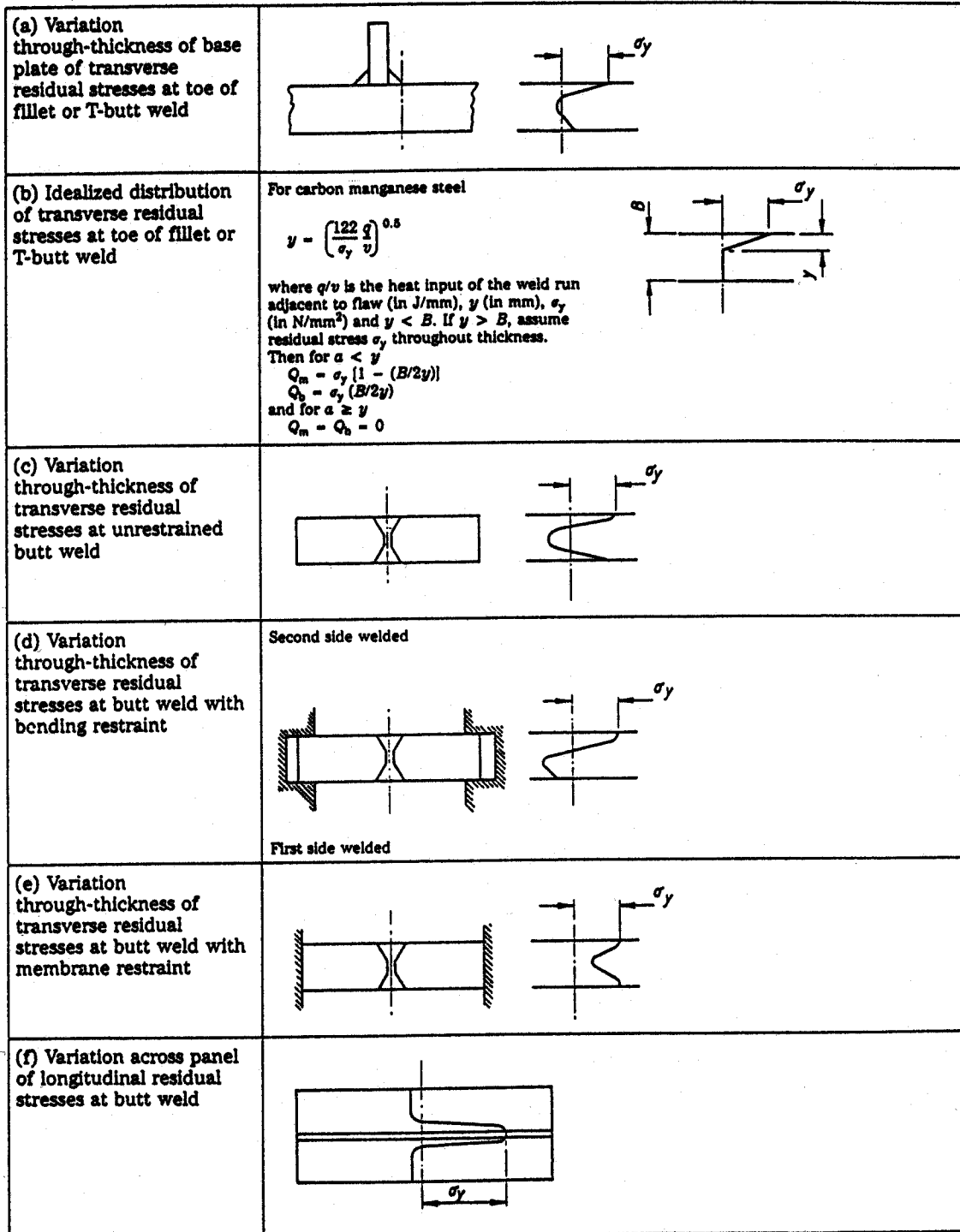


Figure 3.16: Typical Distributions of Residual Stresses at Welds

3.4.6 Finite Element Modeling

In the design of critical structural elements, or when the global structure is too complicated for simple parametric formulae, finite element analysis (FEA) may be used to obtain a reliable description of the overall stiffness and global stress distribution in the hull.

3.4.6.1 Global FEA

The global FEA is generally carried out with a relatively coarse mesh, the main objective being to obtain a good representation of the overall membrane panel stiffness in the longitudinal and transverse directions and for shear, sufficient for determination of nominal stresses. Stiffened panels may be modelled by means of anisotropic elements or, alternatively, using a combination of plate and beam elements.

The extent of the model is dependent on the type of response to be considered and the structural arrangement of the hull. If the FEA based design process involves only several localized details, the required extent of the local model is dependent on the stiffness variation of the hull over a certain length and this has to be captured in the global FEA model. The minimum hull module length required to accurately portray the structural response and provide the additional information not available from the simplified analysis approach typically includes several cargo holds (or watertight compartments of a naval vessel). The exact length requirement depends on the ship's overall geometry and nature and arrangement of the cargo or other loads.

For horizontal and torsional bending response of the hull of an open hatch ship, it is generally required that the extent of the global model cover the complete hull length, depth and breadth (a half breadth model may be used if antisymmetric boundary conditions can be assumed at the centerline). A complete finite element model may also be required for the evaluation of vertical hull girder bending of ships with complex superstructure arrangements (e.g., warships, passenger ships), and for ships of complex cross-section (e.g., catamarans).

Instead of modelling the entire ship hull, a part of the hull (for example, the midship area including three holds) may be modelled. The estimated hull girder loads (e.g., bending moments at the frame of interest) can be applied as concentrated FE model applied loads (e.g., force couples or moments) at each end of the model. This will produce a constant loading away from the model edges at which the loads are applied and thus the stress or strain state of the area of interest may be evaluated. Unit pressure loads will normally be distributed over the appropriate section of the hull. The loads should be balanced in order to give a minimum of reaction forces at the supports (boundary conditions). The loads and boundary conditions in the hull cross section should be evaluated carefully when modelling only a part of the hull to avoid unrealistic stiffness from the forebody/afterbody.

Figure 3.17 shows an example of a global finite element model of a section of a bulk carrier. This model may be used to calculate nominal global stresses and deformations away from areas with stress concentrations. In areas where local stresses in web frames, girders or other areas (for example hatch corners) are to be considered, the global model should have a mesh producing deformations applicable as boundary conditions for local stress analysis. In such cases the global and local models should be compatible. The local model may be directly applied as a substructure or super-element in the global model (if such techniques are available with the FEA software). The substructure technique ensures that forces and deformations in the global and local models are compatible and, if the substructure is detailed enough, local stress results may be obtained directly. The substructure technique is very effective where local structural assemblies (i.e., the substructure) are repeated several times in the overall assembly, but it does present added complexity into the analysis.

More commonly, the global and local analyses are conducted separately. Nodal forces and/or displacements obtained from the global model are applied as boundary conditions for the local model. In general, the stiffness of the local model should be comparable to that of the global model representation so that forces and displacements between the two models are compatible. However, due to the greater level of geometric detail and mesh refinement of the local model, this is rarely achievable. As such it is preferable that nodal forces be transferred from the coarse model to the local model rather than forced displacements. It is important that the extent of the local model is sufficiently large that boundary effects due to prescribed forces or displacements are away from the areas where accurate stresses need to be determined.

The loads to be applied in the global analysis can be produced using any of the methodologies presented in Section 3.3. The global analysis should be conducted for each load case (i.e., vertical bending, horizontal bending, torsional bending, external pressure, internal pressure) individually. Each load case should be analyzed for a unit value of the applied load at the location being considered. In this manner, the stresses derived from subsequent local analysis will correspond to unit loading and therefore be equal to the stress coefficients, A_i , which are required to generate the local stress spectrum from the combined loading spectra.

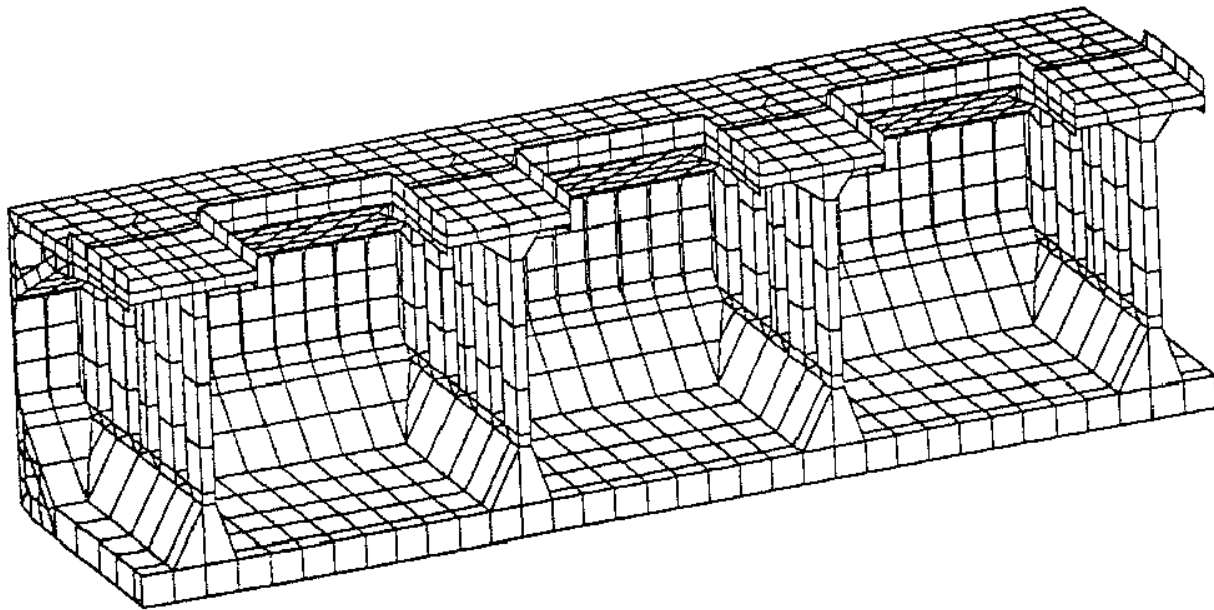


Figure 3.17: Global Finite Element Model of Bulk Carrier (ABS 1994)

3.4.6.2 Local FEA

Local (peak) stresses considering the geometry of the connection detail may be estimated based on analytic formulations, however these approximations are not always available. If appropriate stress concentration factors are not available, the total stress distribution including local peak stresses may be calculated by local FEA. As discussed previously in the section on global FEA, the extent of the local model should be large enough that the calculated results are not significantly affected by assumptions made for boundary conditions and application of loads.

Figure 3.18 [Ma 1994] shows a local finite element model of a ship detail. The local model should have a relatively fine mesh, especially in areas of stress concentration. It is important to have a continuous and not too steep change in the density of the element mesh in the areas where the local stresses are to be analyzed. The geometry of the elements (aspect ratio, corner angles, skewness and warp) at the point of interest should be as near optimal as possible (for example: element length/breadth aspect ratio less than 2, corner angles between 60° and 120° , avoid use of triangular elements with reduced order shape functions).

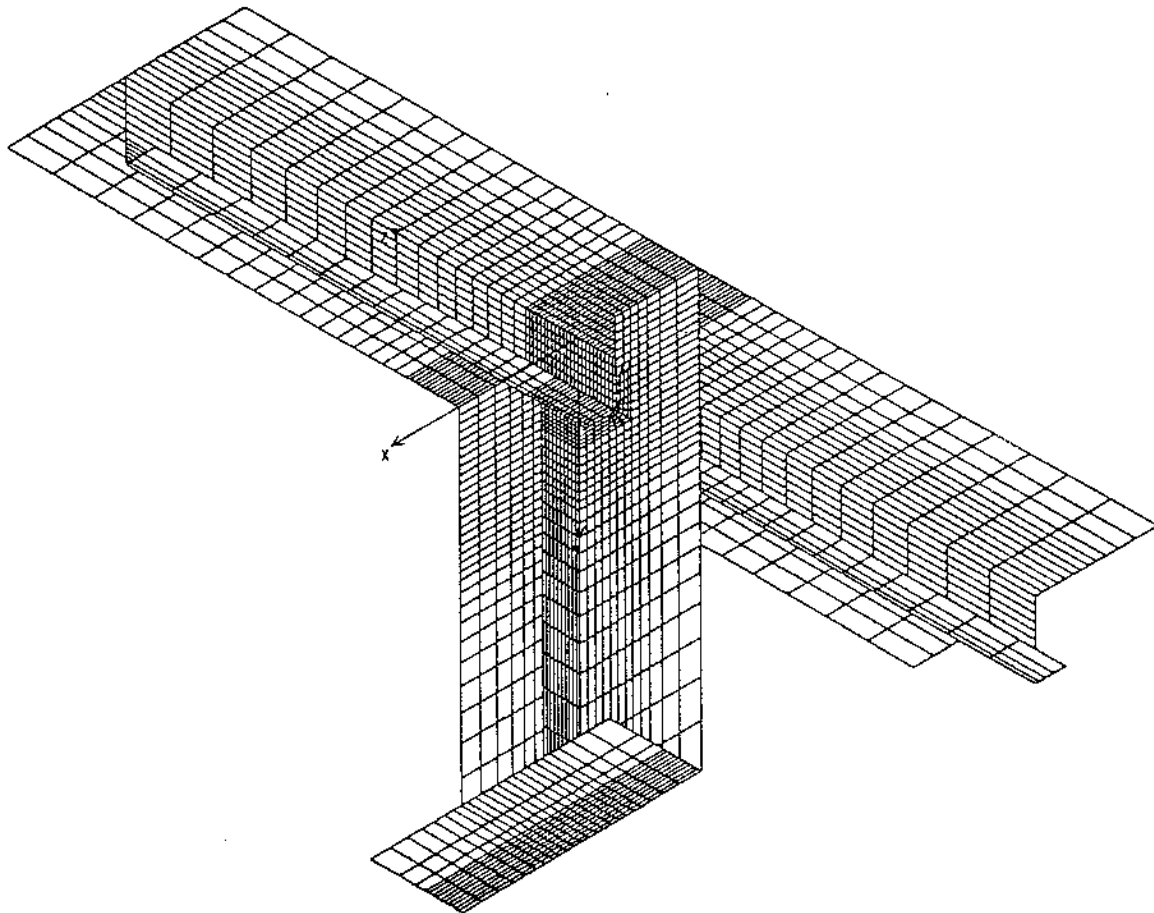


Figure 3.18: Local Finite Element Model of Ship Detail

Finite element size requirements to accurately characterize the local stress distribution for a fracture assessment are dependent on the type of element. The mesh size may be determined based on experience or by benchmark testing a similar mesh for a case where results have been presented in the literature. Figure 3.19 [Cramer et al, 1995] provides some guidance on element sizes for 20-node solid, 8-node shell and 4-node shell element types suitable for determining the hot spot stress.

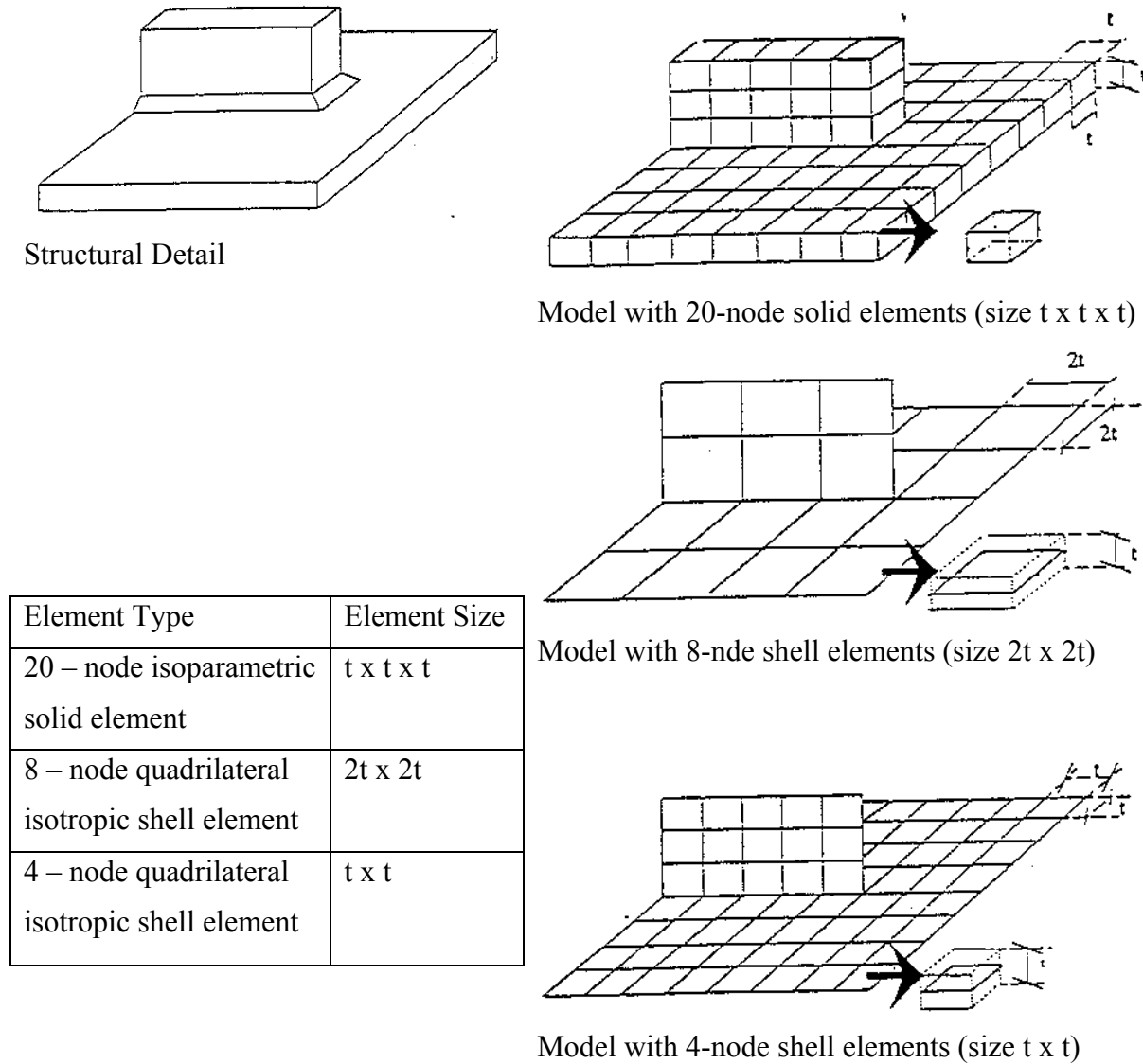


Figure 3.19: Recommended Element Sizes for Local Detail FEA

3.4.6.3 Crack Tip FEA

In cases where published solutions are not readily available for the detail under consideration, finite element methods may be used to calculate SIF solutions. The application of FEM to LEFM requires modelling the stress singularity that occurs at the crack tip. The first attempts to model cracks simply involved the use of very large numbers of conventional finite elements. No attempt was made to take into account the stress singularity in the element formulation. It has been demonstrated that many hundreds of elements are required to achieve perhaps 5% accuracy. As a result, this approach has been abandoned in favour of elements that take explicit account of the crack tip stress singularity. The most important of these formulations include classical solution based singularity elements, polynomial singularity function elements, and modified isoparametric elements.

Isoparametric elements are, perhaps, the most important of these due to their wide availability in commercial FEM programs. Their application to LEFM is based on the ability to represent the $1/\sqrt{r}$ stress singularity by a very simple modification to the standard isoparametric element. By shifting the "mid-side" nodes to the quarter point in a quadratic isoparametric triangular or quadrilateral element, the required singularity results at the nearest node.

Barsoum, in a most important paper, investigated two and three-dimensional quadratic isoparametric elements. He introduced the idea of "collapsing" nodes along one edge of the element, and placing the adjacent nodes at the quarter point (see Figure 3.20).

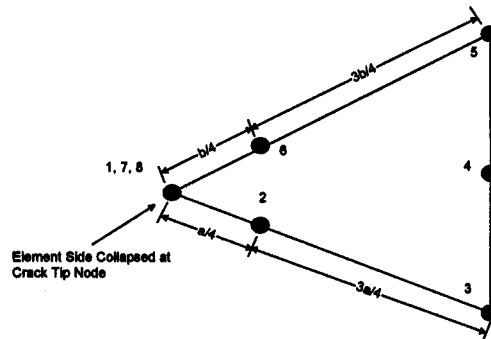


Figure 3.20: Collapsed Node Isoparametric Crack Tip Element

These collapsed or degenerate elements were later shown by the same author to contain the required stress singularity along any ray from the crack tip, whereas the simple modified elements exhibit the singularity only along the boundaries of the element. The demonstrated accuracy of the collapsed form of isoparametric element, together with their wide availability and ease of application, makes them the preferred choice for elastic crack analysis.

The application of FEM for determining SIF is similar to that for local stress analysis. In general, a local model of the detail containing the crack is required with special crack-tip elements applied at the crack tip. Shell element models may be used to derive SIF for through-thickness and 2-D straight-fronted (i.e., $a/2c = 0$) cracks. The analysis of partial thickness elliptical cracks is somewhat more complicated and requires the use of 3-D solid elements. Figures 3.21 and 3.22 show typical FEM meshes for 2-D and 3-D cracks.

The 2-D crack mesh shown in Figure 3.21 was used to model an edge-cracked plate. Four triangular crack tip elements are located at the crack tip in the arrangement shown. The rest of the model uses conventional isoparametric plate or shell elements. In this particular example the crack face lies on a plane of symmetry, therefore only half of the crack is modelled. The nodes between the crack tip and the far edge of the plate are prescribed symmetry displacement conditions, nodes along the crack surface are free to move. Note that the crack tip elements are relatively small (typically about 2% of the crack length) and that elements gradually get larger as the distance from the crack tip increases. This is to ensure that the rapid stress gradient at the crack tip is adequately represented.

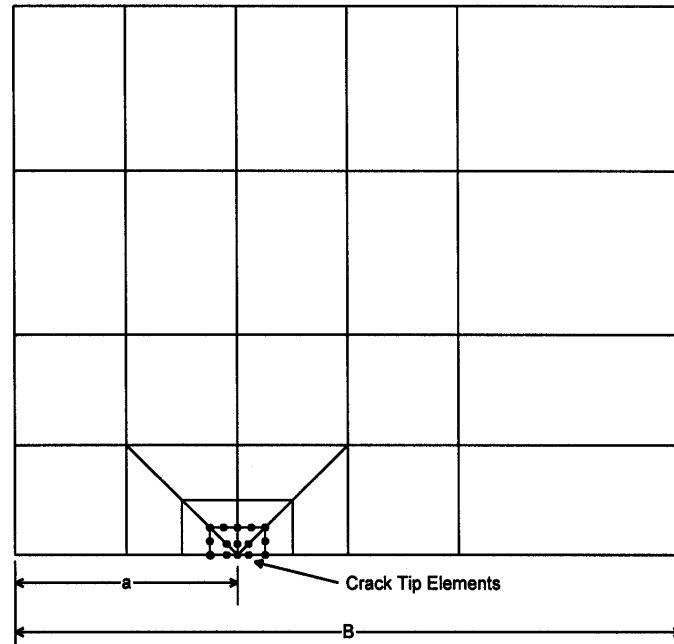


Figure 3.21: Example of 2-D Crack Model of an Edge Cracked Plate

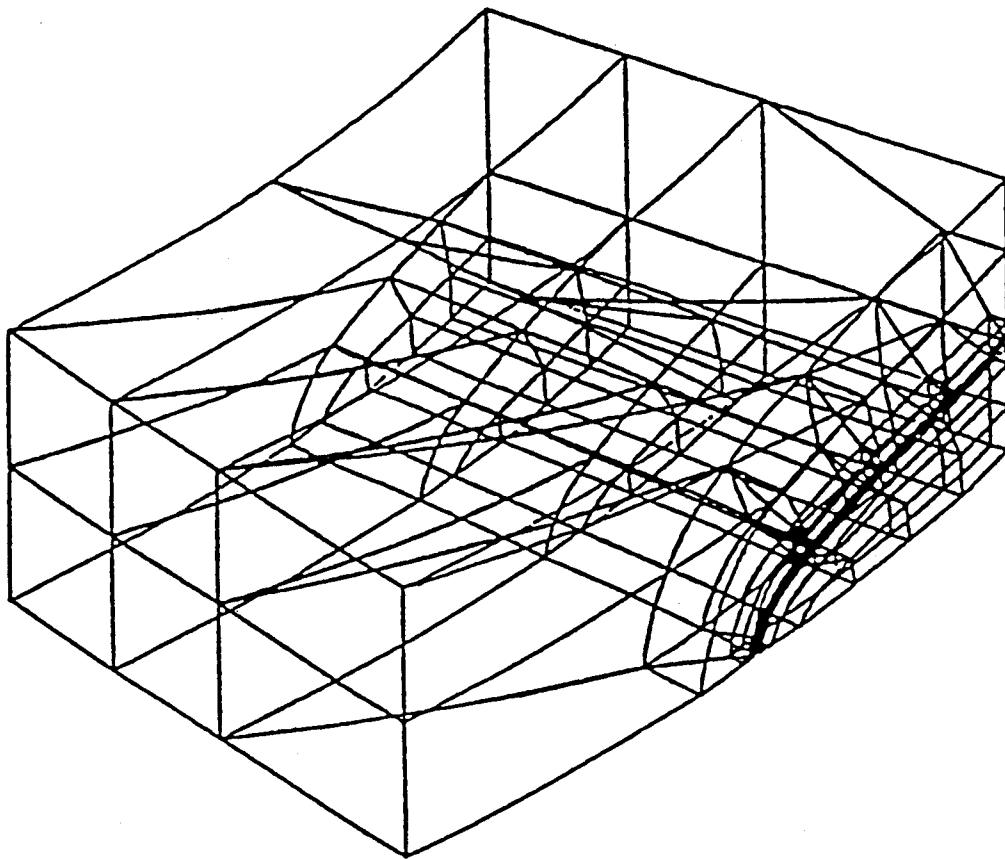


Figure 3.22: Example of 3-D Crack Mesh for Semi-Elliptical Surface Crack

Figure 3.22 shows a 3-D FEM model of a semi-elliptical surface crack in a plate. The design of the 3-D crack mesh requires analogous considerations for element placing and sizing to those discussed for the 2-D crack mesh. As a guide, the size of the crack tip elements normal to the crack front should be less than 5% of the crack length, a , for acceptable accuracy (2-5%). The length to width aspect ratio of solid crack-tip elements should not exceed 4, where the length dimension of the element is measured along the crack front. The 3-D crack model is considerably more complex than the 2-D problem. In general, modelling of 3-D semi-elliptical cracks requires the use of computerized "mesh generation" programs or FEM pre-processors with advanced solids modelling features to facilitate their preparation.

3.4.7 Future Development

The development of a software program to perform the above structural characterization would only be useful if the effort required by the user to enter data is minimized. For this, a Windows based GUI should be developed to simplify the data entry process.

In future, it would likely be beneficial to increase the level of detail of the analytic approach structural component description to explicitly include the stiffener flanges and other bracketing attachments. This improvement in the level of detail will allow more accurate consideration of component failure modes and the consideration of other load effects such as lateral bending, local pressures or torsion.

Ultimately, it would be possible to consider the application of finite element analysis techniques, however, this step requires a significant increase in the data preparation process. To facilitate or automate the FE model generation process, local component finite element models based on the parametric modeling techniques such as those developed by FTL [FTL 1998] could be considered.

It is also suggested that while the current model has been developed based on analytic and user meshed FEA crack tip modeling, these approaches could be improved. Improvements would automate the crack tip meshing and the implementation of weight function solutions to make use of uncracked FE analysis results.

3.5 Failure Assessment

The objective of this step in the solution process is to consider the potential for failure including plastic collapse or fracture failure modes for the ship structure containing cracks. This failure assessment will be completed using a failure assessment diagram approach similar to that outlined in BS 7910. A simplified failure assessment approach that will be used in this analysis was developed based upon a review of available techniques that identified the Level 2 approach in BS 7910:1999 as the most appropriate failure assessment technique. The simplification is made since the stress-strain curve of the material is not likely to be available in most failure assessment cases and the conventional approach is to use the Level 2B FAC. Level 2A Failure Assessment Curve (FAC) for failure assessment following BS 7910:1999 with Amendment 1, was used to develop and test a simplified Level in the case the stress-strain curve is not available.

The method that is used in the failure assessment may be summarised as follows:

- Define the Cracked Detail and Material.
- Estimate the Ultimate State of Cracked Detail (FAC)
- Estimate the Current State of the Cracked Detail (FAP)
- Estimate Fracture Toughness of Material.
- Estimate Load on Cracked Detail.
- Estimate Crack Driving Force in Cracked Detail.
- Estimate Collapse Load of Cracked Detail.
- Determine the Safety Margin of the Cracked Detail

A schematic of this method is presented in Figure 3.23 [Reemsnyder 2002], defining the failure assessment curve (FAC), failure assessment point (FAP), and margin of safety, for scenarios considering no residual stress. The vertical and horizontal axes of the graph in Figure 3.23 represent the fracture and collapse ratios, respectively, indicating the effect of the applied loading towards the onset of fracture or plastic collapse of the flawed structure. As the fracture ratio approaches 1, the flawed structure is said to be at risk of brittle fracture, whereas a structure with a plastic collapse ratio approaching 1 is at risk of a ductile shear or tearing failure.

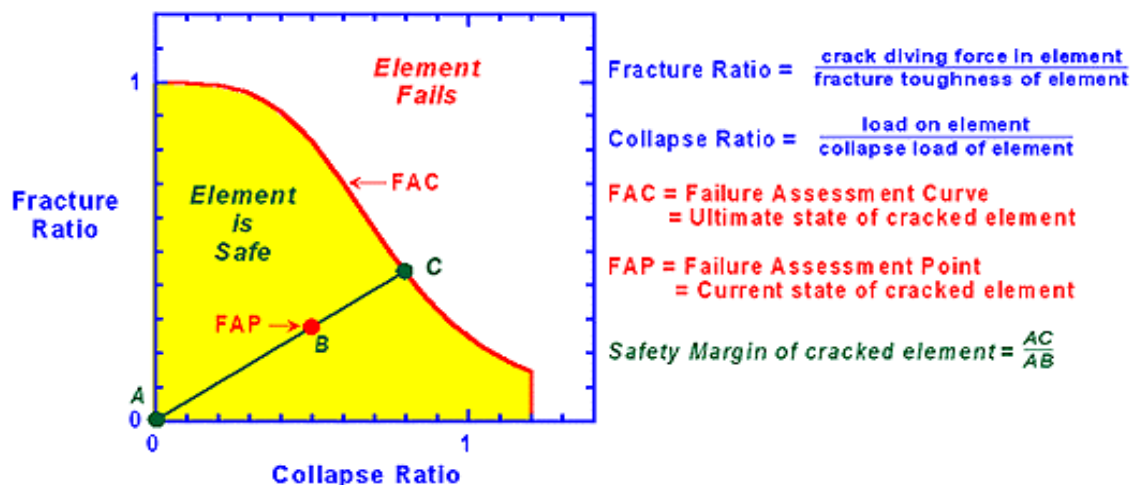


Figure 3.23: A Schematic of the Generic FAC, the FAP and Safety Margin

The cracked detail and material was from a typical ship detail. (These need a single value critical CTOD to determine the fracture component of the ordinate of FAP) The appropriate FAC's are:

- Level 2B (Material Specific).
- Requires stress-strain curve.
- Level 2A (Generalized).
- Material without Lüders strain plateau.
- Material with Lüders strain plateau.

3.5.1 Construction of Failure Assessment Curves

Level 2A FAC is based on the Option 1 FAC of the R6 approach [I. Milne, 1986] that is an empirical fit of Level 2B FAC's for a variety of steels (including an elastic-perfectly plastic material) but biased toward a lower bound. Further elaboration on the FAC and the effect of residual stress are presented in Appendix A1.

The Level 2A FAC of BS 7910:1999 is defined as

$$K_r = (1 - 0.14 \cdot L_r^2) \cdot [0.3 + 0.7 \cdot \exp(-0.65 \cdot L_r^6)] \quad \text{for } L_r \leq L_r^{max} \quad (3.11)$$

or

$$K_r = 0 \quad \text{for} \quad L_r > L_r^{max} \quad (3.12)$$

where L_r is defined as the ratio of the effective net-section stress to the yield stress

$$L_r = \frac{\sigma}{\sigma_y} \quad (3.13)$$

and the cut-off L_r^{max} is defined as

- 1.15 for low alloy steels and welds
- 1.25 for mild steel and austenitic welds
- 1.8 for austenitic steels

For materials showing a yield discontinuity¹, i.e., a Lüders or yield plateau, the Level 2A FAC is cut off at $L_r = 1.0$. If it is impractical to determine a Level 2B FAC, the Level 2A FAC at and beyond $L_r = 1.0$ is determined from the following relations. K_r at $L_r = 1.0$ is determined from

$$K_r = \frac{1}{\sqrt{1 + \frac{E \cdot \epsilon_L}{\sigma_y^u} + \frac{1}{2 \cdot \left(1 + \frac{E \cdot \epsilon_L}{\sigma_y^u}\right)}}} \quad \text{for} \quad L_r = 1.0 \quad (3.14)$$

¹ Amendment 1 to BS 7910:1999 introduces the accommodation of Lüders plateau.

where

$$\varepsilon_L = 0.0375 \cdot \left(1 - \frac{\sigma_y^u}{1000} \right) \quad \text{for} \quad \sigma_y^u < 800 \text{ MPa (116 ksi)} \quad (3.15)$$

ε_L is the Lüders plateau strain and σ_y^u is the upper yield strength. If the upper yield strength is not available, it is conservative to use the 0.2% yield strength. Equation 3.15 is compared to measured values of Lüders plateau in Figure 3.24.

K_r for $L_r > 1.0$ is determined from

$$K_r = K_r|_{L_r=1} \cdot (L_r)^{(n_{lb}-1)/2n_{lb}} \quad \text{for} \quad 1.0 > L_r > L_r^{\max} \quad (3.16)$$

where the lower bound strain hardening exponent n_{lb} is estimated from

$$n_{lb} = 0.3 \cdot \left(1 - \frac{\sigma_y}{\sigma_u} \right) \quad (3.17)$$

with σ_y and σ_u , respectively, the yield and tensile strengths and

$$L_r^{\max} = \frac{\sigma_f}{\sigma_y} \quad (3.18)$$

where σ_f is the mean of σ_y and σ_u .

Equation 3.17 is compared to strain-hardening exponents for a wide range of steel products in Figure 3.25. Also shown in Figure 3.25 is the third-order polynomial that was developed for inclusion in the forthcoming edition of the ASTM CTOD testing standard E 1290. The polynomial is:

$$n_{poly} = 1.724 - 6.098 \cdot \frac{\sigma_y}{\sigma_u} + 8.326 \cdot \left(\frac{\sigma_y}{\sigma_u} \right)^2 - 3.965 \cdot \left(\frac{\sigma_y}{\sigma_u} \right)^3 \quad (3.19)$$

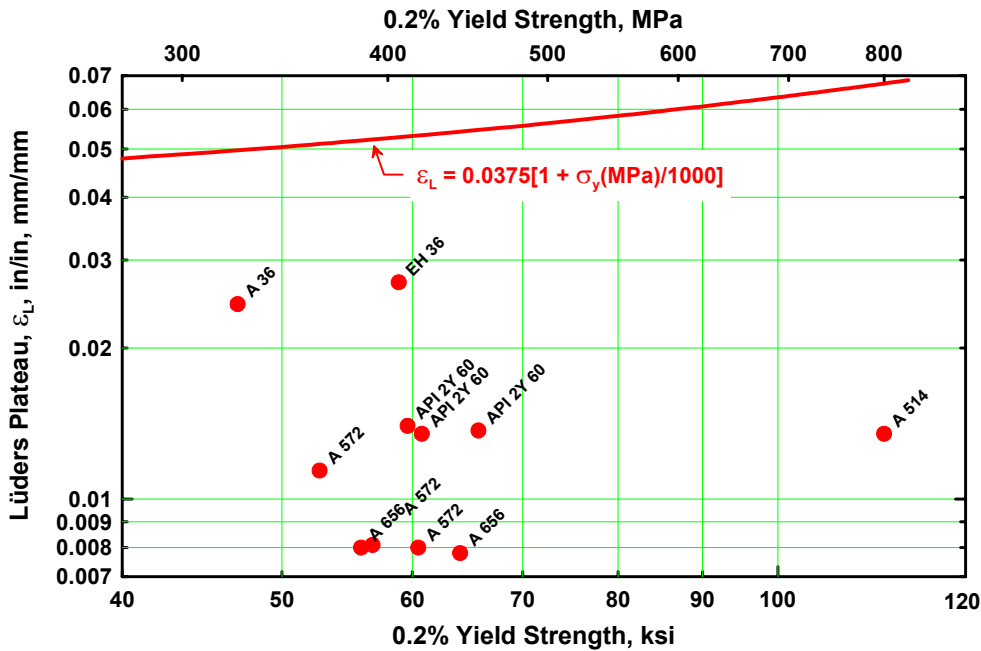


Figure 3.24: Lüders Plateau ϵ_L , Measured Values and Estimation Equation of BS 7910:1999 with Amendment 1

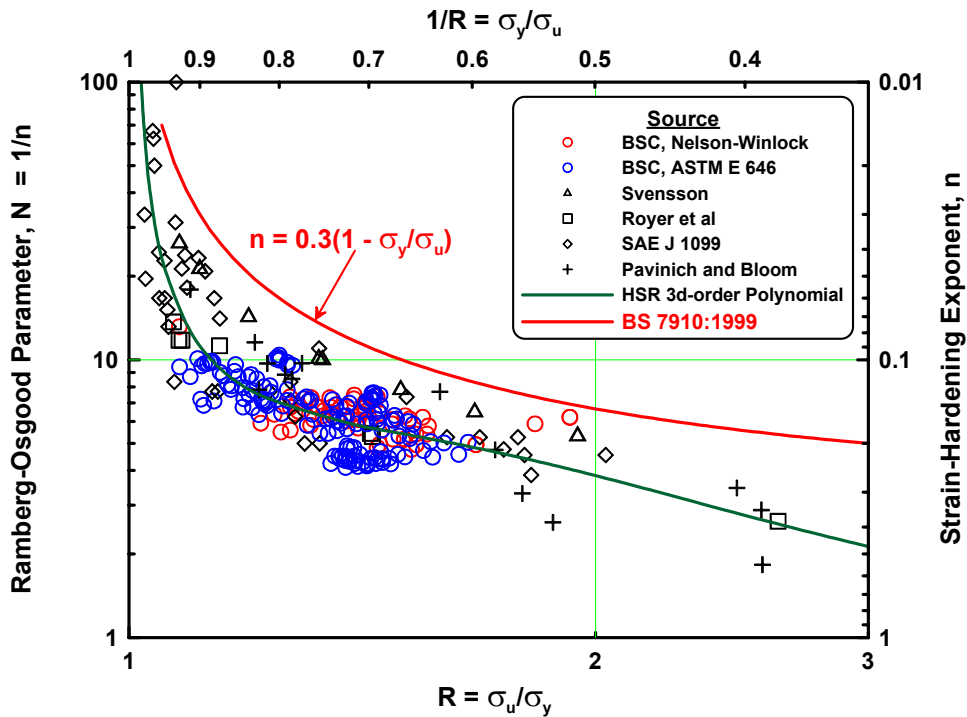


Figure 3.25: Strain Hardening Exponents for Steel Plate, Sheet, and Bar

Level 2B is based on the Option 2 FAC of the R6 approach [I. Milne, 1986] developed from expressions for J-integrals from the EPRI/GE handbook [V. Kumar, 1981] reformulated to use the actual true stress-strain curves. Also, conservative approximations were introduced to make the formulae geometry independent.

The Level 2B, Material Specific, FAC of BS 7910:1999 is defined as:

$$K_r = \frac{1}{\sqrt{\frac{E \varepsilon}{L_r \sigma_y} + \frac{L_r^3 \sigma_y}{2 E \varepsilon}}} \quad \text{for} \quad L_r \leq L_r^{\max} \quad (3.20)$$

and

$$K_r = 0 \quad \text{for} \quad L_r > L_r^{\max} \quad (3.21)$$

where L_r is expressed by equation 3.13, L_r^{\max} is expressed by equation 3.18, and ε is the *true strain* for a *true stress* of $L_r \cdot \sigma_y$ from the material's *true stress-strain curve*.

An example of the comparison to the two types of FAC's for the case of EH36 steel (which has a Lüders plateau) where the stress strain curve was available is presented in Figure 3.26.

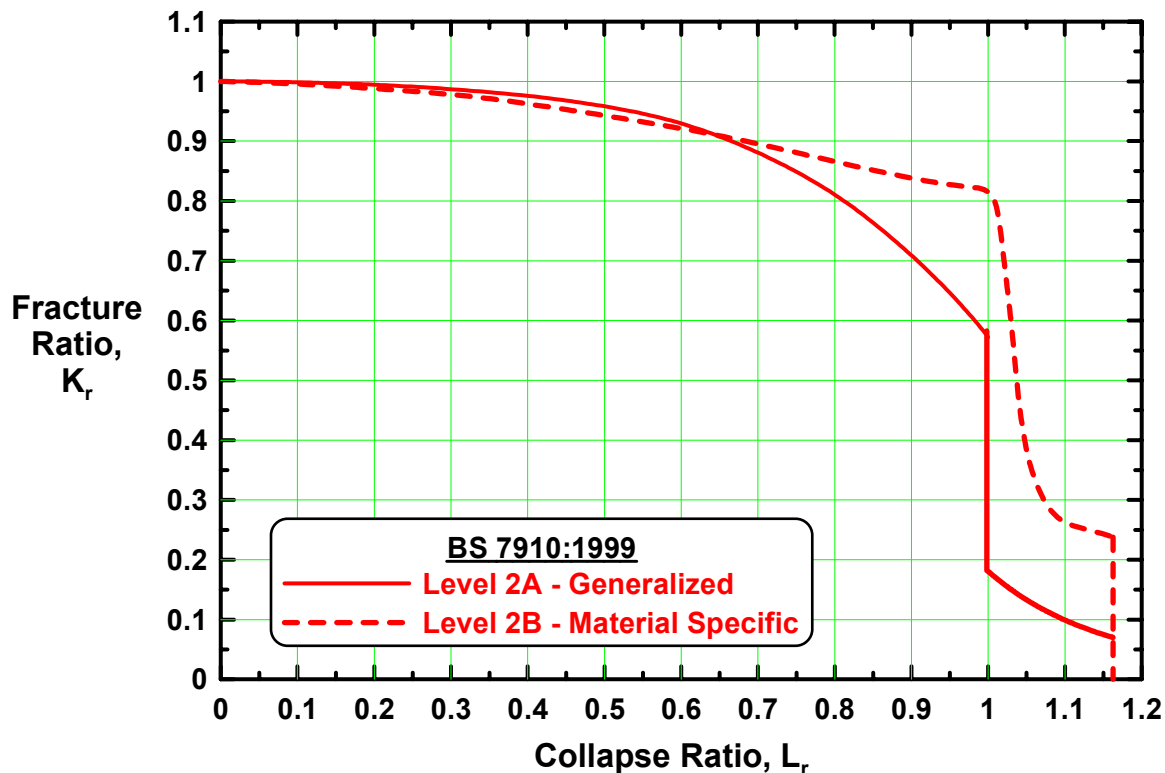


Figure 3.26: BS 7910:1999 Level 2 FAC's – ABS EH 36 Steel.

The simplified Level 2B is based on the recognition that all steels display a linear stress-strain curve to the Lüders plateau:

$$\sigma = L_r \cdot \sigma_y \quad (3.22)$$

and

$$\sigma = E \cdot \varepsilon \quad \text{for } L_r \leq 1 \quad (3.23)$$

equation 3.20 becomes the expression for the Simplified Level 2B FAC

$$K_r = \frac{1}{\sqrt{1 + \frac{L_r^2}{2}}} \quad \text{for } L_r \leq 1 \quad (3.24)$$

and

$$K_r = 0 \quad \text{for } L_r > 1. \quad (3.25)$$

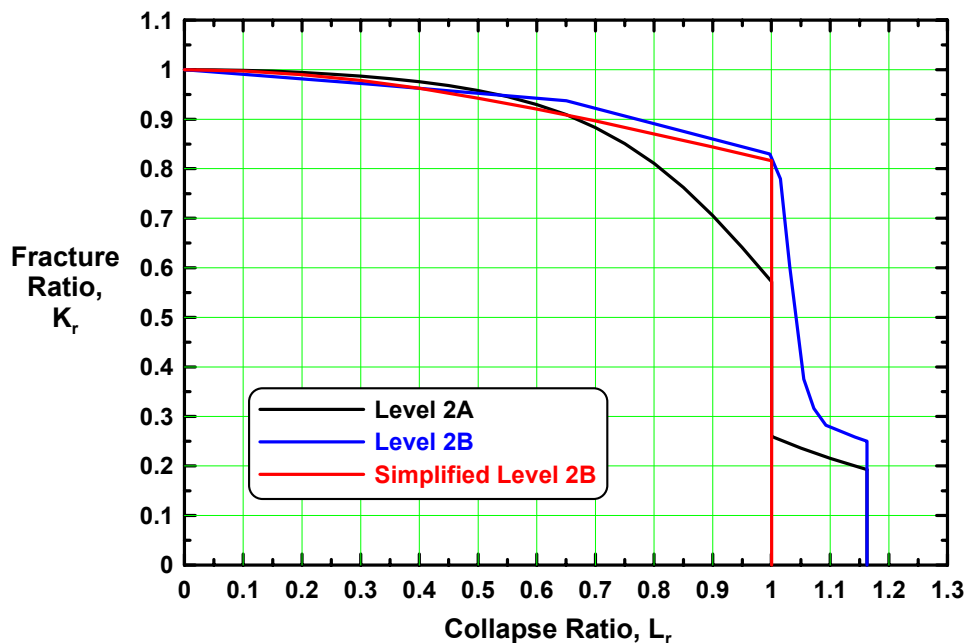


Figure 3.27: Comparison of BS 7910:1999 Level 2 FAC's with the simplified Level 2B Curve – ABS EH 36 Steel.

Figure 3.27 shows that Level 2A FAC is very conservative relative to the Level 2B FAC at values of Collapse Ratio L_r from 0.7 to 1.0. On the other hand, the Simplified Level 2B FAC is a reasonable descriptor of the Level 2B FAC except for values of L_r greater than unity and values of K_r less than 0.3. However, the latter conservatism is likely to be immaterial in most, if not all, fracture sensitive failure assessments.

The Level 2A, 2B, and Simplified 2B FAC's are compared for several grades, except for EH36 presented above, for which stress-strain curves are available. The *measured* yield and tensile strengths, σ_y and σ_u , strain-hardening exponent n and the Lüders plateau ε_L are listed in Table 3.1. The stress-strain curves are compared in Appendix A2. All grades but HSLA 80 demonstrated discontinuous yielding, i.e., a Lüders plateau.

Table 3.1. Steel Grades with Stress-Strain Curves

Grade	σ_y		σ_u		n	ε_L	Source	FAC's, Fig.
	MPa	ksi	MPa	ksi				
A 36	324	47.0	462	67.0	0.211	0.0245	A2.1	A2.1
ABS EH 36	406	58.9	538	78.0	0.202	0.0270	A2.2	NA
API 2Y 60	454	65.8	555	80.5	0.150	0.0180	A2.1	A2.2
HSLA 80	534	77.5	738	107	0.104	n/a	A2.1	A2.3
	607	88.0	690	100	0.0939	n/a	A2.2	
A 514	800	116	862	125	0.0888	0.0135	A2.1	A2.4

In all cases, the comparison leads to the similar conclusions to those arrived in EH36 steel.

3.5.2 Detail: Example of an Assessment of the State of the Cracked Detail

An estimate of the crack driving force K_I is usually determined from an expression of the form:

$$K_I = \sigma \sqrt{\pi c} F \quad (3.26)$$

where, $\sigma = K_f M_k S_{nom}$

and $F = f(a/2c, a/t, 2c/W)$

for a detail having a surface crack (length $2c$, and depth a) at the toe of a fillet weld. K_f is the stress concentration factor (SSC 379) at the toe of the weld, M_k is from BS 7910 (when the crack is in a region of stress concentration) S_{nom} is the nominal stress on the detail.

The fracture ratio K_r is given by:

$$K_r = \sqrt{\frac{\delta_I}{\delta_{mat}}} + \rho \quad (3.27)$$

$$\delta_I = \frac{K_I^2}{X \sigma_y E} \quad (3.28)$$

where K_I includes both σ and σ_{res}

δ_{mat} is the material fracture toughness and ρ is the plasticity correction factor that accommodates the residual stress, and

X and E depends on the state of stress in the cracked detail (see Table 3.2).

Table 3.2. Values of X and E.

	Plane Stress	Plain Strain
X	1	2
E'	E	E/(1-ν ²)

The collapse ratio L_r is given by:

$$L_r = \frac{\sigma_{ref}}{\sigma_y} \quad (3.29)$$

where $\sigma_{ref} = f(\sigma_{membrane}, \sigma_{bending}, \text{geometry})$ the membrane and bending stresses.

3.5.3 Detail: Determine the Safety Margin of the Cracked Detail

The safety margin is obtained after determining the location of the FAP (the x-y pair, L_r and K_r) relative to the applicable FAC, using the FAD shown in Figure 3.23.

Figure 3.28(a) and 3.28(b) show the Failure Assessment Diagrams for an athwart ship through-thickness crack in the weather deck of a product tanker [Reemsnyder 2002]. Three crack lengths, 50, 150, and 600 mm, two values of CTOD toughness, 0.254 and 2.54 mm, and two levels of global residual stress, $\sigma_{res} = 0$ and $\sigma_{res} = \sigma_y/2$, respectively, are considered in Figure 3.28(a) and 3.28(b). The stress intensity factor solution K_I was that of a transverse, through-thickness crack in a plate between longitudinal stiffeners. (The stiffeners modeled the side-shells of the ship.)

The Simplified Level 2B FAC is used for the failure loci and the Failure Assessment Points (FAP) are located by the x-y pair, L_r and K_r . It is assumed that the effective net-section stress was 60 percent of the yield stress, i.e., $L_r = 0.6$. The Fracture Ratio K_r for the FAP's was determined from

$$K_r = \sqrt{\frac{K_I^2}{\sigma_y \cdot E} \cdot \frac{1}{\delta_{mat}}} + \rho = \sqrt{\frac{(K_I^{applied} + K_I^{residual})^2}{\sigma_y \cdot E} \cdot \frac{1}{\delta_{mat}}} + \rho \quad (3.30)$$

where K_I , σ_y , E and δ_{mat} are, respectively, the elastic crack-driving force, i.e., the stress intensity factor, the yield stress, Young's Modulus, and the CTOD fracture toughness. The plasticity correction factor ρ accommodates residual stresses (Reemsnyder 2002) and is computed, in the present case ($L_r < 0.8$), from

$$\rho = 0.1 \cdot \chi^{0.714} - 0.007 \cdot \chi^2 + 3 \times 10^{-5} \cdot \chi^5 \quad (3.31)$$

where

$$\chi = \frac{K_I^{residual}}{K_I^{applied}} \cdot L_r \quad (3.32)$$

It is assumed that

$$\frac{K_I^{residual}}{K_I^{applied}} = \frac{\sigma_{res}}{\sigma}. \quad (3.33)$$

Thus

$$\chi = \frac{\sigma_{res}}{\sigma} \cdot \frac{\sigma}{\sigma_y} = \frac{\sigma_{res}}{\sigma_y}. \quad (3.34)$$

When $\sigma_{res} = 0$, χ and ρ are 0. When $\sigma_{res} = \sigma_y/2$, $\chi = 0.5$ and $\rho = 0.0592$.

The safety margins, given in Table 2.3, are computed from

$$\text{Safety Margin} = \frac{OB}{OA} \quad (3.35)$$

where OB is the length of the ray from the origin of the FAD, through the FAP, to the intersection of the ray with the FAC. OA is the length of the ray from the origin to the FAP.

Note the coordinates of Point O, for the case of $\sigma_{res} \neq 0$, are K_r expressed as equation 3.30 with

$K_I^{applied} = 0$ and $L_r = 0$, e.g., Figure 2.14(b).

Table 3.3: Safety Margins — Failure Assessment Using the Simplified Level 2B FAC.

Crack Length, mm	CTOD Toughness, δ_{mat}			
	0.254 mm (0.01 in)		2.54 mm (0.1 in)	
	$\sigma_{res} = 0$	$\sigma_{res} = \sigma_y/2$	$\sigma_{res} = 0$	$\sigma_{res} = \sigma_y/2$
50	1.67	1.41	1.67	1.67
150	1.40	> 1	1.67	1.67
600	> 1	> 1	1.67	1.27

It is interesting to note that the Safety Margin, when using the Simplified Level 2B FAC, and the assumption of equation 3.33, is

$$\text{Safety Margin} = \frac{OB}{OA} = \frac{1}{L_r} \quad \text{for} \quad \frac{K_r - K_r^{L_r=0}}{L_r} + K_r^{L_r=0} \leq 0.8165. \quad (3.36)$$

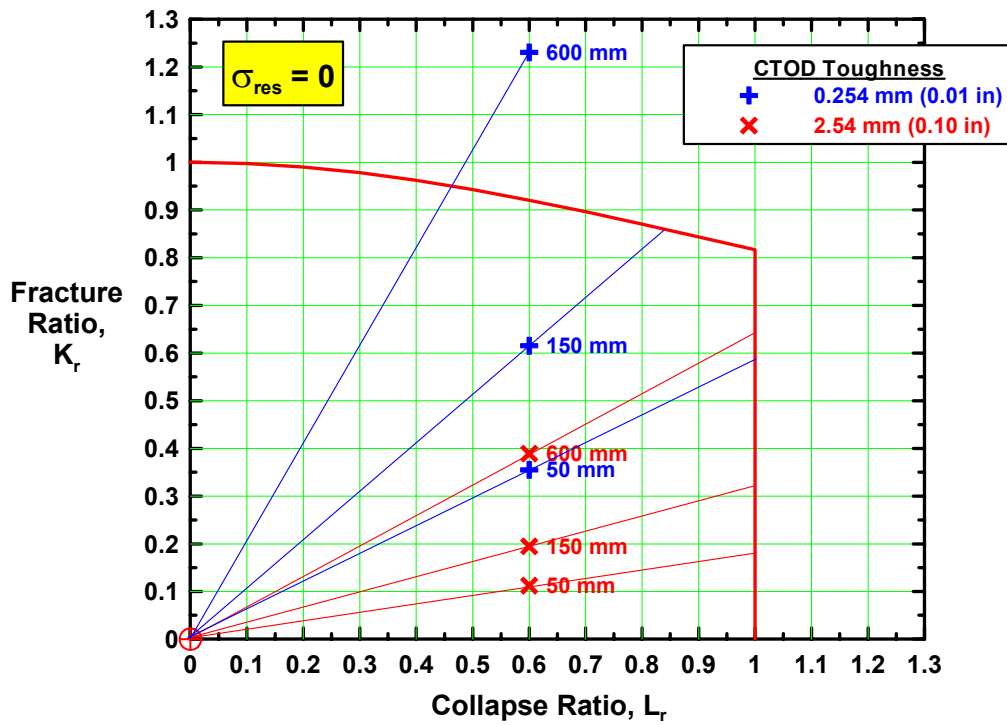


Figure 3.28(a): BS 7910:1999 Simplified Level 2B FAC – ABS A, B, D, E Steels – $\sigma_{res} = 0$.

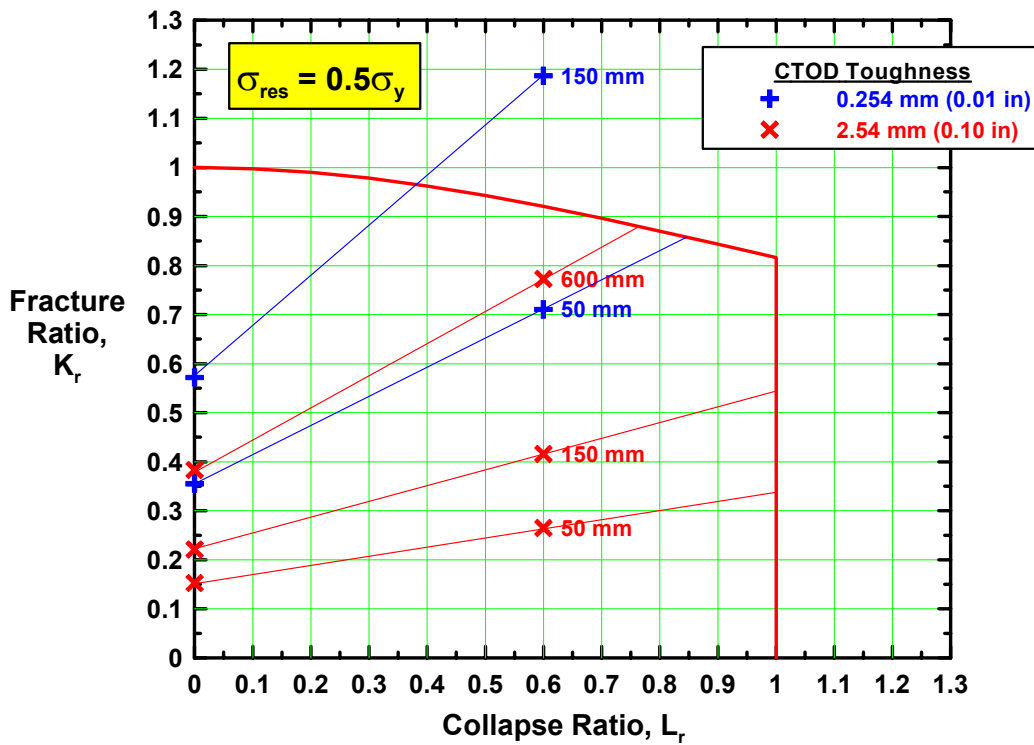


Figure 3.28(b): BS 7910:1999 Simplified Level 2B FAC – ABS A, B, D, E Steels – $\sigma_{res} = \sigma_y$.

3.6 Application of the Results

The results generated by the ship structure fracture assessment will indicate the relative criticality of flaws in a given structural component. This information may be used to define the importance of inspection accuracy in each area of the vessel.

In this project, the model developed based on the techniques described in the previous sections was applied in two limited applications. These applications are used to demonstrate the analysis techniques and to define areas in need of improvement. These example problems include a tanker and a tramp bulk carrier. This work is described in more detail in Section 4 that describes the sample applications and proposed results.

The fracture and plastic collapse analysis techniques to be used in the sample applications can be used to assess vessel or component fracture sensitivity by calculating the severity of a given flaw in a specific location under a particular applied loading condition. These results are developed using a failure assessment diagram approach similar to that shown in Figure 3.28. This flaw acceptability assessment technique may be used throughout the entire vessel to over a wide range of design load scenarios for a given flaw size that would not be detected by an inspector. This approach may be used to estimate the safety of the given ship or its level of damage tolerance.

Alternatively, given the material properties and design temperature the critical flaw size at a given structural detail may be estimated. A sample of this type of result is shown in Figure 3.9 where the critical flaw size is estimated as a function of the applied loading. The applied loading is expressed as a fraction of the peak applied load condition, possibly defined as the material yield stress. This form of results may be used to identify the inspection flaw detection accuracy required in each area of a vessel to assure a consistent level of safety against fracture over the entire vessel.

In a design application, knowing the flaw detection capabilities in vessel inspection, the minimum material toughness requirements for the vessel or structural components may be estimated. An estimate of the probability of failure may also be calculated using the critical flaw sizing capabilities and ocean wave extreme load statistics.

3.7 References

- Almer-Naess, A., Ed., “Fatigue Handbook – Offshore Steel Structures”, Tapir Publishers, Trondheim, Norway, 1985.
- American Bureau of Shipping, “Guide for Fatigue Strength of Tankers”, ABS, 1992.
- Ayyub, B., Souza, G., “Reliability-Based Methodology for Life Prediction of Ship Structures”, SSC Symposium 2000.
- Barsom, J.M., and Rolfe, S.T.: “Fracture and Fatigue Control in Structures-Application of Fracture Mechanics”, 3rd edn., ASTM, (1999)
- Bennett, F.M., and Sinclair, G.M.: “Parameter Representation of Low-Temperature Yield Behaviour of Body-Centered Cubic Transition Metals, ASME Publication 65-MET-11, (1965)
- BS PD6493: 1991, “Guidance on Methods for Assessing the Acceptability of Flaws in Fusion Welded Structure”, BSI, 1991.
- Chalmers, D.W., “Design of Ship Structures”, Ministry of Defence, London, HMSO, 1993.
- Cramer, E., Gran, S., Holtmark, G., Lotsberg, I., Loseth, R., Olaisen, K., and Valsgard, K., “Fatigue Assessment of Ship Structures”, DnV Report No. 93-0432, Rev. 5, 31 Jan. 1995.
- Ellingwood, B., Mori, Y., “Probabilistic Methods for Condition Assessment and Life Prediction of Concrete Structures in Nuclear Power Plants”, Nuclear Engineering and Design, Vol 142, pg. 155-166, 1993.
- FTL “Load Shell for Ship Structural Analysis - LOS³A”, software developed under contract to DREA, 1999.
- FTL, “Fatigue Design Guide for Ship Structures”, US Ship Structure Committee, 1998.
- FTL, “Shipmo PC User’s Manual”, Software developed in co-operation with DREA, 1998
- Glen, I.F., Dinovitzer, A., Paterson, R.B., Luznik, L., and Bayley, C., “Fatigue-Resistant Detail Design Guide for Ship Structures”, Ship Structure Committee Report SSC 405, Project No. SR-1386, 1999.
- Glen, I.F., Paterson, R.B., Luznik, L., “*Sea-operational Profiles for Structural Reliability Assessments*”, Ship Structure Committee Report SSC 406, 1999.
- “Guide on Methods for Assessing the Acceptability of Flaws in Metallic Structures,” *BS 7910: 1999 with Amendment 1*, Brit. Std. Inst., London, 2000.
- Hobbacher, A., “Stress Intensity Factors of Welded Joints”, Engng. Fracture Mechanics, Vol. 46, No. 2, pp173-182, 1993.
- Kumar, V., German. M.D., and Shih, C.F., “An Engineering Approach for Elastic-Plastic Fracture Analysis,” EPRI NP-1931, Project 1237-1, General Electric Company, Research and Development Center, Schenectady, NY, July 1981
- Ma, K.T., Bea, R., “Repair Management System for Fatigue Cracks in Ship Critical Structural Details”, Report No. SMP III-1-1, Dept. Naval Architecture and Offshore Engineering, University of Berkeley, California, December 1994.

- McTaggart, K., “**SHIPMO 7** An Updated Strip Theory Program for Predicting Ship Motions and Sea Loads in Waves”, DREA Technical Memorandum 96/243, 1997.
- Milne, I., Ainsworth, R.A., Dowling, A.R., and Stewart, A.T., “Assessment of the Integrity of Structures Containing Defects,” R/H/R6, Central Electricity Generating Board, Leatherhead, Surrey, May 1986
- Minami, F., Hashida, T., et al: “Dynamic Fracture Toughness Evaluation of Structural Steels Based on the Local Approach - Application of the Local Approach to Fracture Control Design (Part 3)”, J Soc Naval Architects Japan, v 184, Dec 1998, p 453
- Pussegoda, L.N. et.al: “Strain Rate Effects on Fracture Toughness of Ship Plate Steels”, Jour. Offshore Mechanics & Engineering, Transaction of ASME, v. 118, (1996), pp. 127-134
- Reemsnyder, H.S., “Failure Assessment Diagrams” in ASM Handbook, Volume 11, *Failure Analysis and Prevention*, ASM International, Materials Park, Ohio, 2002
- Reemsnyder, H.S., “Failure Assessment Diagrams” in ASM Handbook, Volume 11, *Failure Analysis and Prevention*, ASM International, Materials Park, Ohio, 2002, pp 243-249.
- Reemsnyder, H.S., “Simplified Level 2B Failure Assessment Curve - BS 7910: 1999 with Amendment 1,” November 7, 2002.
- SSC 379 "Improved Ship Hull Structural Details Relative to Fatigue", Stambaugh, K.A., Lawrence, F., and Dimitriakis, S., Ship Structure Committee, Washington DC 1994.
- Stambaugh, K., Lawrence, F., and Dimitriakis, S., “Improved Ship Hull Structural Details Relative To Fatigue”, SSC-379, 1994.
- Tada, M.: “Fracture Toughness Evaluation System of Steel Plates for Welded Structures”, Mitsubishi Juko Giho, v 32 n 5, 1995, p 362
- Xu, S., et al.: “Constitutive Equation for Steels” (2001), private communication
- Yoneya, T., Kumano, A., Yamamoto, N., and Shigemi, T., “Hull Cracking of Very Large Ships”, Integrity of Offshore Structures-5, Paper 15, University of Glasgow, Scotland, 1992.

4. DEMONSTRATION OF THE FAILURE ASSESSMENT TECHNIQUE

The objective of this section is to illustrate the application of the failure assessment techniques, described in the preceding sections, to relatively simple ship structure details. These applications will be used to illustrate the sensitivity of the failure criteria to changes in flaw size, material properties and vessel scantlings.

4.1 Centre Cracked Stiffened Panel

4.1.1 Introduction

The objective of this section is to demonstrate and discuss the application of the simplified Level 2B Failure Assessment Curve (FAC) following BS 7910:1999 with Amendment 1 to the sensitivity failure assessments of a central, through-thickness crack in an edge-stiffened panel.

In the previous section a simplified Level 2B FAC was developed. In this section, the simplified Level 2B FAC is applied to a sensitivity analysis of a central through-thickness crack in a 1024-in (26 m) wide edge-stiffened plate that modeled a ship's deck. The example selected to demonstrate the application of the Simplified Level 2B FAC is an athwartship, through-thickness crack in the weather deck of a product tanker (MV Castor 26m beam). The stress intensity factor solution K_I was that of a central, transverse, through-thickness crack in a plate between longitudinal stiffeners. (The stiffeners modeled the side-shells of the ship.)

This application considers:

1. Crack lengths, 22.8, 45.6, 97.4, 149.2, 179.2 and 209.2 mm (0.90, 1.8, 3.8, 5.9, 7.1 and 8.2 in).
2. Yield Strength, σ_Y , 345 N/mm² (50 ksi).
3. CTOD Fracture Toughness, 0.1 mm and 2 mm (0.004 and 0.08 in).
4. Residual Stress, 0 and 172.5 N/mm² (0 and 25 ksi), i.e., 0 and $\sigma_Y/2$.
5. Geometric conditions, free edge panel ($\beta=0$) and infinitely stiff edge stiffeners ($\beta \rightarrow \infty$)

The two values of CTOD toughness δ_c were selected from BMT Fleet Technology Limited test data [Pusegoda 2002]. Lower shelf and upper shelf values of, respectively, 0.004 in (0.10 mm) and 0.080 in (2.0 mm) were assumed to be representative of ship hull steels.

4.1.2 Stress Intensity Factor and Reference Stress Formulations

The stress intensity factor (SIF) for the edge-stiffened, through-cracked panel [Rook 1976 and Tada 2000] is:

$$K_I = \sigma_m \cdot \sqrt{\pi a} \cdot F\left(\frac{a}{b}, \beta\right) \quad (4.1)$$

where σ_m is the membrane stress, a and b are, respectively, the half-crack length, and panel half-width, and $F(a/b, \beta)$ accommodates the stiffness of the panel edges where

$$\beta = \frac{E' \cdot h'}{E \cdot h} \quad (4.2)$$

with thicknesses h and h' and Young's Moduli E and E' , Figure 4.1.

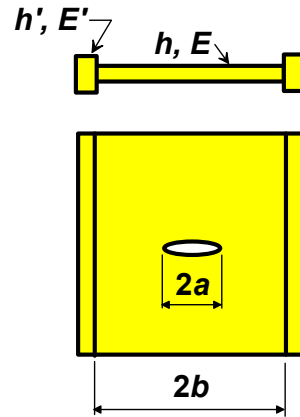


Figure 4.1: Central, Through-Thickness, Cracked Panel with Stiffened Edges

The SIF correction factors $F(a/b, \beta)$ are, for a panel with free edges

$$F\left(\frac{a}{b}, \beta\right)_0 = \sqrt{\sec \frac{\pi a}{2b}}, \quad (4.3)$$

and, for a panel with infinitely stiff (extension and bending) edges²

$$F\left(\frac{a}{b}, \beta\right)_\infty = 0.99952 + 0.014985 \cdot \left(\frac{a}{b}\right) - \dots \quad (4.4)$$

$$\dots - 0.62594 \cdot \left(\frac{a}{b}\right)^2 + 0.65416 \cdot \left(\frac{a}{b}\right)^3 - 0.60157 \cdot \left(\frac{a}{b}\right)^4.$$

The SIF correction factors $F(a/b, \beta)$ from equations (4.3) and (4.4) are shown in Figure 4.2.

² Polynomial fitted to digitized F vs. a/b curve for $\beta \rightarrow \infty$ in Ref. 4.

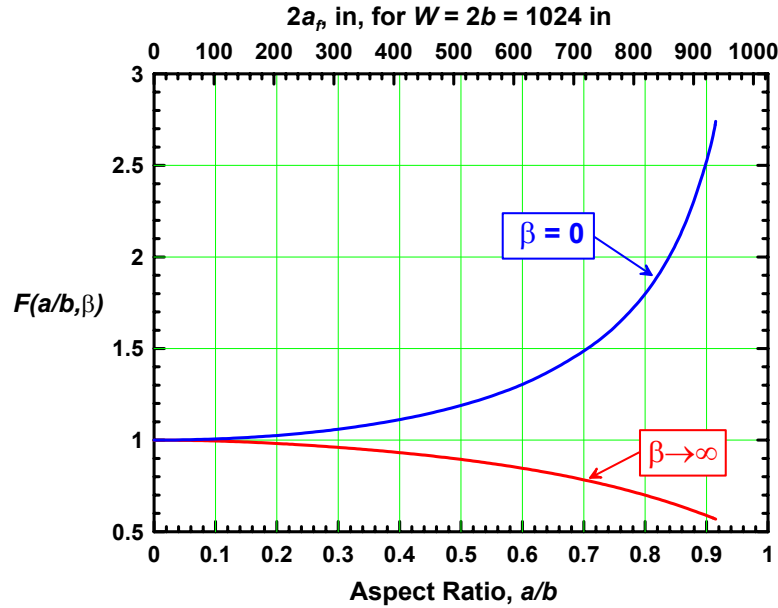


Figure 4.2: Stiffened Edge SIF Correction Factors

The plasticity correction factor ρ in equation (4.10) accommodates the inelastic interaction of the applied and residual stresses and is computed from BS 7910

$$\begin{aligned} \rho &= \rho_1 && \text{for } L_r \leq 0.8 \\ \rho &= 4 \cdot \rho_1 \cdot (1.05 - L_r) && \text{for } 0.8 < L_r < 1.05 \\ \rho &= 0 && \text{for } L_r \geq 1.05 \text{ or } K_I^{\text{residual}} \leq 0 \text{ or } K_I^{\text{applied}} = 0 \end{aligned} \quad (4.5)$$

where

$$\rho_1 = 0.1 \cdot \chi^{0.714} - 0.007 \cdot \chi^2 + 3 \times 10^{-5} \cdot \chi^5 \quad (4.6)$$

with

$$\chi = \frac{K_I^{\text{residual}}}{K_I^{\text{applied}}} \cdot L_r. \quad (4.7)$$

The Collapse Ratio L_r of Eq. 4.7 and 4.9 is expressed as

$$L_r = \frac{\sigma_{ref}}{\sigma_y} \quad (4.8)$$

where the reference stress σ_{ref} is a function of the applied stresses and geometry of the cracked element. The reference stress for the central, through-cracked panel with membrane stress σ_m but zero bending stress σ_b is

$$\sigma_{ref} = \frac{\sigma_m}{1 - \frac{a}{b}}. \quad (4.9)$$

The Fracture Ratio K_r for the Failure Assessment Points (FAP) is determined from:

$$K_r = \sqrt{\frac{K_I^2}{\sigma_y \cdot E} \cdot \frac{1}{\delta_c}} + \rho = \sqrt{\frac{(K_I^{applied} + K_I^{residual})^2}{\sigma_y \cdot E} \cdot \frac{1}{\delta_c}} + \rho \quad (4.10)$$

where K_I , σ_y , E and δ_c are, respectively, the elastic crack-driving force, i.e., the stress intensity factor, the yield stress, Young's Modulus, and the CTOD fracture toughness.

It is assumed that the form of the stress intensity factors for the residual stress σ_{res} and the applied (or membrane) stress σ_m were identical, i.e.,

$$\frac{K_I^{residual}}{K_I^{applied}} = \frac{\sigma_{res}}{\sigma_m} \quad (4.11)$$

4.1.3 Computational Method

For given values of β , σ_y , σ_{res} , and σ_m , an initial value of a (i.e., a_i) was assumed. The value of a was then increased iteratively until the loci of FAP's (computed from equations (4.10) and (4.8)) intersected the FAC.

The computations were performed by an interactive program written in Microsoft Compiler QuickBasic, Version 4.5. Typical screen captures of the analyses are shown in Figures 4.3 to 4.10.

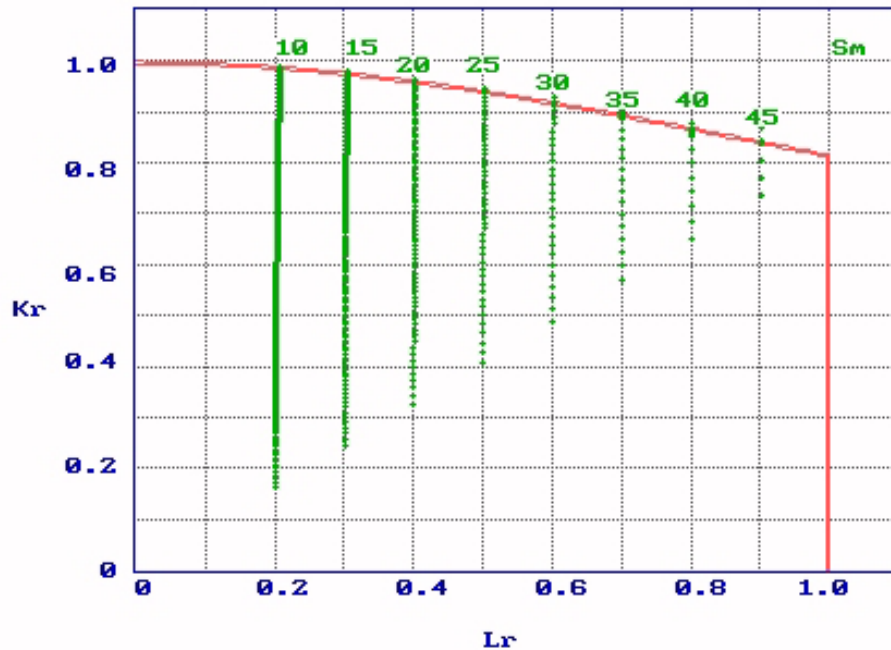


Figure 4.3: Screen Capture - $\beta = 0$, $\sigma_y = 50$ ksi, $\sigma_{res} = 0$, $\delta_c = 0.004$ in, $2a_i = 0.1$ in.

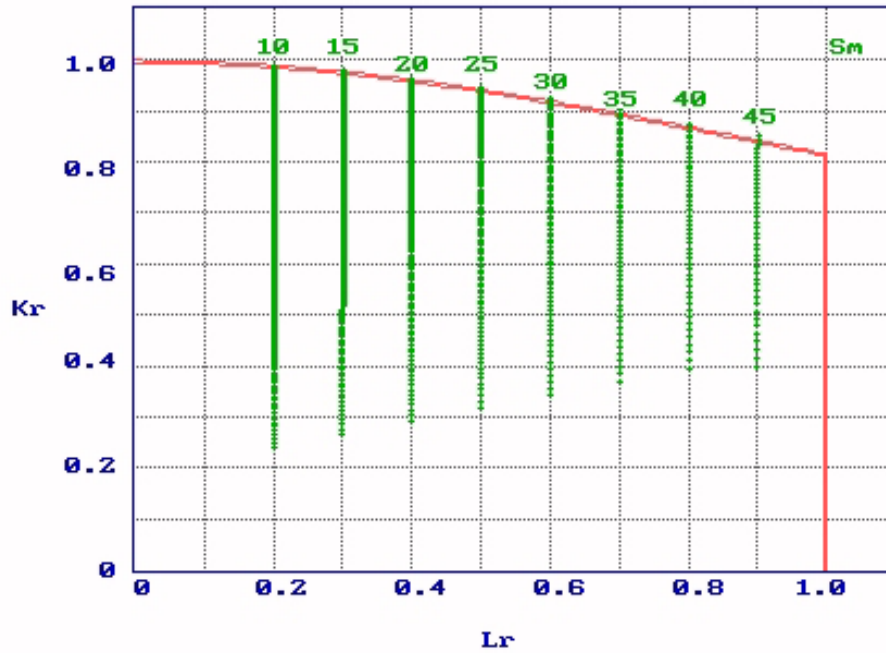


Figure 4.4: Screen Capture - $\beta = 0$, $\sigma_y = 50$ ksi, $\sigma_{res} = 25$ ksi, $\delta_c = 0.004$ in, $2a_i = 0.1$ in.

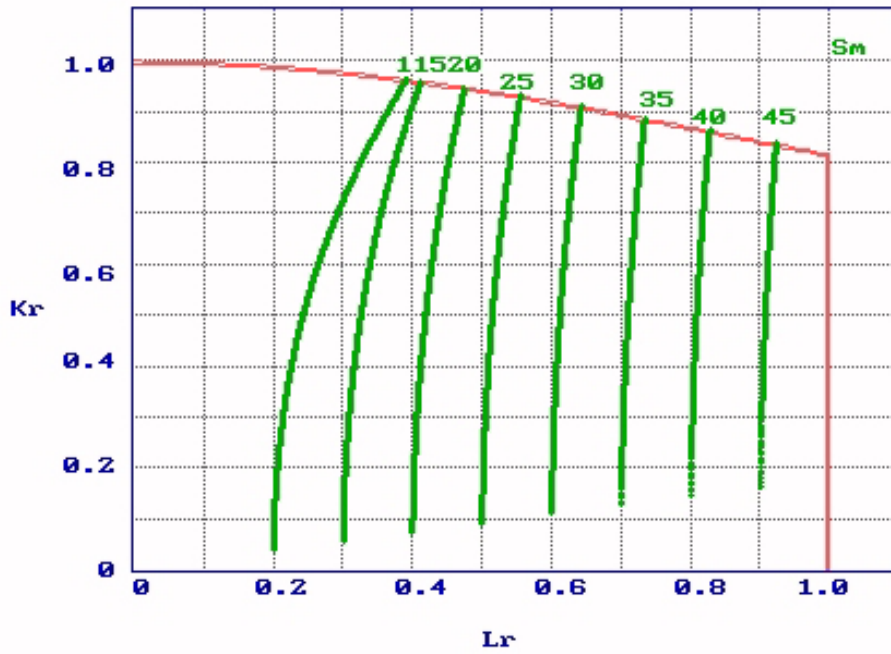


Figure 4.5: Screen Capture - $\beta = 0$, $\sigma_y = 50$ ksi, $\sigma_{res} = 0$, $\delta_c = 0.080$ in, $2a_i = 1.0$ in.

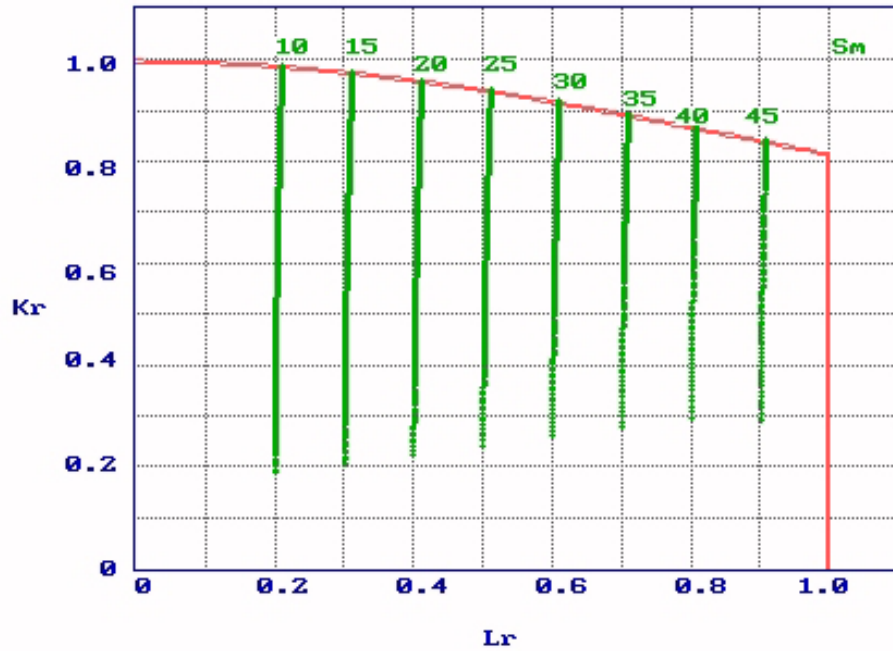


Figure 4.6: Screen Capture - $\beta = 0$, $\sigma_y = 50$ ksi, $\sigma_{res} = 25$ ksi, $\delta_c = 0.080$ in, $2a_i = 1.0$ in.

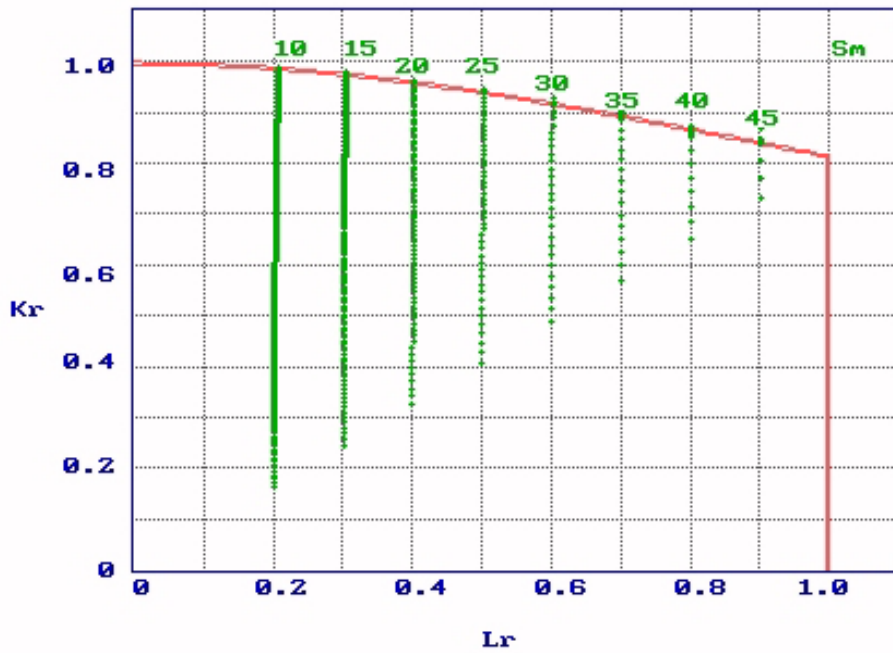


Figure 4.7: Screen Capture - $\beta \rightarrow \infty$, $\sigma_y = 50$ ksi, $\sigma_{res} = 0$, $\delta_c = 0.004$, $2a_i = 1.0$ in.

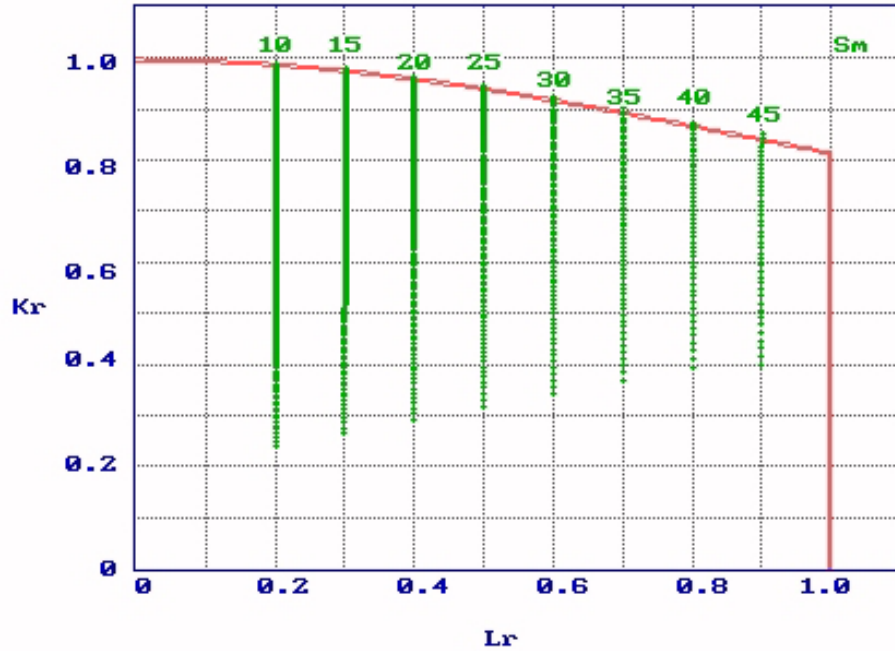


Figure 4.8: Screen Capture - $\beta \rightarrow \infty$, $\sigma_y = 50$ ksi, $\sigma_{res} = 25$ ksi, $\delta_c = 0.004$, $2a_i = 0.1$ in.

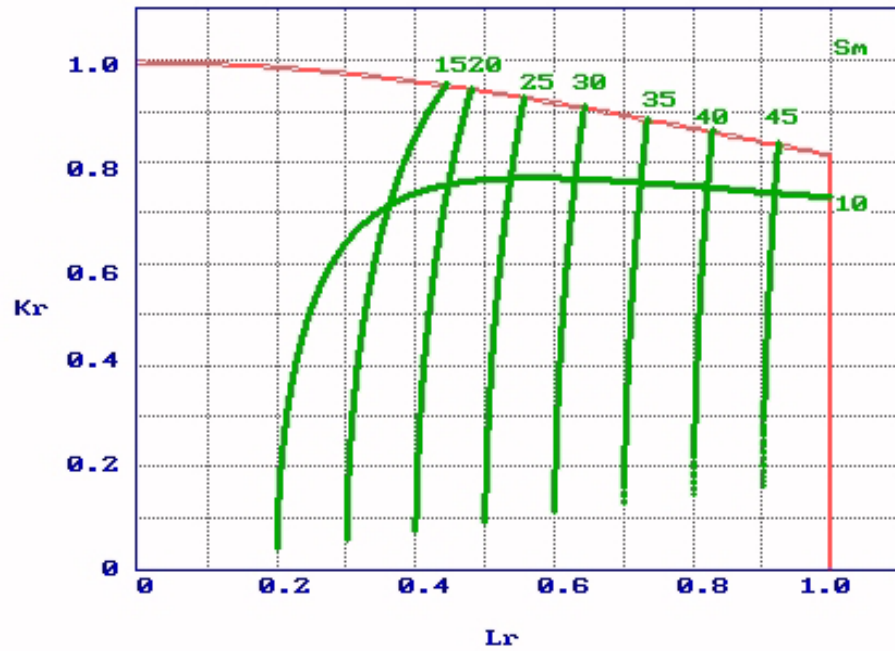


Figure 4.9: Screen Capture - $\beta \rightarrow \infty$, $\sigma_y = 50$ ksi, $\sigma_{res} = 0$, $\delta_c = 0.080$, $2a_i = 1.0$ in.

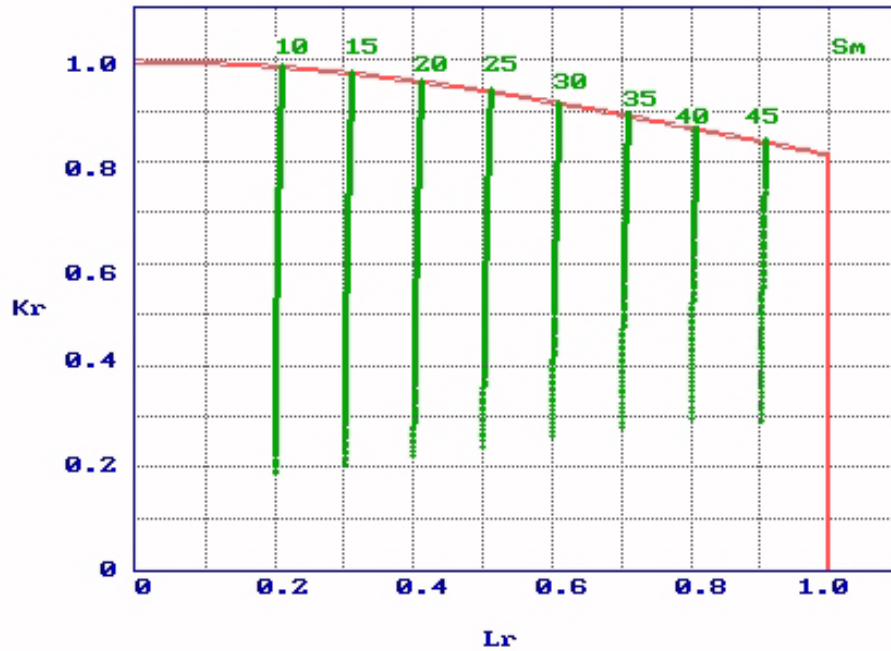


Figure 4.10: Screen Capture - $\beta \rightarrow \infty$, $\sigma_y = 50$ ksi, $\sigma_{res} = 25$ ksi, $\delta_c = 0.080$, $2a_i = 1.0$ in.

4.1.5 Results of Analyses

Tables 4.1 and 4.2, respectively, $\beta = 0$ and $\beta \rightarrow \infty$, list the crack-lengths $2a_f$ and the values of K_r and L_r at the intersections of the loci of FAP's and the simplified Level 2B FAC.

Table 4.1: Results, $\beta = 0$, $\sigma_y = 50$ ksi, $2b = 1024$ in.

(1 ksi = 6.89 MPa, 1 in = 25.4 mm = 0.0254 m)

CTOD δ_c , in	σ_{res} ksi	σ_m ksi	$2a_f$ in	L_r --	K_r --
0.004	0	10	36.7	0.2074	0.9895
		15	15.9	0.3047	0.9776
		20	8.70	0.4034	0.9626
		25	5.34	0.5026	0.9427
		30	3.54	0.6021	0.9210
		35	2.46	0.7017	0.8959
		40	1.78	0.8014	0.8708
		45	1.32	0.9012	0.8436
	25	10	2.66	0.2005	0.9907
		15	1.98	0.3006	0.9784
		20	1.51	0.4006	0.9624
		25	1.17	0.5006	0.9429
		30	0.92	0.6005	0.9205
		35	0.73	0.7005	0.8963
		40	0.58	0.8005	0.8703
		45	0.50	0.9004	0.8439
0.08	0	10	501	0.3919	0.9639
		15	280	0.4128	0.9600
		20	164	0.4760	0.9480
		25	103	0.5559	0.9311
		30	68.8	0.6432	0.9104
		35	48.2	0.7346	0.8878
		40	34.9	0.8282	0.8629
		45	26.0	0.9234	0.8375
	25	10	52.7	0.2109	0.9899
		15	39.3	0.3120	0.9765
		20	30.0	0.4121	0.9602
		25	23.3	0.5116	0.9410
		30	18.3	0.6109	0.9185
		35	14.5	0.7101	0.8938
		40	11.7	0.8092	0.8687
		45	10.0	0.9089	0.8413

Table 4.2: Results, $\beta \rightarrow \infty$, $\sigma_y = 50$ ksi, $2b = 1024$ in.

(1 ksi = 6.89 MPa, 1 in = 25.4 mm = 0.0254 m)

CTOD δ_c , in	σ_{res} ksi	σ_m ksi	$2a_f$ in	L_r --	K_r --
0.004	0	10	36.8	0.2075	0.9895
		15	16.0	0.3048	0.9777
		20	8.70	0.4034	0.9622
		25	5.35	0.5026	0.9431
		30	3.54	0.6021	0.9206
		35	2.46	0.7017	0.8959
		40	1.78	0.8014	0.8704
		45	1.32	0.9012	0.8435
	25	10	2.66	0.2005	0.9903
		15	1.98	0.3006	0.9782
		20	1.51	0.4006	0.9623
		25	1.17	0.5006	0.9428
		30	0.92	0.6005	0.9206
		35	0.73	0.7005	0.8965
		40	0.59	0.8005	0.8706
		45	0.50	0.9004	0.8443
0.08	0	10	819	1.0002	0.7304
		15	334	0.4452	0.9539
		20	173	0.4813	0.9469
		25	105	0.5572	0.9305
		30	69.5	0.6437	0.9105
		35	48.4	0.7347	0.8874
		40	35.0	0.8283	0.8629
		45	26.0	0.9235	0.8374
	25	10	53	0.2109	0.9898
		15	39.5	0.3120	0.9773
		20	30.1	0.4121	0.9607
		25	23.3	0.5116	0.9405
		30	18.3	0.6109	0.918
		35	14.5	0.7101	0.8939
		40	11.7	0.8092	0.8683
		45	10.0	0.9089	0.8414

Figure 4.11 and 4.12, respectively, $\beta = 0$ and $\beta \rightarrow \infty$, show the crack-lengths $2a_f$ versus the membrane stresses σ_m .

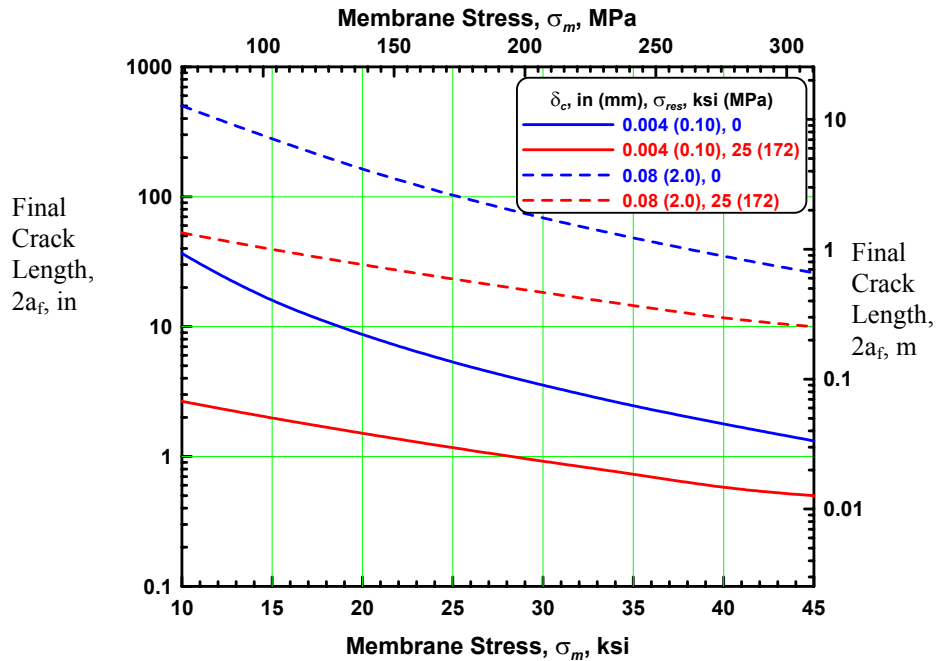


Figure 4.11: Critical Crack Length $2a_f$ vs. Membrane Stress, σ_m , $2b = 1024$ in (26 m), $\beta = 0$.

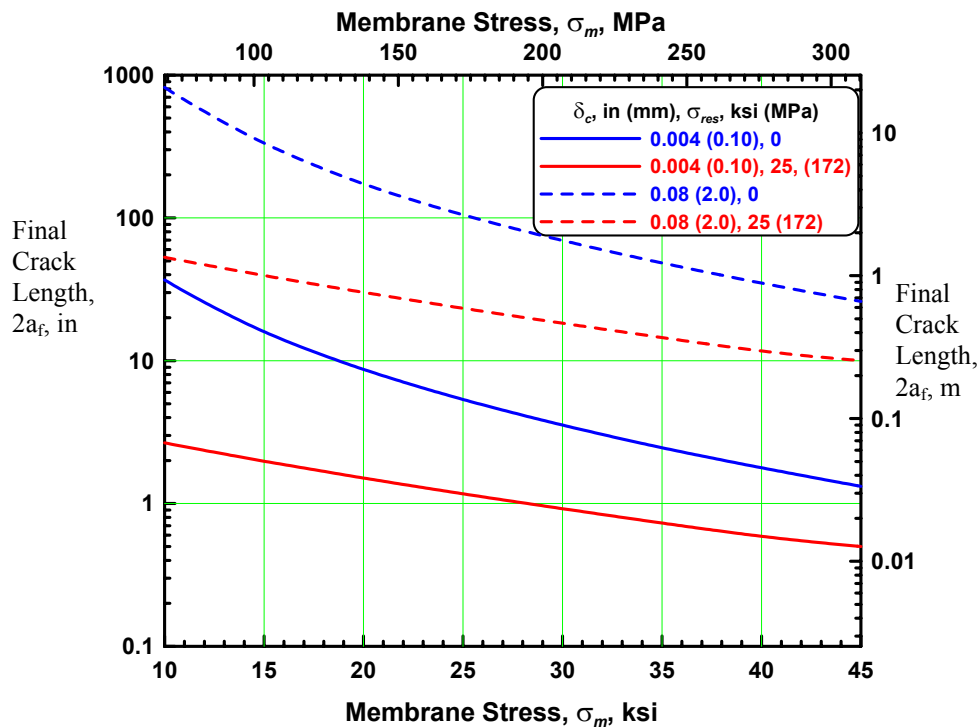


Figure 4.12: Critical Crack Length $2a_f$ vs. Membrane Stress, σ_m , $2b = 1024$ in (26 m), $\beta \rightarrow \infty$.

4.1.6 Discussion

The example calculations presented in this section illustrate the failure analysis of a centre-cracked panel. The sample applications illustrate that, as expected, the critical crack length reduces with:

- increasing applied stress,
- increasing residual stress, and
- decreasing toughness.

The critical crack lengths $2a_f$ are identical for both $\beta = 0$ and $\beta \rightarrow \infty$ except for the cases where the membrane stress σ_m is less than 20 ksi (138 MPa), $\delta_c = 0.08$ in (2.0 mm), and the residual stress σ_{res} is zero. Then the critical crack length for $\beta \rightarrow \infty$ exceeds that of $\beta = 0$. This is due to fact that, for small aspect ratios a/b , i.e., less than 0.2, the SIF correction factors $F(a/b, \beta)$ for both $\beta = 0$ and $\beta \rightarrow \infty$ are practically identical.

Only one critical FAP — $\sigma_m = 10$ ksi (69 MPa), $\sigma_{res} = 0$, $\delta_c = 0.08$ in (2.0 mm), $\beta \rightarrow \infty$ — is controlled by plastic collapse, i.e., $L_r = 1$. All of the other FAP's fall on the FAC for $L_r < 1$ and are controlled by fracture.

4.2 Cracked Deck Longitudinal

4.2.1 Introduction

The objective of this section is to demonstrate the application of the simplified Level 2B Failure Assessment Curve (FAC) following BS 7910:1999 with Amendment 1 to assess failure of a crack in a bulb-flat deck longitudinal. Details regarding the development of the structural model for the composite section, deck plate with cracked deck longitudinal, used in this sample application is reported in Appendix C along with the stress intensity factor derivation.

The composite section is that of a 16-mm-thick deck plate with 280x11 bulb-flat deck longitudinal. The 280x11 bulb-flat was selected so that area of the composite section, i.e., deck-plate + longitudinal, with the bulb-flat matched that of the composite section with a $\angle 150 \times 150 \times 15$ longitudinal, i.e., similar areas to match the hull girder section modulus.

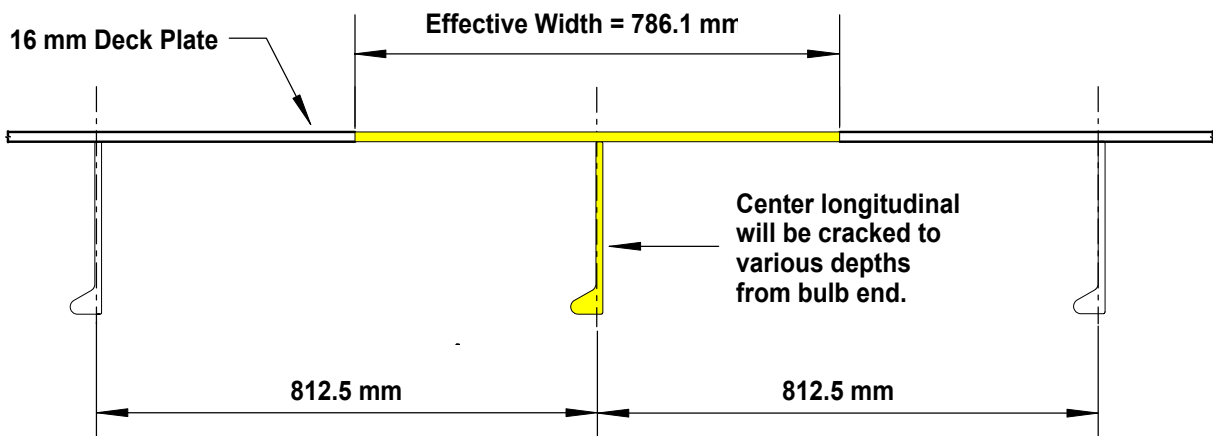
The parameters studied in this application include:

- Crack lengths, 22.8, 45.6, 97.4, 149.2, 179.2 and 209.2 mm (0.90, 1.8, 3.8, 5.9, 7.1 and 8.2 in).
- Yield Strength, σ_Y , 345 N/mm² (50 ksi).
- CTOD Fracture Toughness, 0.1 mm and 2 mm (0.004 and 0.08 in).
- Residual Stress, 0, 86.25 and 172.5 N/mm² (0, 12.5 and 25 ksi), i.e., $\sigma_Y/4$ and $\sigma_Y/2$.

The two values of CTOD toughness, 0.1 and 2 mm, represent, respectively, typical lower shelf and upper shelf toughnesses typical of marine steels.

4.2.2 Model Geometry

The deck plate longitudinal composite section, similar to that of M/V Castor, the subject of the example in the previous section, is derived in Appendix C. In M/V Castor, the deck-plate was 16 mm thick on a span (distance between transverse frames) of 5.54 m with $\angle 150 \times 150 \times 15$ longitudinal stiffeners on 8.125 m centers. The dimensions of the subject model are identical with the exception of the section selected for the deck longitudinal, Figure 4.13. Bulb flats [Corus 2002] were selected in lieu of the angles and several bulb flats were considered. The 280x12 bulb-flat was selected so that the composite section, i.e., deck-plate + longitudinal, with the bulb-flat matched that of the composite section with the angle. Upon the recommendation of Mr. Phillip Rynn, ABS Americas [Rynn 2003], the 280x11 bulb-flat, Table 4.3, was selected as the longitudinal for the model to match the hull girder section modulus using an angle as a deck longitudinal.



280 x 11 Corus Bulb Flats

$$A = 42.6 \text{ mm}^2 \quad I = 3330 \text{ cm}^4$$

Span (Transverse Frame Spacing) = 5540 mm

Figure 4.13: Composite Section – Deck Plate and Bulb Flat Longitudinals

Table 4.3: Properties of Deck Longitudinal.

Section		Area, A, cm ²	Inertia, I, cm ⁴	Comments
Angle	150x150x15	42.74	888	M/V Castor
Bulb Flat	280x11	42.6	3330	Match area of \angle

4.2.3 Shear lag in Deck Plate

The actual width of the deck-plate in the composite section is the spacing of the longitudinals, i.e., 8.125 m. However, due to shear lag, the effective width of the deck-plate in the composite section is less than the actual width, i.e., 7.861 m [Reemsnyder 2003b], Figure 4.13.

4.2.4 Stress Intensity Factor and Reference Stress Formulations

For the fracture mechanics analysis of a cracked bulb-flat deck longitudinal, three crack lengths measured from the bottom of the bulb-flat (bulb depth $d = 42$ mm and web depth $W = 280$ mm)), Figure 4.14, have been selected:

$d/4$, $1/4$ of the bulb-depth, 10.5 mm.

d , bulb-depth, 42 mm.

$d + W/4$, bulb-depth + $1/4$ web-depth, 101.5 mm.

The fracture mechanics analysis is performed on an 11-mm-thick flat-plate longitudinal with a cross-sectional area equal to that of the bulb-flat, i.e., 4260 cm^2 . The three crack lengths studied in the equivalent flat-plate longitudinal were selected so that their respective areas are identical to the areas of the cracks in the bulb-flat longitudinal, Figure 4.14. The equivalent flat-plate longitudinal is 11-mm thick and 387.3 mm deep. The three crack lengths are: (1) 45.6 mm, (2) 149.2 mm, and (3) 209.2 mm, as shown in Figure 4.14.

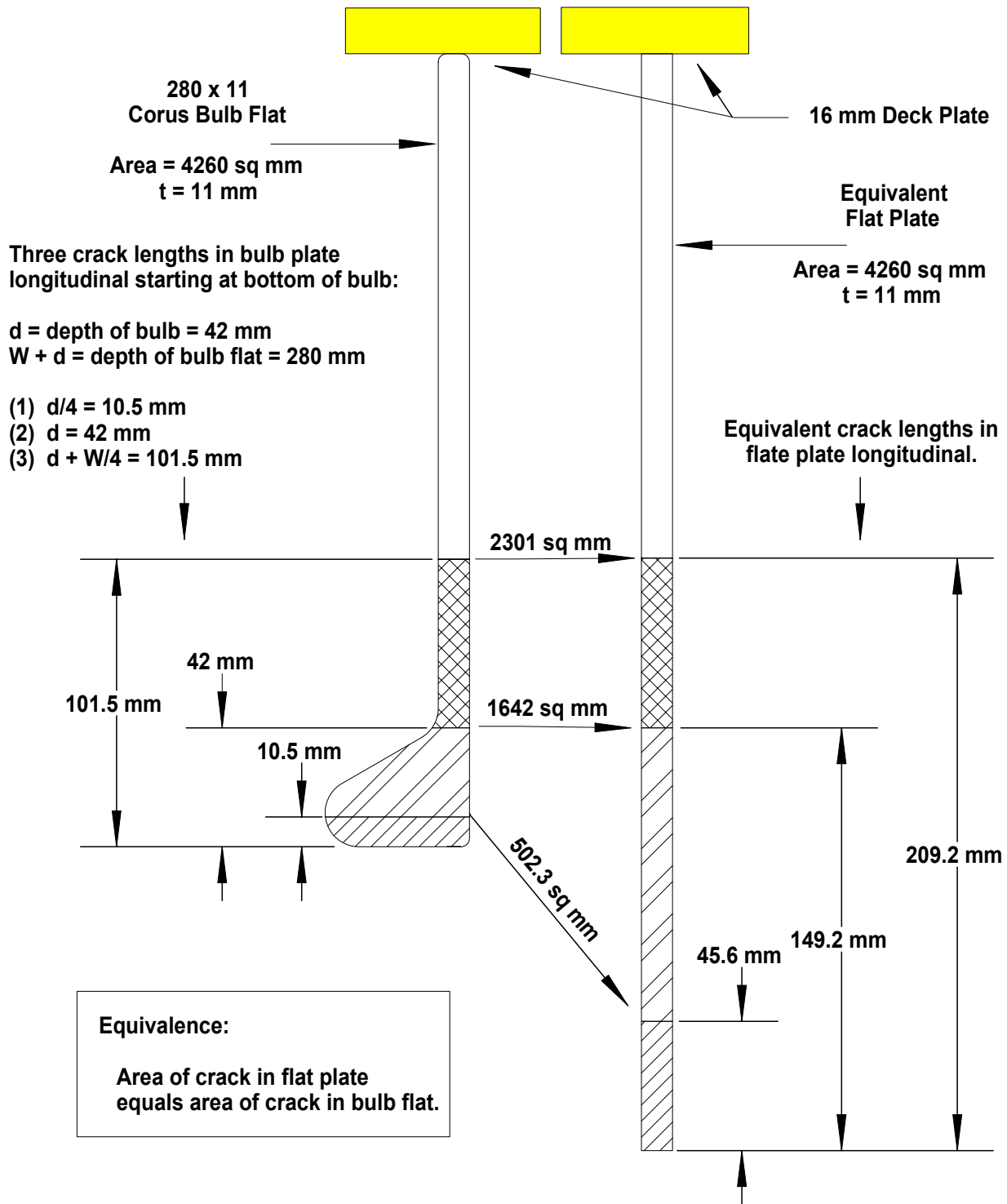


Figure 4.14: Equivalent Flat Plate Longitudinal for Fracture Mechanics Analysis

The composite section was modeled as having two components – a deck plate and a cracked flat-plate longitudinal [Reemsnyder 2003c].

The stress intensity factor solution for the composite section takes the form of:

$$K_I = \sigma_L \cdot \sqrt{\pi a} \cdot F\left(\frac{a}{b}\right) \quad (4.12)$$

where σ_L is the remote or nominal axial stress in the longitudinal, a is the crack length and b is the depth of the longitudinal. The function $F(a/b)$, from [Tada 2000] reflects the boundary conditions of the specific problem:

$$F\left(\frac{a}{b}\right) = \sqrt{\frac{2 \cdot b}{\pi \cdot a} \cdot \tan \frac{\pi \cdot a}{2 \cdot b}} \cdot \left[\frac{0.752 + 2.02 \cdot \left(\frac{a}{b}\right) + 0.37 \cdot \left(1 - \sin \frac{\pi \cdot a}{2 \cdot b}\right)^3}{\cos \frac{\pi \cdot a}{2 \cdot b}} \right] \quad (4.13)$$

The remote stress in the *cracked* longitudinal σ_L is [Reemsnyder 2003c]

$$\sigma_L = \sigma \cdot \frac{1 + \frac{t \cdot b}{t' \cdot b'}}{1 + \frac{4 \cdot a}{L_c} \cdot V_2 + \frac{t \cdot b}{t' \cdot b'}} \quad (4.14)$$

where σ is the remote stress on composite section and V_2 is the displacement (or elongation) along the centerline due to the crack [Tada 2000],

$$V_2(a/b) = \frac{a/b}{(1-a/b)^2} \cdot \left\{ 0.99 - a/b \cdot (1-a/b) \cdot \left[1.3 - 1.2 \cdot a/b + 0.7(a/b)^2 \right] \right\} \quad (4.15)$$

and L_c is the effective length of the composite section. (In the present analysis, L_c is taken as 5.54 m, the transverse frame spacing.)

The reference stress (σ_{ref}) formulation for the composite section of interest is expressed, for the case of *plane stress*, as [Reemsnyder 2003c]

$$\sigma_{ref} = \frac{\sigma \cdot \left(1 + \frac{t \cdot b}{t' \cdot b'}\right)}{1 + 1.072 \cdot \eta \cdot \frac{t \cdot b}{t' \cdot b'} \cdot (1 - a/b)} \quad (4.16)$$

where η is a function of the ligament c , ($c = b - a$) [EPRI 1981]

$$\eta = \sqrt{1 + \left(\frac{a}{c}\right)^2} - \left(\frac{a}{c}\right) \quad (4.17)$$

Based upon this formulation, the fracture ratio K_r for the FAP is defined as before:

$$K_r = \sqrt{\frac{K_I^2}{\sigma_y \cdot E} \cdot \frac{1}{\delta_c}} + \rho = \sqrt{\frac{(K_I^{applied} + K_I^{residual})^2}{\sigma_y \cdot E} \cdot \frac{1}{\delta_c}} + \rho \quad (4.18)$$

where K_I , σ_y , E and δ_c are, respectively, the elastic crack-driving force, i.e., the stress intensity factor, the yield stress, Young's Modulus, and the CTOD fracture toughness. The plasticity correction factor ρ accommodates residual stresses and is computed from

$$\begin{aligned} \rho &= \rho_1 && \text{for } L_r \leq 0.8 \\ \rho &= 4 \cdot \rho_1 \cdot (1.05 - L_r) && \text{for } 0.8 < L_r < 1.05 \\ \rho &= 0 && \text{for } L_r \geq 1.05 \text{ or } K_I^{\text{residual}} \leq 0 \text{ or } K_I^{\text{applied}} = 0 \end{aligned} \quad (4.19)$$

where

$$\rho_1 = 0.1 \cdot \chi^{0.714} - 0.007 \cdot \chi^2 + 3 \times 10^{-5} \cdot \chi^5 \quad (4.20)$$

and

$$\chi = \frac{K_I^{\text{residual}}}{K_I^{\text{applied}}} \cdot L_r. \quad (4.21)$$

It was assumed that:

$$\frac{K_I^{\text{residual}}}{K_I^{\text{applied}}} = \frac{\sigma_{\text{res}}}{\sigma_L}. \quad (4.22)$$

Thus

$$\chi = \frac{\sigma_{\text{res}}}{\sigma_Y} \cdot \frac{1 + \frac{4a}{L_c} \cdot V_2 + \frac{t \cdot b}{t' \cdot b'}}{1 + 1.072 \cdot \eta \cdot \frac{t \cdot b}{t' \cdot b'} \cdot \left(1 - \frac{a}{b}\right)}. \quad (4.23)$$

The values of χ and ρ_1 for values of σ_{res} used herein are listed in Table 4.4. When σ_{res} is zero χ and ρ_1 (and, therefore ρ), are zero.

Table 4.4: Plasticity Correction Factors.

a, mm	χ		ρ_1	
	$\sigma_{\text{res}}/\sigma_Y = 1/4$	$\sigma_{\text{res}}/\sigma_Y = 1/2$	$\sigma_{\text{res}}/\sigma_Y = 1/4$	$\sigma_{\text{res}}/\sigma_Y = 1/2$
22.8	0.2535	0.5071	0.0371	0.0598
45.6	0.2622	0.5244	0.0380	0.0612
97.4	0.2852	0.5704	0.0403	0.0647
149.2	0.3166	0.6332	0.0433	0.0694
179.2	0.3437	0.6875	0.0458	0.0732
209.2	0.3860	0.7719	0.0496	0.0790

4.2.5 Failure Assessment of the Composite Section

The goal of the analyses is the development of critical stress versus crack length plots for the various combinations of parameters. For a given set of parameters, the crack length was held constant and the remote, or nominal, stress σ was increased until the locus of FAP's intersected the Failure Assessment Curve FAC defined as the Simplified Level 2B, BS 7910 [Reemsnyder 2002b]. This intersection defined the critical stress for the given crack length.

An example of the procedure for the cracked composite section with zero residual stress and L_c taken as 5.54 m (the transverse frame spacing) is shown in Figure 4.15. In all cases, except the smallest crack length (45.6 mm) with the higher fracture toughness, failure is estimated to occur in a fracture mode.

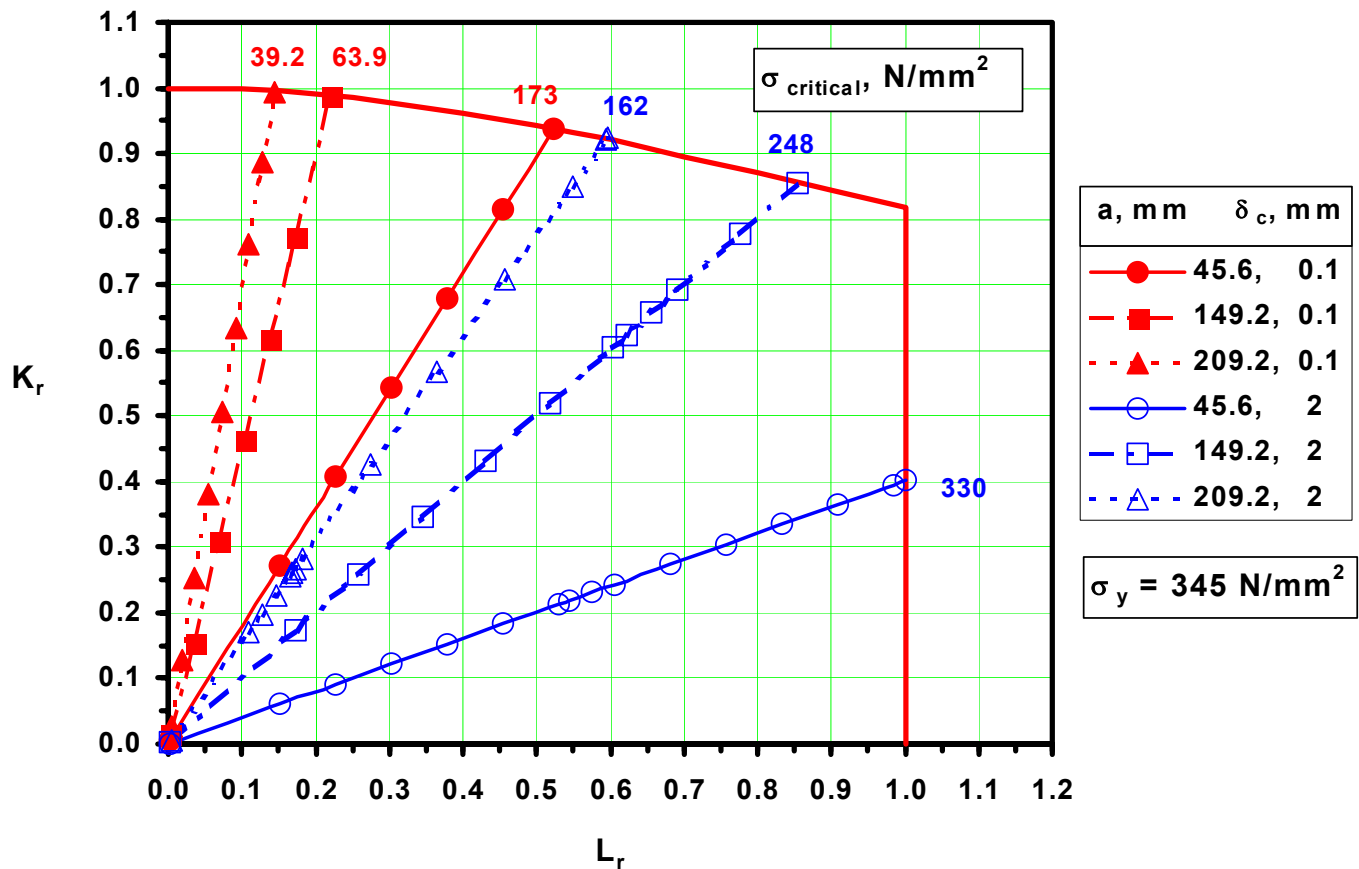


Figure 4.15: Failure Assessment Diagram for Composite Section

The results of all the analyses are shown in Figure 4.16 and Table 4.5 where σ_c is the critical value of the remote (nominal or membrane) stress on the composite section. These results indicate that, in general, the fracture mode of failure is dominant, with the exception of a few low residual stress, high toughness and short crack conditions.

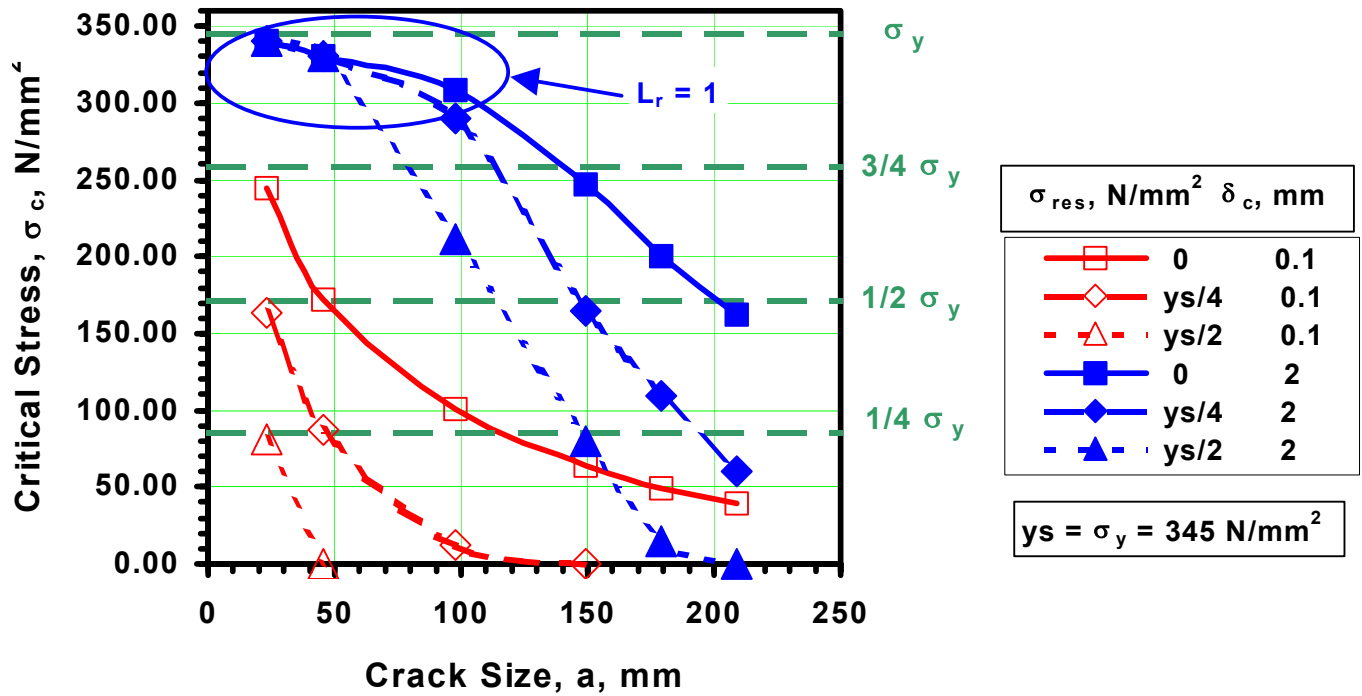


Figure 4.16: Critical Stress vs. Crack Length for Composite Section

Table 4.5: Failure Assessment Results

$\delta_c, \text{ mm}$	$a, \text{ mm}$	Critical Stress, $\sigma_c, \text{ N/mm}^2$		
		$\sigma_{res} = 0$	$\sigma_{res} = \sigma_Y/4$	$\sigma_{res} = \sigma_Y/2$
0.1	22.8	244.1	162.8	81.0
	45.6	172.4	87.1	0
	97.4	101.2	11.8	0
	149.2	63.9	0	0
	179.2	49.7	0	0
	209.2	39.2	0	0
2	22.8	340.4*	340.4	340.5
	45.6	330.0	330.0	330.0
	97.4	308.1	290.5	211.8
	149.2	247.6	164.3	80.4
	179.2	199.9	109.1	14.3
	209.2	162.6	60.0	0

* Values in bold italics indicate that *Plastic Collapse controls*, i.e., $L_r = 1$.

In Table 4.5, zero values of critical stress σ_c indicate that failure occurs in the presence of residual stresses only without a stress due to external loading.

It is noted that the intersection of the locus of FAP's and the FAC define the critical combination of remote (nominal or membrane) stress in the deck σ_c and crack length a in the deck longitudinal at failure. Further, *failure is defined herein as the initiation of crack extension* – stable for upper shelf values of toughness and unstable for lower shelf values of toughness. It is possible that unstable crack extension could be arrested if the crack-arrest toughness is adequate or if sufficient load is shed from the cracked composite section to the adjacent uncracked composite sections.

4.2.6 Effect of Load Shedding

Obviously, as the crack in the deck longitudinal grows, the stiffness of the cracked composite section decreases and the adjacent uncracked composite sections begin to pick up load shed by the cracked section. This load shedding is explored in Figure 4.17 where:

- σ remote (nominal or membrane) stress on the deck system
- σ_{cs} remote stress on the cracked composite section
- σ_{us} remote stress on the adjacent uncracked composite sections
- C_{cs} compliance³ of the cracked composite section (P/ Δ , force/elongation)
- C_{us} compliance of the adjacent uncracked composite sections (force/elongation).

In the analysis of load shedding, it was assumed that the load shed by the cracked composite sections is picked up by the two adjacent uncracked composite sections, one on either side of the cracked section, as shown in Figure 4.13.

Figure 4.17 shows that the load shedding, and change of stiffness, is relatively insignificant until the length of crack in the deck longitudinal approaches 200 mm. Table 4.6 demonstrates the effect of load shedding on the critical applied stress to promote failure.

³ Compliance is the reciprocal of the stiffness Δ/P , elongation/force.

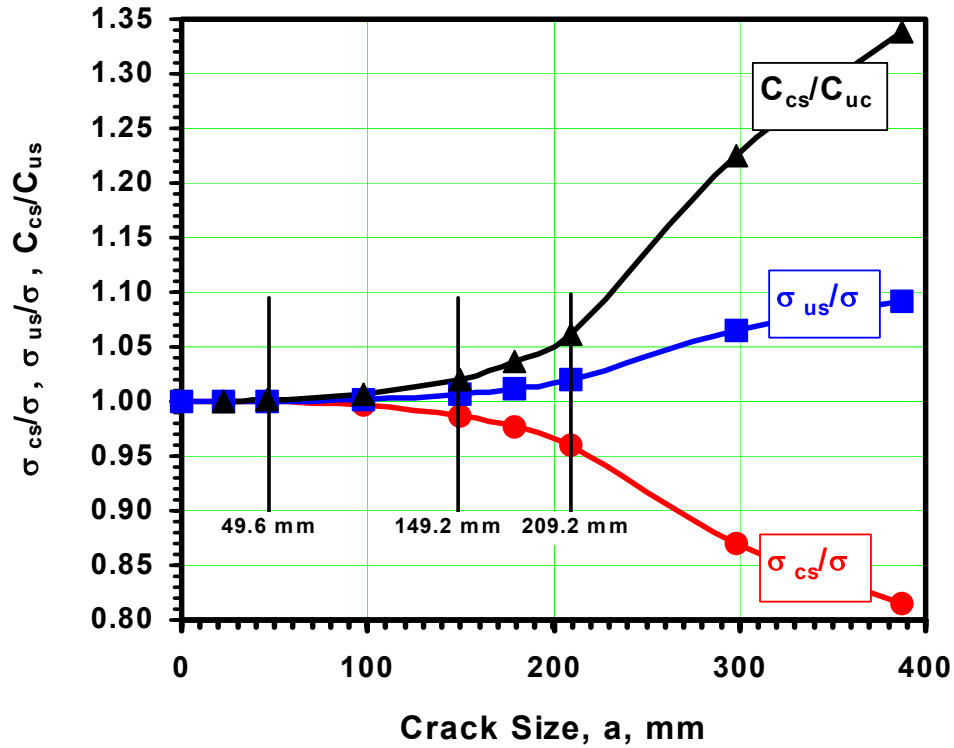


Figure 4.17: Load Shedding in Composite Section

Table 4.6: Increase in Critical Stress due to Load Shedding

a, mm	Percent Increase in σ_c , N/mm ² , with Load Shedding					
	$\delta_c = 0.01$ mm			$\delta_c = 2$ mm		
	$\sigma_{res} = 0$	$\sigma_{res} = \sigma_Y/4$	$\sigma_{res} = \sigma_Y/2$	$\sigma_{res} = 0$	$\sigma_{res} = \sigma_Y/4$	$\sigma_{res} = \sigma_Y/2$
22.8	0	0	0	0	0	0
45.6	0.1	0.1	0	0.1	0.1	0.1
97.4	0.4	0.4	0	0.4	0.4	0.4
149.2	1.3	0	0	1.3	1.3	1.3
179.2	2.3	0	0	2.3	2.3	2.3
209.2	4.0	0	0	4.0	4.0	0.0

4.2.7 Discussion

The examples presented in this section illustrate the failure assessment of cracked deck longitudinal and provide a means of considering stiffeners that are not flat bars. The results indicate that as expected the critical failure stress reduces with:

- increasing crack length,
- increasing residual stress, and
- decreasing toughness.

It is also noted that any beneficial effect from load shedding is insignificant and can be neglected in the failure assessment of the cracked deck—longitudinal composite section.

The effect of reduced buckling resistance concomitant with crack growth was not considered in this analysis.

4.3 References

“An Engineering Approach to Elastic-Plastic Fracture Analysis,” *EPRI NP-1931*, General Electric Co., Schenectady, 1981, p 3-12 – 3-14.

“Guide on Methods for Assessing the Acceptability of Flaws in Metallic Structures,” *BS 7910:1999 with Amendment 1*, Brit. Std. Inst., London, 2000.

“Special Bulb Flats for Plate Stiffening,” Corus Group Ltd., Saltburn, United Kingdom, 2002.

Correspondence with Mr. Phillip G. Rynn, ABS Americas, May 1, 2003.

Pussegoda, L.N., Correspondence, November 13, 2002.

Reemsnyder, H.S. “Example of Application of Simplified Level 2B Failure Assessment Curve BS 7910:1999 with Amendment 1 – Central, Through-Thickness Crack in Edge-Stiffened Panel,” January 16, 2003a.

Reemsnyder, H.S. “Example of Application of Simplified Level 2B Failure Assessment Curve BS 7910:1999 with Amendment 1 – Cracked Deck Longitudinal,” Progress Report 1, May 15, 2003b.

Reemsnyder, H.S. “Example of Application of Simplified Level 2B Failure Assessment Curve BS 7910:1999 with Amendment 1 – Cracked Deck Longitudinal – K-Solution for Composite Model,” Progress Report 2, June 23, 2003c.

Reemsnyder, H.S., “Simplified Level 2B Failure Assessment Curve -- BS 7910: 1999 with Amendment 1,” November 7, 2002b.

Reemsnyder, H.S., “Failure Assessment Diagrams” in ASM Handbook, Volume 11, *Failure Analysis and Prevention*, ASM International, Materials Park, Ohio, 2002a, pp 243-249.

Rook, D.P., and Cartwright, D.J., “Compendium of Stress Intensity Factors,” Her Majesty’s Stationery Office, London, 1976, pp 188-190.

Tada, H., Paris, P.C., and Irwin, G.R., “The Stress Analysis of Cracks Handbook,” 3d Edition, ASME Press, New York, 2000, p 332.

5. DEMONSTRATION OF THE VESSEL FAILURE ASSESSMENT TECHNIQUE

The sample application is presented in terms of the six steps used to describe the approach in the previous sections, including:

- Vessel Particular Identification
- Structural Section and Component Definition
- Load Assessment
- Definition of Local Detail Characteristics
- Failure Assessment, and
- Application of the Results

5.1 Vessel Particular Identification

The MV Bulk Carrier is a geared “handy-size” bulk carrier operating on short-term contracts (tramp service) taking it all over the world. The vessel was constructed in a Brazilian shipyard and entered service in 1987. After three changes of ownership, the MV Bulk Carrier saw a major refit in a Chinese shipyard in 1998 and continues to trade worldwide. The particulars of the MV Bulk Carrier are provided below.

<p>Length: 190 m Beam: 27.6 m Depth: 14.8 m Block Coefficient (C_B): 0.8 Displacement: 47 043 tonnes Max Draft: 10.93 m Service Speed: 15 knots Power Plant: 12,000 HP Slow Speed Diesel</p>	
---	---

Figure 5.1: Bulk Carrier Particulars

5.2 Structural Segment and Component Definition

Typically, for the seakeeping or loads analysis, a vessel like the MV Bulk Carrier would be divided into 20 equally spaced stations, however, for the sake of this analysis, the vessel was divided into 5 segments of equal length as listed in Table 5.1. Figure 5.2 illustrates the five segment division of the vessel.

Each segment has been further divided into two frame types; frame type 1 is a section in way of the open hatch and frame type 2 is a section in way of the deck plate between the hatches. Frame type 1 has 13 component types, and frame type 2 has 14 component types, as illustrated in Figure 5.3(a) and Figure 5.3(b). The number of repetitions of each frame type and assumed loading in each segment are as described in Table 5.1.

Table 5.1: Vessel Segment and Frame Type Distribution

Segment	Distance from Bow (m)	Frame Type 1	Frame Type 2
1	30.5	10	28
2	61.0	24	20
3	91.5	22	27
4	122.0	26	24
5	152.5		48

Each structural component consists of a longitudinal bulb flat and hull plate and these component types may be repeated within a section several times. The hull plate is not considered to be one continuous structural piece, but is defined as flanges of the bulb flats, the width of the flange is the average center to center distance between adjacent bulb stiffeners. Table 5.2 provides a breakdown of the components illustrated in Figure 5.2 for frame types 1 and 2, respectively. Table 5.2 only shows the components for the portside of the ship. The ship is symmetric about its longitudinal centerline and thus each component is repeated.

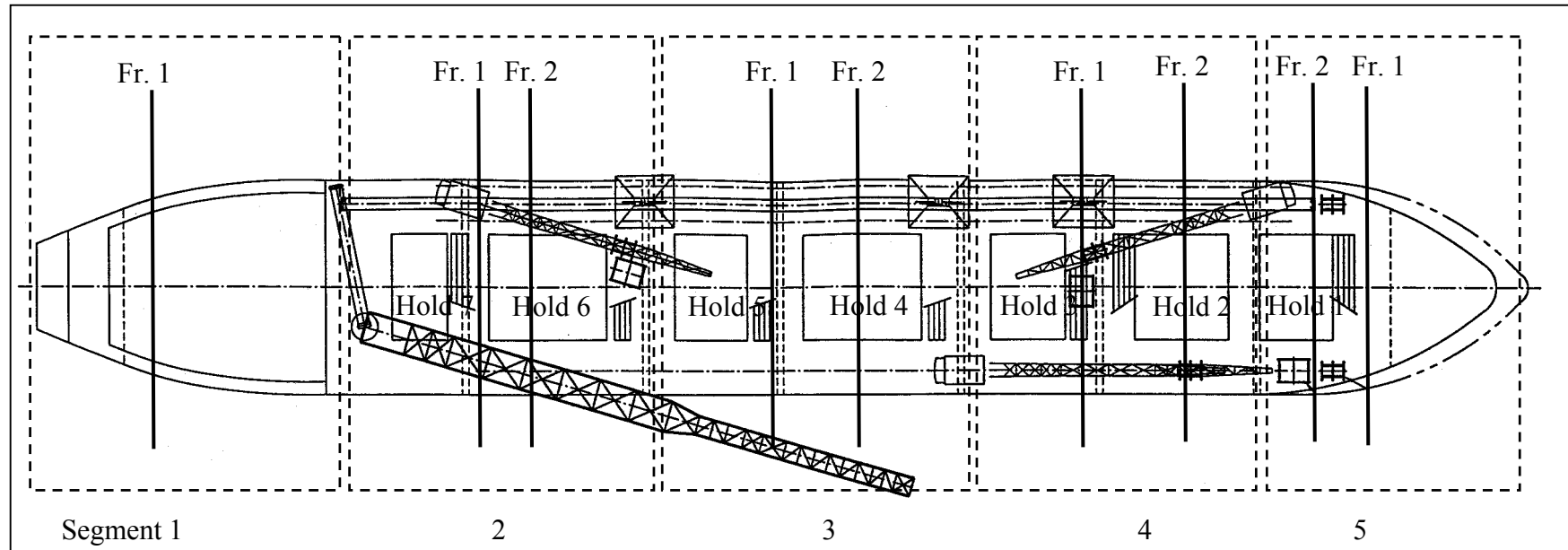


Figure 5.2: General Arrangement of Segments and Frames in the Bulk Carrier

(Only the general location of the frame types for each segment has been shown for clarity)

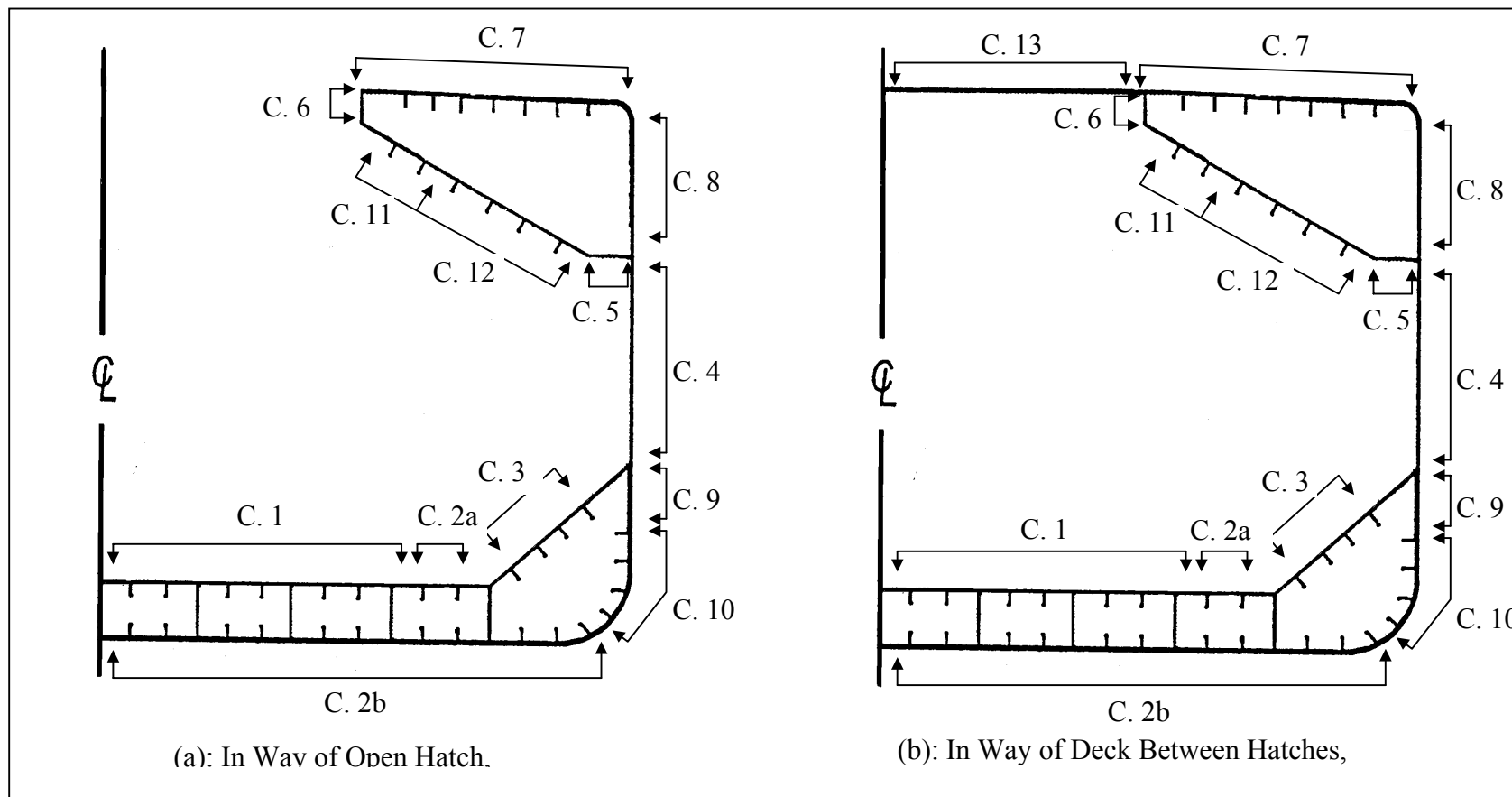


Figure 5.3: Section View of the Bulk Carrier Describing Component Location

(Figure 5.3(a) is the section in way of an open hatch; 5.3(b) is the section in way of the deck between hatches. Both sections shown are the portside half the ship, the ship is symmetric about its longitudinal centerline.)

5.3 Load Assessment

The loading used in the analysis considers extreme load effects comprised of the still water and wave induced moment. The load analysis is completed for ballast and loaded vessel weight distributions individually, however, in practice the relative proportion of time spent in each condition could be considered to develop through life load spectra.

The longitudinal distribution of loads to be applied to the bulk carrier has been idealized to consider the loading on the five longitudinal segments of the vessel. It would be possible to consider different loading conditions for each frame or segment and thus produce more detailed analysis results. The five loading zone condition is used in these examples simply to demonstrate the analysis approach.

The wave and still water bending moments for the bulk carrier were calculated for design operational profiles related to the intended usage of the ship. The combined statistical effects of this service were evaluated as described in SSC 406 - Sea Operational Profiles for Structural Reliability Assessments. The bulk carrier in this example operates on short term contracts which take the vessel all over the world in a year round basis, as shown in the data collection (Glen et. al. 1999). Consequently, the routes for her are the world shipping routes. A typical route from Norfolk (North America) to Hong Kong (Asia) is analyzed in this report. This route includes Marsden Zones 23, 33, 48 56 66, 67, 84, 85, 90, 75, 59, 60, 61, 62 and 40.

The operational characteristics are based upon the joint probability distributions of vessel speed and sea state, shown in Table 5.3 and the joint probability of relative heading and sea state, shown in Table 5.4. This data, as described in SSC 406, describes how hard the vessel is being operated in terms of the likely hood to change direction or speed in light of wave conditions.

Table 5.2: Vessel Component Characteristics for Frame Types 1 and 2**

Segment	Frame Type	Component	N.A. Location*	Plate b_p	Plate t_p	Web t_w	Web h_w	Number
I	1	1	1500	850	20	12	320	9
I	1	2a	1500	850	20	11	280	2
I	1	2b	0	850	20	11	280	11
I	1	3	3092	850	18	11	280	4
I	1	4	7550.00	811	18			7
I	1	5	10735	1000	18			1
I	1	6	14775	650	18			1
I	1	7	15100	850	18	12	320	7
I	1	8	12770	370	18			11
I	1	9	3804	209	18			12
I	1	10	1925	850	18	11	280	4
I	1	11	13087	1000	18	17.5	300	2
I	1	12	11492	1000	18	12	320	4
I	1	13	15100	400	18			17
I	2	1	1500	850	20	12	320	9
I	2	2a	1500	850	20	11	280	2
I	2	2b	0	850	20	11	280	11
I	2	3	3092	850	18	11	280	4
I	2	4	7550.00	811	18			7
I	2	5	10735	1000	18			1
I	2	6	14775	650	18			1
I	2	7	15100	850	18	12	320	7
I	2	8	12770	370	18			11
I	2	9	3804	209	18			12
I	2	10	1925	850	18	11	280	4
I	2	11	13087	1000	18	17.5	300	2
I	2	12	11492	1000	18	12	320	4

* Distance from bottom of hull (keel)

** All dimensions in mm, Geometric parameters described in Section 3.4.2

Table 5.3: Bulk Carrier Joint Probability of Speed and Sea State

Speed (Knots)	Sea State							SUM
	1	2	3	4	5	6	7	
10 - 12	0.0079	0.0000	0.0000	0.0073	0.0133	0.0331	0.0000	0.0616
12 - 14	0.0310	0.0320	0.2172	0.2144	0.1986	0.1532	0.0000	0.8464
14 - 16	0.0000	0.0199	0.0265	0.0290	0.0068	0.0098	0.0000	0.0920
SUM	0.0389	0.0519	0.2437	0.2507	0.2187	0.1961	0.0000	1.0000

Table 5.4: Bulk Carrier Joint Probability of Relative Heading and Sea State

Heading (Degree)	Sea State							SUM
	1	2	3	4	5	6	7	
0	0.0034	0.0100	0.0327	0.0332	0.0242	0.0202	0.0000	0.1236
45	0.0028	0.0072	0.0253	0.0256	0.0194	0.0159	0.0000	0.0963
90	0.0038	0.0116	0.0370	0.0376	0.0272	0.0227	0.0000	0.1400
135	0.0216	0.0190	0.1172	0.1209	0.1141	0.1037	0.0000	0.4964
180	0.0067	0.0065	0.0321	0.0343	0.0317	0.0324	0.0000	0.1437
SUM	0.0383	0.0542	0.2443	0.2516	0.2166	0.1950	0.0000	1.0000

Vessel response to wave encounters were estimated using the linear strip theory program SHIPMO 7 (McTaggart 1997) under the relevant combinations of speed, relative heading, wave height and wave period. More specifically, the ship speeds set in SHIPMO7 were 0, 6, 10, 12, 14 and 16 knots. The heading angles were set at 0, 45, 90, 135 and 180 degrees, where 180 degree represents head seas. Sea states were expressed with BRETSCHEIDER spectrum in terms of wave significant wave heights and peak wave periods. Since the responses and loads are assumed to be linear with respect to wave height, only one wave height was calculated, while the wave zero crossing periods ranged from 3.5 second to 12.5 seconds.

5.3.1 Vertical Bending Moment

The operational profile load analysis indicated that the vessel would be expected to have a mean load zero crossing period of 7.85225 seconds and based upon this and the annual load probability statistics were able to be developed. Table 5.5 presents the probabilities associated with each vertical bending moment magnitude in a given wave encounter (cycle) as well as lifetime load magnitude exceedence probabilities. Figure 5.4 simply displays these load magnitudes and their corresponding probabilities graphically. These results illustrate that the applied moments are higher in the ballast case than in the loaded condition.

The load cycle exceedence probability is related to the life time exceedence probability based on the following equation, assuming that the vessel will encounter 1×10^8 waves in its life time.

$$\text{Prob Ex(lifetime)} = 1 - [1 - \text{Prob Ex(cycle)}]^{100,000,000} \quad (5.1)$$

This formulation assumed that each wave encounter is independant of all others.

Table 5.5: Bulk Carrier Vertical Bending Moment Exceedence Probabilities

	P(exceed) Load Cycle	P(exceed) in life	Segment				
			1	2	3	4	5
Loaded Condition	1.00E-04	1.00E+00	182.7	398.8	439.5	478.1	209.1
	1.00E-06	1.00E+00	294.0	818.8	1069.5	978.1	339.1
	1.00E-08	6.32E-01	406.5	1258.8	1659.5	1443.1	509.1
	1.00E-10	9.95E-03	524.0	1646.3	2174.5	1840.6	689.1
	1.00E-12	1.00E-04	636.5	1986.3	2619.5	2185.6	850.3
	1.00E-14	9.99E-07	737.7	2293.8	3014.5	2493.1	994.1
	1.00E-16	1.11E-08	831.5	2578.8	3374.5	2773.1	1124.1
Ballast Condition	1.00E-04	1.00E+00	580.2	995.0	730.2	868.1	472.0
	1.00E-06	1.00E+00	713.9	1515.0	1450.2	1423.1	699.5
	1.00E-08	6.32E-01	851.4	1980.0	2080.2	1913.1	902.0
	1.00E-10	9.95E-03	975.2	2380.0	2615.2	2323.1	1077.0
	1.00E-12	1.00E-04	1082.7	2730.0	3080.2	2678.1	1229.5
	1.00E-14	9.99E-07	1180.2	3042.5	3500.2	2998.1	1364.5
	1.00E-16	1.11E-08	1267.7	3325.0	3880.2	3288.1	1488.3

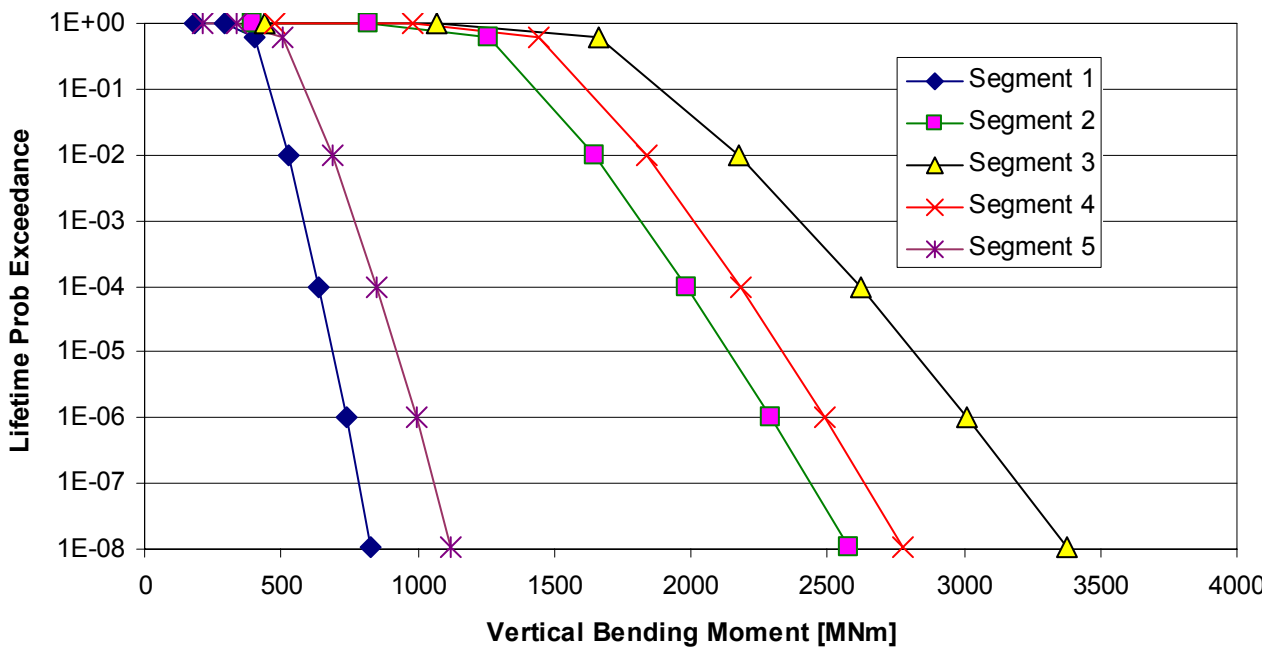


Figure 5.4: Loaded Condition Vertical Bending Moment Exceedence Probability

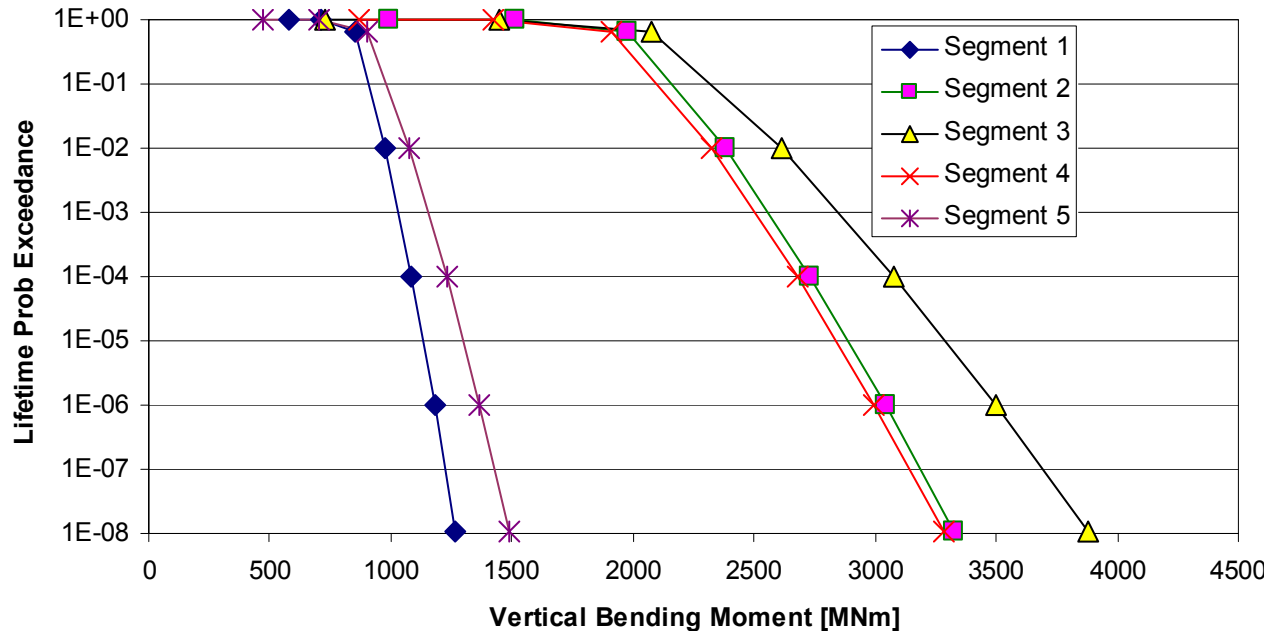


Figure 5.5: Ballast Condition Vertical Bending Moment Exceedance Probability

Load cycle exceedance probabilities indicate the probability of exceeding a given moment magnitude in a single load cycle. This data along with the 20-year design life and the mean zero crossing period (wave period) are used to estimate annual and thus life time statistics. Lifetime load exceedance probabilities = probability of exceeding a given moment magnitude in the lifetime of the vessel (e.g., 20 years or 1×10^8 wave encounters).

5.3.2 Bi-Axial Bending

In order to consider the interaction of horizontal and vertical bending moments, bending moment iso-probability envelopes were assembled. Figures 5.6 through 5.10 illustrate the bending moment envelopes for each segment of the vessel. Since the vessel behaviour is assumed to be symmetric, each of these figures includes both the ballast and loaded vessel condition envelopes by inverting the loaded bending enveloped to plot it on the opposite axis.

The graphs in Figures 5.6 through 5.10 illustrate the interaction of vertical and horizontal bending moment loading. Values on the vertical axis of these graphs may be used to develop the data plotted in the previous section for vertical moment.

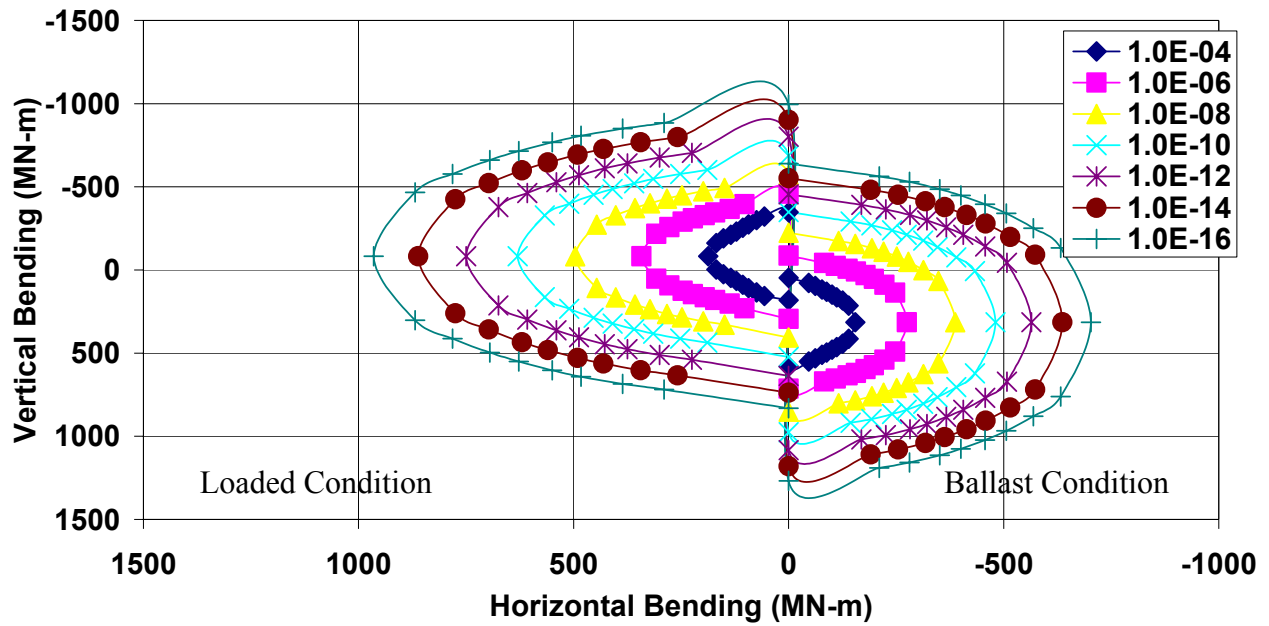


Figure 5.6: Segment 1 Bending Moment Interaction Load Cycle Probability Envelopes

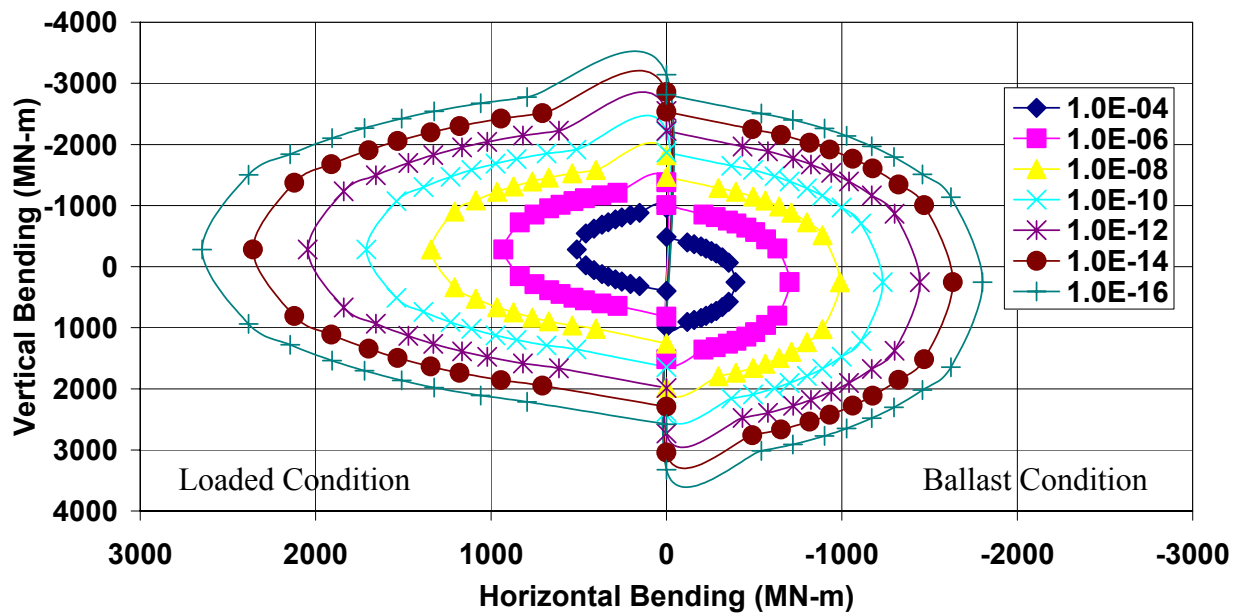


Figure 5.7: Segment 2 Bending Moment Interaction Load Cycle Probability Envelopes

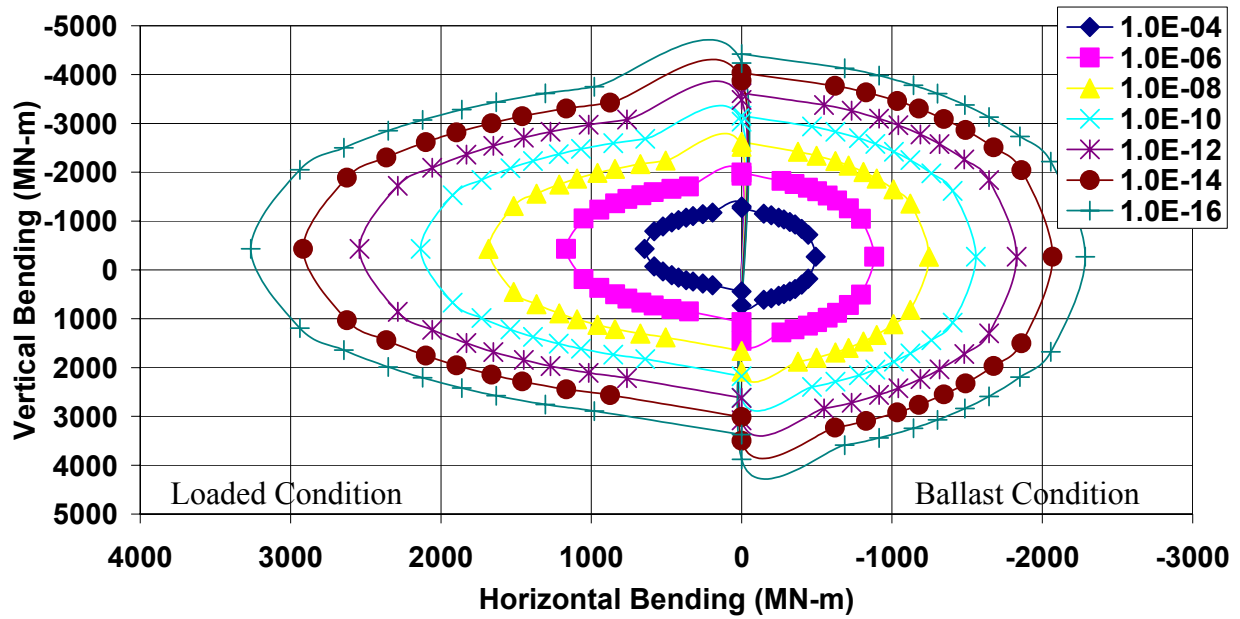


Figure 5.8: Segment 3 Bending Moment Interaction Load Cycle Probability Envelopes

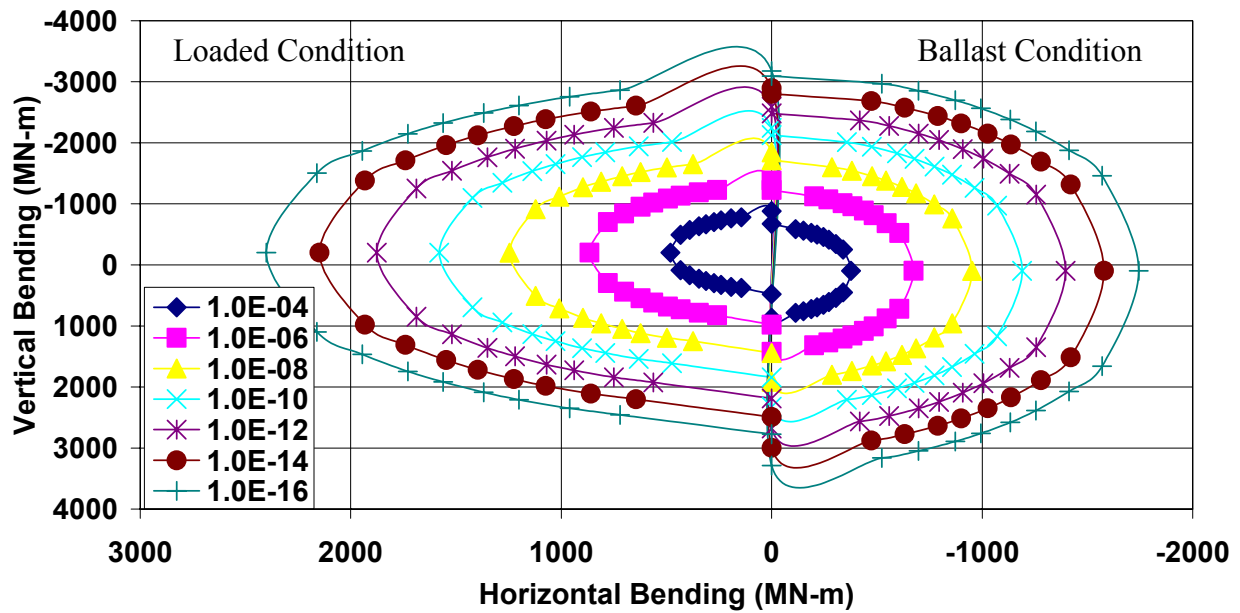


Figure 5.9: Segment 4 Bending Moment Interaction Load Cycle Probability Envelopes

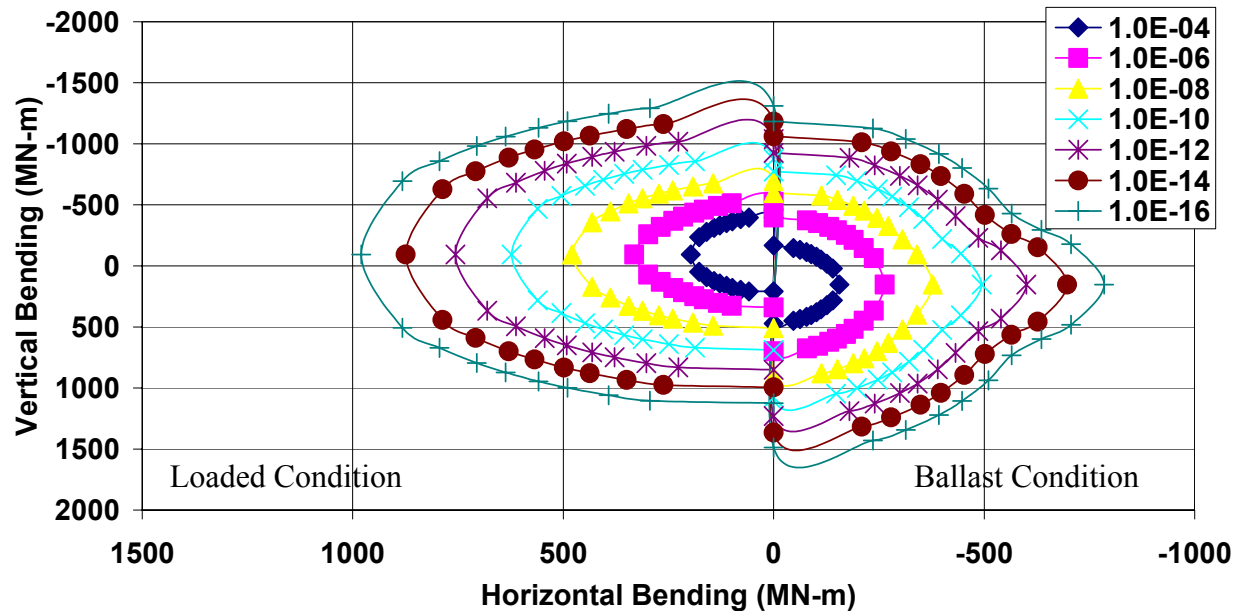


Figure 5.10: Segment 5 Bending Moment Interaction Load Cycle Probability Envelopes

5.4 Definition of Local Detail Characteristics

In this stage of the problem solution process, the characteristics of the previously defined structural details (see Section 3.2) are assigned. The characteristics of interest to this investigation include:

- material properties
- nominal stress transfer functions,
- detail scantling or geometry,
- stress concentration effects,
- stress intensity factor solutions for cracked structural components, and
- residual stress levels.

The information defined at this stage for the analytic approach differs from that used in the numerical (FE) approach. While the analytic approach will use local vessel scantling and geometric data in analytic formulations, the numerical (FE) approach will explicitly identify, stress concentrations, stress intensity factors for given flaw sizes and all of the required stress transfer functions. In the case of the numerical modeling approach, the global and detail finite element model would be assembled in this step.

For the sake of these sample calculations, two cracking locations are being considered: (1) in a stiffened panel in way of the deck opening, and (2) in a stiffened panel forward of the opening as illustrated in Figure 5.10. In these examples, two crack types are considered at each location including: (1) a deck plating through crack, and (2) a deck longitudinal edge crack. The locations of interest and crack types are shown in Figure 5.11.

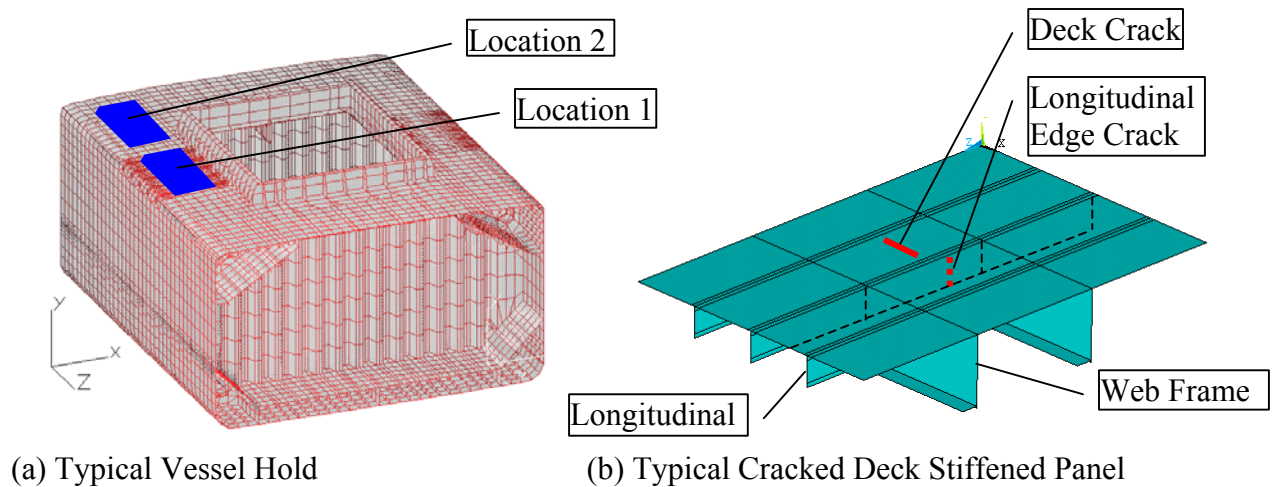


Figure 5.11: Sample Application Cracking Locations of Interest and Crack Types

5.4.1 Material Properties

The material properties used in the analysis are based on the nominal properties of the steel used to fabricate the vessel. The vessel was constructed with AH 32 steel having the following material properties:

- 315 MPa yield stress
- 440 MPa UTS
- 200 GPa modulus of elasticity
- 0.3 Poisson’s Ratio

The fracture toughness transition curve for this steel was conservatively estimated based upon material test data. It is noted, however, that the steel did not have a fracture toughness requirement and as such could be any thing from a very brittle steel to one with high toughness that did not meet the strength requirements of a higher grade of steel that had a fracture toughness requirements. Figure 5.12 presents the fracture toughness transition curve that will be used in this project to demonstrate the effect of operating temperature. The test data and trend line for ABS DH32 is included in the plot as a reference.

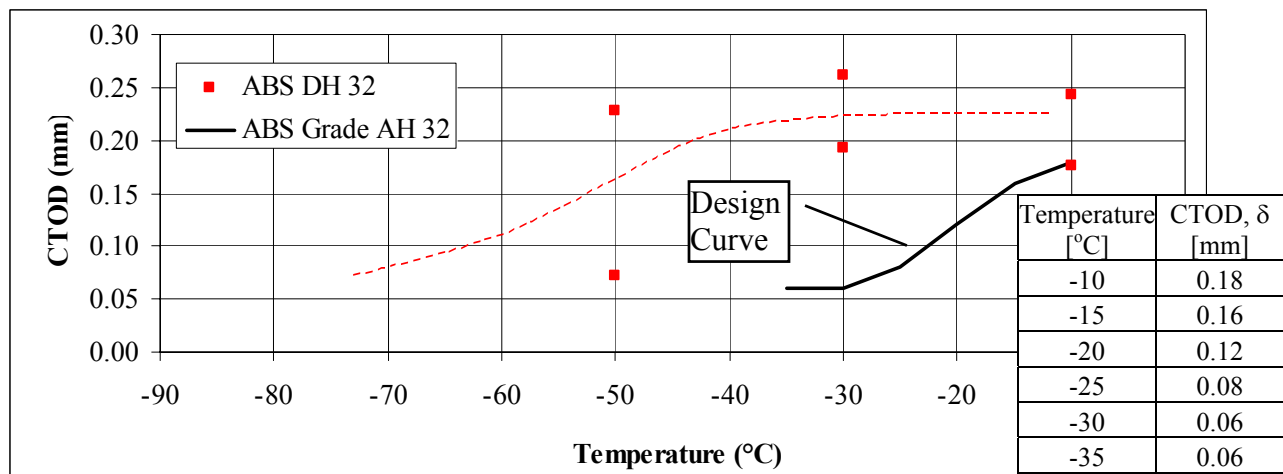


Figure 5.12: Estimated AH36 Fracture Toughness Transition Curve

5.4.2 Stress and Stress Intensity Transfer Function Development

5.4.2.1 Analytic Approach

The nominal stress transfer coefficient is used to relate the applied loading (moment) to the nominal stress. For the analytic approach to the analysis this value is simply the section modulus as listed in Table 5.6 for the open and closed segments of the vessel, locations 1 and 2 (see Figure 5.11), respectively.

Table 5.6: Vessel Analytic Stress Transfer Functions (Section Properties)

Flaw Location	Loading and Frame Type	Moment of Inertia [mm ⁴]	Neutral Axis Distance [mm]	Section Modulus [mm ³]
Deck	Vertical Moment			
	- Open Segment	9.46E+13	9.13E+03	1.04E+10
	- Closed Segment	1.14E+14	8.37E+03	1.36E+10
	Lateral Moment			
Longitudina 1	- Open Segment	3.54E+14	9.83E+03	3.60E+10
	- Closed Segment	3.57E+14	9.83E+03	3.63E+10
	Vertical Moment			
	- Open Segment	9.46E+13	8.91E+03	1.06E+10
	- Closed Segment	1.14E+14	8.15E+03	1.40E+10
	Lateral Moment			
	- Open Segment	3.54E+14	1.03E+04	3.46E+10
	- Closed Segment	3.57E+14	1.03E+04	3.48E+10

The section moduli listed above are used to estimate the nominal stress level as follows:

$$\sigma_{\text{nominal}} = M / S \quad (5.2)$$

where, M is the applied moment, S is the section modulus for the point of interest.

Local stresses considering the geometry of the connection detail may be estimated based on parametric approximations of stress concentration factors for ship details, when these are available. Stress concentration factors (SCF) for a range typical of ship structure details are given by Stambaugh et al (1994), ABS (1992), Cramer et al (1995), and Yoneya et al (1992) for example. Stress concentration factors for typical ship structural details (K_g) and for misalignment effects (K_{te} , K_{ta}) are presented in Appendix B of the Fatigue Design Guide (Glen 1999).

The analyst must exercise extreme care when applying stress concentration factors from different sources to ensure that the correct nominal stress definition is used. For example, in some cases the nominal stress is defined at the intersection point of a connection, in other cases the global nominal stress may be defined at the weld toe or some distance from the weld toe.

Furthermore, the analyst should be aware that sometimes the published stress concentration factor solutions are designed to calculate the "hot spot" stress or the "notch" stress as opposed to the local nominal stress. The analyst should make certain which form of peak stress will result from the application of the SCF.

Local stress concentration effects will be considered using handbook definitions of local stress concentration effects for ship structural details. Figure 5.13 is a sample of the analytic ship structure detail stress concentration factors (SCF) that could be used in a non-numeric analysis. More of these local and global SCF formulations are listed in the SSC Fatigue Design Guide Appendix C. Stress concentration effects are considered explicitly when a numerical (FEA) approach to the problem is considered.

The literature (SSC-405) has the stress concentration factor (SCF) for an opening with geometry shown in Figure 5.11 as 5.0. However, it is noted that this is the SCF for the corner of the opening, and SCF factors away from the corner would be considerably less. To predict the local stresses as a result of the locations proximity to the opening in the deck, a local stress concentration must be determined and applied as follows:

$$\sigma_{\text{nominal}} = M / S * \text{SCF} \quad (5.3)$$

where, SCF is the stress concentration factor for the opening at the location being examined.

In these examples, the stress concentration factor (SCF) applied in the analytic modeling is assumed to be 1.2 to account for the effects of the opening corner on the local stress level. The selection of this value involves engineering judgement and is subjective but may be guided by tabulated stress concentration effect analytic formulations.

A key requirement of local damage tolerance assessment for fatigue and fracture is the ability to evaluate stress intensity factors (SIF) for ship structural details containing cracks. The rigorous derivation of the SIF can be found in most advanced texts on fracture mechanics and so only a brief overview will be presented here. A crack represents a very sharp notch (i.e., notch radius $\rightarrow 0$) and in an ideal elastic body the stresses approach infinity at the crack tip. By studying the conditions near the tip of a crack in an elastic body, it can be shown that the stress and displacement fields can be expressed in terms of three elastic SIF's corresponding to the three modes of fracture (Figure 5.14, [Almer-Naess 1985]): K_I for Mode I (Opening Mode), K_{II} for Mode II (Sliding Mode), and K_{III} for Mode III (Tearing Mode)). Any crack problem can be considered to be a combination of these three basic modes of fracture. However, since there is always a tendency for a brittle fracture to propagate in the direction that minimizes the shear loading (i.e. perpendicular to the maximum principal stress), the first mode is generally regarded as the most important and in this application only the mode I fracture is considered.

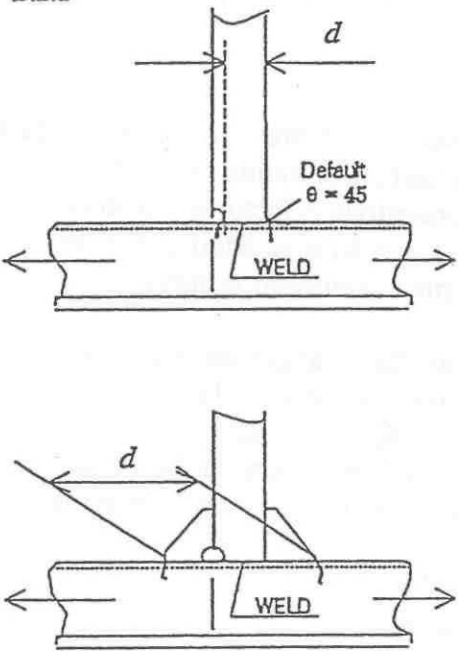
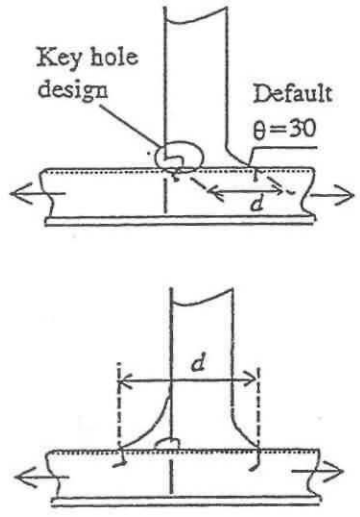
Geometry	K-factor								
<p>B.2.a</p> 	<p>For supporting members welded to stiffener flange:</p> <table border="0"> <tr> <td>$K_g \cdot K_w = 18$</td> <td>$d \leq 50$</td> </tr> <tr> <td>$K_g \cdot K_w = 19$</td> <td>$50 < d \leq 100$</td> </tr> <tr> <td>$K_g \cdot K_w = 2.0$</td> <td>$100 < d \leq 150$</td> </tr> <tr> <td>$K_g \cdot K_w = 2.2$</td> <td>$d > 150$</td> </tr> </table> <p>For supporting members welded to stiffener web by overlap with weld throat thickness as given in $\beta.5a$ (Table $\beta.5$), the above factors are to be multiplied by a factor 1.15</p> <p>Note: The weld connection area between supporting members and stiffener flange must fulfil the requirements in Rules.</p>	$K_g \cdot K_w = 18$	$d \leq 50$	$K_g \cdot K_w = 19$	$50 < d \leq 100$	$K_g \cdot K_w = 2.0$	$100 < d \leq 150$	$K_g \cdot K_w = 2.2$	$d > 150$
$K_g \cdot K_w = 18$	$d \leq 50$								
$K_g \cdot K_w = 19$	$50 < d \leq 100$								
$K_g \cdot K_w = 2.0$	$100 < d \leq 150$								
$K_g \cdot K_w = 2.2$	$d > 150$								
<p>B.2.b</p> 	<table border="0"> <tr> <td>$K_g \cdot K_w = 1.6$</td> <td>$d \leq 50$</td> </tr> <tr> <td>$K_g \cdot K_w = 1.7$</td> <td>$50 < d \leq 100$</td> </tr> <tr> <td>$K_g \cdot K_w = 1.8$</td> <td>$100 < d \leq 150$</td> </tr> <tr> <td>$K_g \cdot K_w = 2.0$</td> <td>$d > 150$</td> </tr> </table> <p>For supporting member welded to stiffener, flange only. It is assumed that the weld is kept clear of flange edge.</p> <p>Note: The weld connection area between supporting members and stiffener flange must fulfil the requirements in Rules.</p>	$K_g \cdot K_w = 1.6$	$d \leq 50$	$K_g \cdot K_w = 1.7$	$50 < d \leq 100$	$K_g \cdot K_w = 1.8$	$100 < d \leq 150$	$K_g \cdot K_w = 2.0$	$d > 150$
$K_g \cdot K_w = 1.6$	$d \leq 50$								
$K_g \cdot K_w = 1.7$	$50 < d \leq 100$								
$K_g \cdot K_w = 1.8$	$100 < d \leq 150$								
$K_g \cdot K_w = 2.0$	$d > 150$								

Figure 5.13: Sample Ship Structure SCF Formulations

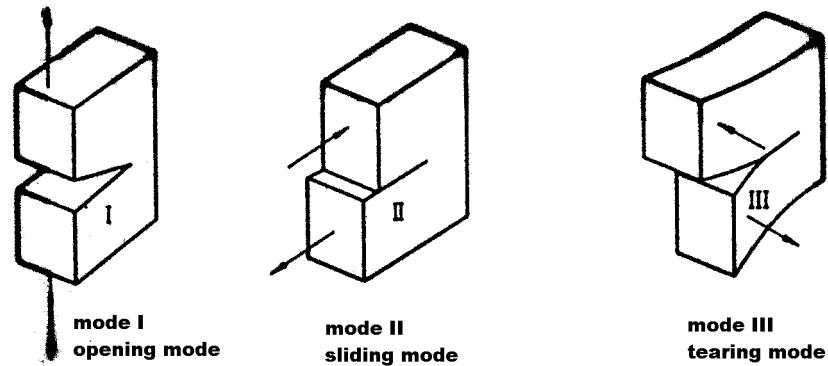


Figure 5.14: Three Modes of Cracking

Various techniques are available to calculate stress intensity factors. When time and resources do not permit the direct (FE based) calculation of K_I , estimates can be obtained using handbook solutions for simplified geometries and loadings that most closely resemble the actual conditions at the crack location. Stress intensity factor solutions are commonly presented in the following form:

$$K_I = \sigma \cdot Y \cdot \sqrt{(\pi a)} \quad (5.4)$$

where:

- σ = a reference local nominal or "field" stress at the crack location
- Y = stress intensity factor correction
- a = crack size parameter

The stress intensity magnification factor, Y , is a function of crack geometry, structural geometry and mode of loading. The reference nominal stress at the crack location is determined from a local stress analysis of the uncracked body. For residual strength assessments, the reference nominal stress corresponds to the stresses under the extreme load condition (including residual stresses). The membrane and bending components of stress usually require separate correction functions and thus the stress intensity factor solution is somewhat more complex than that outlined above.

For the analytic sample applications, the crack tip stress intensity factors and reference stress values were developed based upon analytic formulations. These formulations are presented in Sections 4.1 and 4.2 for the centre cracked panel and the longitudinal edge crack, respectively. The stress intensity factors are developed considering the crack geometry (length) and applied local stress levels.

5.4.2.2 Numerical Approach

The basis for the definition of stress and stress intensity transfer functions lies in the development of a global finite element model. In this case, the global model is a basic shell model created in ALGOR, shown in Figure 5.15. Note the locations chosen for sub-modeling, denoted as "Location 1" and "Location 2".

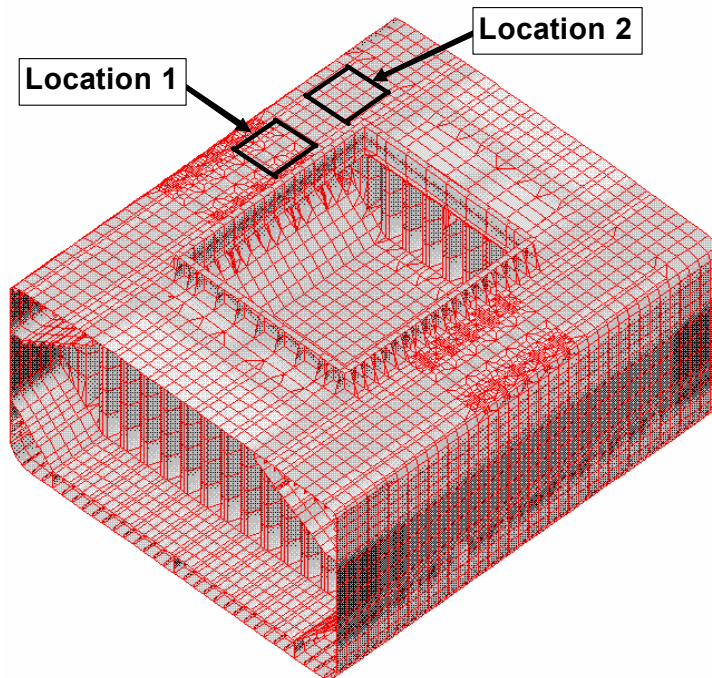


Figure 5.15: ALGOR Shell Finite Element Model

Figure 5.16 shows the basic primary sub-model geometry used in the study of the fracture assessment of the bulk carrier. The primary sub-model structure, completed in ANSYS, includes the deck with three longitudinal stiffeners, and two transverse stiffeners. The coordinate axes used in the solid model, shown in red. Due to the repetitive nature of the ship structure shown in Figure 5.15, the same ANSYS sub-model could be used to model both Location 1 and Location 2 shown in Figure 5.16.

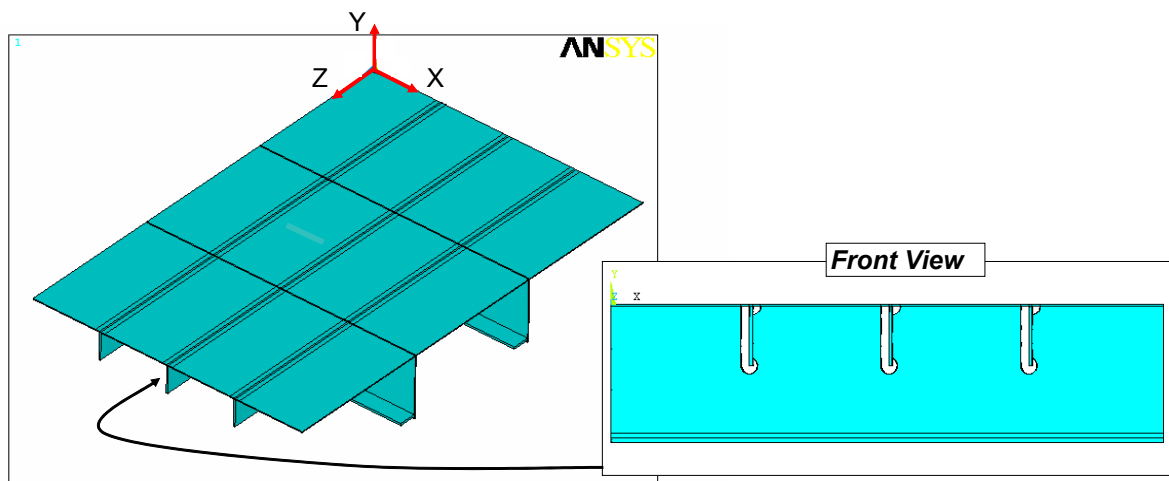


Figure 5.16: Basic ANSYS Primary Shell Solid Model Geometry

To model the two types of cracks (deck and longitudinal edge crack) within the solid geometry shown in Figure 5.11, additional finer mesh sub-models were created. In these examples, three longitudinal edge crack lengths and three-deck transverse through crack lengths were modeled.

Two types of shell sub-models were created, one set of models with cracks, and the other without cracks. The cracked sub-models contained the aforementioned through crack and the other with the edge crack. These cracked models were used to accurately estimate the local displacement fields in the region of the crack. No special crack tip elements were used in these cracked models, as these models would not be used to analyze the crack tip stress intensity factors. These cracked shell sub-models were to be used as a basis for another set of cracked sub-models using brick elements to estimate more accurate displacement results near the crack tip.

The shell sub-model without a crack was used to determine local stresses in the structure due to the proximity to the opening in the deck.

To summarize, the sequence of models and subsequent sub-models is outlined below:

- Create global shell model in ALGOR to represent the repetitive global nature of the full ship structure (see Figure 5.15).
- Create a primary localized uncracked shell model in ANSYS and use the nodal displacements from *Step 1* as boundary conditions (see Figure 5.16).
- Create a primary localized cracked shell model in ANSYS and use the nodal displacements from *Step 1* as boundary conditions. Each crack type (edge and through) and crack length is fully represented.
- Create further localized (secondary) cracked brick sub-models in ANSYS using the displacements from *Step 3* as boundary conditions to fully capture crack tip fields.

For the sub-modeling used in these examples, ANSYS 7.0 was used to create the geometry. A swept mesh was used wherever possible, to avoid using tetrahedral type elements, and achieve more accurate results. When brick elements were used, the structure had at least 2 elements through the thickness. More could have been used, if it was desired to more accurately capture through thickness effects while sacrificing computational time. For the initial shell sub-model, both cracked and uncracked, approximately 6000 SHELL181 elements were used in each, with a solution time in the order of a few minutes.

Displacements for both shell sub-models were taken from the original ALGOR model. These were taken as nodal displacements from the ALGOR model, and applied to the edges of the shell model using linear interpolation between specified ALGOR nodal points.

Both basic shell sub-model meshes are shown below, with the through crack sub-model shown in Figure 5.17, and the edge crack sub-model shown in Figure 5.18. In both figures, the crack location is shown as a yellow line. Note that in Figure 5.17, one is looking down at the deck of the sub-model with the stiffeners hidden underneath, as in Figure 5.16. However, in Figure 5.18, one is looking up at the deck, showing the underlying stiffeners. Both figures give a representation of the location of the through and edge crack locations.

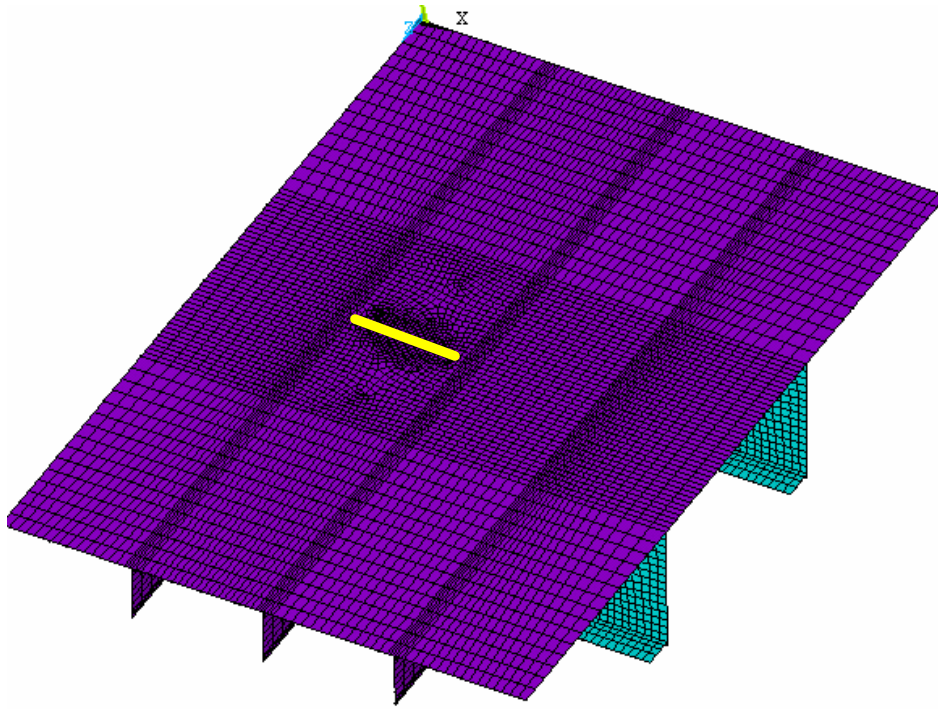


Figure 5.17: Through Crack Shell Finite Element Model

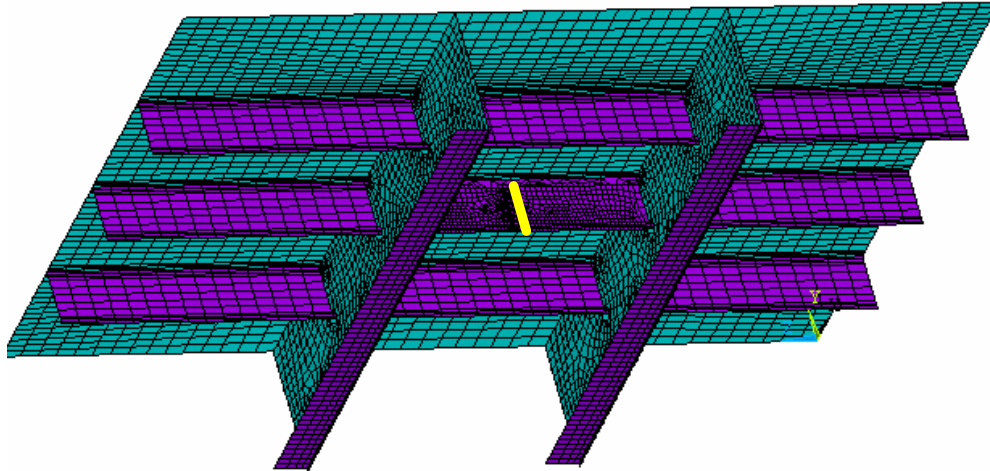


Figure 5.18: Edge Crack Shell Finite Element Model

Figures 5.19 and 5.20 show the solid brick sub-models used to examine the crack tip behaviour in greater detail. Again, the crack location is shown as a yellow line in both figures. These solid brick sub-models use displacements from the cracked shell sub-models as boundary conditions along their edges to simulate their placement within the global model.

For the edge cracked brick sub-model, approximately 12000 SOLID95 elements were used, with a solution time of approximately 10 minutes. The through crack solid model contained a slightly more complex geometry, requiring approximately 30000 SOLID95 elements to mesh it with a satisfactory density. The solution time for this model was approximately an hour. In both models, special crack tip elements were used (see Figures 5.19 and 5.20).

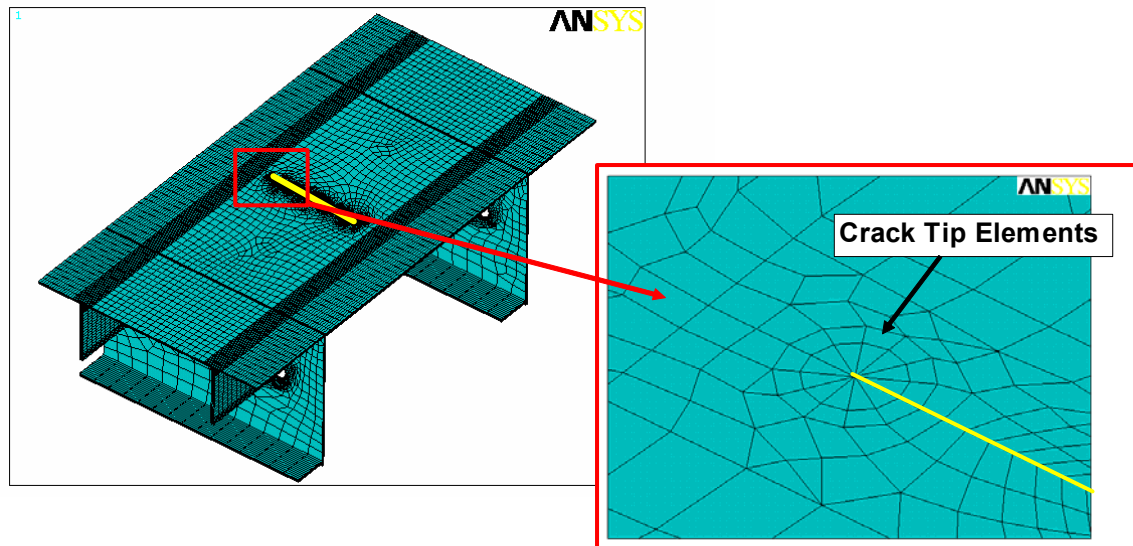


Figure 5.19: Through-Crack Brick Finite Element Model

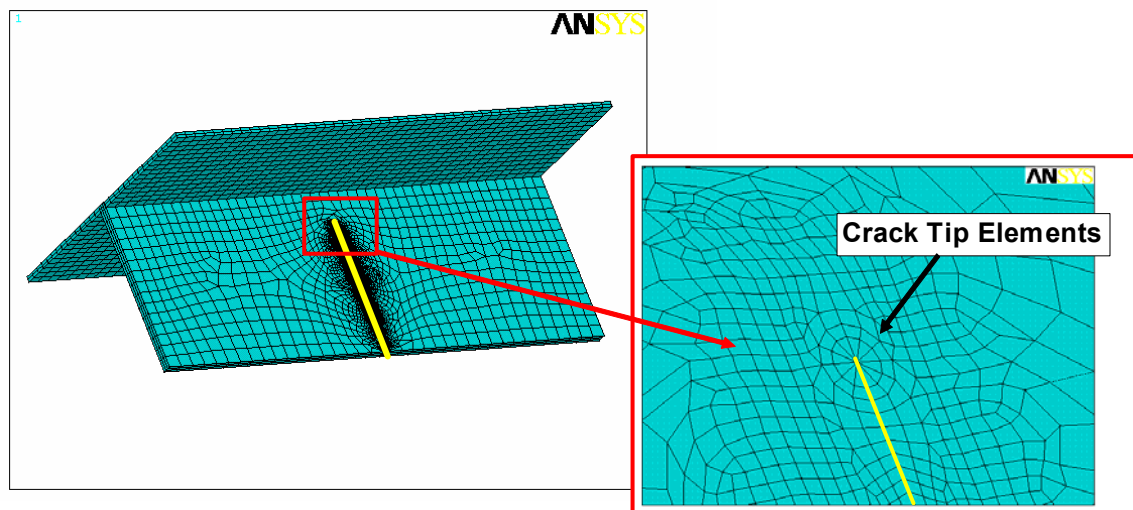


Figure 5.20: Edge Crack Brick Finite Element Model

As mentioned previously, due to the repetitive nature of the ship structure modeled in ALGOR, the same models in ANSYS could be used in two different locations in the global model structure. Thus, each location (see Figure 5.15) was used to assess two crack types with each three lengths each. In addition, to evaluate the effect of vertical wave-induced bending and lateral bending loads, two load cases were considered.

Since the fully numeric analysis approach requires that the crack size be included in the FE model, one a discrete number of crack sizes were assessed. The crack lengths considered in

these examples are described in Table 5.7. It is noted, however, that the results of a series of these analyses could be used to develop a relationship between stress intensity factor and crack size. This is, in general, the basis for the development of the analytic stress intensity factor formulations.

Table 5.7: Crack Model Description

Crack Type	Crack Length [mm]
Deck Plate Through Crack	50
	160
	600
Deck Longitudinal Edge Crack	25
	125
	270

The shell sub-models used in these examples, as mentioned above, are geometrically similar for both cracked and uncracked sub-models. That is, both shell sub-models use the same solid model, depending on the type of crack to be modeled, the crack type and location can vary between an edge crack or through crack. Figure 5.21 shows the view of the solid model along the z-axis of the global model (refer to Figure 5.16). Figure 5.22 shows the same solid model, but along the x-axis. In both of the aforementioned figures, all dimensions shown are in mm. Note that the stiffeners are all evenly spaced throughout the sub-model (i.e., at 850mm intervals transversely, and 1700mm intervals longitudinally).

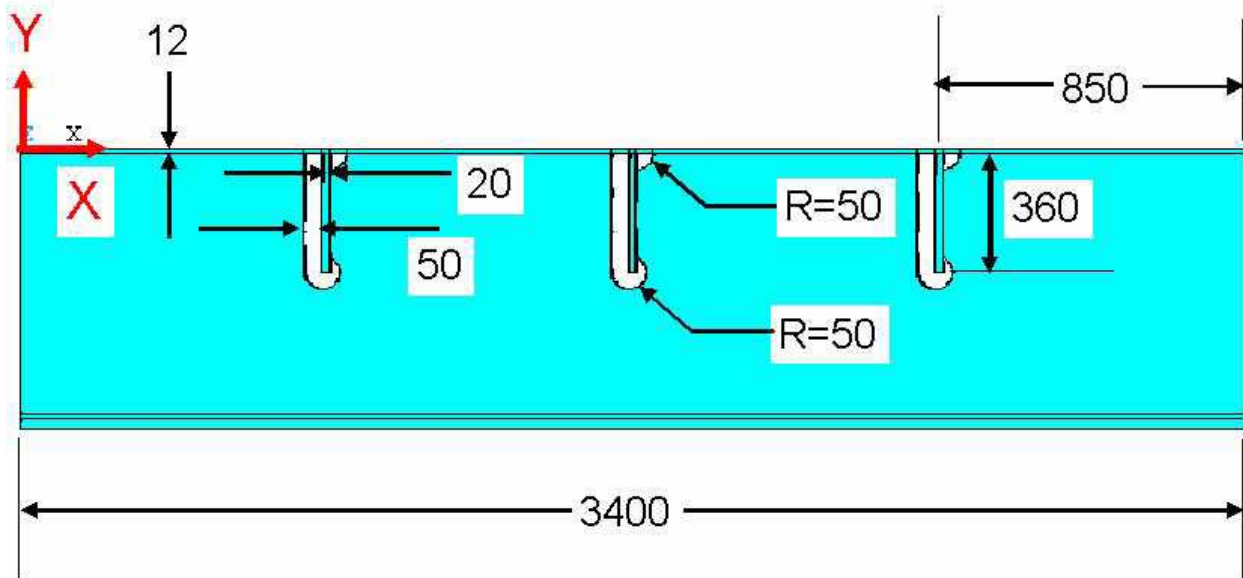


Figure 5.21: View of Solid Model along Z-Axis (All Dimensions in mm)

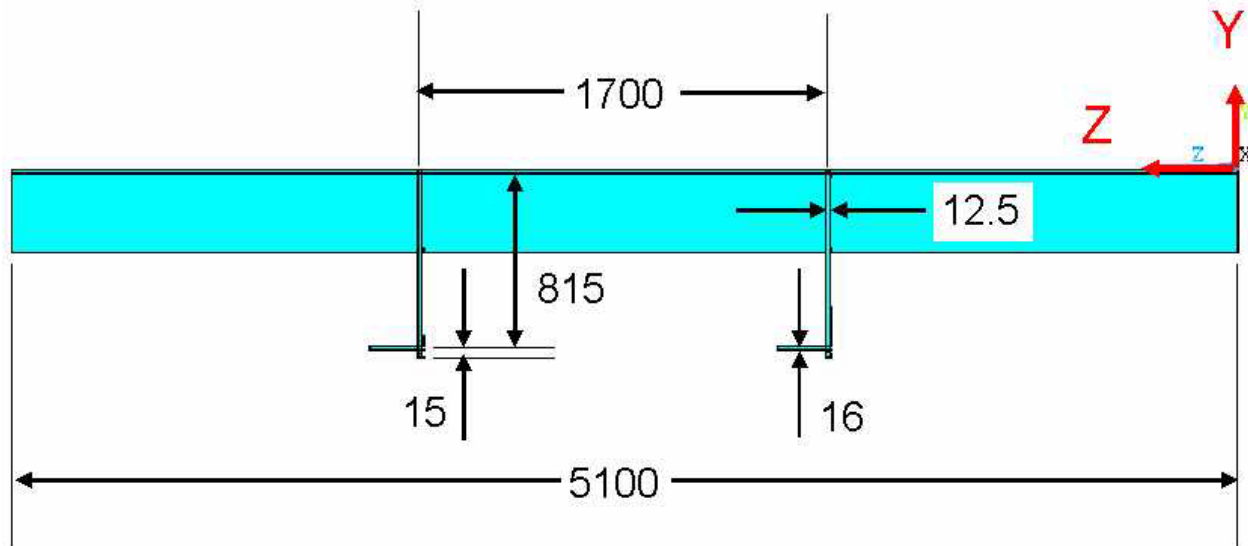


Figure 5.22: View of Solid Model along X-Axis (All Dimensions in mm)

Two load scenarios are applied to the global ALGOR FE model, a moment to produce horizontal bending, and a moment to produce vertical bending. This was achieved by using a force-couple. These are summarized in Table 5.8 below:

Table 5.8: Global FE Model Load Case Summary

<i>Load Case 1</i>	<i>Vertical Bending</i>	
Force Couple	33000	N
Moment Arm	15100	mm
Applied Moment	4.98E+08	Nmm
<i>Load Case 2</i>	<i>Horizontal Bending</i>	
Force Couple	14000	N
Moment Arm	27600	mm
Applied Moment	3.86E+08	Nmm

In terms of the ANSYS model illustrated in Figure 5.16, vertical bending refers to bending in the YZ-plane, whereas horizontal bending refers to bending in the XZ-plane.

Once the finite element analyses were completed, the behaviour of the local details and cracks can be related to the applied loading and crack lengths. The sub-models were used to estimate effective stress concentration factors while the cracked brick sub-models were used to identify stress intensity factors (SIF). The finite element model presented with the ANSYS uncracked shell model was used to derive local stresses in the model due to the deck opening, and these were compared to those predicted analytically, to estimate the SCF of the opening at the crack locations of interest. This step is included for the sake of comparison only.

To simplify the FE model analysis process, the local stress and stress intensity factor solutions were used to develop transfer functions for the behaviour of the structure and cracks at the locations of interest.

The FEA results for each particular crack type and length at each location and load case had a particular stress intensity factor (SIF). The nominal analytic stresses were calculated using the analytic formula presented in Section 5.4.2.1. The local FEA stresses were extracted from the ANSYS uncracked finite element models where the cracks would be located if they were present. Stresses extracted from the FE models were perpendicular to the crack face. Below is a summary of the nominal and local stresses, along with each particular stress concentration factor (SCF), with the SCF defined as:

$$SCF = \frac{\sigma_{local}}{\sigma_{nominal}} \quad (5.5)$$

Tables 5.9 and 5.10 summarize the SIF and local stress data for both crack types, locations, and load cases. FEA local stresses are stresses taken from the uncracked ANSYS shell model at that particular crack plane, whereas analytical local stresses are stresses calculated using Equation (2), with a SCF of 1.2:

Table 5.9: Analytic and Numeric Edge Crack SIF and Stress Summary

LoadCase	Location	Crack Type	Crack Length, d (mm)	Analytical Local Stress (MPa)	FEA Local Stress (MPa)	FEA - K1 (MPa*sqrt(mm))	Analytical - K1 (MPa*sqrt(mm))
1	1	Edge	25	0.0515	0.0430	0.4485	0.5530
			125			1.2557	1.7233
			270			2.3069	2.2519
1	2	Edge	25	0.0427	0.0438	0.4456	0.5802
			125			1.2566	1.8079
			270			2.3280	2.3625
2	1	Edge	25	0.0134	0.0103	0.1102	0.1269
			125			0.3047	0.3954
			270			0.5507	0.5166
2	2	Edge	25	0.0133	0.0111	0.1183	0.1360
			125			0.3160	0.4237
			270			0.5894	0.5536

Table 5.10: Analytic and Numeric Through Crack SIF and Stress Summary

LoadCase	Location	Crack Type	Crack Length, d (mm)	Analytical Local Stress (MPa)	FEA Local Stress (MPa)	FEA - K1 (MPa*sqrt(mm))	Analytical - K1 (MPa*sqrt(mm))
1	1	Thru	50	0.0529	0.0551	0.4594	0.5858
			150			0.6828	1.0011
			600			1.3413	1.5573
1	2	Thru	50	0.0439	0.0576	0.4824	0.6126
			150			0.7224	1.0470
			600			1.4197	1.6286
2	1	Thru	50	0.0129	0.0111	0.0938	0.1185
			150			0.1368	0.2025
			600			0.2689	0.3150
2	2	Thru	50	0.0128	0.0121	0.1016	0.1287
			150			0.1494	0.2200
			600			0.2937	0.3423

It should be noted that for through cracks the SIF shown in the above tables is that of an average between the two end crack tips, as there was no appreciable difference between the two values this averaging was not necessary. The load cases refer the vertical and horizontal bending, respectively. In general, the local stresses and stresses for the analytic and numeric results agree reasonably well while the stress intensity factor results differ by up to 40%.

To permit the evaluation of the effects of various applied load levels, the stress intensity factor solutions developed for specific applied load levels are used to develop transfer functions. These transfer functions will be applied to the moments expected for a given probability level to convert these moments into stresses as a function of probability level. Tables 3.3 and 3.4 show these transfer functions for edge and through cracks, respectively. These transfer functions come about by the following formulae:

$$\sigma_{prob} = M_{prob} \frac{\sigma_{applied}}{M_{applied}} \quad (5.6)$$

where, σ_{prob} is the calculated stress level for a given probability of moment exceedence, M_{prob} is the moment level for a given probability of moment exceedence, $\sigma_{applied}$ is the applied stress level determined analytically or by FEA methods, and $M_{applied}$ is the applied moment used in the FEA and analytic methods. Care must be taken to ensure units are accounted for and consistent.

Similarly, SIF transfer functions ($\sigma_{applied}/K_{applied}$) are developed using:

$$K_{prob} = \sigma_{prob} \frac{K_{applied}}{\sigma_{applied}} \quad (5.7)$$

where, K_{prob} is the calculated SIF for a given probability of stress, $K_{applied}$ is the SIF resulting from the crack length considered undergoing the applied stress level, $\sigma_{applied}$.

Table 5.11: Edge Crack Transfer Functions

Load Case	Location	Applied Moment N.mm	Analysis	Moment to Stress	Stress to K_I Transfer Function		
				Transfer Function (M/ σ)	Crack Length		
					25mm	125mm	270mm
1	1	4.98E+08	FEA	1.16E+10	0.096	0.034	0.019
1	2	4.98E+08	FEA	1.14E+10	0.098	0.035	0.019
2	1	3.86E+08	FEA	3.74E+10	0.094	0.034	0.019
2	2	3.86E+08	FEA	3.48E+10	0.094	0.035	0.019
1	1	4.98E+08	Analytical	9.68E+09	0.093	0.030	0.023
1	2	4.98E+08	Analytical	1.17E+10	0.074	0.024	0.018
2	1	3.86E+08	Analytical	2.88E+10	0.106	0.034	0.026
2	2	3.86E+08	Analytical	2.90E+10	0.098	0.031	0.024

Table 5.12: Through Crack Transfer Functions

Load Case	Location	Applied Moment N.mm	Analysis	Moment to Stress	Stress to K_I Transfer Function		
				Transfer Function (M/ σ)	Crack Length		
					50mm	150mm	600mm
1	1	4.98E+08	FEA	9.04E+09	0.120	0.081	0.041
1	2	4.98E+08	FEA	8.65E+09	0.119	0.080	0.041
2	1	3.86E+08	FEA	3.47E+10	0.119	0.081	0.041
2	2	3.86E+08	FEA	3.19E+10	0.119	0.081	0.041
1	1	4.98E+08	Analytical	9.42E+09	0.090	0.053	0.034
1	2	4.98E+08	Analytical	1.13E+10	0.072	0.042	0.027
2	1	3.86E+08	Analytical	3.00E+10	0.109	0.064	0.041
2	2	3.86E+08	Analytical	3.03E+10	0.099	0.058	0.037

5.4.3 Component Cross-Section Geometry

Section properties ($Y_{cg_{m,n}}$ and $I_{m,n}$) will be estimated based on the geometry of the structural components. Local component geometries will be defined in terms of the as-built area of plating and stiffeners as shown below.

Depending on the location of cracks (e.g., plating vs. stiffening element) of interest, the basic structural component geometry is defined in terms of the component stiffener and plate thickness and lengths as defined above. In assigning these section properties, effective thicknesses will have to be assigned for stiffeners with flanges to ensure that the stiffener area is preserved. In calculating section moments of inertia, the contribution of the component moment of inertia about its own axis will be neglected. The centroid of the component area will be defined by the keel offset ($Y_{m,n,j}$) defined previously for nominal stress calculation.

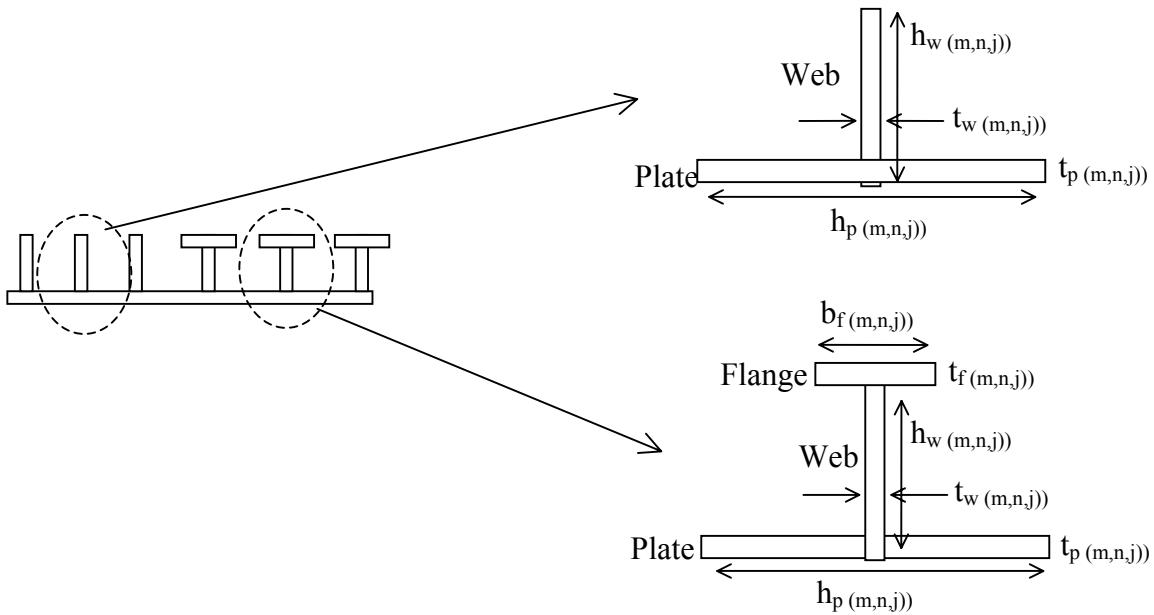


Figure 5.23: Component Geometric Definition

5.4.4 Residual Stress

Residual stresses caused by welding and fabrication are self-equilibrating stresses necessary to satisfy compatibility in the structure. These stresses in themselves do not contribute to plastic collapse since they arise from strain/displacement limited phenomena, and therefore do not influence the abscissa in the Failure Assessment Diagram (FAD) (S_r or L_r) (see Section 3.5). However, residual stresses do add to the crack driving force and therefore have to be included in the calculation of K_{app} for residual strength assessments.

Ideally, one would establish the residual stress magnitude based on actual measurements and resolve them into their membrane and bending components (i.e., σ_{rm} and σ_{rb}). However, that is impractical, therefore, conservative estimates of residual stresses based on findings in the technical literature and on the location of the flaw (weld zone or base metal) and orientation with respect to the weld, are incorporated in the analysis.

The following guidelines can be used to estimate the magnitude of residual stresses to be incorporated into the residual strength assessment. As before, the approach depends on the level of detail of the fracture assessment being performed. For the assessment being performed:

- If the actual distribution of residual stresses is known, then these can be incorporated by linearizing the distribution such that the assumed residual stresses are greater than the actual (measured) stresses over the flaw depth. The linearized residual stress distribution can then be separated into its membrane and bending components.

- A reasonable estimate of residual stresses can be based on some typical residual stress distributions given in (PD6493 1991) for butt, fillet and pipe welds (see Figure 5.24). Parametric equations have been developed corresponding to these distributions and their use can reduce the conservatism in the assumption of "yield strength residual stresses in as-welded joints". Still, the use of these parametric equations pre-supposes some knowledge of the weld joint restraint during fabrication.
- The most conservative approach remains the assumption of uniform, yield strength level, residual stresses as in the Level 1 FAD analysis.

If the reference (net section) stress is deemed high enough to cause plasticity at the crack tips, a certain amount of residual stress relief occurs and the residual stress can be appropriately reduced to the minimum of:

- a) σ_y
- b) σ_r based on approximate distributions
- c) $(1.4 - \sigma_n / \sigma_f) \sigma_y$ for Level 2 FAD with S_r abscissa
- d) $(1.4 - \sigma_n / 1.2\sigma_y) \sigma_y$ for Level 2 FAD's with L_r abscissa

The evaluation of reference stress, σ_n , the stress in the presence of the flaw, is presented in Sections 3 and 4. Clearly, the reference stress must be of the order of 50% of the yield strength in order to get any residual stress relief due to plasticity.

When the flaw tips are in the base metal and away from the weld (2 to 3 plate thicknesses), then the weld residual stresses are negligible. However, there are some longer range assembly and construction stresses that still may be present. These may be relieved to some extent with service (shake down effect) or as the crack grows. However, this effect is difficult to predict and therefore, as a conservative measure, longer range residual stresses equal to 20% of the yield strength are recommended to be included in a fracture analysis.

In the sample applications three residual stress levels were considered. These include 0, 50 and 100% of the material yield stress. Some additional results are presented to demonstrate their effect on the failure assessment.

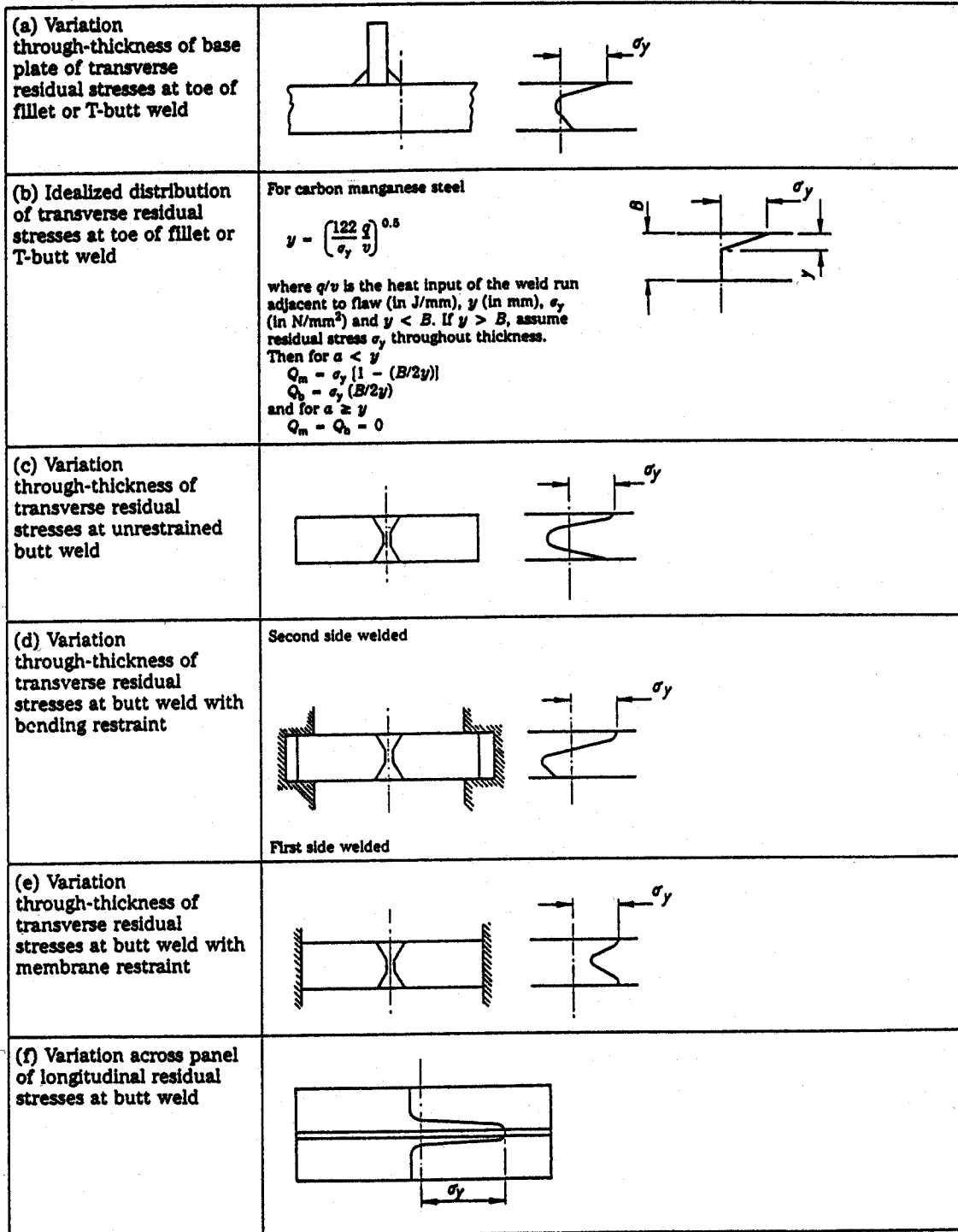


Figure 5.24: Typical Distributions of Residual Stresses at Welds

5.5 Failure Assessment

5.5.1 General Approach

In the failure assessment process, the applied loading data is combined with the structural behaviour transfer functions (stress and stress intensity) and material property data. The general steps in this process for the numerical analysis and analytic analysis processes are outlined below. These may be applied to any ship structure. The steps taken for the analytic or numerical approaches do not differ significantly as shown below.

Step	Analytic	Numerical
1	Collect material property (i.e., CTOD, yield stress, ultimate strength, etc.), residual stress, geometric data required for the assessment and applied loading data.	
2	Develop or collect vessel section modulus data to develop nominal stress transfer functions and stress concentration factors.	Use Global and local finite element models to develop local structural stress responses to global loads
3	Identify appropriate stress intensity factor solutions to relate local stresses and stress intensity factors, $K_I(\sigma_{local})$.	Create local sub-models to relate the applied loading to the crack stress intensity factors, $K_I(\sigma_{local})$.
4	Determine the probability of moment exceedence for the section of the ship being considered. Using the stress transfer functions transform the applied moment exceedence values into stress level probability of exceedence values.	
5	Construct failure assessment diagrams for specific flaw size and location to determine critical stress.	
6	Compare critical stress with stress level probabilities of occurrence/exceedence to complete failure assessment.	

The data described in steps 1 through 3 has been outlined in the previous sections and the sections that follow will illustrate these results by presenting some sample results.

5.5.2 Derivation of Detail Stress Exceedence Probabilities

Stress level exceedence probabilities are developed by applying the nominal stress transfer functions, stress concentration factors to the applied moment probability of exceedence plots similar to those shown in Figures 5.4 or 5.5. It is noted that the stress transfer functions to be applied are related to the sense of the applied loading (e.g., vertical moment stress transfer function needs to be applied to vertical moment exceedence probability data).

Figure 5.25 presents a sample probability of stress exceedence plot developed using the numerical stress transfer functions for location 1 of the vessel (beside the deck opening) applied to the vertical bending moment data. Similar plots can be developed for each location for horizontal and vertical bending moments.

Figure 5.26 is a similar plot developed for the analytic stress transfer functions. Plots similar to 5.25 and 5.26 illustrate that stress levels increase from the ends of the vessel (segments 1 and 5) to the mid ship area (segment 3). It is also noted that the stress levels estimated based upon analytic stress transfer functions develop higher applied stresses for the same applied moments.

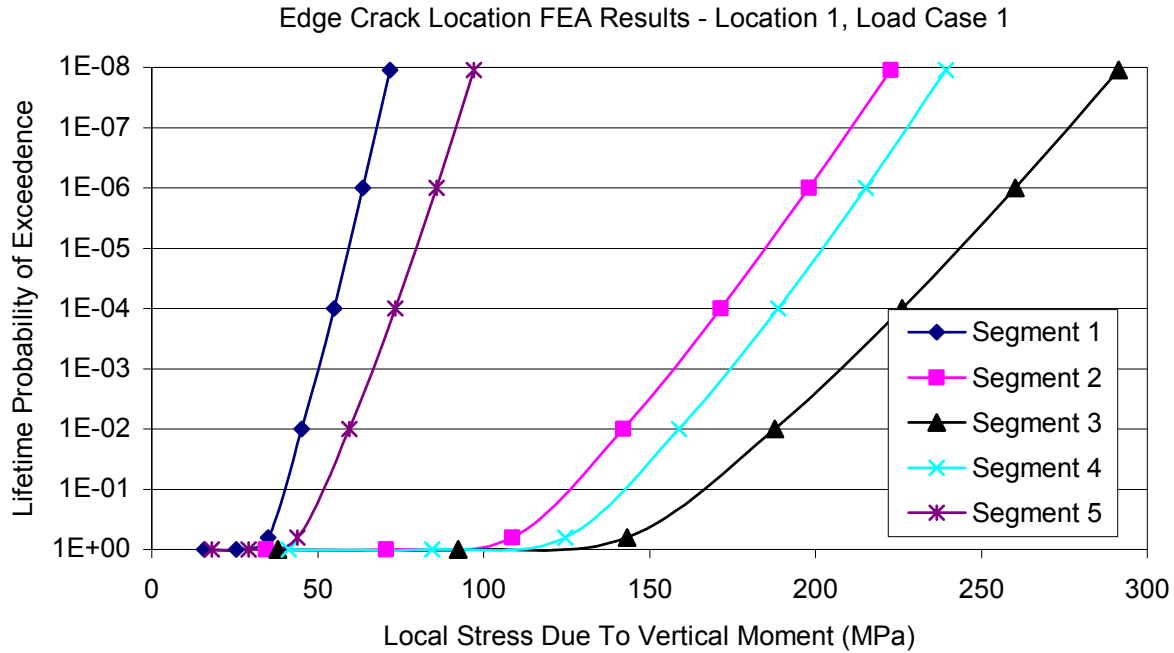


Figure 5.25: Sample Numeric Vertical Bending Moment Local Stress Exceedence Probabilities

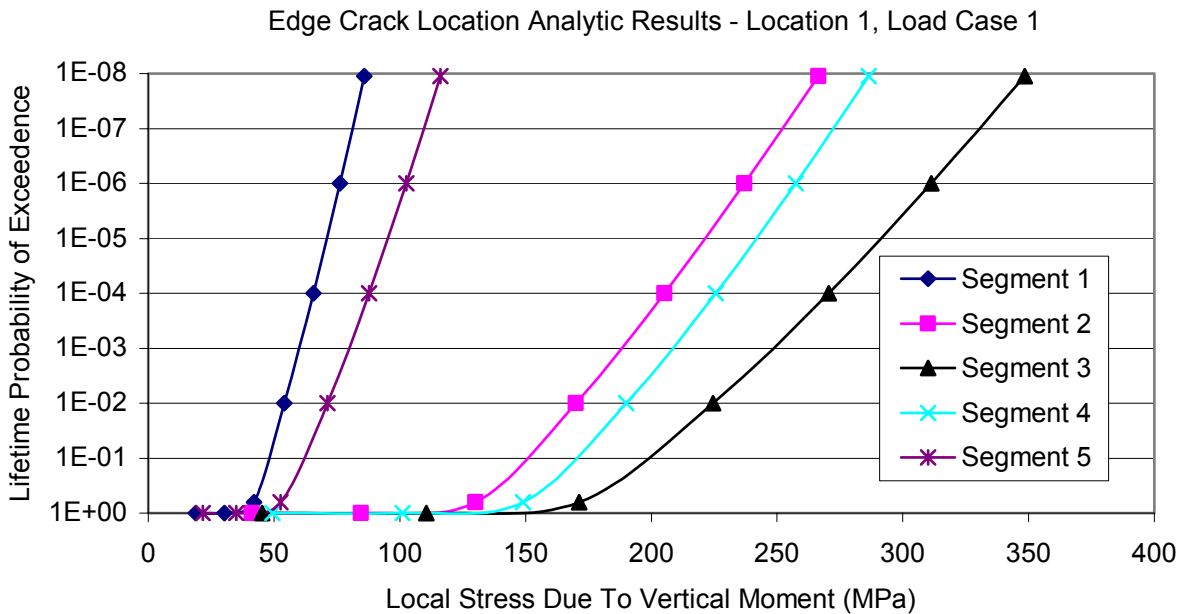


Figure 5.26: Sample Analytic Vertical Bending Moment Local Stress Exceedence Probabilities

When the applied load envelopes shown in Figures 5.6 to 5.10 are considered, the stress transfer functions are applied to each component of the applied loading (vertical and horizontal moment) to estimate a combined total stress for each applied load combination. The maximum stress level associated with all vertical and horizontal moment combinations at a given probability of exceedence are plotted in Figure 5.27 to illustrate the effect of load component interaction on stress exceedence probabilities. These results differ from those considering only vertical or horizontal bending (e.g., Figure 5.25) in that they predict somewhat higher stress levels. Using the previously defined stress intensity transfer functions, similar graphs defining the probability of stress intensity factor value exceedence may be defined.

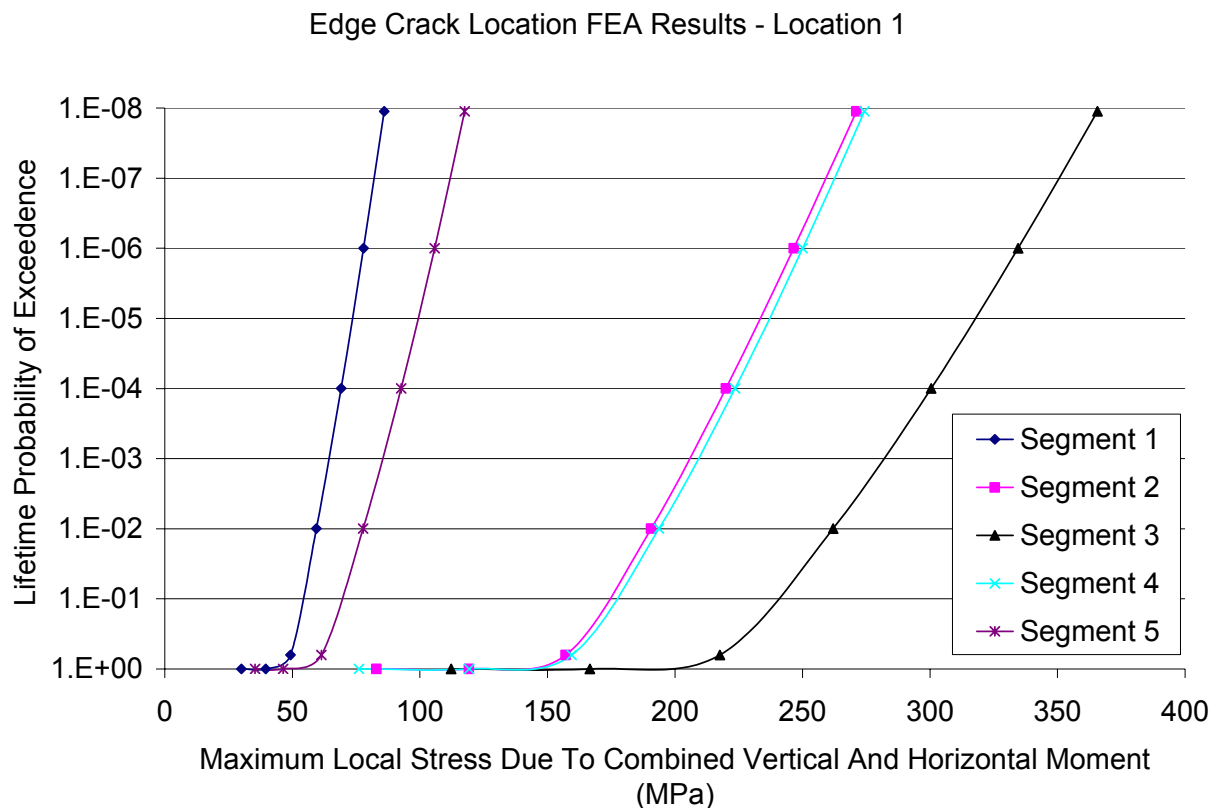


Figure 5.27: Sample Numeric Combined Vertical and Horizontal Bending Moment Local Stress Exceedence Probabilities

5.5.3 Definition of Crack Critical Stress Levels

The next step in the failure assessment is to consider the potential for failure of given crack types, and sizes subjected to various levels of residual stress. This step is completed using the simplified Level 2B failure assessment approach outlined in previous sections. To consider the probabilistic stress levels expressed in the previous graphs (Figures 5.25 to 5.27) the critical stress level for a given crack type and size is derived. A critical stress is defined as the applied loading (wave bending induced) stress that would promote failure (fracture or plastic collapse of the crack). These critical stresses can then be compared to the probability of exceeding a stress level to estimate the probability of failure at various locations in the vessel.

To limit the volume of results presented below, the sample application results consider a range of: vessel stations, crack types and sizes, material properties, and a residual stress levels. Critical stress levels are determined for two CTOD values associated with 10°C and –30°C operating temperatures that could be associated with heated and unheated structural elements. As well, results were generated for several residual stress levels (0%, 15%, 20%, 30%, 50%, and 100% of the yield stress) to demonstrate their effect on the critical stress levels. These parameters were used to develop critical stress levels for each flaw type and size, for a total of 36 critical stress values for each flaw type, or 72 critical stress values for both edge and through cracks and are presented in Tables 5.13 and 5.14.

Note that if a residual stress level is too high, in that it alone promotes failure the reported critical stress level is reported as zero. Failure was considered to occur when the calculated safety factor was less than 1.0. Tables 5.13 and 5.14 give these values for the crack lengths considered for edge and through cracks, respectively. These results, which are independent of location in the vessel, demonstrate several expected trends including:

- critical stress level decreases with increasing residual stress,
- critical stress level decreases with decreasing fracture toughness or decreasing temperature,
- critical stress level decreases with increasing crack size, and
- through cracks are more resistant to failure than edge cracks in that they demonstrate higher critical stress levels. This result is related to the fact that the resistance to failure is carried by two crack tips in and edge crack rather than one as in an edge crack.

Table 5.13: Edge Crack Critical Stresses

Crack Size	CTOD	Residual Stress	Residual Stress	Critical Stress
(mm)	(mm)	% σ_y	(MPa)	(MPa)
25	0.06	0%	0.0	172.9
25	0.06	15%	47.3	162.7
25	0.06	20%	63.0	156.9
25	0.06	30%	94.5	140.4
25	0.06	50%	157.5	70.7
25	0.06	100%	315.0	0.0
125	0.06	0%	0.0	65.2
125	0.06	15%	47.3	42.9
125	0.06	20%	63.0	10.6
125	0.06	30%	94.5	0.0
125	0.06	50%	157.5	0.0
125	0.06	100%	315.0	0.0
270	0.06	0%	0.0	35.8
270	0.06	15%	47.3	0.0
270	0.06	20%	63.0	0.0
270	0.06	30%	94.5	0.0
270	0.06	50%	157.5	0.0
270	0.06	100%	315.0	0.0
25	0.18	0%	0.0	272.5
25	0.18	15%	47.3	264.6
25	0.18	20%	63.0	260.5
25	0.18	30%	94.5	249.3
25	0.18	50%	157.5	217.4
25	0.18	100%	315.0	0.0
125	0.18	0%	0.0	108.9
125	0.18	15%	47.3	95.5
125	0.18	20%	63.0	86.0
125	0.18	30%	94.5	51.6
125	0.18	50%	157.5	0.0
125	0.18	100%	315.0	0.0
270	0.18	0%	0.0	60.7
270	0.18	15%	47.3	36.0
270	0.18	20%	63.0	0.0
270	0.18	30%	94.5	0.0
270	0.18	50%	157.5	0.0
270	0.18	100%	315.0	0.0

Table 5.14: Through Crack Critical Stresses

Crack Size	CTOD	Residual Stress	Residual Stress	Critical Stress
(mm)	(mm)	% σ_y	(MPa)	(MPa)
50	0.06	0%	0.0	208.7
50	0.06	15%	47.3	198.8
50	0.06	20%	63.0	193.9
50	0.06	30%	94.5	180.7
50	0.06	50%	157.5	135.1
50	0.06	100%	315.0	0.0
150	0.06	0%	0.0	145.7
150	0.06	15%	47.3	134.5
150	0.06	20%	63.0	127.7
150	0.06	30%	94.5	107.3
150	0.06	50%	157.5	0.0
150	0.06	100%	315.0	0.0
600	0.06	0%	0.0	69.6
600	0.06	15%	47.3	50.3
600	0.06	20%	63.0	33.0
600	0.06	30%	94.5	0.1
600	0.06	50%	157.5	0.0
600	0.06	100%	315.0	0.0
50	0.18	0%	0.0	296.0
50	0.18	15%	47.3	296.0
50	0.18	20%	63.0	296.0
50	0.18	30%	94.5	296.0
50	0.18	50%	157.5	284.5
50	0.18	100%	315.0	138.9
150	0.18	0%	0.0	229.9
150	0.18	15%	47.3	221.2
150	0.18	20%	63.0	216.4
150	0.18	30%	94.5	203.5
150	0.18	50%	157.5	166.1
150	0.18	100%	315.0	0.0
600	0.18	0%	0.0	87.3
600	0.18	15%	47.3	87.3
600	0.18	20%	63.0	87.3
600	0.18	30%	94.5	58.9
600	0.18	50%	157.5	0.0
600	0.18	100%	315.0	0.0

5.5.4 Definition of Crack Failure Probabilities

The probability of failure for a given flaw type and size based upon an assumed residual stress level may be estimated by superimposing the critical stress level results in Tables 5.13 and 5.14 on the previously developed stress level exceedence plots (Figures 5.25 to 5.27). A sample of this form of result is shown in Figure 5.28 for several through crack conditions. The probability of failure may be estimated by considering the intersection of the critical stress levels with the stress exceedence plots.

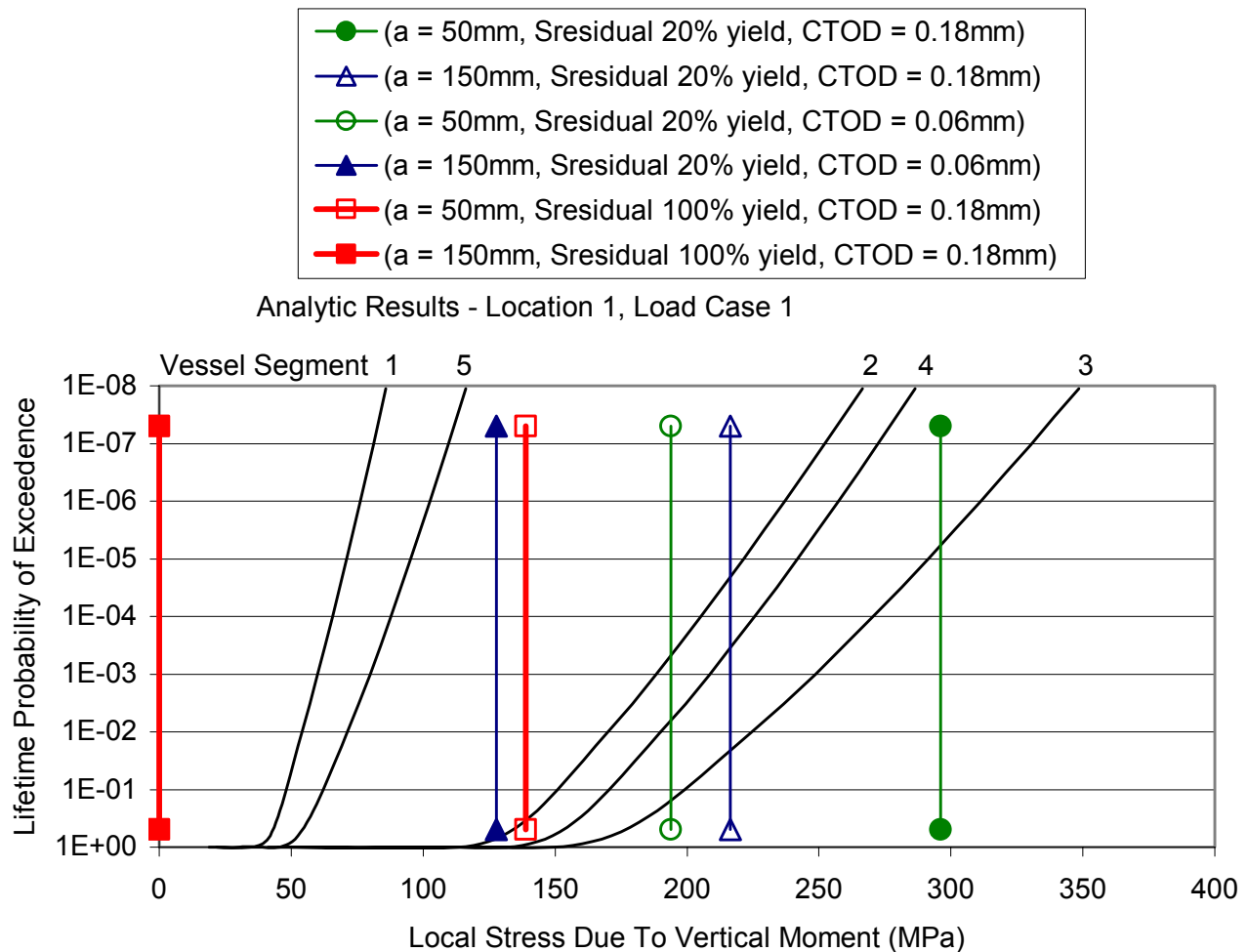


Figure 5.28: Sample Through Crack Probability of Failure Values

Figure 5.28 defines the probability of exceeding specified stress levels in each of the five vessel longitudinal segments. The vertical lines in this graph define critical stress levels for six deck through cracks with given lengths (a), residual stress levels and fracture toughness values. The intersection of a vertical line may be used to define the probability of failure. For example the probability of failure for a 50mm through crack in segment 3 (midship area), assuming a 20% yield level residual stress and a CTOD value of 0.18mm, is approximately 2×10^{-5} over the life of the vessel. The same crack is shown to have less than a 1×10^{-8} probability of failure over the life of the vessel in any other segment of the vessel.

The results illustrated in Figure 5.28 illustrate that increasing flaw size, reducing fracture toughness, and increasing residual stress all serve to increase the probability of failure of a crack. In the limit, the probability of failure of these cracks is 1 indicating that they would certainly fail during the life of the vessel. Similar comparisons of crack critical stress levels could be completed for probabilities of stress level exceedence during a single vessel transit developing mission or transit probabilities of failure and thus be used to define the urgency of maintenance activities.

Alternatively, deterministic failure assessment results may be developed by defining a target or design probability of exceedence. This would define a design stress level in each segment of the vessel. Based upon this, any flaw with a critical stress level less than the design or target stress level would be deemed acceptable.

5.6 Application of the Results

As opposed to assessing individual flaws, as was done in the previous section, maintenance management guidance information may be developed by defining critical crack sizes. A critical crack size is defined as a crack that would be expected to fail at a specified stress level or with a given failure probability. In this section, critical crack sizes (length) are defined for all stations considered in the sample application. These results are presented as an example of the use of the vessel fracture assessment as a maintenance guidance tool for the acceptance of crack like defects.

In this set of calculations, a stress level had to be selected. Local stresses that were calculated analytically for each station at the lifetime probability of vertical moment exceedence level equal to 10^{-6} were considered. Note that vertical bending was considered analytically for Load Case 1 only. For each of these stress states, residual stresses of 0% yield and 100% yield were also considered.

For through cracks, where the critical crack length for a given stress state was calculated to be greater than the length of the panel (in this case, 830mm) the length of the panel was given as the critical crack length.

The results of these calculations are provided in Tables 5.15 through 5.18 for edge and through cracks assuming 0 and 100% (yield stress) residual stress levels. These results illustrate that:

- larger flaws may be accepted at stations further away from the midship (e.g., segment 1 and 5),
- larger flaws are acceptable at location 2 (away from the deck opening) due to lower stress levels,
- the assumption of higher residual stress levels reduces the acceptable flaw size,
- vertical hull girder bending (load case 1) produces higher stress levels and thus results in smaller acceptable flaw sizes, and
- in general, edge cracks become critical at shorter lengths than deck cracks.

Similar analysis results could be completed for a wider range of locations and fracture toughness (temperature) values within each segment of the vessel to define an acceptable flaw size map that could be overlaid on a plan of the vessel to guide inspection result interpretation.

Table 5.15: Edge Crack Critical Crack Lengths; 0% Yield Residual Stress

Load Case	Location	Station	CTOD (mm)	Residual Stress % yield	Residual Stress (MPa)	Analytical Local	Critical
						Membrane Stress (MPa)	Crack Length (mm)
1	1	Segment 1	0.18	0%	0.0	76.2	171.0
2	1	Segment 1	0.18	0%	0.0	25.6	360.0
1	2	Segment 1	0.18	0%	0.0	63.3	360.0
2	2	Segment 1	0.18	0%	0.0	25.4	360.0
1	1	Segment 2	0.18	0%	0.0	236.9	35.3
2	1	Segment 2	0.18	0%	0.0	79.7	162.3
1	2	Segment 2	0.18	0%	0.0	196.7	50.5
2	2	Segment 2	0.18	0%	0.0	79.0	163.8
1	1	Segment 3	0.18	0%	0.0	311.4	19.1
2	1	Segment 3	0.18	0%	0.0	104.7	120.6
1	2	Segment 3	0.18	0%	0.0	258.5	29.4
2	2	Segment 3	0.18	0%	0.0	103.9	121.6
1	1	Segment 4	0.18	0%	0.0	257.5	29.6
2	1	Segment 4	0.18	0%	0.0	86.6	148.0
1	2	Segment 4	0.18	0%	0.0	213.8	43.3
2	2	Segment 4	0.18	0%	0.0	85.9	149.3
1	1	Segment 5	0.18	0%	0.0	102.7	123.2
2	1	Segment 5	0.18	0%	0.0	34.5	360.0
1	2	Segment 5	0.18	0%	0.0	85.3	150.5
2	2	Segment 5	0.18	0%	0.0	34.2	360.0
1	1	Segment 1	0.06	0%	0.0	76.2	95.7
2	1	Segment 1	0.06	0%	0.0	25.6	221.8
1	2	Segment 1	0.06	0%	0.0	63.3	117.9
2	2	Segment 1	0.06	0%	0.0	25.4	222.1
1	1	Segment 2	0.06	0%	0.0	236.9	13.0
2	1	Segment 2	0.06	0%	0.0	79.7	90.7
1	2	Segment 2	0.06	0%	0.0	196.7	19.8
2	2	Segment 2	0.06	0%	0.0	79.0	91.6
1	1	Segment 3	0.06	0%	0.0	311.4	6.7
2	1	Segment 3	0.06	0%	0.0	104.7	62.8
1	2	Segment 3	0.06	0%	0.0	258.5	10.6
2	2	Segment 3	0.06	0%	0.0	103.9	63.5
1	1	Segment 4	0.06	0%	0.0	257.5	10.7
2	1	Segment 4	0.06	0%	0.0	86.6	81.7
1	2	Segment 4	0.06	0%	0.0	213.8	16.5
2	2	Segment 4	0.06	0%	0.0	85.9	82.5
1	1	Segment 5	0.06	0%	0.0	102.7	64.6
2	1	Segment 5	0.06	0%	0.0	34.5	360.0
1	2	Segment 5	0.06	0%	0.0	85.3	83.3
2	2	Segment 5	0.06	0%	0.0	34.2	360.0

Table 5.16: Edge Crack Critical Crack Lengths; 100% Yield Residual Stress

Load Case	Location	Station	CTOD (mm)	Residual Stress % yield	Residual Stress (MPa)	Analytical Local Membrane Stress (MPa)	Critical Crack Length (mm)
1	1	Segment 1	0.18	100%	315.0	76.2	20.7
2	1	Segment 1	0.18	100%	315.0	25.6	22.3
1	2	Segment 1	0.18	100%	315.0	63.3	21.2
2	2	Segment 1	0.18	100%	315.0	25.4	22.3
1	1	Segment 2	0.18	100%	315.0	236.9	11.4
2	1	Segment 2	0.18	100%	315.0	79.7	20.6
1	2	Segment 2	0.18	100%	315.0	196.7	13.7
2	2	Segment 2	0.18	100%	315.0	79.0	20.6
1	1	Segment 3	0.18	100%	315.0	311.4	9.1
2	1	Segment 3	0.18	100%	315.0	104.7	19.3
1	2	Segment 3	0.18	100%	315.0	258.5	10.3
2	2	Segment 3	0.18	100%	315.0	103.9	19.4
1	1	Segment 4	0.18	100%	315.0	257.5	10.3
2	1	Segment 4	0.18	100%	315.0	86.6	20.2
1	2	Segment 4	0.18	100%	315.0	213.8	12.7
2	2	Segment 4	0.18	100%	315.0	85.9	20.3
1	1	Segment 5	0.18	100%	315.0	102.7	19.4
2	1	Segment 5	0.18	100%	315.0	34.5	22.1
1	2	Segment 5	0.18	100%	315.0	85.3	20.3
2	2	Segment 5	0.18	100%	315.0	34.2	22.1
1	1	Segment 1	0.06	100%	315.0	76.2	7.2
2	1	Segment 1	0.06	100%	315.0	25.6	7.8
1	2	Segment 1	0.06	100%	315.0	63.3	7.4
2	2	Segment 1	0.06	100%	315.0	25.4	7.8
1	1	Segment 2	0.06	100%	315.0	236.9	3.9
2	1	Segment 2	0.06	100%	315.0	79.7	7.1
1	2	Segment 2	0.06	100%	315.0	196.7	4.7
2	2	Segment 2	0.06	100%	315.0	79.0	7.2
1	1	Segment 3	0.06	100%	315.0	311.4	3.1
2	1	Segment 3	0.06	100%	315.0	104.7	6.7
1	2	Segment 3	0.06	100%	315.0	258.5	3.5
2	2	Segment 3	0.06	100%	315.0	103.9	6.7
1	1	Segment 4	0.06	100%	315.0	257.5	3.5
2	1	Segment 4	0.06	100%	315.0	86.6	7.0
1	2	Segment 4	0.06	100%	315.0	213.8	4.4
2	2	Segment 4	0.06	100%	315.0	85.9	7.0
1	1	Segment 5	0.06	100%	315.0	102.7	6.7
2	1	Segment 5	0.06	100%	315.0	34.5	7.7
1	2	Segment 5	0.06	100%	315.0	85.3	7.0
2	2	Segment 5	0.06	100%	315.0	34.2	7.7

Table 5.17: Through Crack Critical Crack Lengths; 0% Yield Residual Stress

Load Case	Location	Station	CTOD (mm)	Residual Stress	Residual Stress	Analytical Local	Critical
				% yield	(MPa)	Membrane Stress (MPa)	Crack Length (mm)
1	1	Segment 1	0.18	0%	0.0	78.3	830.0
2	1	Segment 1	0.18	0%	0.0	24.6	830.0
1	2	Segment 1	0.18	0%	0.0	65.0	830.0
2	2	Segment 1	0.18	0%	0.0	24.4	830.0
1	1	Segment 2	0.18	0%	0.0	243.5	94.9
2	1	Segment 2	0.18	0%	0.0	76.4	830.0
1	2	Segment 2	0.18	0%	0.0	202.2	151.0
2	2	Segment 2	0.18	0%	0.0	75.8	830.0
1	1	Segment 3	0.18	0%	0.0	320.0	46.6
2	1	Segment 3	0.18	0%	0.0	100.4	830.0
1	2	Segment 3	0.18	0%	0.0	265.7	76.0
2	2	Segment 3	0.18	0%	0.0	99.6	830.0
1	1	Segment 4	0.18	0%	0.0	264.6	76.8
2	1	Segment 4	0.18	0%	0.0	83.0	830.0
1	2	Segment 4	0.18	0%	0.0	219.7	122.8
2	2	Segment 4	0.18	0%	0.0	82.3	830.0
1	1	Segment 5	0.18	0%	0.0	105.5	830.0
2	1	Segment 5	0.18	0%	0.0	33.1	830.0
1	2	Segment 5	0.18	0%	0.0	87.6	830.0
2	2	Segment 5	0.18	0%	0.0	32.8	830.0
1	1	Segment 1	0.06	0%	0.0	78.3	830.0
2	1	Segment 1	0.06	0%	0.0	24.6	830.0
1	2	Segment 1	0.06	0%	0.0	65.0	830.0
2	2	Segment 1	0.06	0%	0.0	24.4	830.0
1	1	Segment 2	0.06	0%	0.0	243.5	31.3
2	1	Segment 2	0.06	0%	0.0	76.4	830.0
1	2	Segment 2	0.06	0%	0.0	202.2	49.0
2	2	Segment 2	0.06	0%	0.0	75.8	830.0
1	1	Segment 3	0.06	0%	0.0	320.0	15.5
2	1	Segment 3	0.06	0%	0.0	100.4	246.1
1	2	Segment 3	0.06	0%	0.0	265.7	25.2
2	2	Segment 3	0.06	0%	0.0	99.6	251.0
1	1	Segment 4	0.06	0%	0.0	264.6	25.4
2	1	Segment 4	0.06	0%	0.0	83.0	428.5
1	2	Segment 4	0.06	0%	0.0	219.7	40.2
2	2	Segment 4	0.06	0%	0.0	82.3	443.9
1	1	Segment 5	0.06	0%	0.0	105.5	217.8
2	1	Segment 5	0.06	0%	0.0	33.1	830.0
1	2	Segment 5	0.06	0%	0.0	87.6	354.6
2	2	Segment 5	0.06	0%	0.0	32.8	830.0

Table 5.18: Through Crack Critical Crack Lengths; 100% Yield Residual Stress

Load Case	Location	Station	CTOD (mm)	Residual Stress % yield	Residual Stress (MPa)	Analytical Local	Critical
						Membrane Stress (MPa)	Crack Length (mm)
1	1	Segment 1	0.06	100%	315.0	78.3	18.2
2	1	Segment 1	0.06	100%	315.0	24.6	19.8
1	2	Segment 1	0.06	100%	315.0	65.0	18.7
2	2	Segment 1	0.06	100%	315.0	24.4	19.8
1	1	Segment 2	0.06	100%	315.0	243.5	9.3
2	1	Segment 2	0.06	100%	315.0	76.4	18.3
1	2	Segment 2	0.06	100%	315.0	202.2	11.5
2	2	Segment 2	0.06	100%	315.0	75.8	18.3
1	1	Segment 3	0.06	100%	315.0	320.0	7.6
2	1	Segment 3	0.06	100%	315.0	100.4	17.2
1	2	Segment 3	0.06	100%	315.0	265.7	8.7
2	2	Segment 3	0.06	100%	315.0	99.6	17.2
1	1	Segment 4	0.06	100%	315.0	264.6	8.7
2	1	Segment 4	0.06	100%	315.0	83.0	18.0
1	2	Segment 4	0.06	100%	315.0	219.7	10.5
2	2	Segment 4	0.06	100%	315.0	82.3	18.0
1	1	Segment 5	0.06	100%	315.0	105.5	16.9
2	1	Segment 5	0.06	100%	315.0	33.1	19.6
1	2	Segment 5	0.06	100%	315.0	87.6	17.8
2	2	Segment 5	0.06	100%	315.0	32.8	19.6
1	1	Segment 1	0.18	100%	315.0	78.3	54.7
2	1	Segment 1	0.18	100%	315.0	24.6	59.6
1	2	Segment 1	0.18	100%	315.0	65.0	56.3
2	2	Segment 1	0.18	100%	315.0	24.4	59.6
1	1	Segment 2	0.18	100%	315.0	243.5	28.1
2	1	Segment 2	0.18	100%	315.0	76.4	55.0
1	2	Segment 2	0.18	100%	315.0	202.2	34.5
2	2	Segment 2	0.18	100%	315.0	75.8	55.1
1	1	Segment 3	0.18	100%	315.0	320.0	22.9
2	1	Segment 3	0.18	100%	315.0	100.4	51.6
1	2	Segment 3	0.18	100%	315.0	265.7	26.0
2	2	Segment 3	0.18	100%	315.0	99.6	51.8
1	1	Segment 4	0.18	100%	315.0	264.6	26.1
2	1	Segment 4	0.18	100%	315.0	83.0	54.1
1	2	Segment 4	0.18	100%	315.0	219.7	31.7
2	2	Segment 4	0.18	100%	315.0	82.3	54.2
1	1	Segment 5	0.18	100%	315.0	105.5	50.8
2	1	Segment 5	0.18	100%	315.0	33.1	59.1
1	2	Segment 5	0.18	100%	315.0	87.6	53.5
2	2	Segment 5	0.18	100%	315.0	32.8	59.1

6. CRITICAL REVIEW OF THE ANALYSIS APPROACH LIMITATIONS

The analysis approach developed in this project was assembled to demonstrate conceptually the techniques needed to perform vessel failure assessment. In assembling this approach, it was noted that a number of assumptions and short cuts had to be taken to avoid over-complicating the analysis. Further, the completion of this project identified a number of challenges that could not be dealt with in this project. Therefore, this section of the report presents a listing of the limitations of the current approach and, where possible, discusses some improvements or modifications required to overcome these limitations.

This discussion of limitations is presented in terms of the seven step process including:

- Vessel Particular Identification,
- Structural Section and Component Definition,
- Load Assessment,
- Definition of Local Detail Characteristics,
- Failure Assessment, and
- Application of the Results.

The sections that follow describe the perceived limitations of the analysis approach associated with each of these steps.

6.1 Vessel Particular Identification

The first step in the analysis is a data collection effort. The data being collected includes:

- Structural configuration and scantlings,
- Materials, and
- Hull form and weight distribution.

The limitations of the approach taken that could be remedied include:

- Considering the development of a GUI to define standard ship structural systems. This development could both make the data assembly more efficient as well as reduce errors in the data.
- Development of a material property database to support this assessment. Currently there is a need to better understand ship steel material fracture toughness as well as the statistical variability of material properties for commonly used steels and welds.
- The definition of the hull form and weight distribution through the use of a GUI. Standard GUI's exist and were used in the sample applications.

6.2 Structural Section and Component Definition

The second step involves breaking down the structural system into segments, frames and components. This subdivision of the structure in future applications of the proposed approach should consider:

- the development of a database to track the base structural data and thus facilitate the definition of components, frame and segments. In the sample application, a spreadsheet was developed, however, in a useful example a great deal more data is required and this would likely overwhelm a spreadsheet.
- future applications should use a higher degree of structural division to better represent changes in loads and structural behaviour. In the current application only five segment types were defined for which loads were defined.
- more flaw types and locations in the vessel could be considered to better illustrate the sensitivity of these factors on vessel failure resistance.

6.3 Load Assessment

The third step in the analysis involves the definition of the loads applied to the vessel and thus its structure. This is accomplished through a statistical analysis of the loads generated based on a defined operational profile to estimate load distributions for fatigue and ultimate strength calculations. The limitations of the current analysis that should be considered in future applications include:

- consideration of all of the applied load components. The sample application disregarded still water bending moment, however, this effect could have been considered part of the residual stress level. It is also suggested that the combined effects of shear and moment be considered. While this example demonstrated how to combine load effects this area of investigation should be considered further.
- consideration of non-linear load effects. The analysis completed made use of linear strip theory to estimate vessel moments. Since ultimate strength limit states are being considered, non-linear effects need to be considered such as slamming.
- effect of wave statistics needs to be considered. The sample application made use of BMT's Global Wave Statistics whose accuracy for rare events has been questioned. While the accuracy of different wave statistical databases has been dealt with elsewhere, this matter should be explored.

6.4 Definition of Local Detail Characteristics

The fourth step in the process involves the definition of the characteristics of individual structural components. The characteristics of interest to this investigation include:

- nominal stress and stress intensity transfer functions,
- cross-section geometry, and
- stress concentration effects.

In future applications, it is suggested that the following issues be addressed:

- Linear elastic hull girder bending theory was used to estimate the relationship between hull girder applied loads and structural stresses. Non-linear analysis might be more useful to evaluate extreme load events for ultimate strength limit states. This could be accomplished through the use of non-linear beam theory or non-linear FEA, however, the latter would add significantly to the computational complexity of the analysis. If significant plasticity is observed, linear elastic fracture mechanics would not apply.
- The cross-sectional geometry of components was defined in terms of individual stiffened plates with plate and flange dimensions. In the future, an automated means of describing these sections would be worth investigating.
- In the example, only one material type was used. The effect of temperature on fracture toughness was demonstrated for two temperature levels. In reality, a range of materials and temperature levels might be used to model the vessel.

6.5 Failure Assessment

The fifth step in this analysis process is the failure. This step in the analysis process includes:

- definition of the applied stress levels
- definition of critical stress levels, and
- definition of failure or failure probabilities.

In future applications of the failure assessment approach, it is proposed that the following limitations of the demonstrated assessment be dealt with:

- additional consideration to the effects of material grades be considered,
- further applications of the analysis techniques could be used to evaluate the effects of different flaw types and locations within the vessel.
- the failure assessments could be used to define the final flaw size of a fatigue crack. In this result the failure assessment would be combined with a fatigue crack growth analysis to develop a probabilistic damage tolerance assessment.
- the only source of uncertainty in the sample applications stemmed from the wave induced loads. In the future, it is recommended that other sources of uncertainty (weld quality, fabrication quality, material properties, etc.) could be considered.

6.6 Application of the Results

The final step is the application of the results. The scope of the project did not include the extensive development of this step, however, some suggestions are given in the report to indicate how the results could be used. These uses included inspection focusing, repair prioritization, critical detail identification, and illustration of failure mode relative significance. It is suggested that in future applications of the analysis:

- The most important improvement that could be made in the analysis process is the solicitation of potential user input to identify the types of information of interest and the most usable format for the information.
- Repair or maintenance cost data be considered to allow the user to consider the time dependant costs of delayed repairs versus more proactive maintenance.
- Economic criteria could be incorporated to allow weighing the cost of continued operation and maintenance versus the revenues a vessel could generate. This information could be used to make vessel retirement or repair decisions.
- The probabilities of failure could be used to further consider the risk of operation with various maintenance strategies.

7. CONCLUSIONS AND RECOMMENDATIONS

A number of lessons were learned in the development, application and documentation of the vessel fracture assessment approach in this project. A number of shortcomings and limitations of the approach were identified and these are discussed in the previous section. The sections that follow make some general comments regarding the analysis approach and results by way of concluding statements and recommendations for future work.

7.1 Conclusions

The work completed in this project has reviewed the vessel fracture assessment tools, described potential analysis approaches and presented worked sample applications. In addition, potential improvements for these techniques have been discussed to support continued work in this area. Based upon the findings, it is possible to make the following general conclusions:

- The tools to perform vessel fracture assessment as described and demonstrated in this project are available and their use in vessel condition assessment is possible.
- Data to validate the results is not available and therefore it is suggested that an analysis of the type proposed herein be used to draw conclusions on a relative basis.
- A simplified failure assessment approach was developed and demonstrated in this project.
- The sample applications considered the significance of edge and through thickness flaws in several locations in the vessel.
- The results of the sample application indicated that the analysis techniques are capable of identifying critical flaw sizes or structural locations and thus focusing inspection, maintenance or repair efforts. In addition, if completed at the design stage the analysis approach could be used to identify high risk structural areas or define material requirements.
- While sample applications demonstrated the required techniques and identified the data required for the analysis, the volume of data and complexity of the analysis techniques suggests that database systems and automated software would need to be developed before more complex cases could be analyzed.

7.2 Recommendations

While the work completed in this project has provided a great deal of information regarding the application and performance of vessel fracture assessment, a number of issues remain unresolved or require further attention. The comments that follow provide recommendations for future development or investigations for vessel fracture assessment.

- While the sample applications demonstrated the concepts of interest, it is suggested more detailed sample application should be completed to better demonstrate the potential of the approaches developed in this project. The additional detail would include, for example:

- a greater number and variety of materials,
 - a higher degree of structural discretization,
 - additional sources of statistical variability (e.g., material, weld quality, residual stress level, etc.)
 - consideration of additional applied loading components (not just vertical and horizontal bending), and
 - more detailed treatment of different crack types and locations.
- Perhaps a future application of these techniques could also consider repair or renewal rules to better simulate the maintenance of a vessel and thus illustrate the effect of repair techniques.
 - Future applications of the approaches presented in this project would require the development of software tools (databases and GUI's) to facilitate their implementation.
 - Future development or implementation of vessel fracture techniques is dependant on the availability of basic material property and residual stress data. It is suggested that data describing steel fracture toughness or means of non-destructively estimating its value be developed.
 - Additional work be completed to demonstrate how residual stresses are distributed on a ship structure and how they diminish or redistribute with time.

APPENDIX A1
BS 7910 ELABORATION

A1.1 Development of FAD Fracture and Collapse Ratios

The abscissa and ordinate of the Failure Assessment Diagram for a given cracked element⁴ are, respectively, the ***Collapse Ratio*** L_r and the ***Fracture Ratio*** K_r . The ***Collapse Ratio*** is the ratio of the load on the cracked element to the limit load of the cracked element. The ***Fracture Ratio*** is the ratio of the crack driving force in the cracked element to the fracture toughness of the cracked element.

Collapse Ratio

The collapse ratio L_r is, basically,

$$L_r = \frac{P}{P_{LL}} \quad (1)$$

where P is the load on the cracked element and P_{LL} is the limit load of the cracked element.

Eq. 1 may be expressed in terms of stresses as

$$L_r = \frac{P}{P_{LL}} = \frac{\sigma_m \cdot A_{gross}}{\sigma_Y \cdot \alpha \cdot A_{net}} = \frac{\sigma_m}{\sigma_Y \cdot \alpha \cdot A_{net} / A_{gross}} \quad (2)$$

where σ_m , σ_Y , A_{gross} and A_{net} are, respectively, the nominal (or membrane stress) the yield stress, the uncracked area, and the cracked area. The parameter α adjusts the computation of limit load to include the effect of the element's geometry. (Note that bending stresses are ignored for simplification herein.) Eq. 2, ***recognizing that limit load is a function only of the applied stress and not the residual stress*** (see Appendix), may be rearranged as

$$L_r = \frac{P}{P_{LL}} = \frac{\sigma_m \cdot A_{gross} / (\alpha \cdot A_{net})}{\sigma_Y} \quad (3)$$

If the numerator of Eq. 3 is defined as

$$\sigma_{ref} = \sigma \cdot A_{gross} / (\alpha \cdot A_{net}), \quad (4)$$

Eq. 3 becomes

$$L_r = \frac{\sigma_{ref}}{\sigma_Y}, \quad (5)$$

the BS 7910 definition of the ***Collapse Ratio*** L_r .

⁴ The cracked element includes the geometry of the element, the material from which the element is fabricated, and load distribution on the element.

Example of Collapse Ratio

For a through-thickness flaw of length $2a$ in axially loaded panel of thickness t and width W , the load is

$$P = \sigma_m \cdot A_{\text{gross}} = \sigma_m \cdot t \cdot W \quad (6)$$

and the limit load is

$$P_{LL} = \sigma_Y \cdot A_{\text{net}} = \sigma_Y \cdot t \cdot (W - 2a). \quad (7)$$

The Collapse Ratio becomes

$$L_r = \frac{P}{P_{LL}} = \frac{\sigma_m \cdot t \cdot W}{\sigma_Y \cdot t \cdot (W - 2a)} = \frac{\sigma_m}{\sigma_Y \cdot (1 - 2a/W)} = \frac{\sigma_{\text{ref}}}{\sigma_Y} \quad (8)$$

where

$$\sigma_{\text{ref}} = \frac{\sigma_m}{(1 - 2a/W)} \quad (9)$$

which is the BS 7910 definition of σ_{ref} for a through-thickness flaw in an axially loaded panel.

Fracture Ratio

BS 7910 defines the Fracture Ratio, for the linear elastic case, as

$$K_r = \frac{K_I}{K_{\text{mat}}} + \rho = \frac{K_I^{\text{applied}} + K_I^{\text{residual}}}{K_{\text{mat}}} + \rho \quad (10)$$

and, for the plane-stress elastic-plastic case where the crack driving force is characterized by CTOD δ , as

$$K_r = \sqrt{\frac{\delta_I}{\delta_{\text{mat}}}} + \rho = \sqrt{\frac{K_I^2}{\sigma_Y \cdot E} \cdot \frac{1}{\delta_{\text{mat}}}} + \rho = \sqrt{\frac{(K_I^{\text{applied}} + K_I^{\text{residual}})^2}{\sigma_Y \cdot E} \cdot \frac{1}{\delta_{\text{mat}}}} + \rho. \quad (11)$$

In Eq. 10 and 11, K_{mat} and δ_{mat} are the fracture toughnesses characterized by stress intensity factor (SIF) and CTOD δ , respectively.

The SIF's in Eq. 10 and 11 are, for the applied stress,

$$K_I^{\text{applied}} = \sigma_m \cdot \sqrt{\pi a} \cdot Y_m, \quad (12)$$

and, for the residual stress

$$K_I^{\text{residual}} = \sigma_{\text{residual}} \cdot \sqrt{\pi a} \cdot Y_{\text{residual}}, \quad (13)$$

where Y_m and Y_{residual} are expressions that correct the SIF of an infinitely wide panel for the geometry and loading mode of the case of interest.

In Eq. 10 and 11, the parameter ρ corrects the **Fracture Ratio** K_r for the inelastic interaction of the applied and residual stresses and is a function of χ where

$$\chi = \frac{K_I^{\text{residual}}}{K_I^{\text{applied}}} \cdot L_r. \quad (14)$$

For the through-cracked panel and assuming $\mathbf{Y}_m = \mathbf{Y}_{\text{residual}}$, Eq. 0, with Eq. 9, becomes

$$\chi = \frac{\sigma_{\text{residual}}}{\sigma_m} \cdot \frac{\sigma_{\text{ref}}}{\sigma_Y} = \frac{\sigma_{\text{residual}}}{\sigma_m} \cdot \frac{\sigma_m}{\sigma_Y \cdot (1-2a/W)} = \frac{\sigma_{\text{residual}}}{\sigma_Y \cdot (1-2a/W)}. \quad (15)$$

In the case of a non-zero σ_{residual} , χ (Eq. 0) and ρ (a polynomial function of χ) are non-zero. In the case of a zero σ_{residual} , χ (Eq. 0) and ρ (a polynomial function of χ) are zero.

Conclusion

Observing Eq. 8, 10 and 11, it is seen that:

- when σ_m is zero ($K_I^{\text{applied}} = 0$) and σ_{residual} is non-zero ($K_I^{\text{residual}} \neq 0$),
 L_r is zero but K_r is non-zero.
- when σ_m and σ_{residual} are both zero ($K_I^{\text{applied}} = K_I^{\text{residual}} = 0$),
both L_r and K_r are zero.

A1.2 Influence of Residual Stress on Structural Response

Residual stresses may lower the local or general buckling resistance of a compression element or column.

However, in the case of bending elements (where buckling is prevented by appropriate stiffeners) and tension elements, residual stresses reduce only the proportional limit of the load-deflection relation. Residual stresses ***do not*** influence the ultimate capacity, i.e., the plastic limit load, of bending and tension elements. To demonstrate the latter point, take the example of a beam with cross-sectional area A containing a residual stress pattern. The bending moment is

$$M = \int_{\text{Area}} \sigma_m \cdot y \cdot dA + \int_{\text{Area}} \sigma_{\text{res}} \cdot y \cdot dA \quad (16)$$

where σ_m , σ_{res} , and y are, respectively the externally applied membrane or remote stress, the residual stress, and the distance from the neutral axis of the beam to the elemental area dA . (In general, σ_m and σ_{res} are functions of y .) But the residual stress distribution is self-equilibrating, i.e.,

$$\int_{\text{Area}} \sigma_{\text{res}} \cdot y \cdot dA = 0 \quad (17)$$

and thus the bending moment is independent of residual stress with Eq. 17 becoming

$$M = \int_{\text{Area}} \sigma_m \cdot y \cdot dA. \quad (18)$$

Obviously, the upper limit to the bending moment \mathbf{M} is the plastic-hinge-developing plastic moment \mathbf{M}_p which is a function of the limit load \mathbf{P}_{LL} .

APPENDIX A2
SAMPLE FAILURE ASSESSMENT DIAGRAMS FOR VARIOUS SHIP STEELS

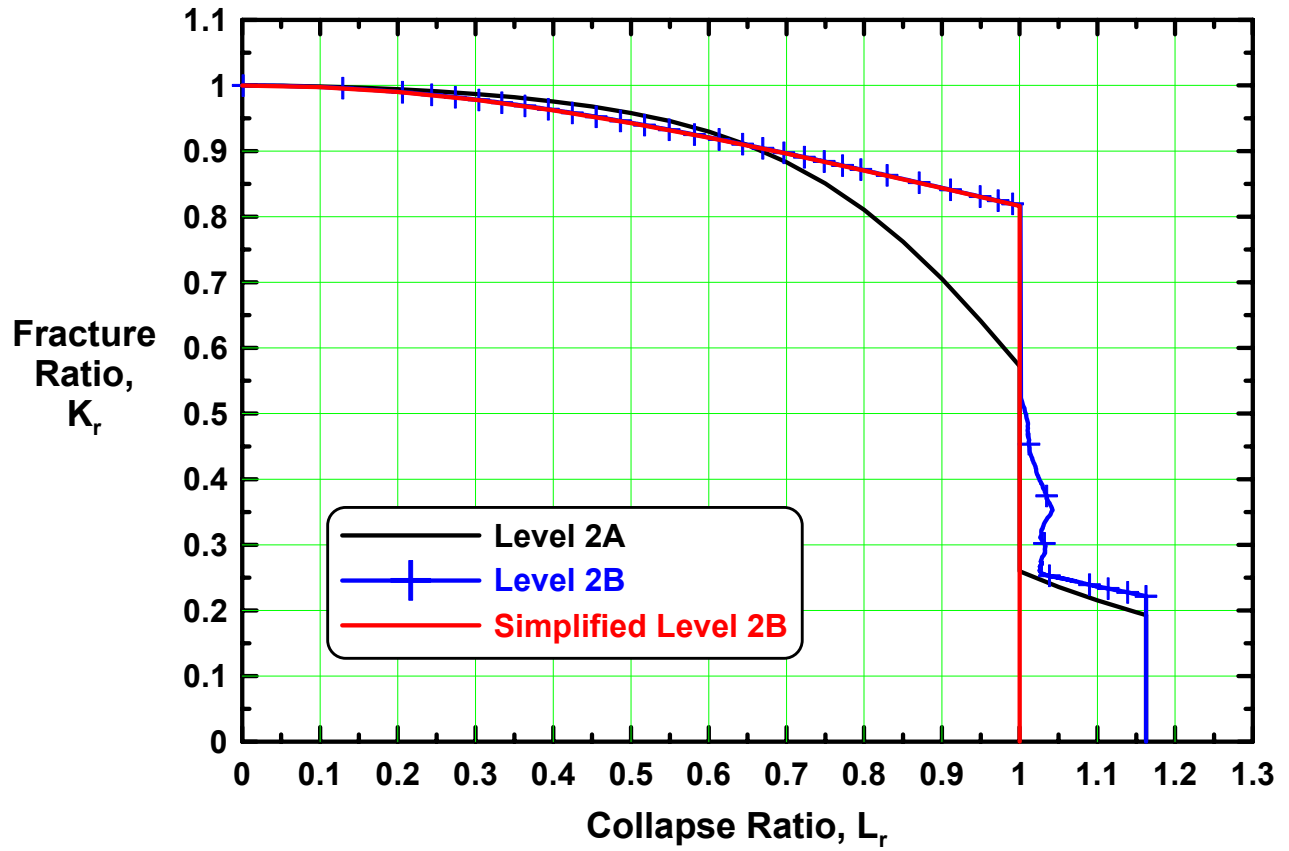


Figure A2.1: BS 7910:1999 Level 2 FAC's – A 36 Steel.

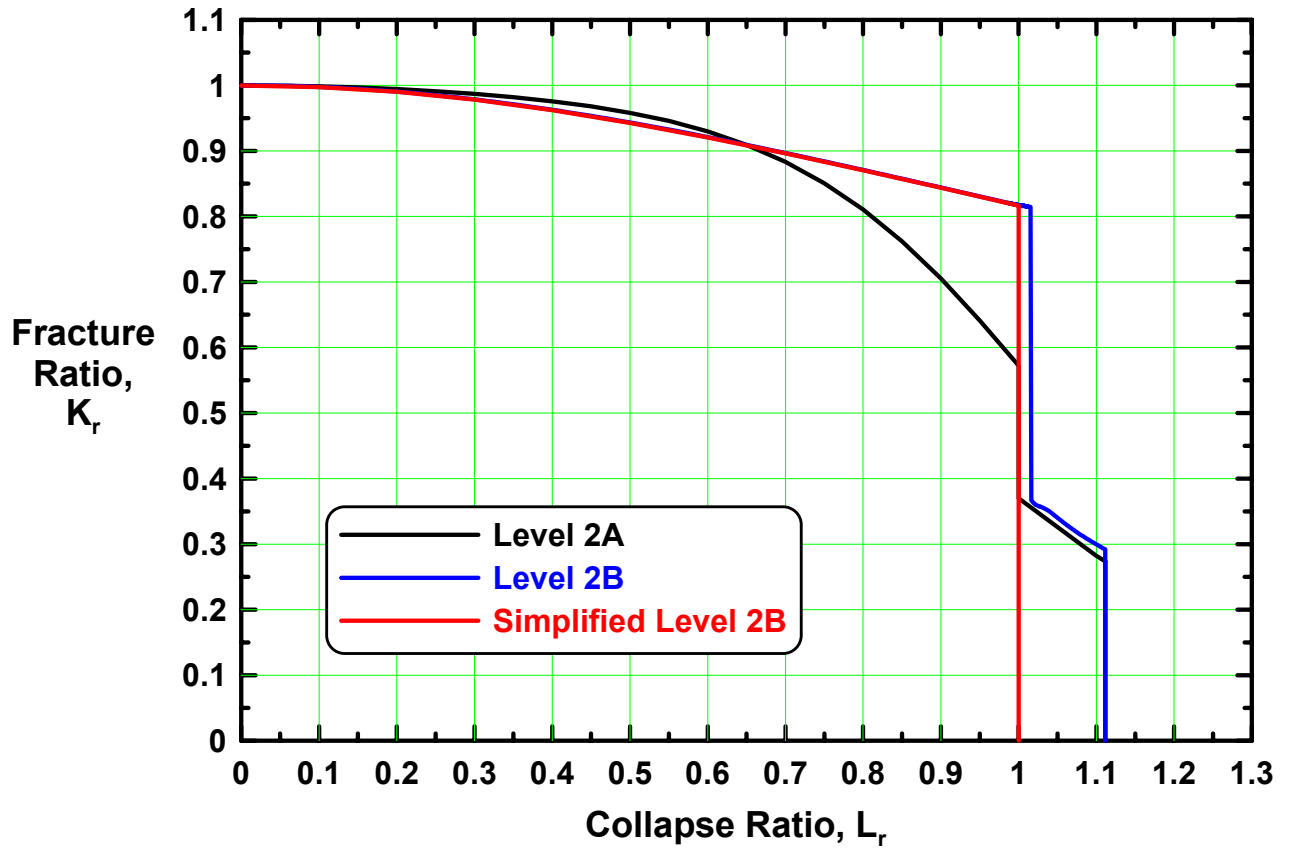


Figure A2.2: BS 7910:1999 Level 2 FAC's – API 2Y 60 Steel.

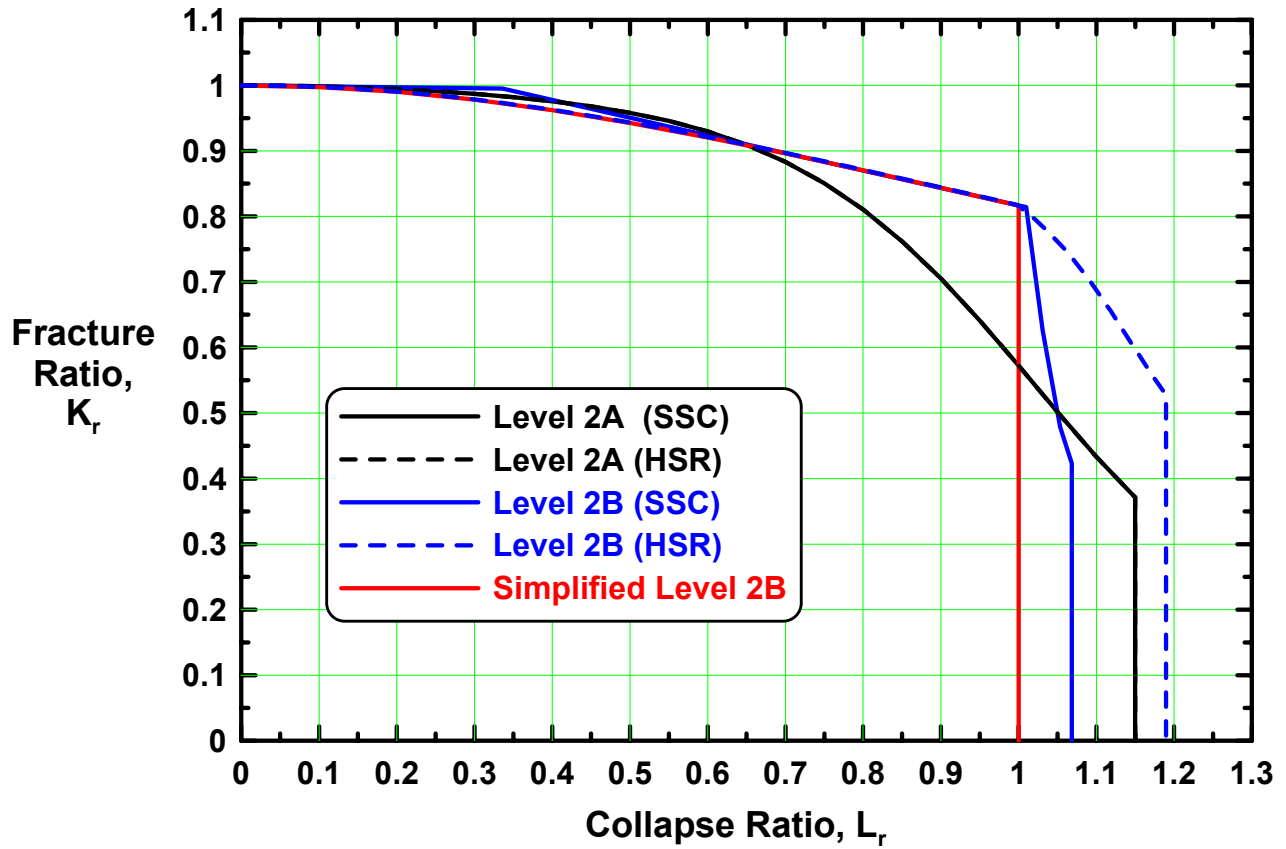


Figure A2.3: BS 7910:1999 Level 2 FAC's – HSLA 80 Steel.

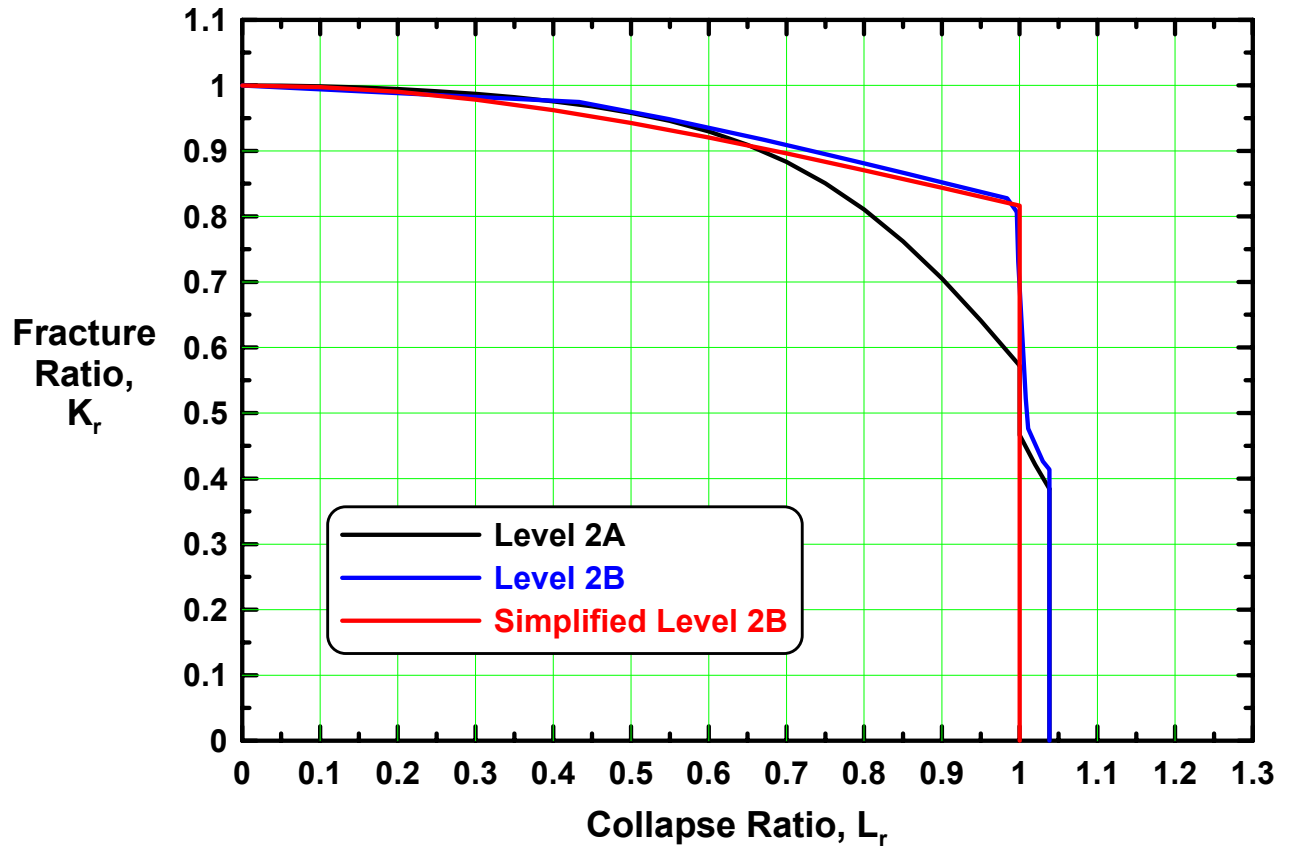


Figure A2.4: BS 7910:1999 Level 2 FAC's – A 514 Steel.

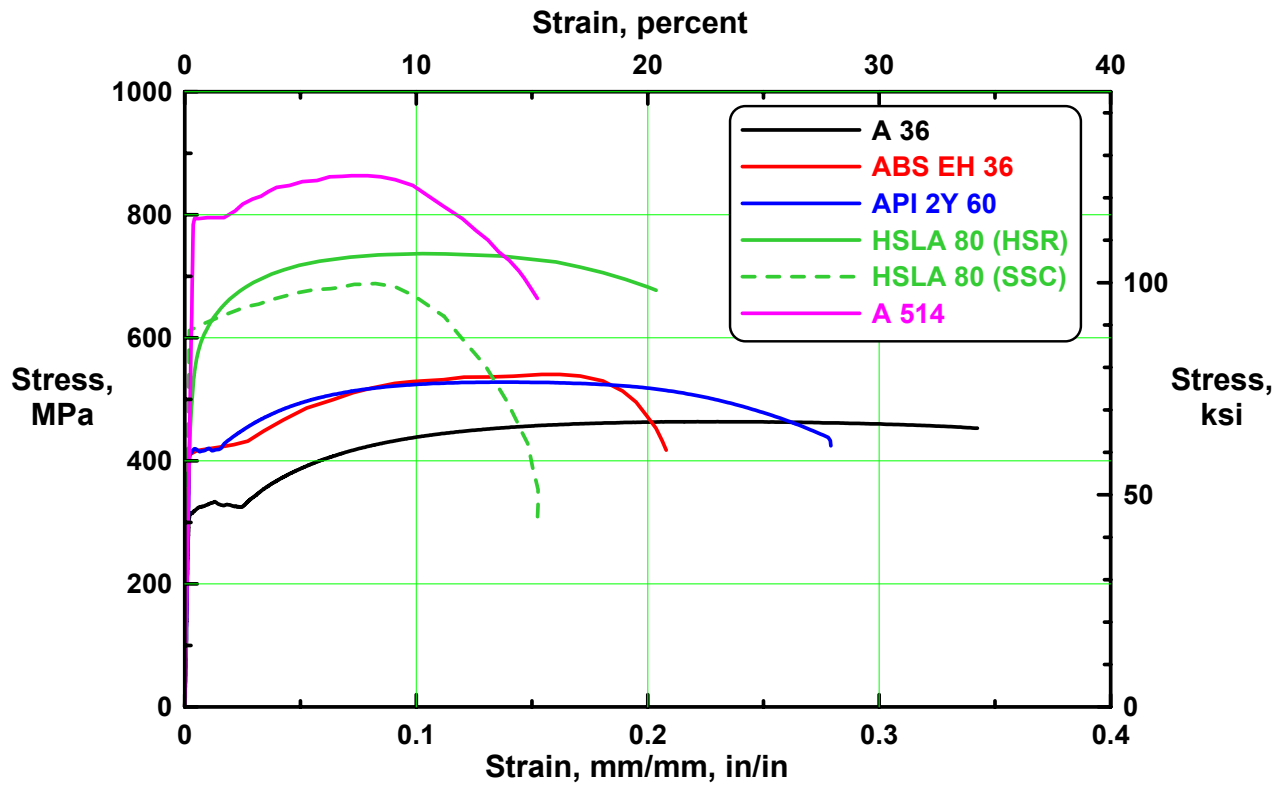


Figure A2.5: Engineering Stress-Strain Curves, Steel Plates

APPENDIX B
MATERIAL FRACTURE TOUGHNESS

1. *Types of Steel in Construction*⁵

Structural steels are available in many grades and may be classified into four major categories: (1) carbon steels, (2) high-strength low-alloy (HSLA or microalloyed) steels, (3) heat-treated carbon steels, and (4) heat-treated alloy steels. The first two categories are available in the as-rolled condition. Chemical compositions and mechanical properties of selected structural steels are listed in, respectively, Tables 1 and 2.

Table 1: Chemical Compositions of Selected Structural Steels

Steel	Chemical Composition (%)					
	C (max.)	Mn	P (max.)	S (max.)	Si	V (min.)
Carbon	0.29	0.60-1.35	0.04	0.05	0.15-0.40	—
HSLA	0.26	0.50-1.65	0.04	0.05	0.15-0.40	0.02
Heat-treated carbon						
Normalized	0.36	0.90 max.	0.04	0.05	0.15-0.40	—
Quenched and tempered	0.20	1.50 max.	0.04	0.05	0.15-0.30	—
Heat-treated alloy						
Normalized	0.20	0.70-1.60	0.04	0.05	0.15-0.50	—
Quenched and tempered	0.21	0.45-0.70	0.035	0.05	0.20-0.35	—

Table 2: Mechanical Properties of Selected Structural Steels

Steel	Minimum Yield Strength		Minimum Tensile Strength		Minimum Elongation in 50 mm (2 in)
	N/mm ²	ksi	N/mm ²	ksi	
Carbon	170-250	25 - 36	310-410	45 - 59	23-30
HSLA	280-450	41 - 65	410-550	59 - 80	18-24
Heat-treated carbon					
Normalized	200	29	420	61	24
Quenched and tempered	550-690	80 - 100	660-760	96 - 110	18
Heat-treated alloy					
Normalized	320	46	350	51	23
Quenched and tempered	620-690	90 - 100	720-800	104 - 116	17-18

Carbon steels consist almost entirely of the element iron but also contain small quantities of carbon, manganese, silicon, phosphorus, sulfur and sometimes copper.

⁵ Much of this section is taken from H. S. Reemsnyder, "Construction Steel," *Encyclopedia of Materials: Science and Technology*, Elsevier Science Ltd., 2001, pp 1564 - 1570.

HSLA steels are carbon steels to which additional alloying elements have been added. Manganese increases strength and toughness whilst ***nickel improves low-temperature toughness. Vanadium or niobium is added to increase strength by grain refinement*** and precipitation strengthening.

Heat-treated carbon and alloy steels may be normalized or quenched and tempered to improve mechanical properties. Normalizing produces essentially the same ferrite-pearlite microstructure as that of carbon and HSLA steels, except that the heat treatment produces a ***finer grain resulting in lower fracture transition temperature*** and more uniform mechanical properties throughout the length of the plate. Quenching and tempering produce a Martensite or Martensite-Bainite microstructure in both carbon and alloy steels. The alloying elements (boron, manganese, molybdenum, chromium, silicon and nickel) make appreciable contributions to the hardening of alloy steels.

As an alternative to, or substitute for, heat treatment of plates, improved properties can be obtained through specific plate-rolling practices. ***Controlled-rolling*** — introduced to increase strength and ***improve toughness of plates*** — tailors the time-temperature deformation process by controlling the rolling parameters: (1) temperature at start of rolling, (2) amount of reduction from start of rolling to finished plate thickness, and (3) plate finishing temperature. Controlled-rolling practices involve deformations at much lower temperatures than hot rolling and are designed specifically for use with the microalloyed steel (HSLA) grades. The increase in strength in controlled steels is achieved through grain-refinement and some precipitation hardening due to the micro-alloying elements. Also, the carbon content of control-rolled steels is much less than that of the carbon steels. The Thermo-Mechanical Control Process (***TMCP***) has evolved from controlled-rolling and ***produces a fine-grained steel*** through a combination of chemical composition and rolling practice. TMCP steels may take one of three forms depending upon the chemical composition, plate thickness, and required properties: (1) Thermo-mechanical Rolling (TMR), Accelerated Cooling (AC), and (3) Direct Quenched and Tempered (DQT)

2. *Parameters Affecting Toughness*

A typical fracture toughness – temperature relation is shown in Figure 1. The sigmoidal relation approaches two horizontal asymptotes — the Upper and Lower Shelves. Fracture on the Upper Shelf is ductile, e.g., microvoid coalescence, whilst fracture on the Lower Shelf is brittle, e.g., transgranular (cleavage) or intergranular. Crack initiation on the Lower Shelf is unstable whilst that on the Upper Shelf is a stable, ductile tearing. (If the Upper Shelf toughness is high enough, it is possible that the cracked element may fail by plastic collapse before tearing.)

In the Transition region, Figure 1, ductile tearing will be terminated by a brittle, unstable crack extension. At the tip of growing crack, the principal stress (operative for mode I fracture) is elevated by the multiaxial stress state and the effective yield strength is increased with strain-rate. Thus, as the ductile crack grows, the principal stress reaches the level of the intrinsic fracture stress and the fracture transitions from ductile to brittle.

Increasing strain-rate and/or constraint, e.g., impact testing and/or increasing specimen thickness, will shift the sigmoidal curve to the right, Figure 1.

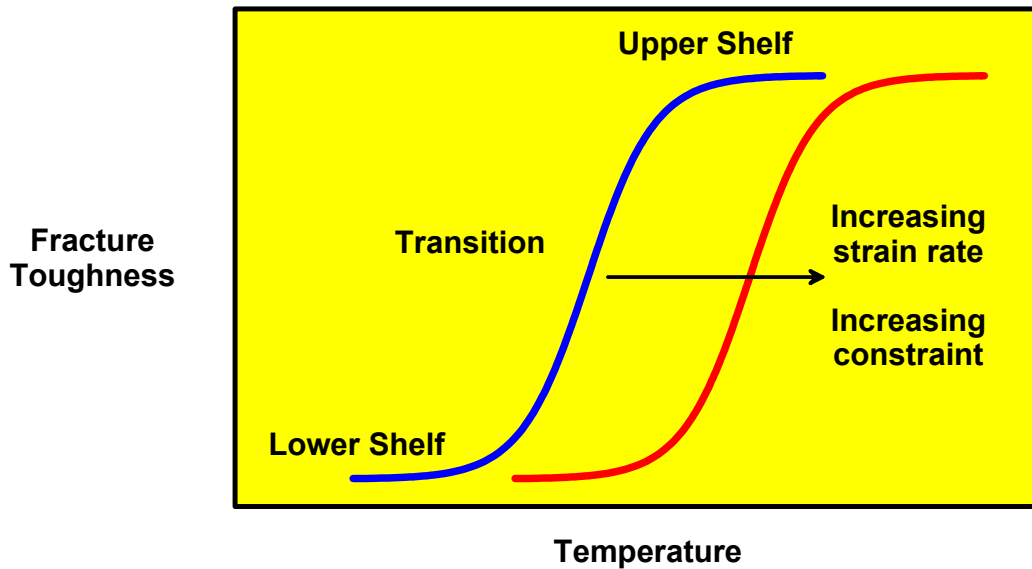


Figure 1: Typical Toughness – Temperature Relation

Fracture toughness is not a single-valued property of a generic steel grade. Instead, the *base-metal* fracture toughness is affected by:

- Metallurgy.
- Geometry.
- Environment.
- Testing.

Metallurgy. Chemistry and ingot-casting practice influence the cleanliness whilst chemistry and thermo-mechanical processing influence the ferrite grain-size. Increasing cleanliness and decreasing grain-size increase the toughness, e.g., low sulfur with ferrite grain refinement. Also, lowering the Sulfur content may raise the upper shelf toughness, Figure 2, whilst ferrite grain refinement, for a given strain rate, may shift the transition to lower temperatures, Figure 2.

Geometry. Thickness and notches (including sudden changes in thickness) affect constraint, i.e., introducing a multi-axial stress state in an otherwise uniaxial or biaxial stress state. Increasing constraint inhibits plastic flow (ductility) and decreases toughness by raising the maximum principal stress.

Environment. Increasing loading rate and decreasing temperature decrease fracture toughness.

Testing. Toughness may vary with specimen configuration even though all other parameters are held constant. Constraint will vary with geometry. Also, the realism of the mathematical models used to compute fracture toughness from test results may vary with specimen configuration.

It should be noted that the fracture toughness of a structural steel is no indication of the fracture toughness of the weld heat-affected zone when that steel is welded. Chemical composition and steel casting and rolling practice may interact with the welding process to reduce the fracture toughness of a welded connection. Thus, these parameters must be controlled closely to insure adequate fracture resistance of the weld heat-affected zone.

3. CTOD Toughness

Fracture initiation toughness is characterized by the crack-driving force and extent of inelastic behaviour. For example, if the fracture phenomenon is essentially linear elastic, toughness may be characterized by the critical value of stress intensity factor K_I , e.g., K_c or K_{Ic} , respectively, the plane stress or plane strain fracture toughness. For the most part, modern structural steels from integrated mills will fracture after significant inelastic behaviour. Then the crack-driving force is characterized by either J-integral or crack-tip opening displacement (CTOD.)

Crack-tip opening displacement (CTOD or δ) is defined as the displacement transverse to the crack-tip defined by the hypotenuse of a 45°-45°-90° right triangle, Figure 2. The apparent advance of the crack-tip is the crack-opening stretch (COS).

One or more of four values of CTOD (or δ) toughness may be determined depending upon the response of the specimen during the fracture toughness test. The response of a particular specimen may be described by its load-displacement (P- Δ) curve, Figure 3, and the values of CTOD correspond to that curve as listed in Table 3.

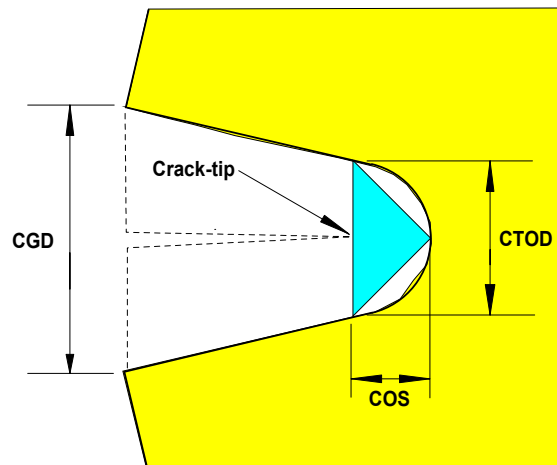


Figure 2: Definition of CTOD

Table 3: CTOD Response

Type of P-Δ	Crack Extension		Value	CTOD Estimated at ...
	Stable	Unstable		
A	No	Yes	δ_c	Maximum load (onset of crack instability)
B	Yes	Yes	δ_i	Intersection of R-curve and blunting line*
			δ_u	Maximum load (onset of crack instability)
C	Yes	No	δ_i	Intersection of R-curve and blunting line*
			δ_m	First achievement of maximum load plateau**
D	No	No	δ_m	First achievement of maximum load plateau**

* Taken as the onset of stable crack extension.

The blunting line is the plot of COS (Figure 2) versus crack extension $\Delta a = a_i - a_0$.

R-curve is the plot of δ versus crack extension $\Delta a = a_i - a_0$.

** Formation of plastic hinge.

The various values of CTOD correspond to the material response with respect to test temperature, Figure 3. The value δ_c and δ_m correspond to the lower and upper shelf toughnesses, respectively, whilst δ_u is the maximum toughness in the transition region. The CTOD at the onset of stable crack extension, δ_i , is determined in the transition region and on the upper shelf. At the higher temperatures it is possible that plastic collapse may occur before appreciable stable crack extension, i.e., Type D response (Figure 3).

The opening displacement at the crack tip (CTOD) is not measured routinely. Instead, the CTOD is estimated from the measurement of the displacement of a clip gage CGD (sometimes called COD) across the crack tips, Figure 2. It is assumed that the CTOD δ is the sum of two components - elastic δ_e and plastic δ_p :

$$\delta = \delta_e + \delta_p. \quad (1)$$

The elastic component of CTOD δ_e is a function of the load P, geometry a_0 (initial crack length), depth W, and specimen thickness B, yield strength at the fracture test temperature σ_{YS} , Young's Modulus E, and Poisson's ratio ν , or

$$\delta_e = (K_I^2)(1 - \nu^2)/m\sigma_{YS}E. \quad (2)$$

where the elastic stress intensity factor K_I for the bend specimen is

$$K_I = Pf(a_0/W)/\sqrt{[BW]} \quad (3)$$

and m, the constraint parameter, is taken as 2 [1]⁶.

⁶ Numbers in brackets denote References.

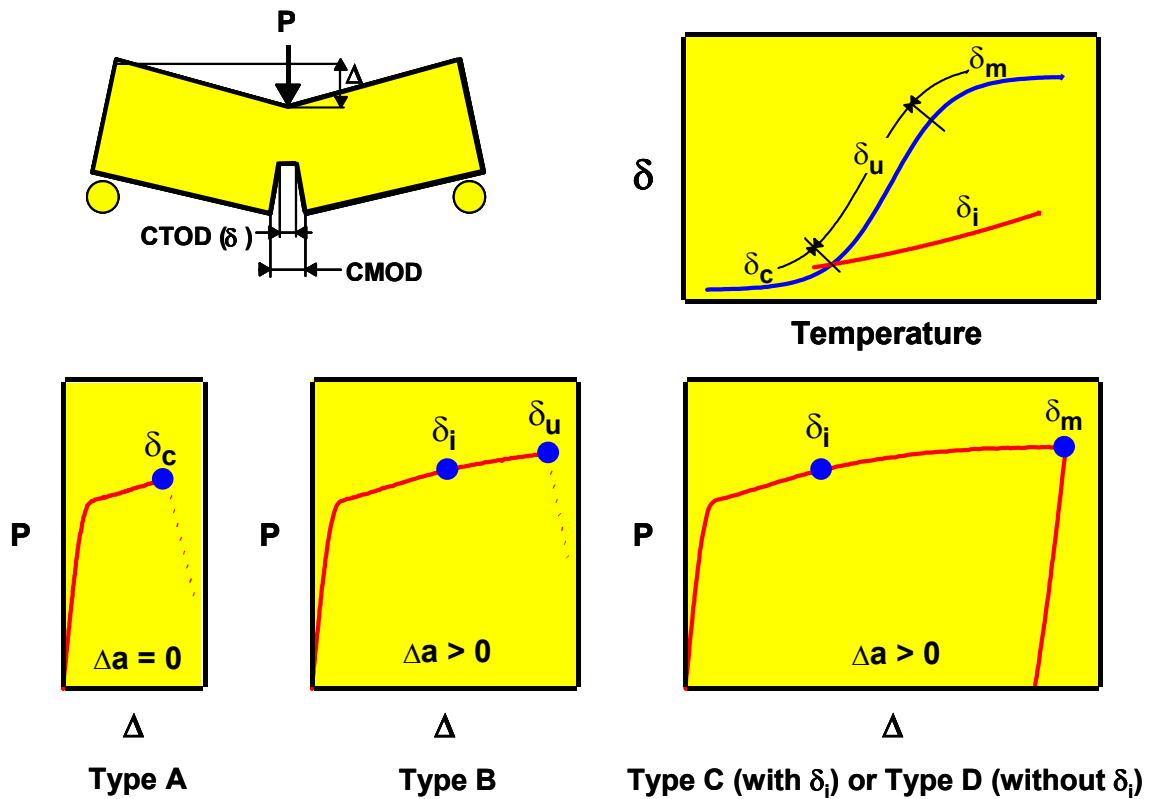


Figure 3: Crack-Tip Opening Displacement (CTOD)

The plastic component δ_p is determined, or inferred, as follows. It is assumed that the specimen behaves inelastically as two rigid bodies rotating about a plastic hinge with the center of rotation CR (Figure 3). Further, it is assumed that distance from the crack tip to the CR (r_p) is either 0.40 or 0.44 of the uncracked ligament b ($b = W - a_0$) for, respectively the British Standard BS 7448 Part 1 [2] and the ASTM standard E 1290 [1]. The plastic component of CTOD δ_p is related to the clip gage displacement CGD by the geometry of similar triangles through the inference expression

$$\delta_p = r_p(W - a_0)V_p/[r_p(W - a_0) + a_0] \tag{4}$$

where V_p is the plastic component of CGD (V).

NOTE: The current version of ASTM E 1290 [3] computes δ_e with an expression for the constraint factor m as a function of aspect ratio a_0/W and the strain-hardening exponent n of the specific material. Also, δ_p is more realistically computed from inference relations developed from elastic-plastic finite element analyses. These relations have been corroborated experimentally for single edge-notched beam specimens [4, 5].

4. Closure

As mentioned above, fracture toughness is not a single-valued property. Instead, it is a set of values that are functions of conditions of both the material and of the fracture toughness test. CTOD fracture toughness must be measured experimentally with *specimen-thicknesses equal to the thickness of the subject material in the structural element* of interest [1, 2, 3]. Also, service strain-rate and temperature should be replicated in the tests.

A common misconception is that an elastic fracture toughness (critical value of K_{I}) can be determined from a simple inversion of Eq. 2, i.e.,

$$K_{I-mat} = \sqrt{[\delta_{mat} m \sigma_{YS} E / (1 - \nu^2)]} \quad (5)$$

where δ_{mat} is the cited or observed CTOD toughness for a specific set of parameters. Such a computation can result in large errors, i.e., unconservative estimates of the critical stress – crack-size relation [6]. In point of fact, the critical value of K_{I} , the relation between critical stress and crack size for the specific element and **NOT** the elastic fracture toughness, could be computed from

$$K_{I-e} = \sqrt{[\delta_e m \sigma_{YS} E / (1 - \nu^2)]} \quad (6)$$

using the elastic component δ_e of the total CTOD δ .

Figure 4, taken from Ref. 6, shows the ratio of δ_e/δ_{mat} versus δ_{mat} for an offshore steel, API 2Y Grade 50T. As ductility to fracture, i.e., δ_p , increases, the ratio δ_e/δ_{mat} decreases from about 0.55 to about 0.05. Thus the error, from Eq. 7, increases from 1.35 to 4.47!

$$K_{I-mat} = K_{I-e} / \sqrt{[\delta_e/\delta_{mat}]} \quad (7)$$

In other words, for a given crack-size the critical stress is overestimated by 1.35 to 4.47! Similarly, for a given stress, the critical crack-size is overestimated by 1.82 to 20! In summary, from Figure 4,

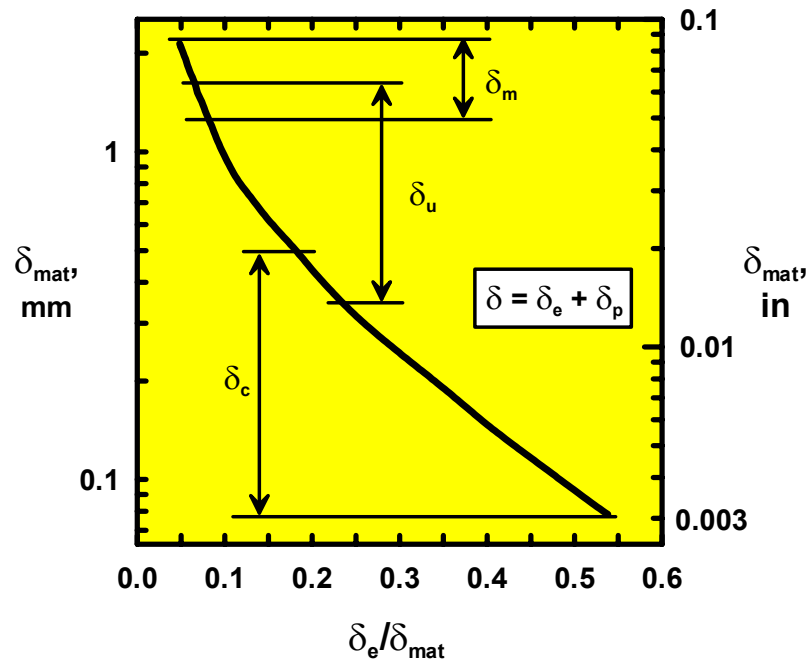


Figure 4: CTOD Toughness, API 2Y Grade 50T [6]

Table 4: Overestimations of Critical Stress and Crack-Size

CTOD	δ_e/δ_{mat}	Overestimate of ...	
		Critical Stress	Critical Crack-Size
δ_c	0.18	2.36	5.56
	0.54	1.36	1.85
δ_u	0.07	3.78	14.2
	0.24	2.04	4.17
δ_m	0.05	4.47	20.0
	0.08	3.54	12.5

Rarely, if every, are the components δ_e and δ_p of the total CTOD δ cited in the literature and, thus, the relation between critical stress and crack size can not be computed from Eq. 6. This apparent dilemma can be solved by recourse to the Failure Assessment Diagram approach [6].

The above argument applies equally well to characterization of elastic-plastic fracture toughness with the J-integral. The relation between CTOD δ and J-integral is

$$J = \delta(m\sigma_Y) \quad (8)$$

where the flow stress σ_Y is the arithmetic mean of the yield and tensile strengths, respectively, σ_{YS} and σ_{TS} . Because J-integral can be partitioned into two components – elastic and plastic

$$J = J_e + J_p = \delta_e(m\sigma_Y) + \delta_p(m\sigma_Y), \quad (9)$$

computing a fictitious elastic fracture toughness from the J-integral toughness J_{mat}

$$K_{I-mat} = \sqrt{[J_{mat}E / (1 - \nu^2)]} \quad (10)$$

results in the same overestimates of Table 4 with δ_c , δ_u , δ_m , δ_e and δ_{mat} replaced by, respectively, J_c , J_u , J_m , J_e and J_{mat} .

The reason for the overestimations of Table 4 is quite simple. Linear elastic fracture mechanics (i.e., fracture toughness expressed as a critical K_I such as K_c or K_{Ic}) assumes that strain energy lost by crack extension becomes the energy to form the new crack surfaces concomitant with crack extension. On the other hand, in elastic-plastic fracture (characterized by either δ_{mat} or J_{mat}), the strain energy lost by crack extension becomes the energy lost in plastic deformation as well as formation of the new crack surfaces concomitant with crack extension.

5. *References*

1. "Standard Test Method for Crack-Tip Opening Displacement (CTOD) Fracture Toughness Measurement," E 1290-89, American Society for Testing and Materials.
2. "Fracture Mechanics Toughness Tests. Part 1. Method for Determination of K_{Ic} , critical CTOD and Critical J Values of Metallic Materials," BS 7448 : Part 1 : 1991, British Standards Institution.
3. "Standard Test Method for Crack-Tip Opening Displacement (CTOD) Fracture Toughness Measurement," E 1290-02, American Society for Testing and Materials.
4. H. S. Reemsnyder, "The Experimental Measurement of the Plastic Component of Crack-Tip Opening Displacement and Comparison with Analytical Estimations," Bethlehem Steel Corporation, 1996.
5. H. S. Reemsnyder, "The Experimental Measurement of the Plastic Component of Crack-Tip Opening Displacement in Mismatched Welds and Comparison with Analytical Estimations," Bethlehem Steel Corporation, 1999.
6. H. S. Reemsnyder, "Failure Assessment Diagrams" in ASM Handbook, Volume 11, *Failure Analysis and Prevention*, ASM International, Materials Park, Ohio, 2002, pp 243 – 249.

APPENDIX C
STRESS INTENSITY FACTOR SOLUTION DERIVATIONS

The present appendix contains the derivations of the equations and expressions used in the analyses of the composite model – deck plate with cracked deck longitudinal.

The Model

The composite section may be modeled as having two components – a *deck plate* and a *cracked flat-plate longitudinal* with the following notations:

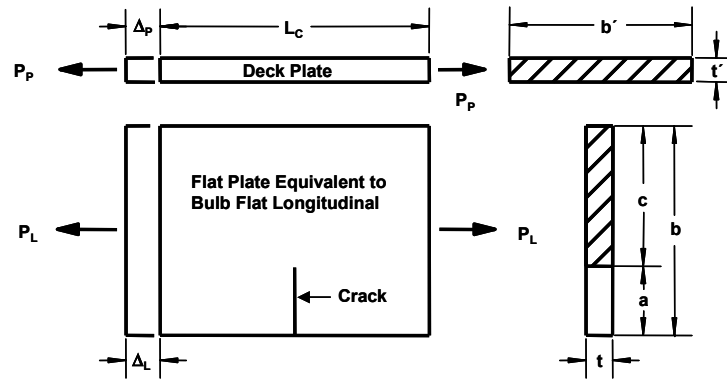


Figure 1: The Model.

Composite Section:

L_c Effective length of composite section.

spacing. use transverse frame 5540 mm

E Young's Modulus. 206,897 N/mm²

P Load on composite section.

P_O Limit load of composite section.

σ Remote stress on composite section.

σ_{ref} Reference stress on composite section.

σ_Y Yield stress. 345 N/mm²

L_r Collapse Ratio of composite section.

K_r Fracture Ratio of composite section.

Deck Plate:

b' **Effective** width of deck plate considering shear-lag. 786.1 mm

t' Thickness of deck plate. 16 mm

A_p **Effective** area of deck plate. 12,577.6 mm²

P_p Load on deck plate.

P_{OP} Limit load of deck plate.

σ_p Remote stress on deck plate.

Δ_p Elongation of deck plate due to load P_p .

Flat Plate Longitudinal:

b Depth of longitudinal. 387.27 mm

t Thickness of longitudinal. 11 mm

a Crack length.

c Ligament, i.e., $c = b - a$.

$A_{L_{uc}}$ Area of **uncracked** longitudinal. 4260 mm²

A_{L_c} Area of **cracked** longitudinal.

P_L Load on longitudinal.

$P_{O_{L_{uc}}}$ Limit load of **uncracked** longitudinal.

$P_{O_{L_c}}$ Limit load of **cracked** longitudinal.

σ_L Remote stress on longitudinal.

$\Delta_{L_{uc}}$ Elongation of **uncracked** longitudinal due to load P_L .

Δ_{L_c} Elongation of **cracked** longitudinal due to load P_L .

Stress Intensity Factor Solutions for a Cracked Plate

Two stress intensity factor solutions for the cracked flat-plate deck longitudinal acting alone are:

Single-edge-notched plate with ends restrained against rotation.

Single-edge-notched plate with ends free to rotate.

These two solutions bound the real situation where the stiffness of the deck-plate and adjacent structure influence the crack-driving force in the cracked longitudinal.

The stress intensity factor solutions take the form of

$$K_I = \sigma_L \cdot \sqrt{\pi a} \cdot F\left(\frac{a}{b}\right) \quad (1)$$

where σ_L is the remote (nominal) axial stress in the longitudinal, a is the crack length and b is the depth of the longitudinal. The function $F(a/b)$ reflects the boundary conditions of the specific problem.

The functions $F(a/b)$ for the case of free end rotation due to Brown and Srawley [1] for $a/b \leq 0.6$ and $L_c/2b \geq 1.0$

$$F\left(\frac{a}{b}\right) = 1.12 - 0.23 \cdot \left(\frac{a}{b}\right) + 10.6 \cdot \left(\frac{a}{b}\right)^2 - 21.7 \cdot \left(\frac{a}{b}\right)^3 + 30.4 \cdot \left(\frac{a}{b}\right)^4 \quad (2)$$

and Tada [2] for any a/b , Figure 2,

$$F\left(\frac{a}{b}\right) = \sqrt{\frac{2 \cdot b}{\pi \cdot a} \cdot \tan \frac{\pi \cdot a}{2 \cdot b}} \cdot \left[\frac{0.752 + 2.02 \cdot \left(\frac{a}{b}\right) + 0.37 \cdot \left(1 - \sin \frac{\pi \cdot a}{2 \cdot b}\right)^3}{\cos \frac{\pi \cdot a}{2 \cdot b}} \right] \quad (3)$$

and for the case of end rotation restraint due to Harris [1]

$$F\left(\frac{a}{b}\right) = \frac{5}{\sqrt{20 - 13 \cdot \left(\frac{a}{b}\right) - 7 \cdot \left(\frac{a}{b}\right)^2}} \quad (4)$$

Stress Intensity Factor Solution for the Composite Model

The effective area of the deck plate is

$$A_p = t' \cdot b', \quad (5)$$

the *uncracked* area of the flat plate longitudinal is

$$A_{Luc} = t \cdot b, \quad (6)$$

and the *cracked* area of the flat plate longitudinal is

$$A_{Lc} = t \cdot b \cdot (1 - a/b). \quad (7)$$

The elongation of the deck plate is

$$\Delta_p = \frac{P_p \cdot L_c}{A_p \cdot E} = \sigma_p \cdot \frac{L_c}{E} \quad (8)$$

and the elongation of the *cracked* flat plate longitudinal is

$$\Delta_L = \Delta_{Luc} + \Delta_{Lc} = \sigma_L \cdot \frac{L_c}{E} + \Delta_{Lc}. \quad (9)$$

From Tada [2], the displacement (or elongation) along the centerline due to the crack is

$$\Delta_{Lc} = \frac{4 \cdot \sigma_L \cdot a}{E} \cdot V_2(a/b) \quad \text{for } \frac{L_c}{2 \cdot b} \geq 1 \quad \text{and plane stress} \quad (10)$$

where, for any a/b, Figure1,

$$V_2(a/b) = \frac{a/b}{(1-a/b)^2} \cdot \left\{ 0.99 - a/b \cdot (1-a/b) \cdot \left[1.3 - 1.2 \cdot a/b + 0.7(a/b)^2 \right] \right\}. \quad (11)$$

For compatibility,

$$\Delta_p = \Delta_L. \quad (12)$$

Substitution of Eq. 8 to 10 inclusive into Eq. 12 gives the relation between remote stress on the deck plate σ_p and the remote stress on the *cracked* flat plate longitudinal σ_L ,

$$\sigma_p \cdot \frac{L_c}{E} = \frac{\sigma_L \cdot L_c}{E} \cdot \left(1 + \frac{4 \cdot a}{L_c} \cdot V_2 \right) \quad (13)$$

or

$$\sigma_p = \sigma_L \cdot \left(1 + \frac{4 \cdot a}{L_c} \cdot V_2 \right). \quad (14)$$

As $a/b \rightarrow 0$, $V_2 \rightarrow 0$ and $\sigma_p \rightarrow \sigma_L$.

For equilibrium,

$$P = P_L + P_p \quad (15)$$

where

$$P = \sigma \cdot (A_{Luc} + A_p), \quad (16)$$

$$P_L = \sigma_L \cdot A_{Luc} \quad (17)$$

and

$$P_p = \sigma_p \cdot A_p. \quad (18)$$

Substitution of Eq. 5, 6, 16, 17 and 18 into Eq. 15 results in

$$\sigma \cdot (A_{Luc} + A_p) = \sigma_L \cdot A_{Luc} + \sigma_p \cdot A_p \quad (19)$$

or

$$\sigma \cdot (t \cdot b + t' \cdot b') = \sigma_L \cdot t \cdot b + \sigma_p \cdot t' \cdot b' \quad (20)$$

$$\sigma_p + \sigma_L \cdot \frac{t \cdot b}{t' \cdot b'} = \sigma \cdot \left(1 + \frac{t \cdot b}{t' \cdot b'}\right). \quad (21)$$

$$\text{As } tb \rightarrow 0, \sigma_p \rightarrow \sigma. \quad \text{As } t' b' \rightarrow 0, \sigma_L \rightarrow \sigma.$$

Substitution of Eq. 14 into Eq. 21 results in

$$\sigma_L \cdot \left(1 + \frac{4 \cdot a}{L_c} \cdot V_2\right) + \sigma_L \cdot \frac{t \cdot b}{t' \cdot b'} = \sigma \cdot \left(1 + \frac{t \cdot b}{t' \cdot b'}\right). \quad (22)$$

or

$$\sigma_L = \sigma \cdot \frac{1 + \frac{t \cdot b}{t' \cdot b'}}{1 + \frac{4 \cdot a}{L_c} \cdot V_2 + \frac{t \cdot b}{t' \cdot b'}}. \quad (23)$$

$$\text{As } a/b \rightarrow 0, V_2 \rightarrow \sigma \text{ and } \sigma_L \rightarrow \sigma. \quad \text{As } t' b' \rightarrow 0, \sigma_L \rightarrow \sigma.$$

The stress intensity factor solution for the *composite section* takes the form of

$$K_I = \sigma_L \cdot \sqrt{\pi a} \cdot F\left(\frac{a}{b}\right) \quad (24)$$

where $F(a/b)$ is expressed as Eq. 40 and σ_L is expressed as Eq. 40.

Limit Loads– The limit loads for the deck plate P_{OP} and the *uncracked* flat plate longitudinal P_{OLuc} are

$$P_{OP} = \sigma_Y \cdot t' \cdot b' \quad (25)$$

and

$$P_{OLuc} = \sigma_Y \cdot t \cdot b. \quad (26)$$

The *plane stress* limit load for the cracked flat plate longitudinal is [3]

$$P_{OLc} = 1.072 \cdot \eta \cdot t \cdot c \cdot \sigma_Y = 1.072 \cdot \eta \cdot t \cdot b \cdot (1 - a/b) \cdot \sigma_Y \quad (27)$$

where η is a function of the ligament c , i.e., $c = b - a$, Figure 2,

$$\eta = \sqrt{1 + \left(\frac{a}{c}\right)^2} - \frac{a}{c} = \sqrt{1 + \left(\frac{1}{b/a - 1}\right)^2} - \left(\frac{1}{b/a - 1}\right). \quad (28)$$

As $a/b \rightarrow 0$, $\eta \rightarrow 1$ and $P_{Lc} \rightarrow 1.072bt\sigma_Y$.

The limit load of the composite section is

$$P_O = P_{OP} + P_{OLc} = \sigma_Y \cdot [t' \cdot b' + 1.072 \cdot \eta \cdot t \cdot b \cdot (1 - a/b)] \quad (29)$$

or

$$P_O = \sigma_Y \cdot t' \cdot b' \cdot \left[1 + 1.072 \cdot \eta \cdot \frac{t \cdot b}{t' \cdot b'} \cdot (1 - a/b) \right] \quad (30)$$

Reference Stress and Collapse Ratio

In the application of the Failure Assessment Diagram (FAD) approach to failure assessment, the coordinates of the Failure Assessment Point are the Fracture Ratio K_r and the Collapse Ratio L_r [4]. The Collapse Ratio is defined as

$$L_r = \frac{\sigma_{ref}}{\sigma_Y} \quad (31)$$

where the reference stress σ_{ref} is a function of the remote stress σ on the cracked element and the geometry of the cracked element.

However, the Collapse Ratio is rigorously defined as

$$L_r = \frac{P}{P_O} \quad (32)$$

where P and P_O are, respectively, the load on the cracked section and the limit load of the cracked section.

Combining Eq. 16, 29, 31 and 40 gives the reference stress σ_{ref} expressed as

$$\sigma_{ref} = \frac{\sigma \cdot \left(1 + \frac{t \cdot b}{t' \cdot b'}\right)}{1 + 1.072 \cdot \eta \cdot \frac{t \cdot b}{t' \cdot b'} \cdot (1 - a/b)}. \quad (33)$$

Thus L_r is expressed as

$$L_r = \frac{\sigma_{ref}}{\sigma_Y} = \frac{\sigma}{\sigma_Y} \cdot \frac{\left(1 + \frac{t \cdot b}{t' \cdot b'}\right)}{1 + 1.072 \cdot \eta \cdot \frac{t \cdot b}{t' \cdot b'} \cdot (1 - a/b)}. \quad (34)$$

Fracture Ratio

The Fracture Ratio K_r (*for zero residual stress*) is defined as [4]

$$\begin{aligned} K_r &= \sqrt{\frac{K_I^2}{\sigma_Y \cdot E \cdot \delta_c}} + \rho = \sqrt{\frac{(K_I^{\text{applied}} + K_I^{\text{residual}})^2}{\sigma_Y \cdot E \cdot \delta_c}} + \rho = \dots \\ &\dots = \sqrt{\frac{(K_I^{\text{applied}})^2 \cdot \left(1 + \frac{K_I^{\text{residual}}}{K_I^{\text{applied}}}\right)^2}{\sigma_Y \cdot E \cdot \delta_c}} + \rho \end{aligned} \quad (35)$$

where K_I , σ_y , E and δ_c are, respectively, the elastic crack-driving force, i.e., the stress intensity factor, the yield stress, Young's Modulus, and the CTOD fracture toughness. Further K_I^{applied} , the crack-driving in the cracked deck longitudinal, is defined by Eq. 24 where σ_L (in Eq. 24) is computed from Eq. 40.

The plasticity correction factor ρ , accommodating residual stresses and the concomitant plastic redistribution of stress, is computed from

$$\begin{aligned} \rho &= \rho_1 && \text{for } L_r \leq 0.8 \\ \rho &= 4 \cdot \rho_1 \cdot (1.05 - L_r) && \text{for } 0.8 < L_r < 1.05 \\ \rho &= 0 && \text{for } L_r \geq 1.05 \text{ or } K_I^{\text{residual}} \leq 0 \text{ or } K_I^{\text{applied}} = 0 \end{aligned} \quad (36)$$

where

$$\rho_1 = 0.1 \cdot \chi^{0.714} - 0.007 \cdot \chi^2 + 3 \times 10^{-5} \cdot \chi^5 \quad (37)$$

and

$$\chi = \frac{K_I^{\text{residual}}}{K_I^{\text{applied}}} \cdot L_r \quad (38)$$

where L_r is defined by Eq. 34.

I assumed that

$$\frac{K_I^{\text{residual}}}{K_I^{\text{applied}}} = \frac{\sigma_{\text{res}} \cdot \sqrt{\pi \cdot a} \cdot F(a/b)}{\sigma_L \cdot \sqrt{\pi \cdot a} \cdot F(a/b)} = \frac{\sigma_{\text{res}}}{\sigma_L} \quad (39)$$

Thus Eq. 40 becomes, with Eq. 34

$$\chi = \frac{\sigma_{\text{res}}}{\sigma_L} \cdot \frac{\sigma}{\sigma_Y} \cdot \frac{1 + \frac{t \cdot b}{t' \cdot b'}}{1 + 1.072 \cdot \eta \cdot \frac{t \cdot b}{t' \cdot b'} \cdot \left(1 - \frac{a}{b}\right)} \quad (40)$$

and, with Eq. 40, Figure 2,

$$\chi = \frac{\sigma_{res}}{\sigma_Y} \cdot \frac{1 + \frac{4a}{L_c} \cdot V_2 + \frac{t \cdot b}{t' \cdot b'}}{1 + 1.072 \cdot \eta \cdot \frac{t \cdot b}{t' \cdot b'} \cdot \left(1 - \frac{a}{b}\right)} \tag{41}$$

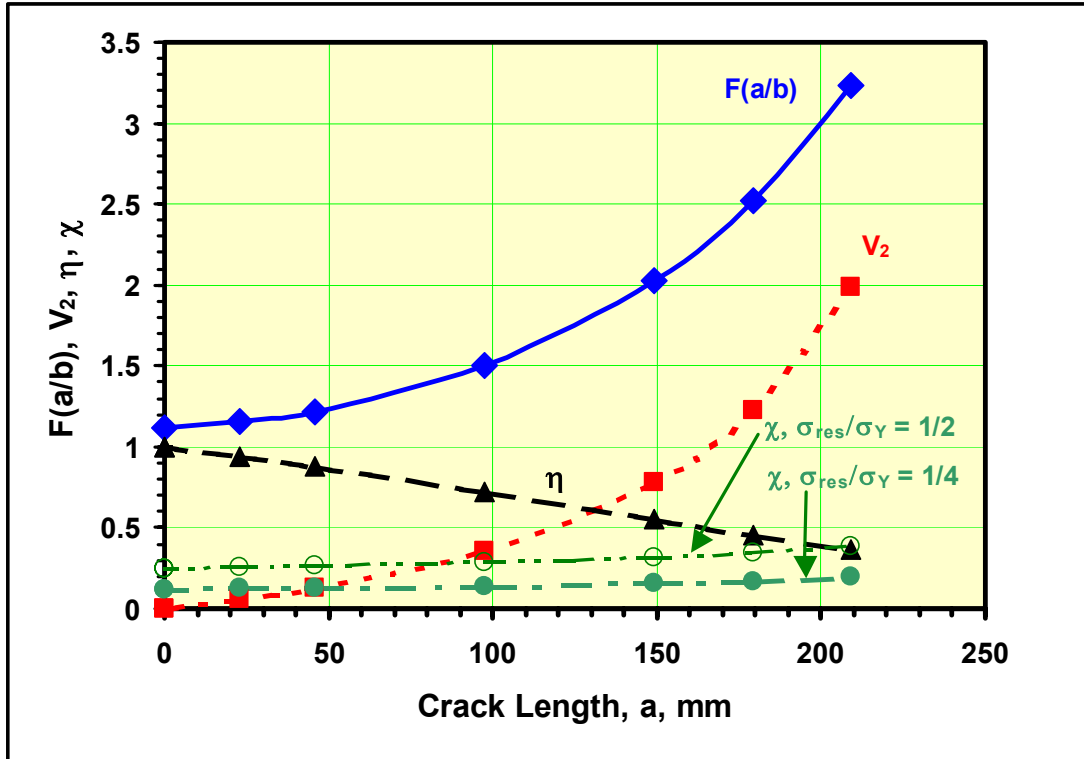


Figure 2: Parameters

Failure Assessment Curve

The Simplified Level 2B Failure Assessment Curve FAC is expressed as [5], Figure 3,

$$K_r = \frac{1}{\sqrt{1 + \frac{L_r^2}{2}}} \quad \text{for } L_r \leq 1 \tag{42}$$

and

$$K_r = 0 \quad \text{for } L_r > 1. \tag{43}$$

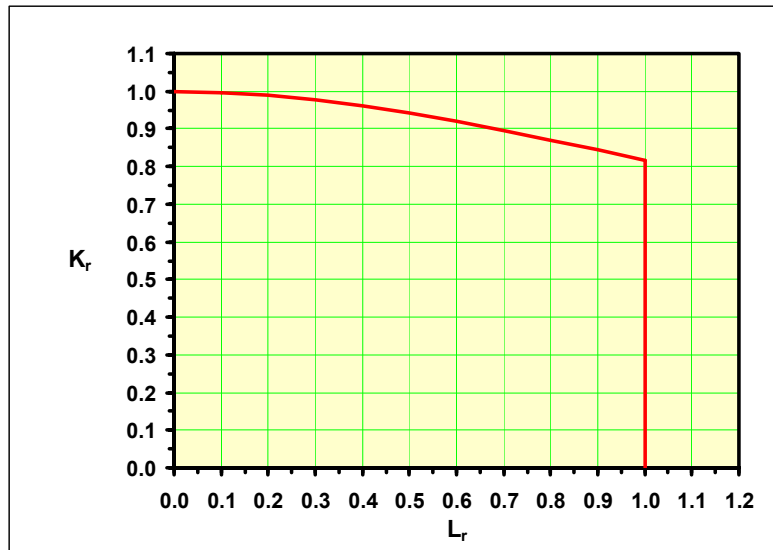


Figure 3: Simplified Level 2B, BS 7910

LOAD SHARING

Assume: *The adjacent composite sections pick up the load shed by the cracked section as the crack grows.*

Notation:

General:

Δ	Elongation of sections due to load P.	
P	Total load on two adjacent uncracked and one cracked composite section.	
L_c	Effective length of composite section, 5540 mm, transverse frame spacing	
E	Young's Modulus	206,897 N/mm ²
σ	Remote stress on deck system.	
σ_Y	Yield stress.	345 N/mm ²
b'	Effective width of deck plate considering shear-lag.	786.1 mm
t'	Thickness of deck plate.	16 mm

Uncracked Composite Section:

Δ_{LUC}	Elongation of uncracked sections due to load P_{US} .
P_{US}	Load on uncracked composite sections.
σ_{US}	Remote stress on uncracked section.
A	Remote area of uncracked section. $A = t'b' + tb$

Cracked Composite Section:

Δ_L	Elongation of cracked section due to load P_{US} , $\Delta_L = \Delta_{LUS} + \Delta_{LS}$
P_{CS}	Load on cracked composite section.
σ_{CS}	Remote stress on cracked section.
A_C	Remote area of cracked section. $A_C = t'b' + tb = A$
a	Crack length.
c	Ligament, i.e., $c = b - a$.
σ_L	Remote stress on cracked longitudinal.
Δ_{LUS}	Elongation of uncracked longitudinal due to load P_{CS} .
Δ_{LS}	Additional elongation of cracked longitudinal due to load P_{CS} .
V_2	Tada correction for computation of Δ_{LC} .

The two adjacent uncracked composite sections and the center cracked composite section will elongate an amount Δ under the total load P where, in the cracked composite section

$$\Delta = \Delta_L = \Delta_{LUS} + \Delta_{LS} = \sigma_L \cdot \frac{L_c}{E} \cdot \left(1 + \frac{4 \cdot a}{L_c} \cdot V_2 \right). \quad (44)$$

where

$$\sigma_L = \sigma_{CS} \cdot \frac{1 + \frac{t \cdot b}{t' \cdot b'}}{1 + \frac{4 \cdot a}{L_c} \cdot V_2 + \frac{t \cdot b}{t' \cdot b'}} \quad (45)$$

and σ_{CS} is the remote stress on the cracked composite section

$$\text{As } a \rightarrow 0, \Delta_{LS} \rightarrow \Delta_{LUS} = \sigma_L L_c / E.$$

and in the uncracked composite sections

$$\Delta = \Delta_{LUC} = \frac{\sigma_L \cdot L_c}{E} \quad (46)$$

where $\sigma_L = \sigma_{US}$, the remote stress on the uncracked section.

Also

$$P = 2P_{US} + P_{CS} \quad (47)$$

or

$$\sigma \cdot (3 \cdot A) = 2 \cdot \sigma_{US} \cdot (A) + \sigma_{CS} \cdot (A_C) \quad (48)$$

where σ is the remote (nominal or membrane) stress in the stiffened deck system.

Eq. 39 becomes, with $A_C = A$

$$\sigma \cdot (3 \cdot A) = 2 \cdot \sigma_{US} \cdot (A) + \sigma_{CS} \cdot (A) \quad (49)$$

or,

$$\sigma_{US} = \frac{3 \cdot \sigma - \sigma_{CS}}{2}. \quad (50)$$

But, combining Eq. 35, 36 and 37

$$\Delta = \Delta_{LUS} + \Delta_{LS} = \sigma_{CS} \cdot \frac{L_c}{E} \cdot \frac{1 + \frac{t \cdot b}{t' \cdot b'}}{1 + \frac{4 \cdot a}{L_c} \cdot V_2 + \frac{t \cdot b}{t' \cdot b'}} \cdot \left(1 + \frac{4 \cdot a}{L_c} \cdot V_2\right) = \Delta_{UC} = \sigma_{US} \cdot \frac{L_c}{E} \quad (51)$$

or

$$\sigma_{CS} = \frac{3 \cdot \sigma}{1 + 2 \cdot \frac{\left(1 + \frac{4 \cdot a}{L_c} \cdot V_2\right) \cdot \left(1 + \frac{t \cdot b}{t' \cdot b'}\right)}{1 + \frac{4 \cdot a}{L_c} \cdot V_2 + \frac{t \cdot b}{t' \cdot b'}}}. \quad (52)$$

As $a \rightarrow 0, \sigma_{CS} \rightarrow \sigma$, Figure 4.

Thus, σ_{CS} is the remote stress in the cracked composite section as load is shed to the adjacent two uncracked composite sections whilst a grows, and

$$\sigma_{US} = \frac{3 \cdot \sigma}{2} \cdot \left[1 - \frac{1}{1 + 2 \cdot \frac{\left(1 + \frac{4 \cdot a}{L_c} \cdot V_2\right) \cdot \left(1 + \frac{t \cdot b}{t' \cdot b'}\right)}{1 + \frac{4 \cdot a}{L_c} \cdot V_2 + \frac{t \cdot b}{t' \cdot b'}}} \right] \quad (53)$$

As $a \rightarrow 0$, $\sigma_{US} \rightarrow \sigma$, Fig. 0.

where σ_{US} is the remote stress in the two uncracked composite sections as load is shed from the cracked composite section whilst a grows.

COMPLIANCE OF COMPOSITE SECTIONS

The compliance (i.e., reciprocal of stiffness) of the *cracked* composite section C_{CS} is

$$C_{CS} = \frac{P_{CS}}{\Delta_L} = \frac{\sigma_{CS}}{A_C} \cdot \frac{E \cdot \left(1 + \frac{4 \cdot a}{L_c} \cdot V_2\right) \cdot \left(1 + \frac{t \cdot b}{t' \cdot b'}\right)}{\sigma_{CS} \cdot L_c \cdot \left(1 + \frac{4 \cdot a}{L_c} \cdot V_2 + \frac{t \cdot b}{t' \cdot b'}\right)} \quad (54)$$

or, with $A_C = t' \cdot b' + tb$,

$$C_{CS} = \frac{E}{t' \cdot b' \cdot \left(1 + \frac{t \cdot b}{t' \cdot b'}\right) \cdot L_c} \cdot \frac{\left(1 + \frac{4 \cdot a}{L_c} \cdot V_2\right) \cdot \left(1 + \frac{t \cdot b}{t' \cdot b'}\right)}{\left(1 + \frac{4 \cdot a}{L_c} \cdot V_2 + \frac{t \cdot b}{t' \cdot b'}\right)} \quad (55)$$

or

$$C_{CS} = \frac{E}{t' \cdot b' \cdot L_c} \cdot \frac{1 + \frac{4 \cdot a}{L_c} \cdot V_2}{\left(1 + \frac{4 \cdot a}{L_c} \cdot V_2 + \frac{t \cdot b}{t' \cdot b'}\right)} \quad (56)$$

The compliance of the *uncracked* composite section C_{US} is

$$C_{US} = \frac{P_{US}}{\Delta_{LUC}} = \frac{\sigma_{US}}{A} \cdot \frac{E}{\sigma_{US} \cdot L_c} = \frac{E}{t' \cdot b' \cdot L_c} \cdot \frac{1}{1 + \frac{tb}{t'b'}} \quad (57)$$

Also

$$\frac{C_{CS}}{C_{US}} = \frac{\left(1 + \frac{4 \cdot a}{L_c} \cdot V_2\right) \cdot \left(1 + \frac{t \cdot b}{t' \cdot b'}\right)}{\left(1 + \frac{4 \cdot a}{L_c} \cdot V_2 + \frac{t \cdot b}{t' \cdot b'}\right)} \quad (58)$$

As $a \rightarrow 0$, $C_{CS} \rightarrow C_{US}$, Figure 4.

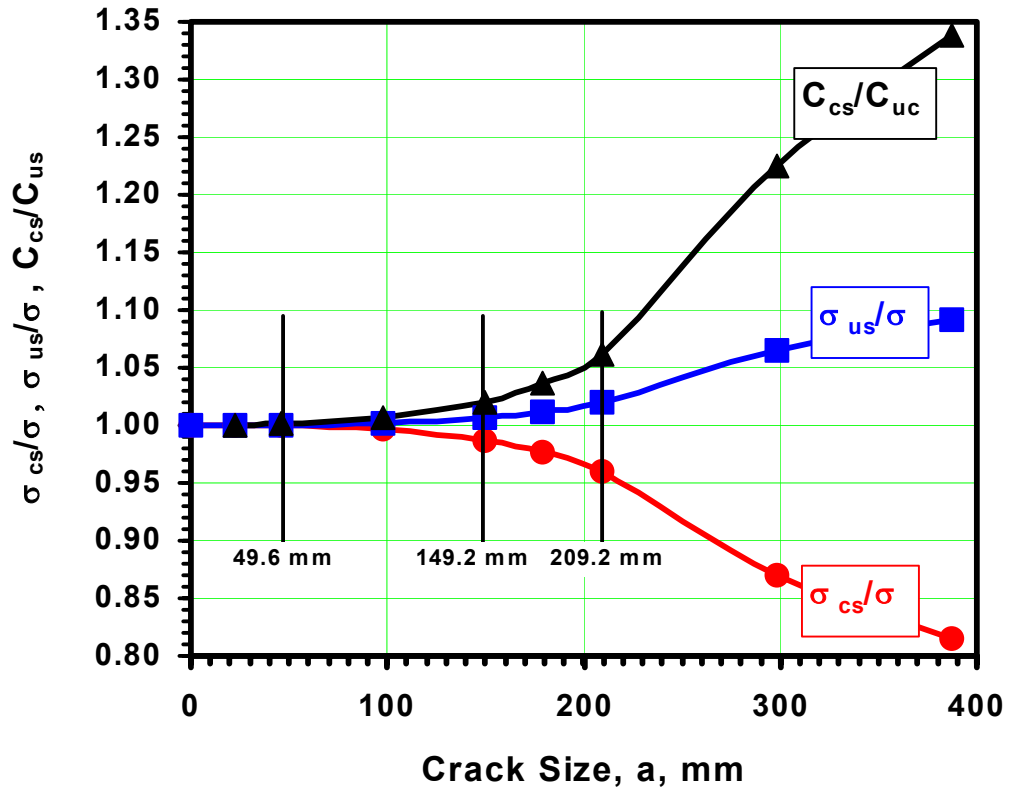


Figure 4: Load Shedding with Crack Growth

REFERENCES

- 1.. D.P. Rooke and D.J. Cartwright, "Compendium of Stress Intensity Factors," HM Stationery Office, London, 1976, pp 84 – 85.
- 2.. H. Tada, P.C. Paris, and G.W. Irwin, , "The Stress Analysis of Cracks Handbook," 3d Ed., ASME Press, New York, 2000, pp 52 – 54.
- 3.. "An Engineering Approach to Elastic-Plastic Fracture Analysis," *EPRI NP-1931*, General Electric Co., Schenectady, 1981, p 3-12 – 3-14.
4. "Guide on Methods for Assessing the Acceptability of Flaws in Metallic Structures," *BS 7910: 1999 with Amendment 1*, Brit. Std. Inst., London, 2000.
5. H.S. Reemsnyder, "Simplified Level 2B Failure Assessment Curve -- BS 7910: 1999 with Amendment 1," November 7, 2002.
- 6.. H.S. Reemsnyder, "Example of Application of Simplified Level 2B Failure Assessment Curve BS 7910:1999 with Amendment 1 – Cracked Deck Longitudinal," Progress Report 1, May 15, 2003.
- 7.. H.S. Reemsnyder, "Example of Application of Simplified Level 2B Failure Assessment Curve BS 7910:1999 with Amendment 1 – Cracked Deck Longitudinal – K-Solution for Composite Model," Progress Report 2, June 23, 2003.
- 8.. H.S. Reemsnyder, "Example of Application of Simplified Level 2B Failure Assessment Curve BS 7910:1999 with Amendment 1 – Cracked Deck Longitudinal – Failure Assessment of Composite Model," Progress Report 3, July 15, 2003.

SHIP STRUCTURE COMMITTEE PARTNERS AND LIAISON MEMBERS

PARTNERS

The Society of Naval Architects and Marine Engineers

Mr. Joe Cuneo
President,
Society of Naval Architects and Marine Engineers

Dr. John Daidola
Chairman,
SNAME Technical & Research Steering
Committee

The Gulf Coast Region Maritime Technology Center

Dr. John Crisp
Executive Director,
Gulf Coast Maritime Technology Center

Dr. Bill Vorus
Site Director,
Gulf Coast Maritime Technology Center

LIAISON MEMBERS

American Iron and Steel Institute
American Society for Testing & Materials
American Society of Naval Engineers
American Welding Society
Bethlehem Steel Corporation
Canada Center for Minerals & Energy Technology
Colorado School of Mines
Edison Welding Institute
International Maritime Organization
International Ship and Offshore Structure Congress
INTERTANKO
Massachusetts Institute of Technology
Memorial University of Newfoundland
National Cargo Bureau
Office of Naval Research
Oil Companies International Maritime Forum
Tanker Structure Cooperative Forum
Technical University of Nova Scotia
United States Coast Guard Academy
United States Merchant Marine Academy
United States Naval Academy
University of British Columbia
University of California Berkeley
University of Houston - Composites Eng & Appl.
University of Maryland
University of Michigan
University of Waterloo
Virginia Polytechnic and State Institute
Webb Institute
Welding Research Council
Worcester Polytechnic Institute
World Maritime Consulting, INC

Mr. Alexander Wilson
Captain Charles Piersall (Ret.)
Captain Dennis K. Kruse (USN Ret.)
Mr. Richard Frank
Dr. Harold Reemsnyder
Dr. William R. Tyson
Dr. Stephen Liu
Mr. Dave Edmonds
Mr. Tom Allen
Dr. Alaa Mansour
Mr. Dragos Rauta
Mr. Dave Burke / Captain Chip McCord
Dr. M. R. Haddara
Captain Jim McNamara
Dr. Yapa Rajapaksie
Mr. Phillip Murphy
Mr. Rong Huang
Dr. C. Hsiung
Commander Kurt Colella
Dr. C. B. Kim
Dr. Ramswar Bhattacharyya
Dr. S. Calisal
Dr. Robert Bea
Dr. Jerry Williams
Dr. Bilal Ayyub
Dr. Michael Bernitsas
Dr. J. Roorda
Dr. Alan Brown
Dr. Kirsi Tikka
Dr. Martin Prager
Dr. Nick Dembsey
VADM Gene Henn, USCG Ret.

RECENT SHIP STRUCTURE COMMITTEE PUBLICATIONS

Ship Structure Committee Publications on the Web - All reports from SSC 392 and forward are available to be downloaded from the Ship Structure Committee Web Site at URL:

<http://www.shipstructure.org>

SSC 391 and below are available on the SSC CD-ROM Library. Visit the National Technical Information Service (NTIS) Web Site for ordering information at URL:

<http://www.ntis.gov/fcpc/cpn7833.htm>

SSC Report Number	Report Bibliography
SSC 429	<u>Rapid Stress Intensity Factor Solution Estimation for Ship Structures Applications</u> L. Blair Carroll, S. Tiku, A.S. Dinovitzer 2003
SSC 428	<u>In-Service Non-Destructive Evaluation of Fatigue and Fracture Properties for Ship Structure</u> S. Tiku 2003
SSC 427	<u>Life Expectancy Assessment of Ship Structures</u> A. Dinovitzer 2003
SSC 426	<u>Post Yield Stability of Framing</u> J. DesRochers, C. Pothier, E. Crocker 2003
SSC 425	<u>Fatigue Strength and Adequacy of Weld Repairs</u> R.J. Dexter, R.J. Fitzpatrick, D.L. St. Peters 2003
SSC 424	<u>Evaluation of Accidental Oil Spills from Bunker Tanks (Phase I)</u> T. McAllister, C. Rekart, K. Michel 2003
SSC 423	<u>Green Water Loading on Ship Deck Structures</u> M. Meinhold, D. Liut, K. Weems, T. Treakle, Woe-Min Lin 2003
SSC 422	<u>Modeling Structural Damage in Ship Collisions</u> Dr. A.J. Brown 2003
SSC 421	<u>Risk Informed Inspection of Marine Vessels</u> Dr. B.M. Ayyub, U.O. Akpan, P.A. Rushton, T.S. Koko, J. Ross, J. Lua 2003
SSC 420	<u>Failure Definition for Structural Reliability Assessment</u> Dr. B. M. Ayyub, P.E. Hess III, D.E. Knight 2002
SSC 419	<u>Supplemental Commercial Design Guidance for Fatigue</u> R.A. Sielski, J. R. Wilkins, J.A. Hultz 2001
SSC 418	<u>Compensation for Openings in Primary Ship Structure</u> J.J. Hopkinson, M. Gupta, P. Sefcsik 2002
SSC 417	<u>Prediction of Structural Response in Grounding Application to Structural Design</u> K.K. Tikka 2001